NOVEL INSIGHTS INTO MEASLES PATHOGENESIS AND IMMUNE SUPPRESSION

Rory D. de Vries

NOVEL INSIGTHS INTO MEASLES PATHOGENESIS AND IMMUNE SUPPRESSION
Rory D. de Vries, 2013

Cover
Confocal microscopy image of an agarose inflated lung slice 6 days post infection after *ex vivo* infection with rMV^{KS}EGFP(3). Image shows a small bronchus stained with TO-PRO-3 for nuclei (red) and β-tubulin IV for cilia (blue). MV-infected cells are shown by EGFP autofluorescence in green.

ISBN: 978-94-6169-342-6
Lay-out: Rory D. de Vries
Print: Optima Grafische Communicatie

Novel Insights into Measles Pathogenesis and Immune Suppression

Nieuwe inzichten in mazelen pathogenese en immuunsuppressie

Proefschrift

Ter verkrijging van de graad van doctor aan de
Erasmus Universiteit Rotterdam
op gezag van de
rector magnificus

Prof.dr. H.G. Schmidt

en volgens besluit van het College van Promoties.

De openbare verdediging zal plaatsvinden op

vrijdag 8 februari 2013 om 9:30 uur
door

Rory Dylan de Vries
geboren te Schiedam

Promotiecommissie

Promotor:	Prof.dr. A.D.M.E. Osterhaus
Overige leden:	Prof.dr. J.J.M. van Dongen Prof.dr. H.P. Endtz Prof.dr. T.B.H. Geijtenbeek
Co-promotor(en):	Dr. R.L. de Swart Dr. W.P. Duprex

The research described in this thesis was conducted at the Erasmus MC department Viroscience, Rotterdam, the Netherlands, with financial support of ZonMW (grant number 91208012) and MRC (grant number G0801001). Furthermore, the research for this thesis was performed within the framework of the Erasmus Postgraduate School Molecular Medicine.

Financial support for printing of this thesis by the following companies and foundations is gratefully acknowledged:
- Erasmus University
- Carl Zeiss BV
- BD Biosciences
- Greiner Bio-one

Molecular Medicine
Postgraduate School

“ It’s not easy being green ”

Kermit

TABLE OF CONTENTS

General introduction

1

General introduction

Based on:

Measles vaccination: new strategies and formulations
Rory D. de Vries, Koert J. Stittelaar, Albert D.M.E. Osterhaus and Rik L. de Swart
Expert Reviews of Vaccines 2008 Oct; 7(8):1215 - 1223 (review)

The pathogenesis of measles
Rory D. de Vries, Annelies W. Mesman, Teunis B.H. Geijtenbeek, W. Paul Duprex and Rik L. de Swart
Current Opinion in Virology 2012 Jun; 2(3): 248 - 255 (review)

Evaluating measles vaccines: can we assess cellular immunity?
Rory D. de Vries and Rik L. de Swart
Expert Reviews of Vaccines 2012 Jul; 11(7): 779 - 782 (key paper evaluation)

Paramyxoviruses

Paramyxoviruses belong to the order *Mononegavirales*, and have a diverse host range. They have a negative-sense single stranded RNA genome of 15,000 – 19,000 nucleotides (nt), encoding 6 – 10 genes [1]. The genome is contained in a helical nucleocapsid, 18 nm in diameter and up to 1000 nm in length, which is surrounded by a lipid bilayer [1]. The envelope is derived from the membrane of the infected cell during budding [2]. Many animal and human paramyxoviruses have been identified, and new ones are still being detected in a wide variety of animals [3–8].

Paramyxoviruses transmit from host-to-host via the respiratory route, and are responsible for significant diseases in humans and animals. The family *Paramyxoviridae* contains two subfamilies, the *Paramyxovirinae* and *Pneumovirinae*. The subfamily *Paramyxovirinae* contains the genera *Morbillivirus* (including measles virus (MV), which causes measles in man), *Rubulavirus* (including mumps virus, which causes mumps in man), *Respirovirus* (including parainfluenzavirus type 3, which causes respiratory tract disease in small children) and *Henipahvirus* (including Hendra- and Nipah virus, which originate from bats and cause lethal outbreaks among humans following infection of intermediate hosts such as horses or pigs, respectively). The genus *Avulavirus* includes Newcastle disease virus (NDV), which is an important pathogen of birds causing high mortality rates and a large worldwide economic impact [1]. The subfamily *Pneumovirinae* contains the genera *Pneumovirus* (including human respiratory syncytial virus (HRSV) and bovine respiratory syncytial virus (BRSV)) and *Metapneumovirus* (including human metapneumovirus (HMPV)). HRSV and HMPV are important causes of respiratory tract disease in children [9,10], while BRSV causes outbreaks of respiratory tract disease in calves [10].

In this general introduction, the biology of the members of the genus *Morbillivirus* will be discussed, focusing primarily on the prototype morbillivirus MV. How is the genome organized, how and where does the virus replicate, how does it infect the host and cause disease, how does it interact with the immune system and finally how is it transmitted? Furthermore, current vaccination strategies to interrupt endemic MV transmission and potentially eradicate measles will be discussed, alongside with what might be the consequences if the virus were to be globally eradicated.

Morbilliviruses

The viruses discussed in this thesis belong to the genus *Morbillivirus*. All morbilliviruses are highly infectious, spread via the respiratory route, cause profound immune suppression and have the propensity to cause large outbreaks with high morbidity and mortality among all age classes in previously unexposed populations. Morbilliviruses are relatively host-restricted, meaning that they mainly cause disease in a limited number of natural host species (Figure 1). The only primate pathogen in this genus is MV. Other morbilliviruses are canine distemper virus (CDV), which causes distemper in dogs and a number of other carnivore species, phocine distemper virus (PDV), which leads to distemper in several seal species, dolphin and porpoise morbillivirus (DMV and PMV), which cause disease in cetacean species and peste des petits ruminants (PPRV), which causes disease in small ruminants such as goats

and sheep [11]. Only recently, feline morbillivirus (FmoPV) was identified as a new member of the genus that causes disease in cats [8]. Rinderpest virus (RPV) was an important cause of disease in cattle and other large ruminants, which not only had a devastating effect on cattle herds world-wide but also on human populations that depended on them [12,13]. RPV is the second virus to be eradicated by targeted vaccination campaigns [13,14].

Even though each of the morbilliviruses normally targets a specific host species, it is unlikely that adaptation resulted from parallel evolution between the viruses and their respective hosts, as the evolutionary diversification of mammals is much older than that of the morbilliviruses [15]. It is therefore more likely that these viruses evolved from a common ancestral virus that adapted to different mammalian hosts following cross-species jumps [11], see also Figure 1. Therefore it is not surprising that to this day morbilliviruses occasionally cross species barriers and cause disease in 'non-natural host' species.

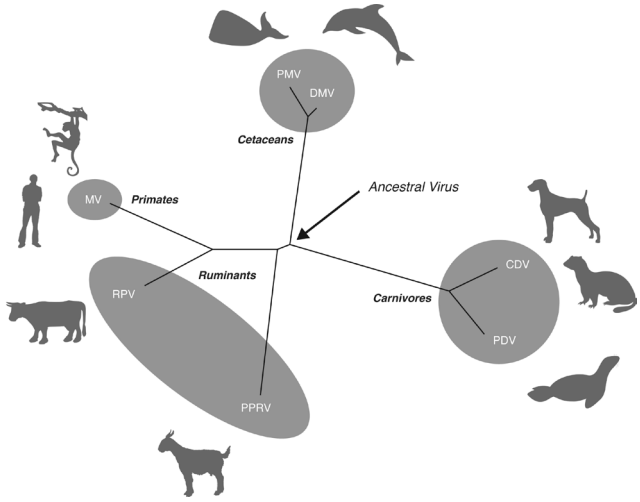

Figure 1. *Phylogenetic tree showing relationships between the morbilliviruses and their respective hosts, based on partial sequences of the P gene. The branch lengths are proportional to the mutational differences between the viruses and the hypothetical common ancestor that existed at the nodes in the tree. Adapted from: [11]. This tree does not include feline morbillivirus.*

Morphology, genome organization and viral proteins

Morbillivirus particles are pleiomorphic and average in size from 100 – 300 nm [16], see also schematic representation in Figure 2A and B. The genome consists of single-stranded RNA of negative polarity, typically 15,500 – 16,000 nt in length, consisting of six genes that encode 8 proteins (Figure 2C). Genes are transcribed by a start-stop mechanism from a single promotor at the 3' end of the genome leading to a so-called transcription gradient, which means that the mRNAs transcribed from the genes closest to the 3' end are present in greater abundance than those transcribed from the genes at the 5' end [17,18]. This is due to the chance that between each open reading frame (ORF) the virus-associated RNA-dependent RNA-polymerase

(RdRp) may dissociate from the genome, and thus has to re-initiate transcription at the 3' end.

The nucleoprotein (N) mRNA is produced first since it is at the promotor-proximal position of the genome. The main function of the N protein is to encapsidate the genomic RNA, with which the viral polymerase interacts during transcription and replication. Since one N protein covers 6 nt, the genome lengths of morbilliviruses always obey the "rule of six" (*i.e.* the genome length must be a multiple of six nt) [19].

The second gene in the morbillivirus genome is the phosphoprotein (P) gene, which encodes two different mRNAs and three proteins, P, V and C protein. The P protein is a co-factor of the RdRp [20], essential in transcription and replication. The C and V proteins are either translated from an overlapping reading frame or as co-transcriptionally edited products of the P mRNA [21,22]. The V protein is important in immune inhibition, potentially interfering with the type 1 interferon pathway by binding to DBB1, mda-5, STAT1 and STAT2 [23–28]. The C protein has been suggested to modulate the viral polymerase activity and play a role in interference with the innate immune system [29,30]. Recombinant (r) MV defective for C is growth-defective in peripheral blood mononuclear cells (PBMC) and less virulent *in vivo* [31,32].

The matrix (M) protein is assumed to associate with the inner leaflet of the virus envelope [33,34] (Figure 2A). However, a recent publication using electron cryotomography revealed that in MV particles the M protein coats the N-coated viral RNA, rather than localizing to the envelope [35] (Figure 2B). The M protein has an important role in the morphogenesis of viral particles [36], and may be the driving force in viral budding. M is thought to interact with both the N protein [37] and the cytoplasmic tails of the viral envelope glycoproteins to ensure incorporation of the viral genome into nascent virions [38,39].

The mRNAs encoding the two viral transmembrane glycoproteins, the fusion (F) and hemagglutinin (H) proteins, are transcribed after M. The F glycoprotein mediates membrane fusion, either between the virus particle and a host cell (virus-to-cell fusion) or between two adjacent host cells (cell-to-cell fusion). The H glycoprotein mediates attachment of the viral particle to host cell receptors. The F glycoproteins form trimers while H is present as a dimer of dimers, which interact to form the fusion complex [40]. Upon binding the cellular receptor, the H glycoprotein undergoes a conformational change and triggers the fusion activity of the F glycoprotein [41,42]. Therefore, the combination of the F and H glycoproteins is critical for viral entry and cell-to-cell spread.

The transcription unit encoding the large (L) protein mRNA is located at the 5' end of the genome and accounts for more than 40% of the genome length. The L protein acts both as a transcriptase and as a replicase, in a complex with P [20,43–45].

Virus life-cycle

A schematic representation of the morbillivirus life-cycle is shown in Figure 2D. To initiate infection of a target cell, the H glycoprotein interacts with an entry receptor present on the cell surface. After virus binding and fusion of the viral membrane with that of the host cell, the minimal unit of infectivity, the ribonucleoprotein (RNP) complex, is released into the cytoplasm. The RNP is comprised of the viral genome associated with the N, P and L proteins. In the cytoplasm, the RdRp is responsible for primary transcription during the first 6 hours post infection (h.p.i.). In the second phase of infection (6 – 12 h.p.i.), newly synthesized RdRp leads to an exponential increase in mRNA synthesis. In the third phase of infection (12 – 24 h.p.i.), the emphasis shifts from transcription to genome replication: RdRp switches from functioning as a transcriptase to functioning as a replicase.

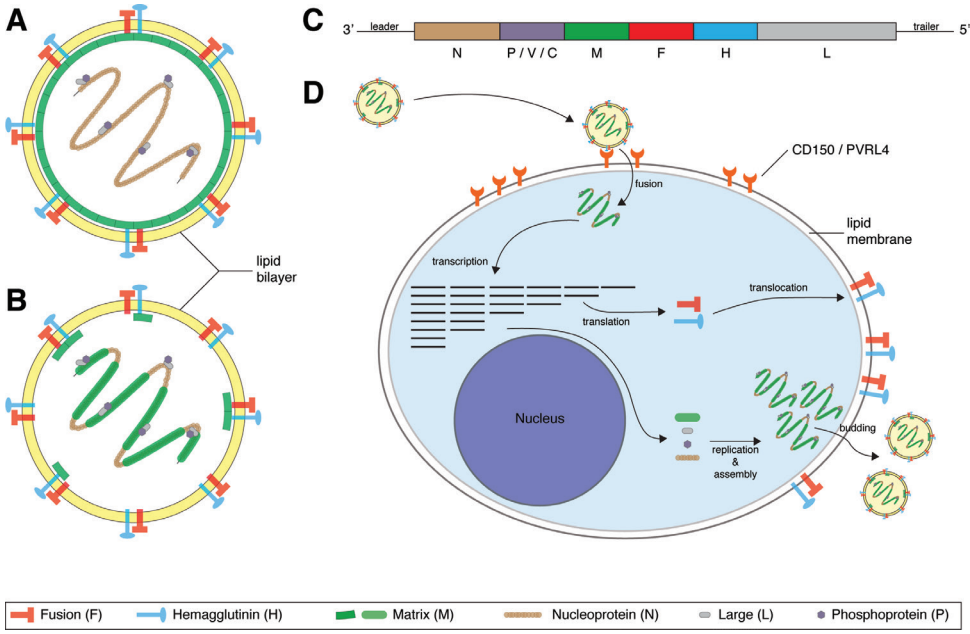

Figure 2. *(A, B) Schematic representation of an MV virion. The enveloped virus contains six proteins: the transmembrane glycoproteins F and H, the N protein coating the genomic RNA and the P and L proteins in a complex associated with the nucleoprotein. For the location of the M protein two models exist [35]. M is either present directly beneath the lipid bilayer (A) or directly interacts with the nucleoprotein (B). (C) Schematic representation of the MV genome. The P gene also encodes the V and C protein. Gene lengths are not shown on scale. (D) Schematic representation of the MV replication cycle. MV enters via interaction between the H glycoprotein and a cellular receptor followed by fusion, replicates in the cytoplasm, and assembled virions bud at the plasma membrane.*

During the viral replication cycle, the F and H glycoproteins are modified in the Golgi apparatus and translocated to the cell membrane [46]. The presence of these glycoproteins at the cell membrane can generate syncytia or multi-nucleated giant cells, which are often seen in the lungs or lymphoid tissues of morbillivirus-infected hosts. Newly formed RNP associates with the M protein, which is recruited to the plasma membrane. Here, new viral particles are generated by budding from

lipid rafts. The interaction between the M protein and the cytoplasmic tails of the trans-membrane glycoproteins ensures that new viral particles have an envelope containing F and H glycoproteins on its surface. The M protein and the RNP are incorporated into the newly formed virus particles.

Reverse genetics

Even though RNA viruses typically have high mutation rates, morbilliviruses are monotypic [47] and remain surprisingly stable during outbreaks or in situations of endemic circulation [48–50]. Molecular clones of MV are also remarkably stable. Reverse genetics enabled the first rMV to be rescued in 1995. The system was based on the expression of the anti-genomic RNA of laboratory-adapted MV strain Edmonston in 293 cells stably expressing T7 RNA polymerase and the N and P proteins, into which the L protein was transfected transiently [51]. This resulted in a clone that was designated rMV^{Edtag}. Since the initial rescue of rMV^{Edtag} many different rMV have been generated, which have been critical in advancing our understanding of morbillivirus biology and pathogenesis. In 2000, Takeda *et al.* described the recovery of a cloned wild-type strain of MV from a wild-type Japanese MV strain, using an Epstein-Barr virus-transformed marmoset B lymphocyte cell line (B95a), named rMV^{IC323} [52]. An additional transcription unit (ATU) encoding enhanced green fluorescent protein (EGFP) was cloned into this virus at the promotor-proximal position resulting in a virus known as rMV^{IC323}EGFP [53], which could be used for sensitive detection of infected cells. Furthermore, rMV^{IC323}EGFP has been used in the macaque model to study measles pathogenesis [54].

In addition to the rMV that include EGFP within an ATU, many other rMV have been generated. These include viruses in which complete genes were replaced by genes from other MV strains [55] and viruses in which an ORF has been modified by site-directed mutagenesis. This last method has been extensively used to generate recombinant viruses with reduced binding affinity to their entry receptor, by introducing mutations in the H gene [56]. Furthermore, rMV with segmented genomes have been rescued that included three different reporter proteins [57]. Finally, several rMV have been generated as candidate oncolytic viruses [58,59].

Measles virus

Measles

MV is the only virus within the genus *Morbillivirus* that targets primates as its natural host. It is thought to have evolved from RPV in an environment where humans and cattle lived in close proximity [60,61]. Therefore, measles is often referred to as a disease of civilization. Although non-human primates are highly susceptible to MV infection, their population sizes do not reach sufficient numbers to sustain endemic transmission. Measles is therefore essentially a disease of man, and remains an important cause of childhood morbidity and mortality in developing countries. In 2010, 139,300 deaths were attributed to measles [62]. MV is highly contagious, is transmitted via the respiratory route and causes systemic disease. Mortality mainly results from secondary complications due to measles-induced immune suppression.

Clinical symptoms

After initial infection via aerosol inhalation, MV replicates in the lymphoid tissues of the upper respiratory tract. After a relatively long incubation phase, during which no clinical signs are observed, patients go into a prodromal phase where they develop fever and upper respiratory tract symptoms. A few days later full-blown measles develops with the appearance of Koplik's spots, the pathognomonic feature of MV infection, on the buccal mucosa [16]. The hallmark of measles is a maculopapular rash that appears around 14 days post infection (d.p.i.) [63], starting behind the ears and eventually covering the entire body. Within a few days symptoms usually start to subside, and in absence of further complications patients recover rapidly (Figure 3).

Measles is associated with immune suppression, leading to an increased susceptibility to opportunistic infections (Figure 3). This is the primary reason why a significant percentage of measles patients develop complications, resulting in a plethora of clinical symptoms [64–67]. For instance, bacterial pneumonia is a common complication and a major cause of measles-associated deaths [68]. In addition, there are rare but severe central nervous system complications associated with measles, including acute post-infection measles encephalitis (APME), measles inclusion body encephalitis (MIBE) and subacute sclerosing pan encephalitis (SSPE) [69–72].

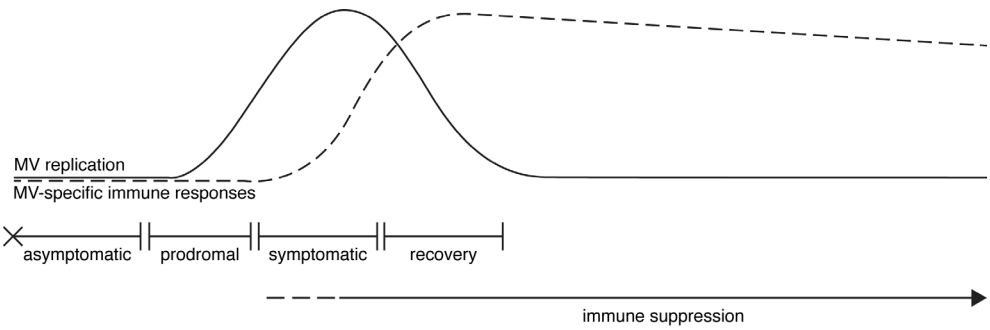

Figure 3. *Schematic representation of different phases in measles. Measles starts with an asymptomatic phase followed by a prodromal phase, where MV replicates but the only clinical symptom at this time is fever. At the moment the MV-specific immune responses start, symptoms are observed. During the recovery phase, the immune responses inhibit MV replication and symptoms disappear. However, after recovery the period of immune suppression continues, which can last for several weeks to months.*

The mortality due to measles is directly linked to the socio-economic status of the infected population. Mortality rates may reach 25% in refugee camps or overcrowded populations, 5 – 10% in developing countries, but is usually less than 0.1% in industrialized countries [73,74].

Epidemiology

MV is highly contagious, with an estimated reproductive number (R_0) or average number of secondary cases produced by an infectious individual of 12 – 18 [73]. Many of the features of MV transmission in unvaccinated populations have been

deduced from studies performed by Peter Panum, who investigated a measles epidemic in the Faro Islands in 1846. He estimated that MV-infected individuals are capable of transmitting virus to susceptible contacts for a total of 7-9 days, starting several days before until few days after onset of rash [75].

In previously unexposed, immunologically naive populations, MV infects individuals of all age groups. However, in populations where measles has previously been endemic older members of the community are generally immune, with the result that measles becomes primarily a childhood disease [16]. Maintenance of MV in a population requires a continuous supply of susceptible individuals. If the population is too small, endemic transmission cannot be maintained [76]. A population size of at least 250,000 – 500,000 is necessary to establish measles as an endemic disease [77]. Children become susceptible to measles as soon as they lose their passively acquired maternal antibodies. Since women with vaccine-induced immunity usually have lower MV-specific antibody levels than women with naturally acquired immunity, their infants become susceptible at a younger age [78].

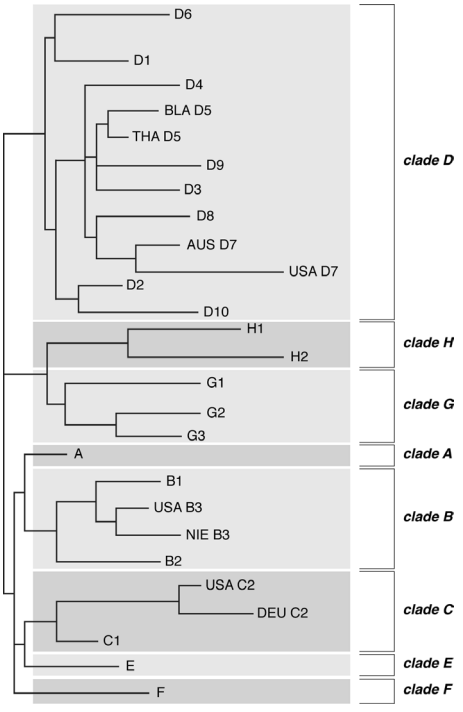

Figure 4. *Dendrogram showing the relationships among the measles WHO reference strains representing the 23 known measles genotypes (on basis of the 450 nt N-terminus of N), divided into clade A – H. Vaccine strains belong to genotype A. Adapted from [211].*

An important consequence of the high transmissibility of MV is that vaccination coverage of >95% is required to eliminate endemic transmission [79,80]. Immunization directly alters the epidemiology of measles and the kinetics of MV transmission. If vaccination coverage is high, but <95%, outbreaks can still occur. However, the period between epidemics is increased as the vaccination coverage increases, since a pool of susceptibles needs to accumulate [81]. Due to reduced awareness

of the severity of measles and unsubstantiated claims of dangers associated with vaccination, vaccination rates in a number of industrialized countries have started to fall over the last decade. Indeed, in Europe this has resulted in large outbreaks of measles in a number of countries, with 28,887 cases, 8 deaths and 26 cases of acute encephalitis reported in 2011 [82]. The lesson learned is that global vaccination approaches are required, since measles cannot be controlled anywhere if it is not controlled everywhere [83].

MV is serologically monotypic, and infection by a MV strain anywhere in the world will result in protection from all globally circulating MV strains. Indeed, the live-attenuated MV vaccines developed in the 1960s still provide protection from measles [84]. However, sequence analysis of the variable carboxy-terminus of the N gene or the complete H gene has allowed the genetic distinction of globally circulating MV strains into eight clades (A – H), further sub-divided into 23 genotypes [47,85] (Figure 4). The division of MV into these genotypes is useful for surveillance purposes, since by molecular epidemiology outbreaks of MV can be traced to specific individuals and locations, and global measles transmission pathways can be identified [83,86]. All live-attenuated MV vaccine strains belong to genotype A.

Diagnosis

The WHO case definition of measles is an individual with fever, maculopapular rash, and cough, coryza or conjunctivitis [63]. However, measles diagnosis on the basis of clinical symptoms is unreliable, especially under low incidence conditions. Several other infectious agents can cause measles-like clinical symptoms, e.g. rubella virus, parvovirus B19, human herpesvirus type 6, dengue virus, Epstein-Barr virus, *Mycoplasma pneumoniae* and *Rickettsia conorii* [87,88]. In contrast, MV infection of immunocompromised individuals may cause severe disease in the absence of classical measles symptoms [89]. Therefore, laboratory diagnosis of measles is of critical importance [90].

The most commonly used method of laboratory diagnosis is IgM serology [91]. MV-specific IgM can either be detected in serum, dried blood spots or oral fluid [90]. In the first few days after onset of rash IgM levels may still be low, and a second serum sample may be required. Alternatively, seroconversion or a more than four-fold rise in IgG antibody titer can also be used as serological evidence of a recent MV infection. Measles can also be diagnosed by isolating MV in cell culture from urine, nose swabs, throat swabs or white blood cells. However, this is only possible at early time-points after the initial infection, since the virus is rapidly cleared as clinical signs and symptoms develop (Figure 3). Furthermore, CD150-expressing cell lines are required for accurate and rapid virus isolation. Direct detection of viral RNA by real-time reverse transcriptase polymerase chain reaction (RT-PCR), using primers directed against conserved regions of the MV genome, can also be used as rapid sensitive virus detection method. In surveillance studies oral fluid or dried blood spots are frequently used as clinical specimens, as they allow the combination of IgM serology, RT-PCR and sequence analysis for molecular epidemiological purposes [90,92,93].

Measles pathogenesis

Animal models of measles

Over the past decades, multiple small animal models have been developed for the study of measles pathogenesis, including transgenic mouse models and a cotton rat model [94–96]. However, non-human primates are the optimal animal model for measles. Both rhesus (*Macaca mulatta*) and cynomolgus (*Macaca fascicularis*) macaques are highly sensitive to infection with wild-type MV and develop clinical signs and pathologic lesions similar to those described in humans [97–102]. Moreover, natural infections following contact with MV-infected humans have been frequently reported [99,103]. Within this thesis, the combination of a highly susceptible non-human primate animal model and virulent rMV strains expressing fluorescent reporter proteins is described [53,104] that has allowed detailed studies on the full spectrum of measles pathogenesis.

Animal morbilliviruses

Measles pathogenesis has been studied by experimental MV infections of different animal species. However, as an alternative, studies of animal morbilliviruses in their natural hosts, mostly CDV in ferrets, have provided important insights into morbillivirus pathogenesis. Using a rCDV strain expressing EGFP, von Messling *et al.* have illuminated the tropism of CDV and found many similarities to MV [105]. CDV initially replicated in T- and B-lymphocytes in lymphoid organs and CDV-infected ferrets developed rash, high fever and viremia. An initial exclusively lymphoid phase was followed by widespread epithelial cell infection. Furthermore, the ferrets were severely immune suppressed and usually died within 2-3 weeks post inoculation, although this strongly depended on the virus strain used [105–108]. In addition, a hallmark of CDV infection of both ferrets and dogs is the frequent spread of the virus into the central nervous system (CNS). This directly demonstrates a key limitation of using an animal morbillivirus as a model for measles. MV rarely causes CNS complications in humans and is normally not lethal, and therefore dramatically differs from CDV infection of ferrets.

Entry receptors

Infection of cells by MV is initiated by binding of the H glycoprotein to a cellular receptor [109]. The first cellular receptor to be identified was CD46, a protein that is ubiquitously expressed by nearly all human nucleated cells [110,111]. However, shortly after its discovery it became evident that only vaccine and laboratory-adapted MV strains utilize CD46 to infect cells [112] and that its use was an artifact of the adaptation of MV in tissue culture.

In 2000 signaling lymphocyte activation molecule (SLAM), also known as CD150, was identified as a cellular receptor for wild-type strains of MV [113,114]. The usage of CD150 as an entry receptor is conserved throughout the genus *Morbillivirus*, with MV, CDV and RPV causing infection via CD150-dependent fusion [115]. Strains of CDV and MV genetically engineered to have low affinity for CD150 were attenuated *in vivo* in ferrets and macaques, respectively [116,117]. CD150 is mainly expressed

on subsets of lymphocytes and dendritic cells (DC) [118–122], but also on activated Langerhans' cells (LC) and macrophages [118,123]. Experimental infections of rhesus and cynomolgus macaques with an rMV expressing EGFP have shown that $CD150^+$ lymphocytes and DC were predominantly infected during the peak of virus replication. However, infection of $CD150^-$ epithelial cells by wild-type MV strains was also observed *in vitro* and *in vivo* [54,124–129]. In 2011, two research groups independently identified polio virus receptor-related 4 (PVRL4), a protein expressed by epithelial cells at adherens junctions, as a cellular receptor for MV [130,131]. Since PVRL4 is localized on the basolateral side of epithelial cells, its identification as a MV receptor is compatible with the observation that differentiated epithelial cells cannot be infected apically, and hence are unlikely to be initial target cells for MV infection [125].

Attachment receptors

In addition to CD150 and PVRL4, a number of MV attachment receptors have been described. These bind a virus particle to the cell surface, but do not facilitate fusion of the viral envelope with the cellular plasma membrane. The C-type lectin DC-specific intercellular adhesion molecule-3-grabbing non-integrin (DC-SIGN) has been shown to play an important role in attachment of MV to DC [132]. Different DC subsets express various C-type lectins. The C-type lectins DC-SIGN and Langerin, expressed on DC and LC respectively, have both previously been shown to play an important role in the pathogenesis of human immunodeficiency virus type-1 (HIV-1) infections [133–136]. Whereas DC-SIGN enhances HIV-1 transmission and DC are now considered as the 'Trojan horse' through which HIV-1 enters a host, it was postulated that Langerin functions as an innate barrier to HIV-1. LC at mucosal surfaces were speculated to have a protective effect against HIV-1 infection [134]. The role of DC-SIGN and Langerin in the pathogenesis of measles is the topic of chapter 1 of this thesis.

Early target cells

MV initiates infection in the respiratory tract and as such the early target cells were originally thought to be respiratory epithelial cells [16]. However, since these cells do not express CD150 or PVRL4 on their apical cell surface, this is now considered unlikely. A rMV unable to bind to PVRL4 was shown to cause systemic infection in macaques [137], whereas rMV unable to bind to CD150 was severely attenuated *in vivo* [116]. This suggested that the initial infection of cells in the respiratory tract is most likely a CD150-dependent event and excludes epithelial cells as the primary targets for initiation of infection. This was confirmed by *in vitro* experiments, where primary differentiated normal human bronchial epithelial (NHBE) cells could not be infected with MV apically [124,125,127–129]. In this thesis, aerosol infection of macaques with a new pathogenic rMV strain expressing EGFP was used to elucidate what cells are initially infected by MV.

Peak replication phase

Measles has a long incubation phase, with fever occurring on average at 10 d.p.i. and rash at approximately 14 d.p.i. [16,138]. The peak of virus replication is reached

before the onset of recognizable symptoms, and clinical symptoms coincide with viral clearance (Figure 3). It is therefore difficult to perform pathogenesis studies in humans.

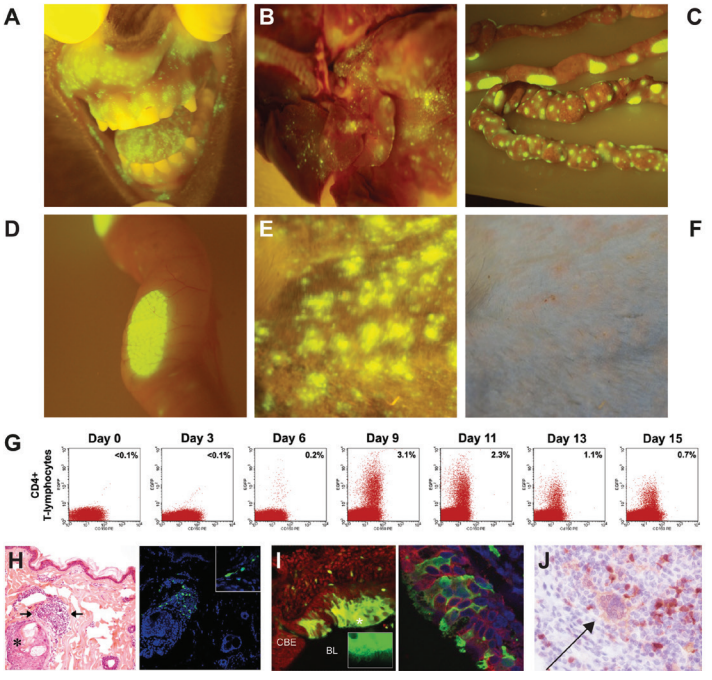

Figure 5. *Measles pathogenesis studies in non-human primates: (A – F) Macroscopic EGFP fluorescence in macaques 9-11 d.p.i.: gingiva and buccal mucosa (A) [Ludlow et al, manuscript in preparation], lungs (B) [Ludlow et al, manuscript in preparation], small intestine with gut-associated lymphoid tissue (C) [318], higher magnification of Peyers' patches (D) [318], EGFP fluorescence (E) or normal light (F) photo of skin rash [357]. (G) Detection of EGFP fluorescence by flow cytometry: EGFP expression in CD150⁺ CD4⁺ T-lymphocytes at different time points after infection [54]. (H) H&E or fluorescence image of MV infection in the skin, demonstrating fluorescence in immune cells [54]. (I) EGFP fluorescence in ciliated bronchial epithelial cells (CBE). BL: bonchial lumen [54]. (J) During peak of MV replication, multi-nucleated giant cells are frequently observed in the lymphoid tissues (arrow).*

The use of an rMV expressing EGFP to experimentally infect macaques has led to an enormous increase in the understanding of MV pathogenesis. At the peak of replication lymphoid organs and tissues are the major sites of replication *in vivo* [54,126,139,140], including the bronchus-associated lymphoid tissues (BALT) of the lungs (Figure 5B, C and D). Multi-nucleated giant cells are frequently observed in lymphoid tissues before the onset of rash [141,142] (Figure 5J). Furthermore, the gingiva, buccal mucosa and the tongue were also brightly fluorescent (Figure 5A), corresponding with infection of lymphoid aggregates within these tissues. Initial infection in the respiratory tract is followed by dissemination via a cell-associated viremia (Figure 5G). MV predominantly infects CD150⁺ T-lymphocyte and B-lymphocytes both in lymphoid tissues and peripheral blood [54], which contradicts earlier studies in which monocytes were reported to be the main cell type disseminating MV during viremia [16]. After the peak of replication, macaques

develop a typical skin rash (Figure 5E and F), corresponding with the infection of lymphoid or myeloid cells (Figure 5H) and epithelial cells (Figure 5I).

After initial replication in the lungs and lymphoid organs, MV spreads into other tissues, including submucosal tissues, tongue, buccal mucosa, trachea, nose and skin. MV dissemination mainly takes place in the form of MV-infected cells, rather than as cell-free virus [143]. From this point, MV-infected lymphocytes are rapidly cleared by the immune system, but infection lingers on in epithelial cells [125]. This may be an indication that MV is more cytolytic in lymphocytes than in epithelial cells. However, it could also be explained by the fact that epithelial cells are more difficult to reach for MV-specific cytotoxic T-lymphocytes, which are required for clearance of infected cells.

Immune responses and viral clearance

Measles is a self-limiting infection, meaning that the immune system is capable of clearing the virus. Clearance is predominantly mediated by cellular immune responses, illustrated by the fact that hypogammaglobulinemic children recover normally from MV infection [144,145], whereas children with deficits in cellular immunity develop severe disease and display prolonged viral shedding [144,146,147]. This could be partly due to the spread of MV via cell–to-cell transmission, thus potentially avoiding neutralizing antibodies in the bloodstream. *Ex vivo* experiments have shown that $CD8^+$ MV-specific T-lymphocytes predominate shortly after acute measles [148], indicating that these cells play a role in viral clearance. However, in classical ^{51}Cr-release assays both $CD4^+$ and $CD8^+$ MV-specific T-cell clones (TCC) had cytolytic activity against MV-infected autologous target cells [148–150], indicating that both subsets are capable of killing MV-infected cells. Recent *in vivo* experiments in non-human primates have corroborated the importance of cellular immunity in MV clearance [151–154].

MV-specific IgM, IgG and IgA antibodies start to appear at the time of viral clearance. Virus neutralizing (VN) serum antibodies directed against the surface glycoproteins F and H are considered the main correlate of protection against MV infection [155,156]. Neutralizing antibodies, either induced by vaccination or natural infection, confer lifelong protection against measles infection. As a proof of principle, it was shown that passive transfer of antibodies leads to protection [157].

Exit of the host and transmission

MV is mainly transmitted by aerosols, either in the form of cell-free virions or debris from MV-infected cells. It has been speculated that infection of epithelial cells during the late stage of the disease contributes to MV transmission [130,131]. Here, MV-infected lymphocytes or DC present in the respiratory submucosa [125] transmit the virus to epithelial cells via PVRL4. Productive infection of polarized epithelial cells can lead to apical shedding of MV into the airway lumen, potentially resulting in transmission to the next host [130,131,158]. In this thesis an alternative model for MV transmission is discussed, in which extensive epithelial damage of lymphoid tissues in the upper respiratory tract contributes to MV transmission.

Immune suppression

Measles is associated with a transient but profound immune suppression, the clinical importance of which is best illustrated by the observation that measles mortality is typically caused by secondary infections in the respiratory and digestive tracts [64–66]. Multiple observations have been described which illustrate the impact of this immune suppression *in vivo*, including suppression of Mantoux responses [159,160], lymphopenia [161] and impaired responses to vaccination [162,163]. Decreased lymphoproliferative responses [164–166], altered cytokine response profiles [167] and impairment of antigen-presenting cell function [168,169] have been described *in vitro*. The relevance of these observations in relation to enhanced susceptibility to opportunistic infections and immune suppression remains unclear. The paradox of measles is that the acute phase of the disease is not only associated with a dramatic immune suppression, but also with immune activation [170] and induction of robust MV-specific humoral and cellular immune responses that result in lifelong immunity. In this thesis a new model for measles-associated immune suppression is discussed, which was based on *in vivo* observations and confirmed by *in vitro* studies [54,171].

Measles prevention and eradication

Formalin-inactivated MV vaccine

The best means of preventing measles is by immunization. Large-scale vaccination programs against measles started in the 1960s after successful isolation and growth of the Edmonston strain of MV in tissue culture by John Enders [172], with formalin-inactivated (FI) or Tween-ether-inactivated whole-virus vaccines adjuvanted with alum. Vaccination resulted in high seroconversion rates but neutralizing antibody titers were short lasting, necessitating multiple immunizations [173]. Furthermore, this vaccine was incapable of inducing cytotoxic T-lymphocyte responses [174] and a substantial number of children vaccinated with these inactivated vaccines developed enhanced disease upon natural infection with MV, referred to as atypical measles [175,176]. Inactivated MV vaccines were discontinued in 1967 due to these adverse effects.

Live-attenuated MV vaccines

In parallel with the development of FI MV vaccines, live-attenuated MV vaccines (LAV) were introduced in the early 1960s [177]. The first attenuated MV used as a vaccine caused rash and fever in 20 – 50% of the vaccines [178], requiring its replacement with more attenuated strains. The worldwide use of LAV resulted in a major decrease in measles mortality [179], and the vaccine has an impressive safety record, even in HIV-seropositive subjects and immunocompromised individuals [180]. By introducing a two-dose regimen [181,182] and by organizing mass-vaccination campaigns [183], the number of deaths attributed to measles has been significantly reduced over the last decade [184].

Even though major progress has been made in interrupting endemic MV transmission, there are several limitations to the use of LAV. These include the dependency on cold-chain maintenance, a risk, albeit minimal, to immunocompromised individuals

[185], the requirement for professional healthcare workers, the availability of sterile needles and the need to safely dispose of contaminated sharps. In addition, seroconversion rates observed after vaccination with LAV vary considerably. The presence of maternal antibodies and immunological maturity of the recipient has the most significant influence on the success rate of measles vaccination [186,187]. Under ideal conditions, 95% of children seroconvert when vaccine is administered at 12 months of age [188], 85% at 9 months [189] and only 67% below 9 months [190]. Two alternative approaches can be used to protect infants in this age group. If vaccination coverage in older age groups is sufficiently high, MV circulation will be interrupted, thus reducing MV exposure. As an alternative, new measles vaccines and delivery systems that could be used in young infants are being researched with varying success rates [191].

Global eradication of morbilliviruses

In 2011 the Food and Agriculture Organization formally declared that rinderpest had been eradicated from the globe. RPV is a close relative of measles virus, and only the second virus to be eradicated by targeted vaccination after smallpox [13,14]. The potential for measles eradication was first proposed in the 1980s, although it was considered premature in a period when interruption of endemic MV circulation had not been achieved even in industrialized countries [192]. In 2001, the Measles Initiative was established, now named the Measles and Rubella Initiative, a partnership formed by the American Red Cross, the Centers for Disease Control and Prevention, UNICEF and WHO, which aimed to reduce global measles mortality (www.measlesrubellainitiative.org), by initiating mass immunization campaigns and a two-dose vaccination regimen. The program has achieved an impressive reduction of mortality and interruption of endemic MV circulation in large parts of Africa.

Measles eradication is biologically feasible, since humans are the only reservoir for MV, the virus is monotypic, vaccines are available and persistent infections are rare [193,194]. Even though the initial success of the Measles and Rubella Initiative and the eradication of RPV suggest that measles eradication is possible, the current polio virus eradication program illustrates that the endgame of eradication can be extremely difficult [195,196]. The pitfalls that still exist, potentially undermining measles eradication, are waning vaccine immunity and declining vaccination coverage.

The measles post eradication era

Following the eradication of smallpox, vaccination was discontinued. This created a niche for closely related orthopox viruses of other mammals to cross the species barrier into humans [197,198]. A similar threat exists for the morbilliviruses. Morbilliviruses are cross-protective, and global eradication of RPV and MV may create niches for other morbilliviruses to fill. Surprisingly this risk has been claimed to be low [199], but adaptation of for example CDV, which is already observed in primates [200], to humans may have catastrophic consequences. Therefore, it will be important to continue measles vaccination, even when MV is eradicated. In this thesis the potential for CDV to adapt to macaques and/or humans is discussed [196].

Measles as a vaccine vector

With the potential of animal morbilliviruses crossing the species barriers into the human population, and the necessity to continue measles vaccination, vaccine uptake could be facilitated by using MV as a viral vector for the expression of foreign antigens. MV vaccines are safe and effective, and potentially useful and effective vectors since the virus is highly stable and the generation of rMVs through reverse genetics is feasible and well understood [201–203]. Several studies have shown that rMV induces humoral and cellular immunity against both MV and co-expressed proteins derived from other pathogens [202–209]. One study reported that rMV could protect macaques from measles after challenge with a wild type MV, demonstrating that the rMV still induces MV-specific immunity in non-human primates [209]. A major drawback when using rMV as a viral vector is pre-existing immunity against the virus in the population. Most experiments described with rMV were performed in animals without pre-existing immunity. Although LAV, DNA and recombinant protein vaccines have also been used as booster vaccinations, pre-existing MV-specific immunity may be a problem when induction of protective immunity against other pathogens is required.

Outline of this thesis

This thesis focuses on multiple aspects of the pathogenesis of measles. In chapter 2, the C-type lectin attachment receptors for MV are discussed. The focus in this chapter is on the role of DC-SIGN in transmission of MV from DC to T-lymphocytes and the discovery of Langerin on LC as an attachment receptor for MV. The roles of DC-SIGN and Langerin in MV antigen presentation are further elucidated and discussed.

Chapter 3 focuses on the early events after MV infection. Until 2010 it was thought that respiratory epithelial cells were the initial target cells for MV. However, in this thesis the development of an aerosol infection model for macaques is described, and by using rMVs expressing EGFP, this hypothesis was re-evaluated. Following description of the discovery of DC and alveolar macrophages (AM) as the initial target cells, the role of DC in initiation and dissemination of a MV infection is discussed.

To complement the focus on the pathogenesis of wild-type MV strains, the tropism of attenuated MV strains has also been evaluated. Even though LAV is highly efficacious, the tropism and spread of these attenuated viruses is largely unknown. In chapter 4, a pathogenic rMV is compared with a tissue culture-adapted attenuated rMV, and the similarities and differences in tropism are discussed.

Following description of the early events after infection and the tropism of wild-type and attenuated MV strains, the later time-points after MV infection were investigated. In chapter 5, the focus is on how MV is transmitted from host to host. While the importance of epithelial cell infection is emphasized in the current literature, in this thesis an alternative model is proposed, where virus-mediated and immune-mediated disruption of the epithelium of lymphoid tissues in the respiratory tract may also contribute to shedding of MV or MV-infected cellular debris.

Chapter 6 focuses on the mechanisms underlying measles-associated immune suppression. Based on the accumulated observations made in a series of experimental rMV infection studies in the macaque model, a new model is proposed in which the clearance of MV-infected memory T-lymphocytes and follicular B-lymphocytes by measles-specific $CD8^+$ T-lymphocytes is of primary importance.

In chapter 7, the virulence and tropism of rCDV strains was evaluated in naive and MV-vaccinated macaques. This study demonstrated that non-adapted CDV strains can replicate in $CD150^+$ myeloid and lymphoid cells of non-human primates. The outcomes of this study are potentially of importance for MV vaccination strategies after global eradication.

In conclusion, the studies described in this thesis address the early, intermediate and late stages of measles pathogenesis, and the potential of animal morbilliviruses to cross the species barrier and infect primates.

ATTACHMENT RECEPTORS

2

ATTACHMENT RECEPTORS

DC-SIGN and CD150 have distinct roles in transmission of measles virus from dendritic cells to T-lymphocytes

Lot de Witte, Rory D. de Vries, Michiel van der Vlist*, Selma Yüksel, Manja Litjens, Rik L. de Swart and Teunis B.H. Geijtenbeek*

* both authors contributed equally

PLoS Pathogens 2008 Apr 18; 4(4): e1000049

Abstract

Measles virus (MV) is among the most infectious viruses that affect humans and is transmitted via the respiratory route. In macaques, MV primarily infects lymphocytes and dendritic cells (DCs). Little is known about the initial target cell for MV infection. Since DCs bridge the peripheral mucosal tissues with lymphoid tissues, we hypothesize that DCs are the initial target cells that capture MV in the respiratory tract and transport the virus to the lymphoid tissues where MV is transmitted to lymphocytes. Recently, we have demonstrated that the C-type lectin DC-SIGN interacts with MV and enhances infection of DCs *in cis*. Using immunofluorescence microscopy, we demonstrate that DC-SIGN$^+$ DCs are abundantly present just below the epithelia of the respiratory tract. DC-SIGN$^+$ DCs efficiently present MV-derived antigens to CD4$^+$ T-lymphocytes after antigen uptake via either CD150 or DC-SIGN *in vitro*. However, DC-SIGN$^+$ DCs also mediate transmission of MV to CD4$^+$ and CD8$^+$ T-lymphocytes. We distinguished two different transmission routes that were either dependent or independent on direct DC infection. DC-SIGN and CD150 are both involved in direct DC infection and subsequent transmission of *de novo* synthesized virus. However, DC-SIGN, but not CD150, mediates *trans*-infection of MV to T-lymphocytes independent of DC infection. Together these data suggest a prominent role for DCs during the initiation, dissemination, and clearance of MV infection.

Author Summary

Despite the availability of an effective vaccine, measles virus (MV) is still a major cause of childhood morbidity and mortality in developing countries. Almost all non-vaccinated children catch the highly contagious virus during an MV outbreak. This suggests an efficient route for primary infection. However, the main target cells for MV replication, CD150$^+$ lymphocytes, are barely present in the respiratory tract where MV enters the body. Here we demonstrate an alternative route of MV transmission: dendritic cells that are abundantly present in the subepithelial tissues of the respiratory tract may capture MV through binding to either CD150 or DC-SIGN. Although some virus particles are processed for antigen presentation, others escape from degradation. After virus capture, DCs migrate to the lymphoid tissues where they encounter CD150$^+$ lymphocytes and transmit the virus, after which viral replication is started. Our data provide new insights into the transmission of measles virus, and suggest a dual role for DCs in the pathogenesis of measles.

Introduction

Measles is a systemic disease, caused by measles virus (MV) infection of respiratory and lymphoid tissues. MV is a member of the *Paramyxoviridae* family, genus *Morbillivirus*. The virus is highly contagious and is spread via the respiratory route [16]. Although the course and symptoms of measles are well characterized, little is known about the cellular events underlying the disease. The target cells for MV at the site of transmission and during the systemic phase of the disease are still under debate [16,54,171,212]. Moreover, the interaction of MV with the immune system, paradoxically resulting in induction of strong MV-specific immunity, but also immunosuppression, has not been fully clarified.

It was previously thought that MV initially infects epithelial cells of the respiratory tract, and is disseminated during viremia by infected monocytes [212,213]. However, these cells only express CD46, the receptor for attenuated MV strains, but do not express CD150 (SLAM), the primary receptor for wild-type MV [113,114]. CD150 is mainly expressed on subsets of lymphocytes, thymocytes, macrophages and mature dendritic cells (DCs) [214]. Moreover, we have recently shown that lymphocytes, but not monocytes, are the predominant cells infected *in vivo* during measles in macaques [54]. Moreover, lymphocytes are not in large numbers present at respiratory epithelial surfaces compared to lymphoid tissues and therefore we hypothesize that other cells are the targets for MV at sites of entry.

DCs are professional antigen presenting cells (APCs) that have a sentinel function in the immune system; DCs capture antigens in the periphery and, upon activation, migrate to the lymphoid tissues to present the antigens to T-lymphocytes, resulting in a pathogen-specific immune response [215]. We hypothesize that DCs mediate transmission of MV: DCs capture MV in the respiratory tract, but instead of degradation the virus is protected and transported into the lymphocyte-rich area in the lymphoid tissues, where it is efficiently transmitted to $CD150^+$ lymphocytes. A similar role for DCs has been described for HIV-1, where DCs capture HIV-1 via the C-type lectin dendritic cell-specific ICAM-3 grabbing non-integrin (DC-SIGN) and mediate transmission of HIV-1 to T-lymphocytes by *de novo* production of virus or transferring the virus particles directly to the T-lymphocytes (*trans*-infection) [135,216]. We have previously shown that DC-SIGN also mediates binding of MV to DCs, which enhances DC infection through CD150 *in cis* [132]. Moreover, in infected macaques MV-infected DCs have been observed in conjunction with infected T-lymphocytes, suggesting transmission of virus between both cell types [54].

Here we set out to investigate the role of DC-SIGN and CD150 in both antigen presentation and MV transmission by DCs. MV capture by DCs leads not only to antigen presentation but also to efficient transmission to T-lymphocytes. Both the tissue distribution and functional studies demonstrate that CD150 and DC-SIGN have distinct functions in MV transmission by DCs. The identification of their function in antigen presentation and MV transmission will lead to a better understanding of MV pathogenesis.

Materials & Methods

Antibodies

The following antibodies were used: CD150-specific mouse antibody 5C6 [217], DC-SIGN-specific mouse antibodies AZN-D1 and AZN-D2 [135], DCN46 and DCN46 conjugated with PE (BD Pharmingen, San Diego, CA, USA), CD3-specific mouse antibody SK-7 conjugated with PerCP (BD Pharmingen, San Diego, CA, USA), goat anti-mouse IgG antibody conjugated with PO (Jackson Immunoresearch, West Grove, PA, USA), HLA-DR- (Immu357) and CD86- (HA5.2B7) specific mouse antibodies conjugated with PE (Immunotech, Marseille, France), goat anti-mouse antibody conjugated with FITC (Zymed Laboratories Inc., South San Francisco, CA. USA), Alexa488- or Alexa594-labeled anti-mouse antibodies (Molecular probes, Eugene, OR, USA).

Cells

Vero-CD150 cells [218] were grown in Dulbecco's Modified Eagle's Medium (DMEM; Gibco Invitrogen, Carlsbad, CA, USA) supplemented with 4500 mg/L glucose; 110 mg/l sodium pyruvate; 4 mM L-glutamine; 10% heat-inactivated fetal calf serum (FCS); 20 U/ml penicillin and 20 µg/ml streptomycin, at 37°C with 5% CO_2. The $CD4^+$ HLA-DQw1-restricted T-cell clone GRIM99 [150,219] recognizes an epitope in the MV fusion protein (EVNGVTIQV). GRIM61 and GRIM99 are also MV-specific $CD4^+$ T cell clones, for which the epitopes have not been mapped [150]. LB5 is a $CD4^+$ T cell clone of unknown specificity. All clones were cultured in RPMI-1640 (RPMI-1640, Gibco Invitrogen, Carlsbad, CA, USA) supplemented with 4 mM L-glutamine; 10% heat-inactivated human AB serum (Sigma-Aldrich, St. Louis, MO, USA); 20 U/ml penicillin, 20 µg/ml streptomycin and 10^{-5} M 2-mercapto-ethanol in 96-well round bottom plates. Epstein-Barr virus-transformed B-lymphoblastic cell line (B-LCL-GR) [150,219] was used as autologous APC, and was cultured in RPMI-1640 supplemented with L-glutamine, penicillin, streptomycin and 10% FCS. Immature moDCs were cultured as described before [220]. In short, human blood monocytes were isolated from buffy coats by Ficoll density centrifugation, followed by selection of $CD14^+$ cells using magnetic beads (MACS, Milteny Biotec GmbH, Bergisch Gladbach, Germany). Purified monocytes were cultured in RPMI-1640 medium supplemented with 4 mM L-glutamine; 10% FCS; 20 U/ml penicillin and 20 µg/ml streptomycin and differentiated into immature moDCs in the presence of IL-4 and GM-CSF (500 and 800 U/ml, respectively; Schering-Plough, Brussels, Belgium).

PBMCs were isolated from buffy coats by Ficoll density centrifugation, activated with phytohemagglutinin (PHA, 3 µg/ml; Sigma-Aldrich, St. Louis, MO, USA), and cultured in complete RPMI-1640 medium. At day 3 the cells were washed and cultured with IL-2 (100 units/ml). As determined by flow cytometry >80% of the activated PBMC were $CD3^+$ and therefore these cells are referred to as T-lymphocytes throughout the text. The $CD4^+$ and $CD8^+$ T-lymphocytes were enriched at day 3 after PHA stimulation by negative selection using MACS beads. To label DCs and T-lymphocytes, the cells were stained with the PKH26 red fluorescent cell linker kit (Sigma-Aldrich, USA) for general cell membrane labeling, according to the manufacturers protocol.

Viruses
The recombinant MV strain ^{IC323}EGFP [53] was propagated on Vero-CD150 cells. For virus production, Vero-CD150 cells were infected with a multiplicity of infection (MOI) of 0.01 in DMEM supplemented with 2% of FCS. After 90 minutes cells were washed to remove unbound virus and were subsequently grown in DMEM supplemented with 10% FCS. Cells and supernatant were harvested when 80% cytopathic effect was observed. To release cell-bound virus, the cells were sonicated (3 times, 10 seconds, Sonicor Instrument Corporation, Copiaque, N.Y., USA). The cells were centrifuged (10 minutes, 1000 g) and the supernatant was snap-frozen in liquid nitrogen before titration on Vero-CD150 cells. The titer of the virus-stock used was 1 x 10^6 $TCID_{50}$/ml. Purified $MV^{Edmonston}$ with a concentration of approximately 1 mg/ml, was inactivated by UV-irradiation (30 minutes, 15W 312 nm) and is referred to as UV-MV throughout the text.

Immunofluorescence microscopy
Tissues of healthy human donors were obtained through the pathology department of the VU University Medical Center, according to the institutional ethical guidelines. Cryosections (7 µm) were fixed with 100% acetone and stained with primary antibody combinations against DC-SIGN (DCN46, IgG2b, 10 µg/ml) and anti-CD150 (5C6, IgG1, 10 µg/ml) or a buffer control for 18 hours at 4°C. Sections were counterstained with isotype-specific Alexa488- or Alexa594-labeled anti-mouse antibodies. Nuclei were stained with Hoechst (Molecular Probes, Eugene, OR, USA). After mounting, sections were examined with a Nikon Eclipse E800 fluorescence microscope and recordings were made with a digital NIKON DXM1200 camera. Two persons used the photographs to quantify the staining in the different tissues independently. To determine the density of DC-SIGN$^+$- or CD150$^+$ cells, the number of positive cells was divided by the total number of cells, based on the nuclei staining. To determine the co-localization, the double-stained cells were divided by the total number of stained cells. Based on the control sections, auto-fluorescence was often observed in the lower respiratory tract and is indicated in the pictures.

Antigen presentation assays
Monocytes were isolated from an HLA-DQw1-matched donor using CD14 MACS beads and differentiated into immature DCs as described above. Subsequently, these DCs or autologous BLCL-GR (5 x 10^3 cells) were used as APCs in an interferon-γ (IFNγ) ELISPOT assay as previously described [221]. Briefly, APCs were plated into 96-well V-bottom plates in complete RPMI-1640 containing IL-4 and GM-CSF and pre-incubated with mannan (0,25 mg/ml) for 30 minutes at 37°C. Next, the cells were incubated with different dilutions of UV-MV at 37°C or a positive control peptide (EVNGVTIQV; 1 mM). After overnight incubation the CD4$^+$ T-cell clones were added to the APCs (5 x 10^3 cells per well), the plates were briefly centrifuged (1 minute, 300 g) and subsequently incubated at 37°C for 1.5 hour. Subsequently the cells were transferred to nylon bottom plates (Nalge Nunc International, Rochester, NY) coated with a monoclonal antibody specific for human IFNγ (1-D1K; Mabtech, Stockholm, Sweden), and incubated at 37°C for five hours. Finally, plates were washed with phosphate-buffered saline (PBS) containing 0.05% Tween 20 (Merck, Darmstadt,

Germany). Spots were visualized by incubation with a secondary biotinylated mAb against IFNγ (7-B6-1; Mabtech), followed by staining with streptavidin–alkaline phosphatase (Mabtech), and nitroblue tetrazolium–5-bromo-4-chloro-3-indolyl-phosphate (Kirkegaard & Perry Laboratories, Gaithersburg, MA, USA). Finally, the color reaction was stopped by washing the plates with water and spots were counted with an automated ELISPOT reader (automated ELISAspot assay video analysis systems; distributed by Sanquin Reagents, Amsterdam, The Netherlands).

In parallel, the same APCs were also used to stimulate the same T-cell clone for IFNγ production in supernatant. Briefly, APCs (1 x 10^4 cells) were used to stimulate the T-cell clone (3 x 10^4 cells) in round-bottom plates, and were incubated at 37°C for 24 hours before supernatants were harvested. To determine the contribution of DC-SIGN and CD150, the APCs were pre-incubated with mannan (0,25 mg/ml), anti-DC-SIGN (AZN-D2; 20 µg/ml) or anti-CD150 (5C6; 20 µg/ml) for 30 minutes at 37°C. The IFNγ concentrations in the supernatants were determined by ELISA (Biosource International, CA, USA).

MV infection, transmission and co-culture Assays

For infection and transmission assays DCs (5 x 10^4 cells) were seeded in a V-bottom plate and pre-incubated with mannan (0,25 mg/ml), anti-DC-SIGN (AZN-D2; 20 µg/ml) or anti-CD150 (5C6; 20 µg/ml) for 30 minutes at 37°C, before incubation with rMV^{IC323}EGFP at 37°C for 2 hours (5 x 10^4 $TCID_{50}$, unless stated otherwise). After 2 hours the cells were washed and transferred to a flat-bottom plate. To measure transmission, activated T-lymphocytes (2 x 10^5 cells) were added. If indicated the fusion inhibitory peptide (FIP) Z-d-Phe-L-Phe-Gly-OH (Z-FFG; 0.2 mM; Bachem, Heidelberg, Germany) was added 2 hours later. For co-culture assays T-lymphocytes (2 x 10^5 cells), either or not together with DCs (5 x 10^4 cells), were pre-incubated with 0,25 mg/ml mannan and infected with different concentrations of rMV^{IC323}EGFP.

All cells were cultured for three days at 37°C in complete RPMI-1640 containing IL-4 and GM-CSF. The cultures were monitored using a Leica DMIL fluorescence microscope, and pictures were taken using a Leica DFC 320 camera (Leica Microsystems, Wetzlar, Germany). At day 3 the cells were harvested, washed and fixed with 4% PFA and EGFP expression was measured by flow cytometry. DCs had higher auto-fluorescence compared to T-lymphocytes the EGFP$^+$ gate for both population was set at the uninfected control sample. To determine the infection of specific cell populations, the cells were stained with directly labeled antibodies against DC-SIGN and CD3 before analysis. The absolute number of infected DCs (DC-SIGN$^+$/EGFP$^+$) and T cells (CD3$^+$/EGFP$^+$) of the total counted sample by flow cytometry (=10^5 events) were used to determine the efficiency of transmission.

Statistical analysis

To determine the variation in MV transmission among the different DC donors, the infection of T-lymphocytes was normalized to the "medium" control condition, which was set at 100%. Subsequently, the percentages of infection from the different donors were used in a one-way analysis of variance (ANOVA). When the overall *F*

test was significant, differences among the donors were further investigated with the *post hoc* Bonferroni test using Graphpad Prism software. A probability of $p < 0.05$ was considered statistically significant.

Results

DC-SIGN⁺ dendritic cells are present in the respiratory tract and closely interact with CD150⁺ cells in lymphoid tissues

MV enters the body in the respiratory tract; however the initial target cells at the site of entry remain unknown. DC-SIGN and CD150 are the major receptors for wild-type MV strains, of which only CD150 can function as entry receptor. DC-SIGN is abundantly expressed by DCs in peripheral tissues, such as the dermis, foreskin, gut and cervix and on DCs and specialized macrophages in the lymphoid tissues [135,222–224]. However, little is known about the expression of DC-SIGN and CD150 in the respiratory tract. Therefore we investigated the presence of DC-SIGN⁺ and CD150⁺ cells in the different respiratory tissues by immunofluorescence microscopy. DC-SIGN was abundantly present in buccal, pharyngeal, tonsillar, tracheal and bronchial sub-epithelial tissues (Figure 1A and S1, Table 1). Similar to previous reports [225], scattered DC-SIGN⁺ DCs were also observed in the lungs, mainly in the interstitium of the alveoli (Table 1).

Table 1. *DC-SIGN⁺-dendritic cells are present in the sub-epithelial tissues of the respiratory tract. # The number of DC-SIGN⁺- or CD150⁺- cells was determined by counting the number of positive cells, divided by the total number of cells, based on the nuclei staining. The double-positive cells were divided by the total number of stained cells, to determine the co-localization. 0 = 0 – 1%, + = 1 – 5%, ++ = 5 – 25%, +++ = 25 – 100% of the cells, n = number of donors analyzed per tissue, LT = lymphoid tissue.*

	Tissues		CD150#	DC-SIGN	Co-localization	n
URT	Buccal cavity	Epithelium	0	0	0	1
		Sub-epithelium	+	+++	0/+	
	Pharynx	Epithelium	+	0	0	1
		Sub-epithelium	+	+++	0	
	Tonsillar crypt	Epithelium	0/+	0	0	2
		Sub-epithelium	+	+++	0	
LRT	Trachea	Epithelium	+	0	0	2
		Sub-epithelium	0/+	++	0	
	Bronchus	Epithelium	0	0	0	2
		Sub-epithelium	0	++	0	
	Lung	Interstitium	0/+	0/+	0	2
LT	Tonsil	Follicle	+++	+++	++	3
		Inter-follicular	+++	+++	++	
	Lymph node	B-cell area	+++	+	+	1
		T-cell area	+++	++	++	
		Medullary sinus	+++	+++	+++	

Monocyte-derived DCs (moDCs) in culture express CD150, and expression levels are increased upon maturation [119,226]. *In situ*, CD150 expression was detected on cells in the sub-epithelial tissues of the upper respiratory tract, but we observed very little expression in the lower respiratory tract (Figure 1A and S1, Table 1). Although some CD150$^+$ cells were present in the epithelia of the tonsillar crypts and the pharynx, the expression of CD150 in these tissues was low compared to that in lymphoid tissues (Figure 1A and S1, Table 1). These cells might represent macrophages or lymphocytes that can be targets for MV infection and their infection might explain why infection is observed in epithelial tissues *in vivo* [54]. We also observed some auto-fluorescence in the epithelia of the tracheal, bronchial and tonsillar epithelium, probably caused by mucus (Figure 1A and S1). In the upper respiratory tract, we rarely detected co-localization of CD150 and DC-SIGN, suggesting that DC-SIGN$^+$ DCs, abundantly present just below the epithelia in the respiratory tract, express no or low levels of CD150 (Figure 1A and S1, Table 1).

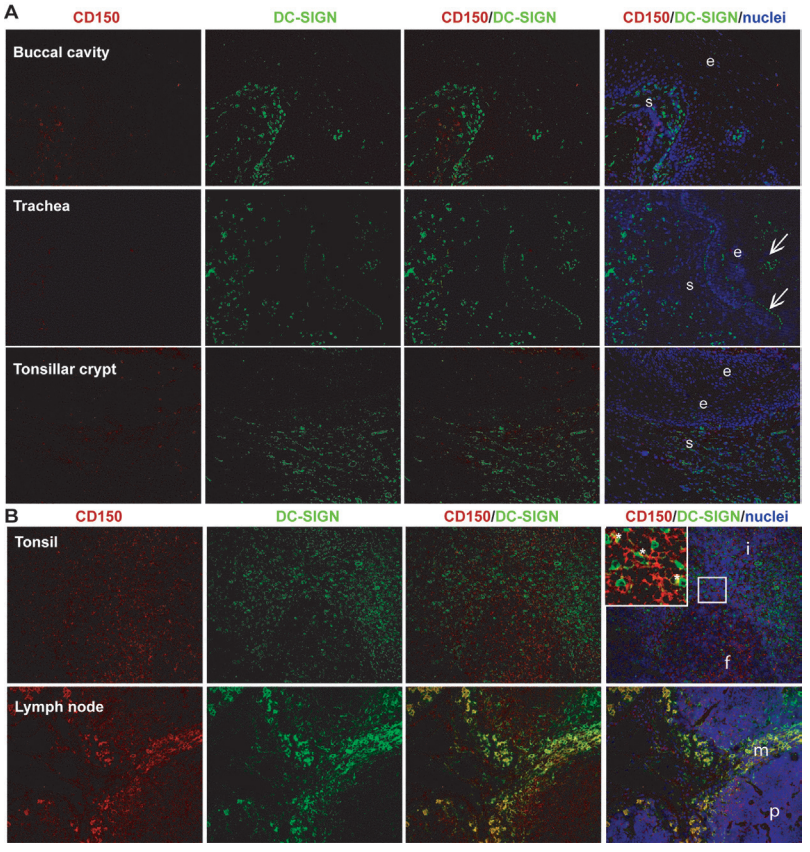

Figure 1. *DC-SIGN$^+$-dendritic cells are present in the sub-epithelial tissues of the respiratory tract. (A,B) Cryosections of different tissues from healthy donors were stained for the expression of DC-SIGN (green) and CD150 (red) using specific antibodies, and for the nuclei using Hoechst (blue). The sections were analyzed by fluorescence microscopy. (A,B) Representative photos with a magnification of 100x are depicted (e = epithelium; s = sub-epithelial tissue, i = inter-follicular, f = follicles, m = medullary sinus, p = paracortex, arrow = auto-fluorescence, * = co-localization).*

During viremia, MV-infected cells enter the lymphoid tissues. Here, DC-SIGN$^+$ DCs might facilitate infection of lymphocytes, similar to HIV-1 [135]. We therefore investigated the expression of DC-SIGN and CD150 in lymph node and tonsil. As previously described [223,225], DC-SIGN$^+$ cells were mainly located around the medullary sinuses and in the paracortex (T-cell areas) of the lymph node as well as in the inter-follicular tissue (T-cell area) of the tonsil (Figure 1B, Table 1). However, DC-SIGN$^+$ cells were also found in the B cell follicles of the tonsil. Notably, DC-SIGN$^+$ cells were located in close contact with the CD150$^+$ cells (Figure 1B). Strikingly, strong co-localization of DC-SIGN and CD150 was observed in the medullary sinuses (Figure 1B, Table 1). Together these data suggest that DC-SIGN$^+$ cells are not only important in the initial phase of MV infection, but might also be involved in MV infection in the lymphoid tissues during the systemic phase of the infection.

DC mediate antigen presentation of measles virus to CD4$^+$ T-lymphocytes

DC-SIGN is an attachment receptor for MV and mediates infection of DCs through CD150 *in cis* [132]. We investigated whether MV capture by DC-SIGN$^+$ DCs also leads to antigen processing and presentation to MV-specific CD4$^+$ T-lymphocytes. We performed an antigen presentation assay using MV-specific CD4$^+$ T cell clones [150,219]. As APCs we used moDCs, expressing high levels of DC-SIGN [135] or an autologous Epstein-Barr virus-transformed B-lymphoblastic cell line (B-LCL). The APCs were incubated with different dilutions of MV that was UV-inactivated to exclude DC and T-lymphocyte infection. Subsequently the APCs were co-cultured with the MV-specific CD4$^+$ T-cell clones. At the highest concentrations, UV-MV induced DC maturation, since CD86 was upregulated, whereas DC-SIGN was downregulated (Figure 2A). Notably, in contrast to LPS stimulation, HLA-DR was not upregulated by MV. T-cell activation was measured by the detection of IFNγ production by ELISPOT and ELISA. We used two different MV-specific T cell clones (GRIM99 and GRIM61) that matched and one that mismatched (GRIM 76) the HLA type of the donor DCs. DCs incubated with UV-inactivated MV specifically activated the HLA-matched MV-specific T cell clones, whereas the mismatched MV-specific T cell clone was not activated (Figure 2B and C). Moreover, an irrelevant T cell clone (LB5) was not activated by the DCs (Figure 2B). Thus, MV capture by DCs leads to specific antigen processing and presentation of MV peptides in the context of MHC-class II molecules. MV-derived antigen presentation by DCs was more efficient at low antigen concentrations than presentation by autologous B-LCL (Figure 2B); while the peptide control response was not significantly different (239 ± 216 versus 264 ± 218).

To investigate whether DC-SIGN and CD150 are involved in antigen presentation, moDCs were pre-treated with specific blocking antibodies to CD150, DC-SIGN and with the C-type lectin inhibitor mannan. Both mannan and anti-DC-SIGN inhibited activation of the MV-specific T-cell clone, demonstrating that DC-SIGN supports MV antigen uptake and processing for antigen presentation (Figure 2B and C). Notably, antibodies against CD150 also inhibited T-cell clone activation, although to a lesser extent than antibodies against DC-SIGN. The role of DC-SIGN and CD150 was not dependent on post-entry effects, since addition of the antibodies just before the

T-lymphocytes were added did not affect MV antigen presentation to the CD4+ T-cell clone (data not shown). Thus, viral uptake by DC-SIGN and to a lesser extent CD150 leads to virus degradation and antigen presentation of MV-derived antigens to CD4+ T-lymphocytes.

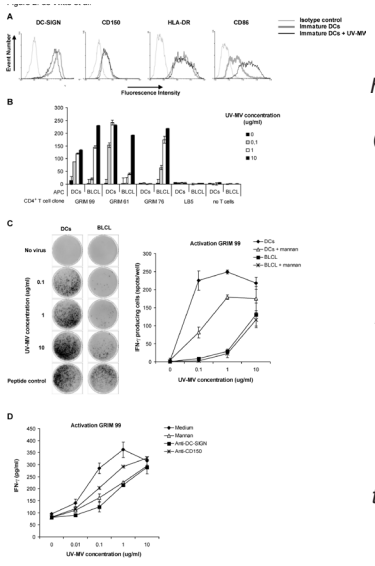

Figure 2. *Dendritic cells mediate antigen presentation of measles virus to CD4+ T-lymphocytes. (A) DCs (1 x 10^5 cells) were incubated with different concentrations of UV-MV. After 24 hours, the cells were stained for CD150, HLA-DR, CD86 and DC-SIGN using specific antibodies and analyzed by flow cytometry. (B,C) DCs or autologous B cells (B-LCL) (5 x 10^4 cells) were pre-incubated with mannan and incubated with UV-MV or a positive control peptide overnight. The MV-specific CD4+ T-cell clones, GRIM99, GRIM61 and GRIM76 and the non-specific T-cell clone LB5 were added and T cell activation was determined by ELISPOT. GRIM99, GRIM61 and LB5 were dependent on HLA-DQw1 as expressed by the DCs, whereas GRIM76 was HLA-mismatched to the DCs used. Images of the ELISPOT (left) and the mean of the spot counts per well are depicted (right). Error bars represent the standard deviation of duplicates. (D) DCs (1 x 10^4 cells) were pre-incubated with mannan, anti-DC-SIGN or anti-CD150 and subsequently incubated with different concentrations of UV-MV. After 6 hours the MV-specific CD4+ T-cell clone (5 x 10^4 cells) was added to the wells. After 24 hours the supernatant was harvested and the amount of IFNγ analyzed by ELISA. Standard deviations represent the standard deviation of duplicates. A representative experiment out of two is shown.*

Measles virus replicates in clusters of dendritic cells and T-lymphocytes that are interconnected by infected dendrites

DCs capture HIV-1 via DC-SIGN [135], and facilitate the infection of T-lymphocytes by transferring the virus through the infectious synapse [227]. Since DC-SIGN+ DCs and CD150+ lymphocytes closely interact in the lymphoid tissues and the upper respiratory tract (Figure 1), we investigated the role of DCs in MV transmission in DC-T-lymphocyte co-cultures. To analyze viral transmission of DCs to T-lymphocytes we used the recombinant MV^{IC323}EGFP strain. This MV strain has similar characteristics as its parental IC-B wild-type strain [52], but infected cells produce high amounts of EGFP. The concentration of EGFP in the cells is directly related to the level of virus replication. The entry receptor for this virus is CD150, and not CD46, similar as MV wild-type strains [113]. DCs were infected with rMV^{IC323}EGFP, and subsequently co-cultured with PHA-stimulated T-lymphocytes expressing high levels of CD150. After two days the infected cells were analyzed by fluorescence microscopy. MV infection induced the formation of large clusters, which contained multiple EGFP+ syncytia (Figure 3A). Most infected cells were observed in clusters, and notably long EGFP+ dendritic processes were observed that interconnected these clusters (Figure 3A). To investigate which cells were present in the clusters, either DCs or T-lymphocytes were stained with a red dye before infection. Staining of either cell type demonstrated that both infected DCs and T-lymphocytes were present in the EGFP+ clusters (Figure 3B), reminiscent of the *in vivo* infection of DCs and T-lymphocytes observed in lymphoid tissues of macaques [54].

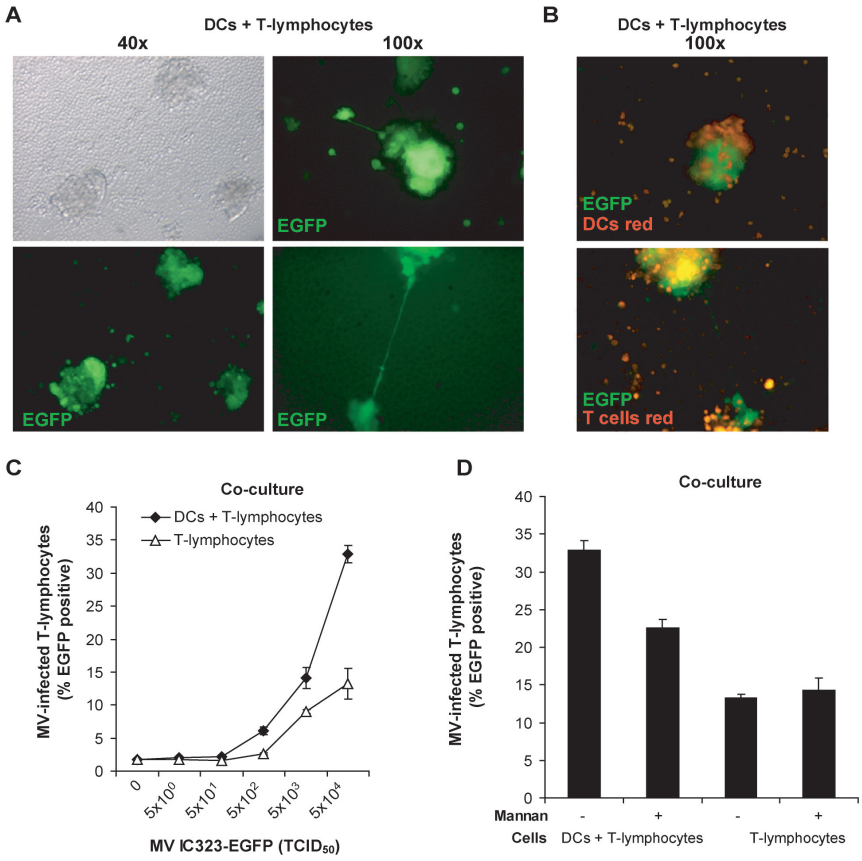

Figure 3. *Dendritic cells facilitate measles virus infection of T-lymphocytes in clusters that are interconnected. (A–D) T-lymphocytes (2 x 10^5 cells), alone or in the presence of DCs (5 x 10^4 cells), were pre-incubated with mannan and infected with rMV^{IC323}EGFP ($TCID_{50}$ 5 x 10^4 unless depicted otherwise) and cultured for 72 hours. (A,B) The infection was analyzed by fluorescence microscopy. The magnification is depicted. (B) DCs or T-lymphocytes were labeled red using the membrane dye PKH26 prior to the experiment and infection by rMV^{IC323}EGFP is shown by EGFP expression (green). (C,D) The infection of DCs and T-lymphocytes was analyzed by measuring EGFP expression by flow cytometry. Standard deviations represent the standard deviation of triplicates. A representative experiment out of two is shown.*

To investigate whether DCs enhance the infection of lymphocytes, T-lymphocytes or DC-T-lymphocyte co-cultures were infected with different concentrations of rMV^{IC323}EGFP and subsequently analyzed by flow cytometry. MV could readily infect activated T-lymphocytes, but addition of DCs enhanced infection two-fold (Figure 3C and D). To investigate the role of DC-SIGN in MV transmission in a DC-T-lymphocyte co-culture, DCs were pre-incubated with mannan and infection was measured. Mannan partially prevented the increased infection of the lymphocytes in the DC-T-lymphocyte co-cultures, demonstrating that DC-SIGN is involved in the enhanced infection in the DC-T-lymphocyte co-culture, probably by increasing viral transmission to T-lymphocytes (Figure 3D).

Dendritic cells transmit measles virus to T-lymphocytes independently of *de novo* virus production

To investigate whether DCs transmit MV to their target cells, DCs were incubated with rMV^{IC323}EGFP for two hours, washed extensively to remove unbound virus and subsequently co-cultured with activated T-lymphocytes. In DC cultures without T-lymphocytes, low percentages of MV-infected DCs were detected, whereas in the DC-T-lymphocyte co-cultures large clusters of MV-infected cells and syncytia were observed (Figure 4A upper panels). These data strongly suggest that DCs capture MV and transmit the virus to T-lymphocytes independently of *de novo* synthesis of virus by infected DCs, since only a few infected DCs were observed (Figure 4A). This process is referred to as *trans*-infection. However, HIV-1 studies have shown that DCs can also mediate transmission of *de novo* synthesized HIV-1 [216]. DCs in the respiratory tract *in situ* express high levels of DC-SIGN and no or low amounts of CD150 (Figure 1), suggesting that DCs are not productively infected by MV. Therefore, we investigated whether DCs mediate *trans*-infection. As demonstrated, DCs transmit MV efficiently to T-lymphocytes in a co-culture (Figure 4A) but *de novo* synthesis in DCs cannot be excluded, since both DCs and T-lymphocytes are infected in the DC-T-lymphocyte co-culture (Figure 4B). To exclude *de novo* synthesis of virus in DCs, we used the fusion inhibitor peptide (FIP, 200mM) [228], which was added to the co-cultures 2 hours after addition of the T-lymphocytes to MV-infected DCs. We observed large clusters of EGFP$^+$ cells in the presence of FIP (Figure 4A). FIP prevents fusion of MV with cell membranes and of membranes of MV-infected cells with those of neighboring cells. Therefore FIP blocks infection and syncytium formation [229]. Thus, T-lymphocytes expressing EGFP must have been infected during the 2 hours co-cultivation with MV-infected DCs before FIP was added (Figure 4B). This is a time frame that excludes *de novo* synthesis of MV by the DCs. In contrast to the condition without FIP, no syncytium formation was observed in DCs and T-lymphocytes cultured in the presence of FIP, confirming that FIP indeed prevented fusion. Moreover, incubation of DCs with different concentrations of MV demonstrated that T-lymphocytes were the major MV-infected cell population in the DC-T-lymphocyte co-culture (Figure 4C), demonstrating that DCs mediate *trans*-infection. To determine the efficiency of the *trans*-infection, the absolute number of infected cells was calculated (Figure 4D). A 6-fold higher number of T-lymphocytes compared to DCs were infected in the co-cultures. This demonstrates that *trans*-infection of T-lymphocytes by DC-bound MV is more efficient than *cis*-infection of DCs. Thus, DCs efficiently mediate transmission of MV to T-lymphocytes, and this process primarily occurs independently of *de novo* synthesis of MV.

Measles virus *trans*-infection of T-lymphocytes by dendritic cells is dependent on DC-SIGN, but not CD150

DC-SIGN and CD150 are both important for binding of MV to DCs and subsequent infection. Indeed, MV-infection of DCs is inhibited by antibodies against CD150 and DC-SIGN, as well as by mannan (Figure 5A) [132]. MV transmission by *de novo* synthesis of MV particles depends on infection of DCs and therefore these data suggest that transmission through *de novo* synthesis of virus is dependent on both CD150 and DC-SIGN.

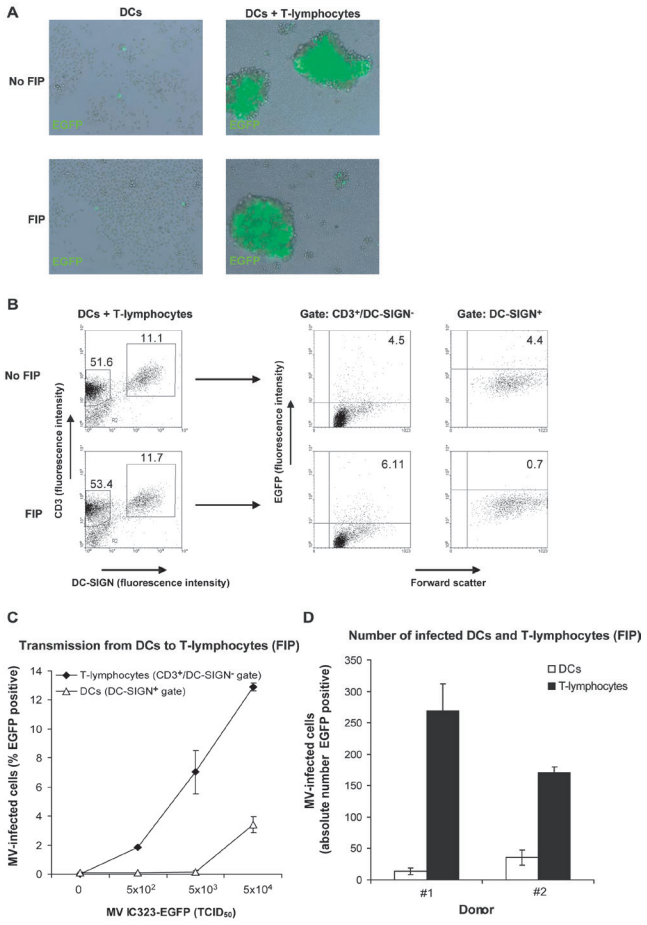

Figure 4. *Dendritic cells mediate viral transmission of measles virus independently of de novo virus production. (A–D) DCs (5 x 10⁴ cells) were incubated with rMV^{IC323}EGFP (5 x 10⁴ TCID$_{50}$, unless depicted otherwise) and after 2 hours the cells were extensively washed. T-lymphocytes (2 x 10⁵ cells) were added and if indicated the fusion inhibitory peptide (FIP) was added after 2 hours. After 72 hours the infection was analyzed by (A) fluorescence microscopy and (B–D) flow cytometry. (A) The cultures are depicted as an overlay of EGFP and brightfield. (B,C) The cells were harvested, washed and stained for CD3 and DC-SIGN. EGFP expression was measured by flow cytometry. (B) The percentage gated is depicted in the regions or quadrants. (C) Transmission of different concentrations of rMV^{IC323}EGFP is analyzed. (D) The absolute numbers of EGFP⁺ DCs and T-lymphocytes in the analyzed samples were calculated and depicted. Error bars represent the standard deviation of triplicates. A representative donor out of seven is shown.*

To investigate whether DC-SIGN is involved in MV *trans*-infection of T-lymphocytes, DCs were pre-treated with mannan or antibodies against DC-SIGN and transmission was measured in the presence of FIP. In all donors, both mannan and antibodies against DC-SIGN inhibited *trans*-infection (Figure 5B), although donor variations were observed. Direct infection of T-lymphocytes after pre-treatment with the blocking agents demonstrated that these compounds do not interfere with the infection of the target cells (Figure 5B). Allogeneic DCs induce T-lymphocyte activation and as such

might increase CD150 expression and subsequently MV infection of T-lymphocytes. Therefore, we used autologous T-lymphocytes for donors #5–7. In this setting, *trans*-infection was also observed and was dependent on DC-SIGN (Figure 5B), indicating that *trans*-infection is independent of T-lymphocyte activation. To analyze whether these differences were significantly different throughout the donors, data were normalized to the medium condition (Figure 5C), demonstrating that DC-SIGN is important for transmission of MV from DCs to T-lymphocytes (Figure 5C). Since CD150 is important for MV binding to DCs and subsequent infection, we investigated whether this receptor is also important for *trans*-infection of T-lymphocytes. Strikingly, antibodies against CD150 did not block the *trans*-infection and even slightly increased the transfer to T-lymphocytes (Figure 5D). These results demonstrate that DC-SIGN mediates both DC infection *in cis* and *trans*-infection, whereas CD150 is only involved in infection, and thus CD150 and DC-SIGN have distinct roles in MV transmission by DCs to T-lymphocytes.

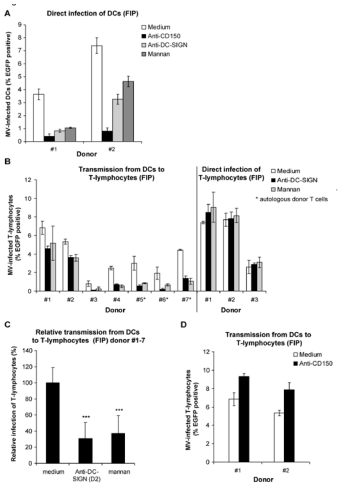

Figure 5. *Trans-infection of measles virus by dendritic cells is dependent on DC-SIGN, but not on CD150. (A–D) DCs (5 x 10^4 cells) or (B) T-lymphocytes from different donors were pre-incubated with mannan, anti-DC-SIGN or anti-CD150 (for donor #1 and #2), before incubation with rMV^{IC323}EGFP (5 x 10^4 $TCID_{50}$). (A) The cells were cultured in the presence of FIP for 3 days and analyzed by flow cytometry. (B–D) After 2 hours the cells were washed and T-lymphocytes (2 x 10^5 cells) were added. For donor #5 – 7 autologous T-lymphocytes were used as target cells. The fusion inhibitory peptide (FIP) was added after 2 hours. After 72 hours the cultures were analyzed by flow cytometry. (B) Transmission by different donors of DCs is depicted. As a control for the specificity of mannan and anti-DC-SIGN T-lymphocytes were pre-treated and directly infected. Error bars represent the standard deviation of triplicates. (C) The results of the different donors in (B) (#1 – 7) were normalized to the medium control to determine the statistical differences by ANOVA. Error bars represent the standard deviation of the mean of the different donors, *** = p < 0,01 versus the medium control.*

DCs transmit MV to both CD4$^+$ and CD8$^+$ T-lymphocytes

In peripheral blood of experimentally infected macaques, MV infection of both CD4$^+$ and CD8$^+$ T-lymphocytes was observed [54]. Therefore we investigated whether DCs mediate transmission of MV to both T-lymphocyte subsets *in vitro*. CD4$^+$ and CD8$^+$ T-lymphocytes were purified from PHA-stimulated human peripheral blood mononuclear cells (PBMCs), and both expressed high levels of CD150 (Figure 6A). DCs were infected with rMV^{IC323}EGFP, and after extensive washing, co-cultured with either CD4$^+$ or CD8$^+$ T-lymphocytes. In both co-cultures, EGFP expression was observed in large clusters containing EGFP$^+$ syncytia, demonstrating that DCs mediate transmission to both T-lymphocyte subsets (Figure 6B). To measure whether DCs mediate *trans*-infection, FIP was added two hours after addition of the T-lymphocytes to the MV-infected DCs. *Trans*-infection to both subsets is efficient and mediated by DC-SIGN, since pre-treatment of DCs with mannan inhibited infection of T-lymphocytes in both cultures (Figure 6C). Thus, DCs transmit MV to both CD4$^+$ and CD8$^+$ T-lymphocytes.

Discussion

Two hallmarks of measles are that the virus is highly contagious and infection results in strong MV-specific cellular immune responses. Both viral transmission and antigen presentation should therefore occur through efficient and robust processes. Since DCs are professional APCs and have been demonstrated to mediate transmission of several viruses, we have investigated the role of DCs in both processes for measles. Here we have shown that a subset of DCs, the DC-SIGN$^+$ DCs, mediates both transmission and antigen presentation of MV to T-lymphocytes. The receptors DC-SIGN and CD150 are both involved in DC infection and antigen presentation, whereas only DC-SIGN is involved in MV trans-infection of T-lymphocytes.

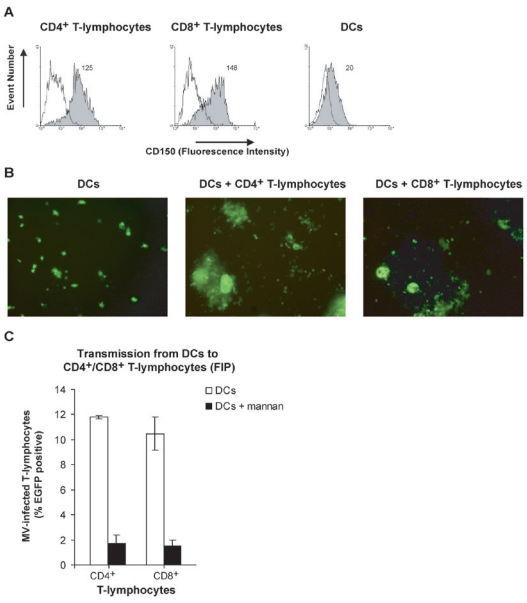

Figure 6. *Dendritic cells mediate transmission of measles virus to both CD4$^+$ and CD8$^+$ T-lymphocytes. (A) PBMCs were activated for three days, and the cells were enriched for CD4$^+$ T-lymphocytes or CD8$^+$ T-lymphocytes. T-lymphocytes and DCs are stained for the expression of CD150 and analyzed by flow cytometry. Open histograms represent isotype-control and filled histogram the specific antibody staining. The mean of the specific staining is depicted. (B,C) DCs (5 x 10^4 cells) were pre-incubated with mannan before incubation with rMV^{IC323}EGFP (5 x 10^4 TCID$_{50}$). After 2 hours the cells were washed and cultured in the presence of the CD4$^+$ or CD8$^+$ T-lymphocytes for three days. (B) The cultures were analyzed by fluorescence microscopy and pictures were made at a magnification of 200x. (C) The fusion inhibitory peptide (FIP) was added after 2 hours. The cells were harvested and EGFP expression was measured by flow cytometry. Standard deviations represent the standard deviation of triplicates. A representative experiment out of two is shown.*

DC-SIGN$^+$ DCs have previously been identified in several subepithelial and lymphoid tissues [135,223]. Here, we have identified DC-SIGN$^+$ DCs in the sub-epithelial tissues of the human mouth, pharynx, trachea and bronchi, and the presence of scattered DC-SIGN$^+$ cells in the lung. CD150 is expressed on *in vitro* cultured macrophages and DCs and is increased upon maturation [119,226,230]. However, CD150 was previously not detected on immature DCs in skin and lung *in situ* [120] and we could not detect CD150 on DC-SIGN$^+$ DCs in respiratory epithelia, suggesting that these DCs are not susceptible to MV infection and DCs capture MV through DC-SIGN. However, expression of low levels of CD150 that might support MV infection cannot be excluded using immunofluorescence microscopy. DC-SIGN strongly enhances infection of DCs through CD150 [132], and therefore low levels of CD150 might be enough for efficient infection of DCs.

Different mechanisms are involved in virus transmission by DC-SIGN, since HIV-1 capture by DC-SIGN can result both in *cis*- and *trans*-infection [135,231]. However, DC-SIGN binding of HIV-1 also leads to virus degradation and presentation in the context of MHC [135,231–233]. Interestingly, we observed that both DC-SIGN and CD150 are involved in MV processing and presentation of MV-derived peptides to the MV-specific $CD4^+$ T-cell clone GRIM99. B cells are able to present MV antigens to T cells [234]. B-LCL express high levels of CD150, but no DC-SIGN and MV capture leads to virus degradation and presentation of MV peptides to the autologous $CD4^+$ T-cell clone and this was previously demonstrated to be dependent on endocytosis [234]. Notably, DCs were more efficient in antigen processing and presentation than the autologous B-LCL and antibodies against DC-SIGN inhibited antigen presentation to a larger extent than antibodies against CD150. Thus, although both DC-SIGN and CD150 are involved, DC-SIGN is more important for antigen presentation of MV by DCs.

MV is a highly contagious virus [16] suggesting that it has a very efficient entry into the respiratory tissues. However, the number of $CD150^+$ target cells in the respiratory tract is low, suggesting that these are not the first targets for MV at the site of entry. In contrast, the tissue is lined with DC-$SIGN^+$ DCs and these DCs are better candidates since DC-$SIGN^+$ DCs efficiently capture MV and mediate transmission of MV to T-lymphocytes *in vitro*. MV transmission to non-stimulated lymphocytes by DCs was inefficient (data not shown), which is in line with a previous report that demonstrated that transmission of MV from DCs to T cells isolated from blood is inefficient [168]. This is probably due to low expression of CD150 on blood-derived lymphocytes. However in lymphoid tissues, where DCs migrate to, CD150 is highly expressed on T and B-lymphocytes and on monocytes [214,235].

Recently it was demonstrated that DCs specifically transmit HIV-1 to HIV-1-specific T-lymphocytes [233] suggesting that immunological synapse formation enhances viral transmission, due to prolonged interactions during antigen presentation and T cell activation. However, we did not observe differences between transmission to autologous- and allogeneic T-lymphocytes, suggesting that prolonged immunological synapse interactions occurring during allogeneic but not autologous DC-T-lymphocyte interactions are not necessary for MV transmission. This might be due to differences in infectivity between both viruses.

MV transmission can occur independently of *de novo* synthesis of virus in DCs (referred to as *trans*-infection). Using specific blocking antibodies, we have demonstrated that *trans*-infection is dependent on DC-SIGN but not on CD150. This is physiologically relevant, since DC-$SIGN^+$ DCs in the respiratory tract express no or low levels of CD150, and are therefore not susceptible to MV infection. Both DC-SIGN and CD150 are important for binding of MV to DCs [132]. However, our data show that binding of MV to DC-SIGN and CD150 results in different internalization pathways. Although both DC-SIGN and CD150 lead to virus degradation for antigen presentation, CD150 binding also results in viral entry, whereas only the interaction of DC-SIGN with MV leads to viral protection for *trans*-infection. Indeed, inhibition of

CD150 resulted in enhanced *trans*-infection due to less degradation or fusion and therefore increasing the amount of virus for the DC-SIGN-mediated transmission. Several donors were tested for the involvement of DC-SIGN in *trans*-infection of MV. The contribution of DC-SIGN varied between the donors, suggesting that another attachment receptor might play a role, such as syndecan-3 for HIV-1 [236]. In macaques, both $CD4^+$ and $CD8^+$ T-lymphocytes are infected during the viremic phase of measles disease [54]. It is unclear whether viral transmission can also occur to $CD8^+$ T-lymphocytes. Interestingly, we observed MV transmission by DCs to both $CD4^+$ and $CD8^+$ T-lymphocytes, indicating the formation of an infectious synapse between DCs and $CD8^+$ T-lymphocytes, similar to DCs and $CD4^+$ T-lymphocytes [227].

During MV infection in macaques, lymphoid tissues are major sites of MV replication [54]. In human lymphoid tissues, $CD150^+$ and $DC\text{-}SIGN^+$ cells are in close contact, which can contribute to massive replication of MV. This is supported by our *in vitro* observations that $DC\text{-}SIGN^+$ DCs enhance infection of T-lymphocytes in co-cultures and MV infection is predominantly observed in the clusters of DCs and T-lymphocytes. Notably, long $EGFP^+$ dendrites were frequently observed between clusters, suggesting that viruses spread between clusters through these dendrites. Although these dendrites might be a MV-specific effect, which facilitates virus spread, these dendritic processes might also have a physiological function in the immune system, such as the interchange of antigenic information. The fact that MV infection in DC-T-lymphocyte co-cultures was observed in clusters was highly reminiscent to the infectious foci that we have previously observed in tissues of infected macaques [54]. This pattern and enhanced infection in DC-T-lymphocyte co-cultures suggest that the virus is much more efficiently transmitted by direct cell-cell contact than as cell-free virus.

In contrast to the APCs in the peripheral tissues, the borders of the medullary sinuses of the lymph node contain a population of cells that express high amounts of both DC-SIGN and CD150. These $DC\text{-}SIGN^+$ cells have been previously shown to express CD68 and lack the expression of DEC205, suggesting that these cells are medullary macrophages [223,224]. These cells are in contact with the lymph and therefore encounter tissue-derived antigens. Based on the high expression of both CD150 and DC-SIGN, and the fact that DC-SIGN can enhance infection *in cis* [132], it is likely that these cells become infected during measles and might contribute to further virus transmission.

In conclusion, these data provide us with an alternative view on how MV might disseminate from the site of infection to their main target cells, the lymphocytes: $DC\text{-}SIGN^+$ DCs, which are abundantly present in the sub-epithelial tissues of the respiratory tract, capture MV and process the virus for antigen presentation, but a part of the virus escapes from degradation. In previous studies dendrites of sub-epithelial DCs have been shown to pass the tight junctions of the epithelium of the gut and respiratory tract and sample the mucosal surfaces [237], which could result in efficient capture of the virus. Moreover, MV induces activation of the DC via TLRs

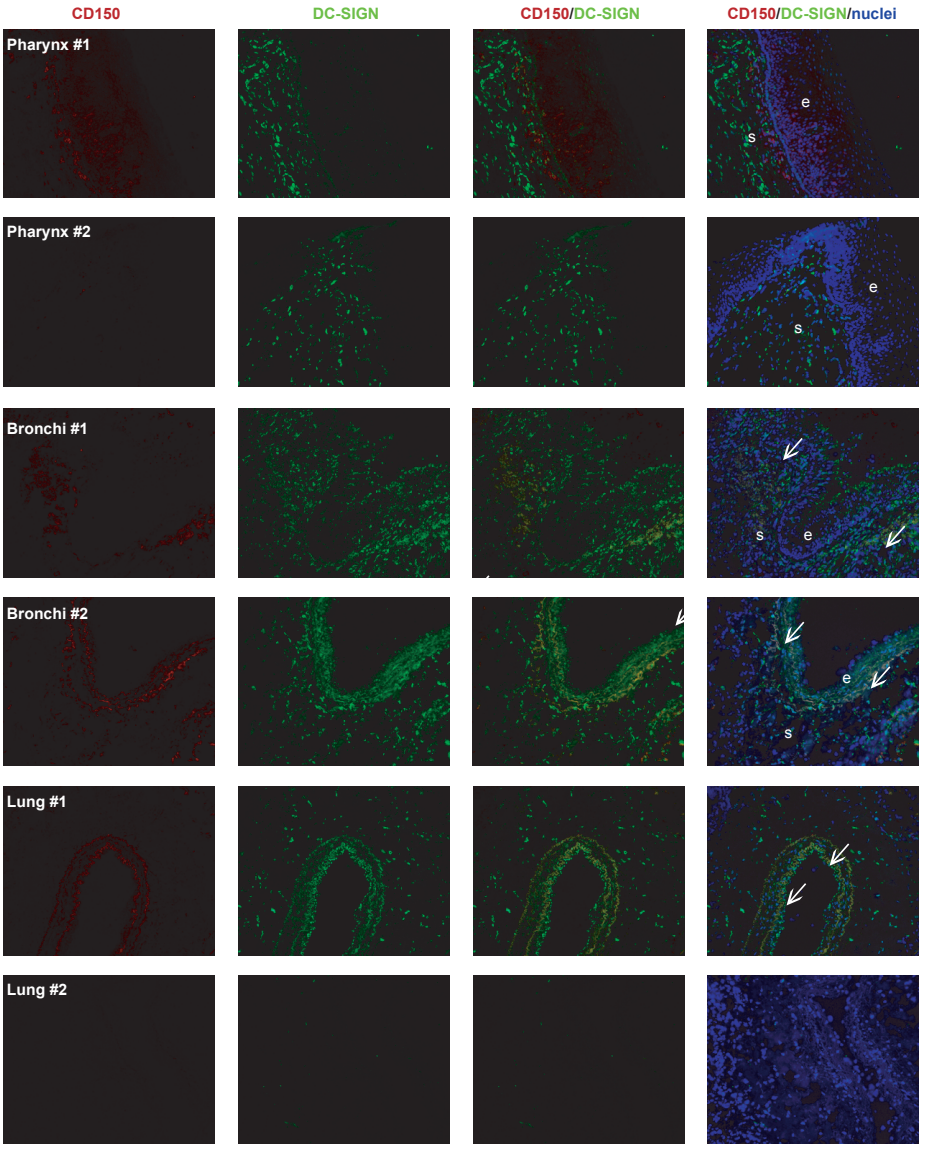

Figure S1. *DC-SIGN⁺-dendritic cells are present in the sub-epithelial tissues of the respiratory tract. Cryosections of different tissues from healthy donors were stained for the expression of DC-SIGN (green) and CD150 (red) using specific antibodies, and for the nuclei using Hoechst (blue). The sections were analyzed by fluorescence microscopy. Representative photos with a magnification of 100× are depicted (e = epithelium; s = sub-epithelial tissue, arrow = auto-fluorescence).*

[238], which will induce migration of DCs from the peripheral tissues to the lymphoid tissues. Although DCs might encounter $CD150^+$ cells in the underlying mucosal tissues, the abundant expression of CD150 in lymphoid tissues strongly suggests lymphoid tissues as the major site of MV transmission and replication. A similar mechanism might play a role in spreading the virus throughout the body, even to privileged tissues such as the brain, and could therefore be involved in complications such as subacute sclerosing panencephalitis (SSPE). Moreover, during viremia, DCs might increase infection and tissue destruction. In the future, *in vivo* studies will be required to prove the importance of MV transmission by DCs.

Funding
This work was supported by a grant from the Dutch Scientific Research (NWO; no. 917-46-367, LdW), Dutch AIDS foundation (2007036, MvdV), and the VIRGO consortium, an innovative cluster approved by the Netherlands Genomics Initiative and partially funded by the Dutch government (BSIK 03012, SY and RLdS).

Acknowledgments
We are grateful to Dr. Y. Yanagi, who provided the Vero-CD150 cells and the plasmid encoding the rMV^{IC323}EGFP virus, Dr. W. P. Duprex, who rescued the virus, Prof. S. Schneider-Schaulies, who provided us with the antibodies against CD150, and Dr. R. S. van Binnendijk, who provided us with the purified $MV^{Edmonston}$.

Author Contributions
Conceived and designed the experiments: LdW RDdV TG. Performed the experiments: LdW RDdV MvdV SY ML. Analyzed the data: LdW RDdV MvdV SY ML RLdS TG. Wrote the paper: LdW RDdV TG.

ATTACHMENT RECEPTORS

Human Langerhans cells capture measles virus through Langerin and present viral antigens to CD4$^+$ T cells but are incapable of cross-presentation

Michiel van der Vlist, Lot de Witte, Rory D. de Vries*, Manja Litjens, Marein A. de Jong, Donna Fluitsma, Rik L. de Swart and Teunis B.H. Geijtenbeek*

* both authors contributed equally

European Journal of Immunology 2011 Sep; 41(9): 2619 - 2631

Abstract

Langerhans cells (LCs) are a subset of DCs that reside in the upper respiratory tract and are ideally suited to sense respiratory virus infections. Measles virus (MV) is a highly infectious lymphotropic and myelotropic virus that enters the host via the respiratory tract. Here, we show that human primary LCs are capable of capturing MV through the C-type lectin Langerin. Both immature and mature LCs presented MV-derived antigens in the context of HLA class II to MV-specific $CD4^+$ T cells. Immature LCs were not susceptible to productive infection by MV and did not present endogenous viral antigens in the context of HLA class I. In contrast, mature LCs could be infected by MV and presented *de novo* synthesized viral antigens to MV-specific $CD8^+$ T cells. Notably, neither immature nor mature LCs were able to cross-present exogenous UV-inactivated MV or MV-infected apoptotic cells. The lack of direct infection of immature LCs, and the inability of both immature and mature LCs to cross-present MV antigens, suggest that human LCs may not be directly involved in priming MV-specific $CD8^+$ T cells. Immune activation of LCs seems a prerequisite for MV infection of LCs and subsequent $CD8^+$ T-cell priming via the endogenous antigen presentation pathway.

Introduction

DCs induce adaptive immunity by presenting antigens in the context of HLA class I (HLA-I) and II (HLA-II) to $CD8^+$ and $CD4^+$ T cells, respectively [239]. Virus-specific $CD8^+$ cytotoxic T cells (CTLs) are crucial to clear viral infections and are classically induced by virus-infected APCs that present endogenous viral antigens in the context of HLA-I. However, DCs can also capture exogenous antigens and present these in the context of HLA-I molecules, a process referred to as cross-presentation which is thought to be important in both viral and tumor immunity [240,241].

It is becoming evident that different DC subsets have specialized functions in anti-viral immunity, *e.g.* by inducing preferentially $CD4^+$ or $CD8^+$ T-cell responses or by inducing innate immunity against pathogens [242,243]. Langerhans cells (LCs) are a subset of DCs that are, in humans, characterized by expression of CD1a, the C-type lectin Langerin and the presence of Birbeck granules [244]. LCs reside in the epidermis and stratified epithelial tissues [245–247]. Recently, we have shown that LCs form a barrier against HIV-1; LCs capture HIV-1 through Langerin, resulting in internalization of HIV-1 into Birbeck granules and preventing subsequent HIV-1 transmission [134]. However, little is known about the role of human LCs and Langerin in antigen presentation.

Capture of exogenous antigens by LCs leads to induction of $CD4^+$ T-cell responses [248–250]. However, the ability of LCs to cross-present exogenous antigens to $CD8^+$ T cells has been debated [251–254]. Klechevsky *et al* [249] have shown that *in vitro*-generated human LCs from either $CD34^+$ cells or monocytes are capable of cross-presenting influenza-virus proteins to $CD8^+$ T cells. However, these *in vitro*-generated LCs might be different from primary immature LCs.

Here, we have investigated the antigen capture and presentation capacity of human primary LCs during measles virus (MV) infection. MV is the causative agent of measles, which remains an important cause of morbidity and mortality in developing countries. MV is a lymphotropic and myelotropic virus and DCs have been implicated in its transmission [54,255]. MV is one of the most infectious viruses that infect humans and is transmitted via the respiratory route. CD150 is the primary receptor for wild-type MV [113], whereas the laboratory-adapted $MV^{Edmonston}$ also uses CD46 as entry receptor [111]. Wild-type MV initially replicates in mononuclear cells in the alveolar lumen, the bronchus-associated lymphoid tissue and the regional lymph nodes of the respiratory tract, followed by viremia and systemic disease [54,256]. Although measles is associated with immune suppression, MV paradoxically induces a strong cellular and humoral immune response that efficiently clears the virus and results in lifelong immunity [109]. Human DC-$SIGN^+$ DCs transmit MV to lymphocytes [132,255] and DCs have been shown to become infected by MV *in vivo* in macaques [54]. Also, LCs have been shown to be susceptible to MV infection, albeit after exposure to mechanical stress [257,258]. These data strongly suggest that different DC subsets are involved in MV dissemination, but little is known about the role of human LCs as professional APCs during measles.

Here, we show that Langerin functions as an attachment receptor for MV that is involved in virus capture but not infection of LCs. MV binding to both immature and mature LCs led to processing and presentation of viral antigens to MV-specific $CD4^+$ T cells. Mature LCs, in contrast to immature LCs, were infected by MV and presented antigens in the context of HLA-I molecules to MV-specific $CD8^+$ T cells. Notably, neither immature nor mature LCs were able to cross-present viral antigens derived from UV-inactivated MV or MV-infected apoptotic cells to MV-specific $CD8^+$ T cells. This study shows that Langerin on LCs is involved in MV capture. Notably, we show that primary human LCs are incapable of cross-presenting antigen from exogenous MV particles or MV-infected apoptotic cells. These results suggest that without prior activation, immature LCs do not induce $CD8^+$ T-cell responses to MV.

Materials & Methods

Antibodies

The following antibodies were used: anti-CD150 (A12, Abd Serotec; 5C6 [217]), anti-Langerin (10E2, IgG1 [134]; DCGM4, Beckman Coulter; polyclonal goat, R&D Systems), anti-MV-F (A5047 [259]), anti HLA-DR (Q5/13) [260], anti HLA-DR1 (MEM-267, Genetex), rabbit anti-LAMP-1 polyclonal, anti-HLA-B27 FITC (HLA-ABC-m3, Abcam), anti-HLA-DQw1 (Genox 3.53, Novus Biologicals), rabbit anti-HLA-DR polyclonal (Santa Cruz biotechnology Inc), anti-CD1a (NA1/34, Dako Cytomation Denmark); anti-CD1a FITC or APC (HI149), anti-HLA-DR (Immu357), CD80 (B7-1) and CD86 (HA5.2B7) conjugated with PE (Pharmingen), anti-CD83 PE (HB15a, Immunotech), goat anti-mouse IgG PO, goat anti-mouse IgG Fcg fragment (Jackson Immunoresearch), goat anti-mouse IgG conjugated with FITC (Zymed Laboratories), Alexa488-, Alexa546-, Alexa594- and Alexa633-labeled isotype-specific anti-mouse antibodies (Molecular probes).

Cells

All research involving human tissues were approved by the VU University Medical Center Medical and Academic Medical Center review board. CHO-CD150 [132], Vero-CD150 cells [261], THP-1 and the Epstein-Barr virus-transformed B-lymphoblastic cell lines (BLCL-OUW, BLCL-GR, BLCL-WH, BLCL-JP) [150,219] were cultured as described [134,255,262]. The $CD4^+$ T-cell clone Hd7 [263], $CD4^+$ T-cell clone GRIM-F99 [150] and the $CD8^+$ T-cell clone WH-F40 [234] were cultured as described before. Immature moDCs were cultured as previously described [220]. Primary LCs were isolated from normal healthy skin obtained from plastic surgery as described before [134].

Viruses

The wild-type MV strain WTF [264], the laboratory-adapted $MV^{Edmonston}$, the recombinant pathogenic MV^{IC323}EGFP [53] and the recombinant attenuated strain $MV^{Edmonston}$EGFP [265] were propagated on Vero-CD150 cells and purified by discontinuous sucrose gradient ultracentrifugation. Purified MV strains were UV-inactivated (30 min, 15 W, 312 nm, 1.5 J/cm^2).

Immunofluorescence microscopy
Cryosections (7 µm) were stained with primary antibody against CD1a (10 µg/mL) in combination with either CD150 (10 µg/mL), Langerin (10E2, 10 µg/mL) or a buffer control for 18 h at 41°C as described before [255].

Langerin-binding assay
Different concentrations UV–MV WTF virions were coated onto Maxisorp plates (NUNC, Denmark), blocked with 5% BSA in 20 mM Tris; 150 mM NaCl; 1 mM $CaCl_2$; $MgCl_2$; pH 8 (TSA) and incubated with Jurkat-Langerin lysate (1 x 10^8 cells/mL). Langerin binding was detected with DCGM4 (10 µg/mL) followed by goat anti-mouse-PO. Specificity was determined by pre-incubation with a saturating concentration of mannan (1 mg/mL).

FITC-labeled MV binding assay
Purified MV^{IC323}EGFP and $MV^{Edmonston}$ were dialyzed against 0.1% formalin and labeled with FITC (0.1 mg/mL in 0.5 mol/L bicarbonate buffer, pH 9.5). Unbound FITC was removed by dialyzation against PBS. 2 x 10^4 THP-1 or THP-Langerin were pre-incubated with medium, mannan (1 mg/mL) or blocking antibodies 10E2 or 5C6, before incubation with MV-FITC.

MV infection
CHO, CHO-DC-SIGN and CHO-CD150 cells (1 x 10^5 cells) were infected with MV^{IC323}EGFP or WTF (multiplicity of infection (MOI): 1). Syncytia and EGFP expression were analyzed 2 d post-infection using a DMIL microscope with a DFC320 camera (Leica Microsystems). For flow cytometry, the fusion inhibitory peptide Z-D-Phe-l-Phe-l-Gly (FIP [228]) (0.2 mM) (Bachem) was added. After 2 d, cells were stained with anti-MV-F. Cells were fixed in 2% paraformaldehyde (PFA) in PBS. Immature LC suspensions (10 - 20% $CD1a^+$) and mature LCs were infected with MV^{IC323}EGFP or $MV^{Edmonston}$EGFP (MOI: 1) for 3 d. LCs were stained for CD1a.

Electron microscopy
Mature LCs were incubated with DCGM4 (10 µg/mL) and fixed as described before [134]. Cryosections were immuno-labeled with anti-mouse antibodies (15 nm protein A gold label) to detect bound and internalized DCGM4 and either one of the following antibodies: goat anti-Langerin, anti-Lamp-1, rabbit anti-HLA-DR (10 nm protein A gold label) and analyzed as described before [134].

Internalization assay
Mature LCs or BLCL-OUW transfectants (2 x 10^5) were incubated with DCGM4 (25 µg/mL) for internalization, washed and fixed with PFA (3% in PBS). Cells were permeabilized using saponine (0.1%), stained with anti-Lamp-1 (0.5 µg/mL) and analyzed by confocal microscopy (Leica AOBS SP2 CSLM, DMIRE2 microscope, PL APO 63x/NA1.30). Images were acquired using Leica confocal software (version 2.61).

Antigen presentation assays
Primary LCs were screened to match HLA-profiles of the T-cell clones. Monocytes were isolated from an HLA-DQw1/HLA-B27- matched donor. APCs (1 x 10^4 cells/well) were pre-incubated with serial dilutions of DCGM4 or AZN-D1 (isotype), washed and co-cultured with 2 x 10^4 Hd7 T cells. After 24 h, IFNγ production was measured by ELISA (Cytoset, Biosource). HLA-matched LCs or moDCs (5 x 10^3 cells) were used as APCs in an IFNγ ELISPOT as previously described [221]. Where indicated, the cells were incubated with a mix of TNFα (100 ng/mL, Strathmann Biotec), poly I:C (10 µg/mL) and LPS (*Salmonella typhosa*, 100 ng/mL, Sigma). In parallel, IFNγ production in supernatant was measured by ELISA (Biosource International). To determine the contribution of Langerin, the APCs were pre-incubated with mannan (0.25 mg/mL), anti-Langerin (20 µg/mL), anti-CD150 (20 µg/mL) or an isotype control (20 µg/mL).

Flow cytometry
Flow cytometry was performed on a FACScan or FACSCalibur (BD Biosciences). Gating strategies were as follows: live gated on forward and sideward scatter. Where indicated in the text, live cells were further gated on CD1a. Finally, infection and binding are depicted as percentage positive cells in the current gate.

Results

Langerin is a receptor for MV but does not mediate viral entry
Langerin interacted with MV in a dose-dependent manner as measured by a soluble Langerin-binding ELISA (Figure 1A). This interaction is specific for the carbohydrate recognition domain of Langerin since binding was inhibited by mannan, which blocks Langerin (Figure 1A). Next, Langerin-transduced THP-1 cells (Supporting Information Figure 1) were incubated with FITC-labeled MV^{IC323}EGFP and laboratory-adapted $MV^{Edmonston}$, and binding was measured by flow cytometry. Binding of both MV strains to Langerin-transduced THP-1 cells was higher compared to mock-transduced cells and could be blocked by mannan (Figure 1B and C). Thus, Langerin is a receptor for both wild-type and laboratory-adapted MV strains.

Next, we investigated whether Langerin is involved in the interaction of human LCs with MV. Primary human mature LCs efficiently captured both MV strains, which was blocked by anti-Langerin and anti-CD150 to a similar extent (Figure 1D). Moreover, mannan reduced binding to a similar extent as anti-Langerin. Thus, primary LCs capture MV through both Langerin and CD150.

To investigate whether Langerin mediates fusion and viral entry, Chinese hamster ovary (CHO) cells were transduced with Langerin (Supporting Information Figure 1). CHO, CHO-Langerin and CHO-CD150 cells were incubated with wild-type MV (WTF) or MV^{IC323}EGFP [52]. Both viruses infected CHO-CD150 cells, but were unable to infect Langerin- or mock-transfected CHO cells (Figure 1E, Supporting Information Figure 2), demonstrating that Langerin is not an entry receptor for MV.

Next, we investigated infection of immature and mature LCs with MV^{Edmonston} and MV^{IC323}EGFP. Mature LCs, in contrast to immature LCs, were infected by both strains (Figure 1F – I). Infection of mature LCs with the laboratory-adapted MV^{Edmonston} was inhibited by anti-CD150 and anti-CD46, whereas the infection with the wild-type MV^{IC323}EGFP was inhibited by anti-CD150 (Figure 1H and I). Anti-Langerin did not affect infection of LCs with either MV strain (Figure 1H and I). Thus, Langerin is a binding receptor for MV that is involved in MV capture but does not mediate viral entry.

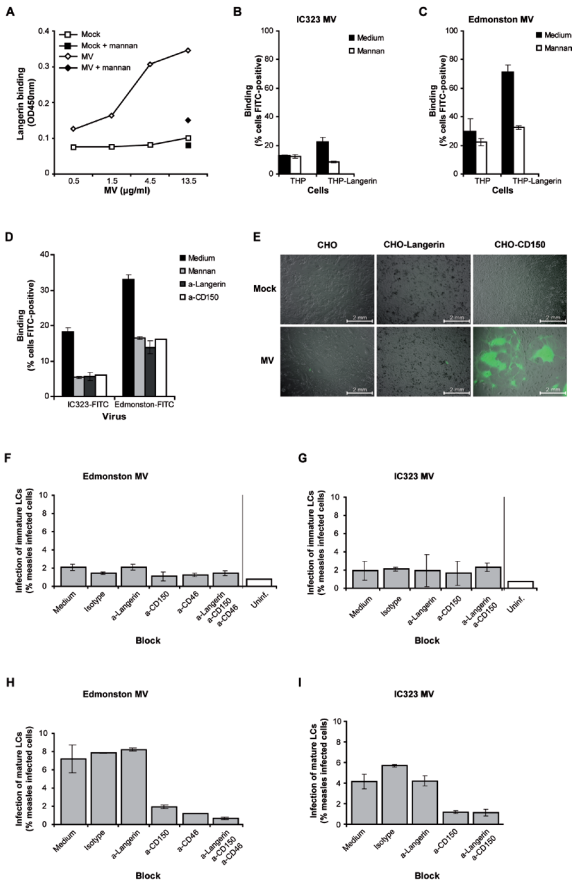

Figure 1. *Langerin is a receptor for measles virus. (A) Different concentrations of wild type MV or a mock control were coated and Langerin binding was detected by anti-Langerin. Mannan was used to determine specificity of the interaction between Langerin and MV. Data are representative of two independent experiments. (B–D) Langerin-transduced THP-1 cells, mock-transduced THP-1 cells (B,C) and primary human mature LCs (D) were incubated with FITC-labeled MV^{IC323}EGFP (B,D) or Edmonston (C,D) and binding was determined by flow cytometry. Mannan (B-D), and anti-Langerin or anti-CD150 (D) were used to determine the specificity. Data show average ± SD and are representative of two independent experiments. (E) CHO, CHO-Langerin and CHO-CD150 cells were infected with MV^{IC323}EGFP. Infection was assessed by syncytium formation and EGFP expression. Original magnification 10x. (F-I) Primary immature (F,G) or mature (H,I) LCs were infected with MV^{IC323}EGFP (G,I) or MV^{Edmonston}EGFP (F,H). The percentages of CD1a^{+} EGFP^{+} cells are depicted. Data show average ± SD and are representative of two independent experiments.*

LCs are abundantly present in epithelium of the upper respiratory tract

LCs have been extensively characterized in mucosal tissues involved in HIV-1 infection [246,266], but little is known about the distribution of LCs in the respiratory tract where MV enters the host. We have analyzed the density and phenotype of LCs in the respiratory tract by staining different epithelial tissues for CD1a, Langerin and CD150. LCs were observed in tongue, buccal cavity, tonsil, pharynx and bronchi (Figure 2A; data not shown). LCs were mainly located in the epidermis and epithelia. Furthermore, the density of LCs was high in the upper respiratory tract and decreased while descending toward the lungs, where LCs were only scarcely detected (data not shown).

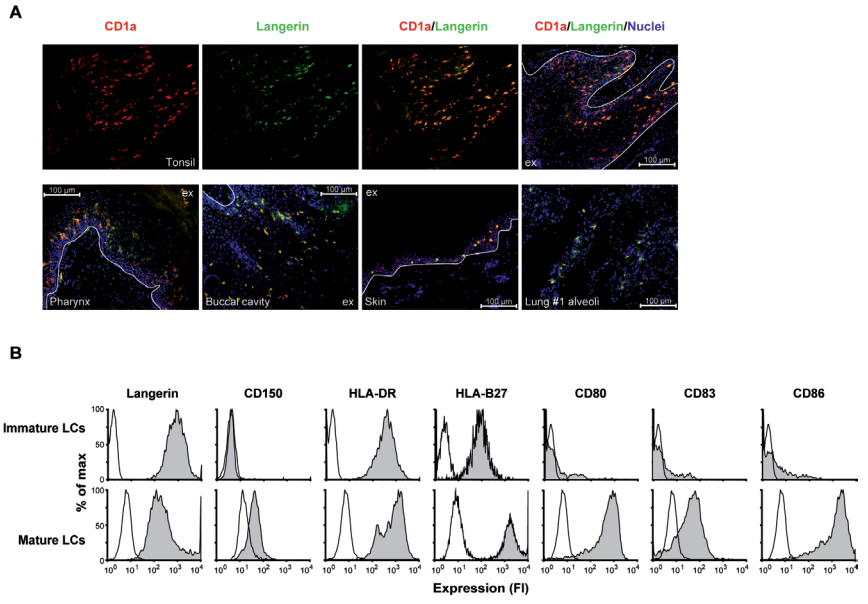

Figure 2. *Human LCs are present in the upper respiratory tract and express Langerin. (A) Cryosections of human tissues were stained for CD1a (red), Langerin (green) and Hoechst (blue) and analyzed by fluorescence microscopy. The border between the epithelium/epidermis and subepithelium/dermis (white line), and the lumen or external environment (ex) are depicted. (B) Immature and mature LCs were analyzed by flow cytometry. Open histograms: isotype control; filled histograms: specific antibody. The data are representative for three donors.*

Langerin was expressed on more than 95% of LCs in the skin and upper respiratory tract (Figure 2A; data not shown). In lungs a donor variation was observed, since LCs from one donor expressed Langerin on the cell membrane and/or intracellular, whereas in two other donors, 80 and 20% of the $CD1a^+$ cells expressed Langerin (data not shown). Only a small population of LCs (<10%; data not shown) in both upper and lower respiratory tracts was positive for CD150 (Supporting Information Figure 3, arrows), indicating that the majority of LCs in respiratory tract are $CD150^-$ and that immature LC are among the first cells to encounter MV in the upper respiratory tract.

Isolation of human immature LCs from the respiratory tract is not possible on a scale that allows functional experiments. Therefore, we have used epidermal LCs from skin because these cells are immature upon isolation and express Langerin and CD1a but no CD150, similar to LCs observed in respiratory tract (Figure 2). The isolation procedure did not activate the cells since expression of co-stimulatory molecules CD80, CD83 and CD86 remained very low or negative, whereas expression of HLA-I and HLA-II was intermediate (Figure 2B). To obtain LCs with a more mature phenotype, epidermal sheets were cultured for two days and the emigrated LCs were isolated. Emigrated LCs were partially mature since these cells expressed CD150 and high levels co-stimulatory molecules as well as HLA-I and II molecules (Figure 2B). Furthermore, Langerin expression was lower on emigrant LCs, which further highlights the more mature phenotype compared to isolated immature LCs. Throughout this paper we will refer to emigrant LCs as mature LCs, and to isolated LCs as immature LCs.

Antibodies to Langerin are internalized and presented in the context of HLA-II
We next investigated the internalization pathway of human Langerin by using an antibody against Langerin to exclude the involvement of other receptors. Human Epstein–Barr virus-transformed B-lymphoblastic cell line (BLCL)-OUW expressing Langerin (Supporting Information Figure 1) or mature primary human LCs were pulsed with a murine IgG1 monoclonal antibody specific for Langerin for 1h at 37°C. The antibody against Langerin was internalized and co-localized with the lysosomal marker Lamp-1 (Figure 3A). Immuno-electron-microscopic analysis showed that the anti-Langerin antibody was internalized into Birbeck granules (Figure 3B) and the internalized antibody co-localized with a polyclonal antibody used to detect Langerin, suggesting that the internalized antibody was still attached to Langerin (Figure 3B). A part of the internalized anti-Langerin antibody was observed in vesicles that were positive for Lamp-1 and/or HLA-DR (Figure 3C and D). Moreover, the internalized antibody was also detected in multi-vesicular bodies (Figure 3C and D, arrows) and incidentally in multi-laminar bodies (Figure 3D, complete left), which co-localized with HLA-DR (Figure 3D). These data suggest that Langerin-captured antigens are internalized into Birbeck granules and are at least partly targeted to the lysosomes, where antigen processing can occur.

We investigated whether the antibodies against human Langerin are processed and presented in the context of HLA-II molecules to $CD4^+$ T cells. We used the $CD4^+$ T-cell clone Hd7 that recognizes a peptide derived from murine IgG1 presented in a HLA-DR1-restricted manner [263]. Both HLA-DR1-matched primary mature LCs and the Langerin-expressing B-cell line were pulsed with an anti-Langerin antibody or an isotype control antibody. Next, the cells were co-cultured with the $CD4^+$ T-cell clone and IFNγ production was measured to determine T-cell activation [263]. BLCL-OUW cells expressing Langerin incubated with the anti-Langerin antibody-induced T-cell proliferation that was neither observed with mock-transduced cells nor with the isotype control antibody (Figure 3E). Primary LCs targeted with the anti-Langerin antibody-induced T-cell proliferation in a dose-dependent matter, which resulted from Langerin-mediated trafficking, since incubation with the isotype control antibody did

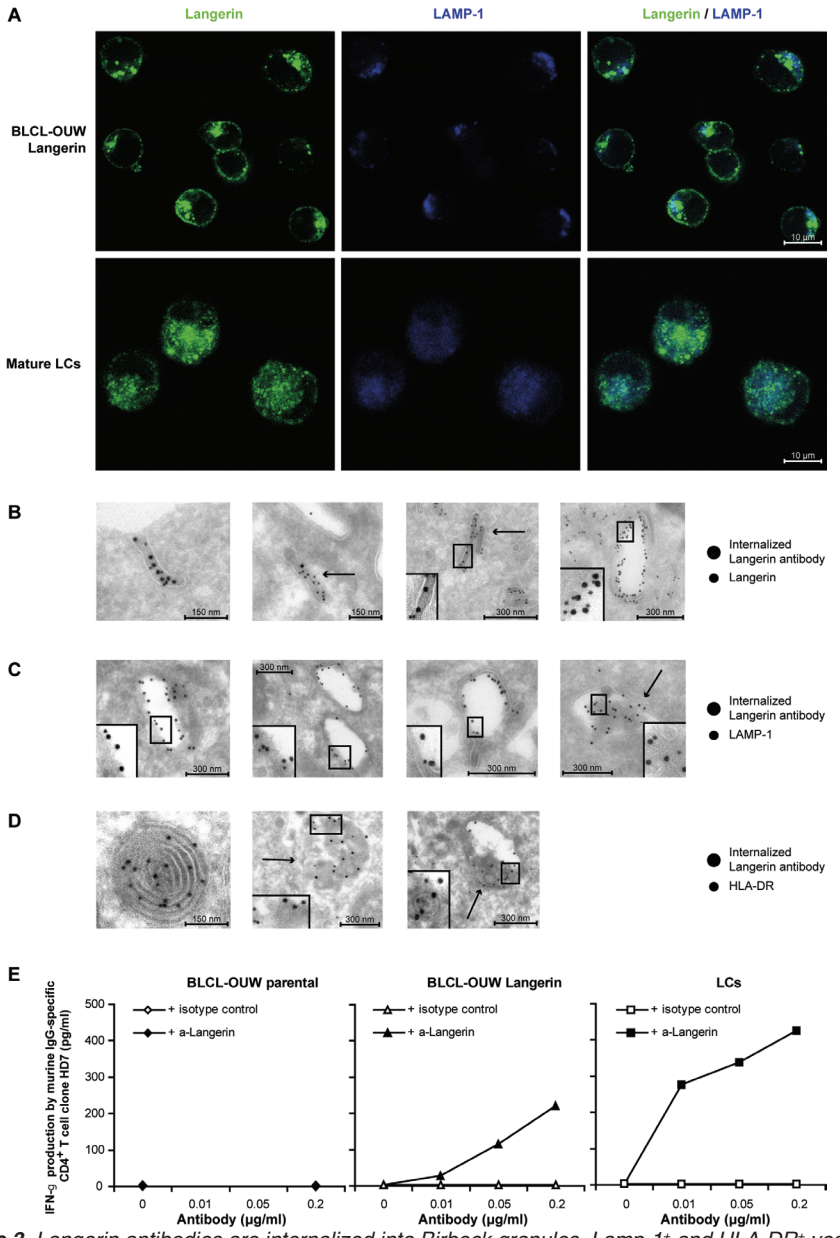

Figure 3. *Langerin antibodies are internalized into Birbeck granules, Lamp-1⁺ and HLA-DR⁺ vesicles, and are presented in the context of HLA-II. (A) BLCL-OUW-Langerin cells and mature LCs were stained with anti-Langerin (green) and anti-Lamp-1 (blue) for confocal microscopy. Representative for two independent experiments, original magnification 63×. (B–D) Mature LCs were incubated with DCGM4. The internalized antibodies were detected using immuno-gold-labeling antibody (15 nm). Cells were stained with goat-anti-Langerin (B), Lamp-1 (C) or HLA-DR (D) and detected using immuno-gold-labeling (10 nm) for electron microscopy. Inlays: co-localization of 10 and 15 nm gold-labeling. Arrows: Birbeck granules (B), multi-vesicular bodies (C,D). (E) BLCL-OUW, BLCL-OUW-Langerin or mature LCs were incubated with DCGM4 or an isotype control and IFNγ production of the co-cultured CD4⁺ HD7 T cells was measured. Data are representative of three independent experiments.*

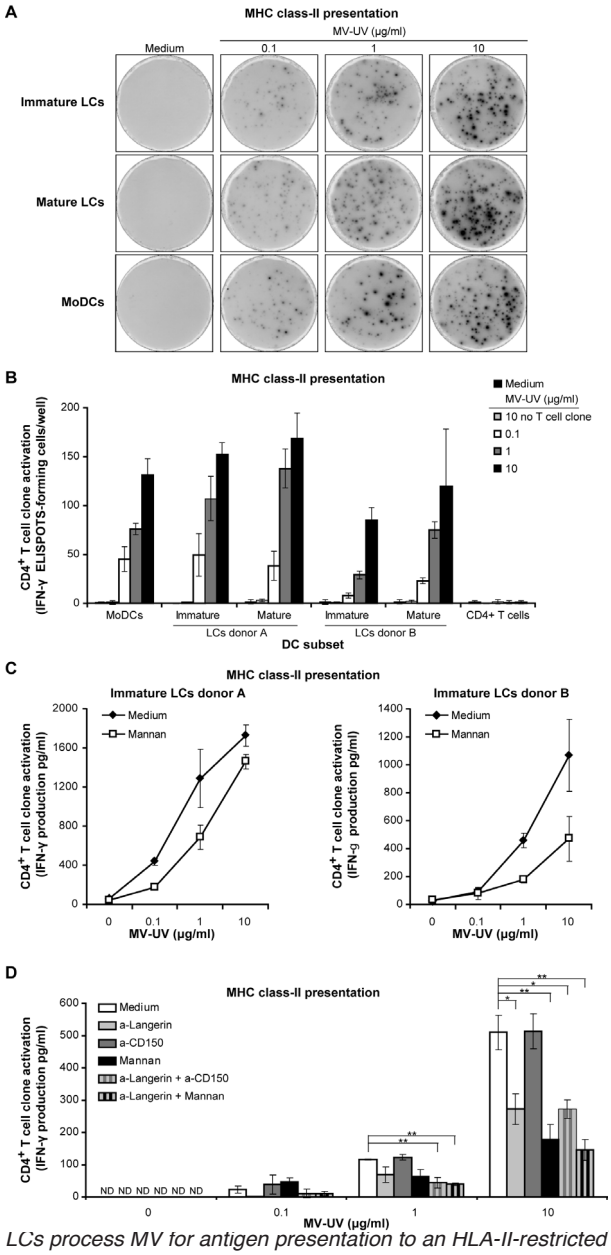

Figure 4. *Human LCs process MV for antigen presentation to an HLA-II-restricted MV-specific CD4+ T-cell clone. Immature LCs, mature LCs or DCs were incubated with MV-UV. (A,B) Activation of the co-cultured CD4+ T-cell clone GRIM-F99 was measured by ELISPOT. (A) Representative for three experiments. (B) Data represent average±SD of duplicates. (C,D) Immature LCs were pre-incubated with (C) medium (♦) or mannan (□), or (D) with anti-CD150, anti-Langerin, or mannan. Production of IFNγ was determined by ELISA. Data represent average ± SD of duplicates. *p < 0.05, **p < 0.01, tested by one-way ANOVA. ND: not detectable.*

not result in T-cell clone activation (Figure 3E). Thus, antigens targeted to Langerin expressed by primary human LCs are processed and presented in the context of HLA-II to $CD4^+$ T cells.

MV captured by LCs results in HLA-II-restricted antigen presentation

We investigated whether binding of MV by LCs results in antigen presentation to MV-specific $CD4^+$ T cells using the $CD4^+$ T-cell clone GRIM-F99 that recognizes a peptide derived from the MV envelope glycoprotein F in the context of HLA-DQw1 [150,234]. Activation of the T-cell clone GRIM-F99 does not require full co-stimulation. Human LCs expressing HLA-DQw1 were pulsed with UV-inactivated Edmonston MV (MV-UV) and co-cultured with the MV-specific $CD4^+$ T cells. Immature LCs directly isolated from skin were compared with mature LCs that had migrated out of the skin (Figure 2B). Both immature and mature LCs stimulated the MV-F-specific $CD4^+$ T-cell clone GRIM-F99 in a dose-dependent manner at comparable levels as monocyte-derived DCs (moDCs, Figure 4A and B). The $CD4^+$ T-cell clone alone did not produce IFNγ. Activation of the T-cell clone was comparable for both immature and mature LCs, which might be because activation of the T-cell clone is less dependent on co-stimulation of naive T cells. We observed for different donors that mannan partially inhibited antigen presentation of MV-derived peptides to the $CD4^+$ T-cell clone (Figure 4C). Antibodies against Langerin inhibited antigen presentation to a similar extent as mannan, whereas the combination of antibodies against Langerin and mannan did not result in more inhibition than the inhibitors alone (Figure 4D). These data confirm that Langerin is the only C-type lectin involved in MV capture on LCs. CD150 inhibition did not affect antigen presentation of MV, which is supported by the lack of CD150 expression on immature LCs (Figure 2B). Other receptors or uptake mechanisms might also be involved since the inhibition with Langerin inhibitors was partial. These data demonstrate that human LCs capture MV resulting in efficient antigen processing and presentation in the context of HLA-II molecules, which is partially dependent on Langerin.

LCs do not cross-present MV antigens

Immature LCs, in contrast to mature LCs, were not efficiently infected by MV (Figure 1F – I). We have used the MV-specific $CD8^+$ T-cell clone WH-F40 that recognizes a peptide derived from the MV envelope glycoprotein F in the context of HLA-B27, to investigate the potential of LCs for HLA-I-restricted antigen presentation. HLA-$B27^+$-typed immature LCs, mature LCs and moDCs were incubated with infectious MV or with the minimal 9-amino acid MV peptide. Next, the MV-F-specific $CD8^+$ T-cell clone was added and T-cell activation was measured [148]. All peptide-loaded DCs and LCs were able to induce IFNγ production by the MV-specific $CD8^+$ T-cell clone (Figure 5A and B), demonstrating that the expression of HLA-B27 and/or co-stimulatory molecules was sufficient in all three DC subsets. However, immature LCs did not activate the $CD8^+$ T-cell clone upon incubation with infectious MV, whereas moDCs and mature LCs both activated the $CD8^+$ T-cell clone (Figure 5A and B). These data suggest that immature LCs do not present MV antigens to $CD8^+$ T cells because these cells are not productively infected by MV.

To address the potential of LCs for cross-presentation, we tested all the three DC subsets for activation of the MV-specific CD8⁺ human T-cell clone after incubation with UV-inactivated MV. Inactivation was complete since the UV-inactivated viruses were not able to infect susceptible cells (data not shown). Under these conditions, moDCs reproducibly showed a dose-dependent potential for cross-presentation, which was enhanced when moDCs were matured by a maturation cytokine cocktail (Figure 5C). In contrast to moDCs, neither immature nor mature LCs were capable of activating MV-specific CD8⁺ T cells after incubation with different concentrations of UV-inactivated MV. Repeated antigen pulse over several days or activation with a maturation cocktail also failed to induce cross-presentation by LCs (Figure 5C; data not shown). These results demonstrate that antigen cross-presentation of cell-free MV by human primary LCs is inefficient and independent of activation state.

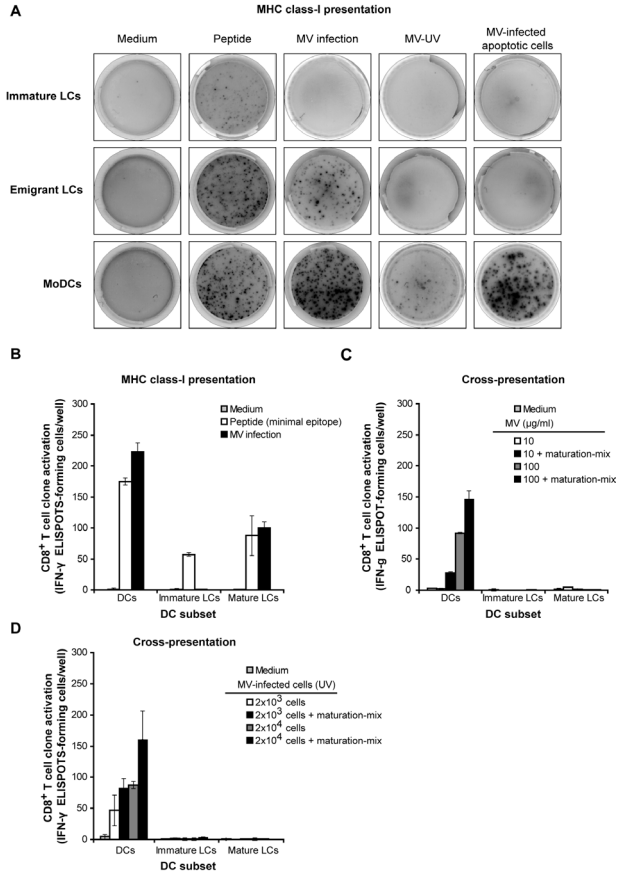

Figure 5. *Human LCs are incapable of cross-presenting MV antigens to an HLA-I-restricted MV-specific CD8⁺ T-cell clone. (A–D) Immature LCs, mature LCs or DCs were incubated with MV Edmonston or a minimal-peptide (B), MV-UV (C) or MV-infected HLA-mismatched BLCL-JP (D) and activation of the co-cultured CD8⁺ T-cell clone WH-F40 was measured by ELISPOT. In (C,D) APCs were incubated with maturation stimuli (TNFα, poly I:C and LPS) together with addition of the antigen. (A) Representative for two independent experiments. (B–D) Data are representative for two independent experiments and depict average ± SD of duplicates.*

Apoptotic virus-infected cells might be an important source for MV antigens *in vivo*. Therefore, we investigated cross-presentation of MV antigens derived from MV-infected cells by incubating the different DC subsets with UV-inactivated MV-infected BLCL-JP. The HLA-I type of the BLCL-JP was mismatched with the MV-specific T-cell clone to exclude antigen presentation by this MV-infected BLCL. Similar to that observed with cell-free virus particles, neither immature nor mature LCs were able to cross-present MV-derived peptides to the $CD8^+$ T cells when incubated with MV-infected apoptotic cells (Figure 5D). In contrast, moDCs efficiently cross-presented MV antigens derived from infected apoptotic cells to the specific $CD8^+$ T-cell clone in a dose-dependent manner (Figure 5D). Further activation of LCs by maturation stimuli did not induce cross-presentation. In summary, both immature and mature human primary LCs were incapable of cross-presentation of exogenous MV particles or MV-infected apoptotic cells to specific $CD8^+$ T cells.

Discussion

Different DC subsets can have distinct functions and therefore might differ in their antigen presentation capacity. Here, we have investigated the function of human LCs in MV infection and their ability to present MV-derived antigens to $CD4^+$ and $CD8^+$ T cells. We have identified Langerin as a binding receptor for MV on LCs that is involved in antigen presentation of MV-derived antigens to $CD4^+$ T cells. Immature LCs were not infected by MV and did not present viral antigens in the context of HLA-I. In contrast, mature LCs were productively infected, resulting in activation of MV- specific $CD8^+$ T cells by presentation of peptides derived from *de novo* synthesized MV proteins via the classical class I antigen presentation route. However, neither immature nor mature LCs were able to cross-present exogenous UV-inactivated MV particles or apoptotic MV-infected cells to $CD8^+$ T cells. These data suggest that primary human LCs are not efficient in activating $CD8^+$ T cells required for anti-viral immunity. Induction of naive HLA-I- restricted T-cell responses is therefore more likely to be mediated by other DC subsets.

MV is transmitted via the respiratory route, and thus the initial targets must be present in or on respiratory mucosal surfaces. LCs that express the C-type lectin Langerin are abundantly present in the epithelium of the upper respiratory tract. Our data show that Langerin is an attachment receptor for MV on LCs. Viruses captured by Langerin, but not CD150, on immature LCs are processed and presented to $CD4^+$ T cells. This is not specific to MV, because antibodies targeted to Langerin are also presented to $CD4^+$ T cells. Since Langerin is also an attachment receptor for HIV-1 [134], Herpes Simplex Virus-2 [267] and fungi [268], our data support a role for Langerin as a pathogen receptor. The MV envelope glycoproteins F and H contain high mannose structures [269] that are likely recognized by Langerin, similarly as shown for C-type lectin DC-SIGN [132]. This is further supported by the high similarity between the folding of the carbohydrate-binding domain of Langerin and DC-SIGN [270].

The fate of pathogens interacting with Langerin on LCs is not clear. Langerin recycles between the plasma membrane and early endosomes and is associated

with Birbeck granules [244]. Langerin internalizes HIV-1 [134] and Langerin-antibodies into Birbeck granules [247]. In contrast to previous observations [247], we observed that internalized antibodies are routed into Lamp-1$^+$ and HLA-II$^+$ vesicles. The importance of Langerin in routing antigens to the HLA-II presentation pathway is supported by our data showing that both anti-Langerin and MV captured by Langerin are processed and presented to CD4$^+$ T cells. Anti-Langerin as well as mannan partly inhibited presentation of MV antigens by HLA-II, suggesting that other receptors or other uptake mechanisms also contribute to antigen uptake. Our data suggest that pathogens captured by Langerin are processed for priming of CD4$^+$ T cells.

Classically, exogenous antigens are presented in the context of HLA-II, whereas endogenous-derived peptides are presented in the context of HLA-I molecules. However, several DC subsets have the capacity to cross-present exogenous antigens in the context of HLA-I molecules [240], a process that is relevant in infection by viruses that circumvent the classical HLA-I processing pathways. Murine myeloid DCs cross-present viral antigens and induce anti-viral CD8$^+$ T cells [271]. Murine LCs were reported to cross-present antigens [254] although a role for Langerin$^+$ dermal DCs was not excluded. More recently, *in vivo* studies indicate that murine Langerin$^+$ dermal DCs, but not LCs, are responsible for the induction of CD8$^+$ T-cell responses [272,273]. Our data show that human primary LCs cannot cross-present UV-inactivated MV and MV-infected apoptotic cells *in vitro*. Immature moDCs efficiently cross-presented UV-inactivated MV and infected apoptotic cells. In contrast, immature LCs were not able to cross-present exogenous-derived antigens to MV-specific CD8$^+$ T cells. The inability to cross-present MV antigens was independent of activation state of LCs, since neither immature nor mature LCs were able to cross-present MV antigens despite stimulation with a maturation cocktail. In a previous study, *in vitro*-generated human LCs were shown to cross-present an influenza-virus matrix protein to CD8$^+$ T cells [249]. The difference between both studies might be due to the origin of LCs. We have isolated primary LCs from epidermal sheets whereas Klechevsky *et al* used *in vitro*-generated monocyte- or CD34$^+$-derived LCs. It cannot be excluded that these *in vitro*-generated LCs differ from primary LCs in their antigen presentation pathways. Furthermore, cross-presentation by LCs might also depend on the uptake route: here, we used complete viruses and virus-infected cells that were internalized through receptors such as Langerin and CD150, whereas soluble proteins might be taken up via other routes. Further studies are required to investigate whether the inability of primary LCs to cross-present MV is a general phenotype, or specific for MV.

Our data show that immature LCs were not susceptible to MV infection whereas mature LCs were. Previously, immature LCs were found susceptible for MV [257], but they might have been more activated as others showed that mechanical stress facilitates LC activation and MV infection [258]. Therefore, differences in activation status of LCs determine susceptibility to MV.

MV infection has been shown to affect DC function; MV-infected DCs are unable to stimulate a mixed lymphocyte reaction and can induce lymphocyte unresponsiveness

through expression of MV glycoproteins [274,275]. Therefore, it is possible that MV interferes with the cross-presentation antigen-processing pathway of primary LCs. However, no MV replication could occur because the virus was UV-inactivated. Moreover, moDCs were able to cross-present to $CD8^+$ T cells after uptake of both MV and MV-infected apoptotic cells. Furthermore, MV-infected mature LCs are capable of presenting endogenous MV antigens in the context of HLA-I molecules. Taken together these results strongly suggest that capture of MV by primary LCs results in presentation of antigens in the context of HLA-II molecules, but does not lead to cross-presentation of MV to $CD8^+$ T cells.

Different studies have suggested a balance between efficient targeting of antigens for presentation in HLA-I or HLA-II [242,251,276]. Langerin internalizes antigens into Birbeck granules that might prevent antigens from entering the cross-presentation route or prevent triggering of pattern recognition receptors that could be required for cross-presentation [277]. However, we did not observe cross-presentation after activating LCs using different TLR ligands or other maturation stimuli.

In conclusion, our data suggest that LCs have a specialized function in MV infection; LCs are refractory to MV infection and do not induce MV-specific $CD8^+$ T cells. These data suggest that other DC subsets are responsible for inducing $CD8^+$ T-cell responses during MV infection. The finding that LCs are incapable of cross-presentation of MV *in vitro* might have implications for vaccine development where LCs are targeted to induce efficient $CD8^+$ T-cell responses.

Funding

This work was supported by a grant from the Dutch Scientific Research (NWO; no 917-46-367: L. de Witte, M. Litjens, M. A. W. P. de Jong NWO Vici 91810619: T.B.H. Geijtenbeek), Dutch AIDS foundation (2007036) (M. van der Vlist), ZonMw (91208012) (R. D. de Vries) and the VIRGO consortium (BSIK 03012) (R. L. de Swart).

Acknowledgements

The authors are grateful to A. Lanzavecchia for providing the HD7 T-cell clone, Y. Yanagi for providing the Vero-CD150 cells and the MV^{IC323}EGFP plasmid, W. P. Duprex for rescuing the MV^{IC323}EGFP virus and providing the $MV^{Edmonston}$EGFP virus, S. Schneider-Schaulies for providing the CHO-CD150 cells, the MV WTF strain, the purified UV-inactivated WTF and the antibodies to CD150 and MV-F, and R. S. van Binnendijk for providing the MV-specific T-cell clones and the purified UV-inactivated MV Edmonston. They also thank Y. van Kooyk for critical discussion.

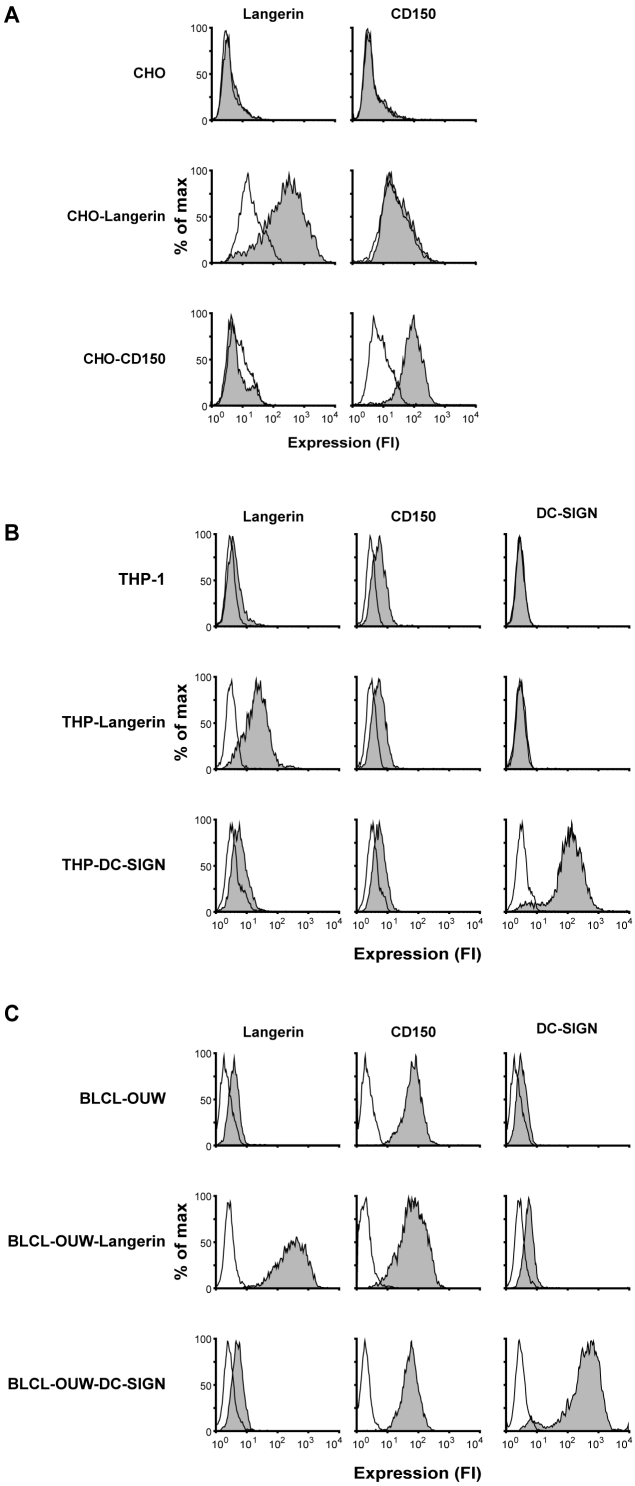

Supporting information figure 1. *Expression profiles of cell lines used. (A–C) Cells were analyzed for the expression of several markers by staining with antibodies and analysis by flow cytometry. Open histograms represent isotype control staining; filled histograms represent specific antibody staining. The data are representative at least two experiments.*

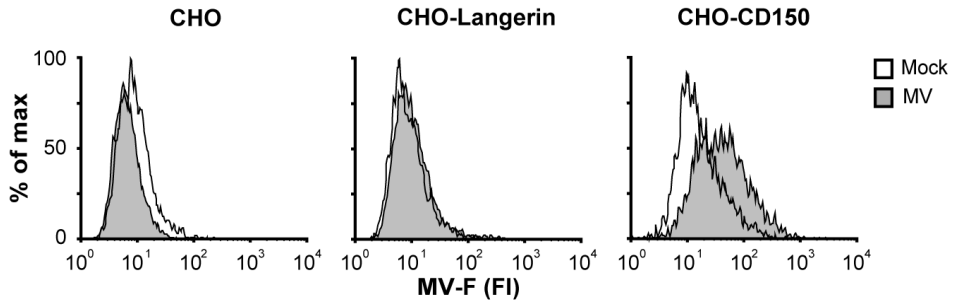

Supporting information figure 2. *Langerin is not an entry receptor for measles virus. Parental CHO, CHO-Langerin and CHO-CD150 were infected with MV-WTF. After 48 h infection was detected by staining for envelope glycoprotein F by flow cytometry.*

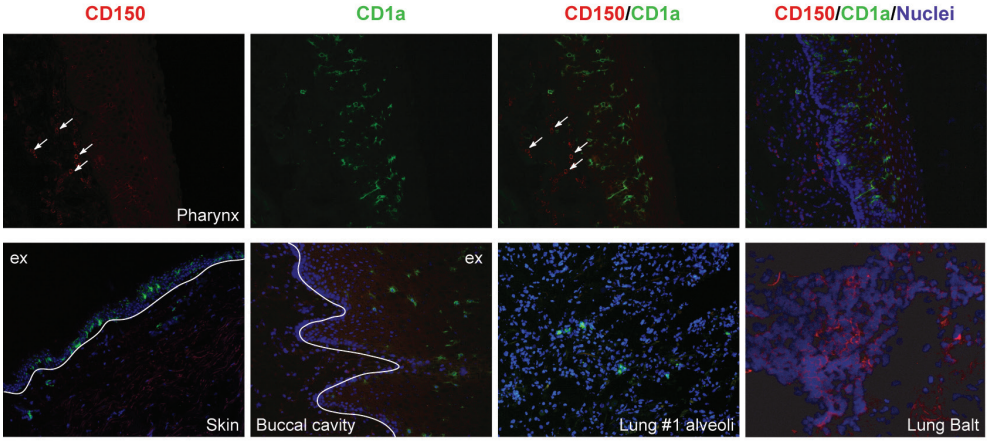

Supporting information figure 3. *CD150 and CD1a staining of respiratory tissue. Cryosections of different human tissues were stained for LC-marker CD1a (green) and CD150 (red). Nuclei were stained using Hoechst (blue). Sections were analyzed by fluorescence microscopy. The border between the epithelium/epidermis and subepithelium / dermis (white line), the site of the lumen or external environment (ex) and CD150$^+$ cells (arrows) are depicted. Background staining is present in the lungs and bronchi, probably due to auto-fluorescent mucus. Representative pictures are depicted.*

EARLY EVENTS AFTER MV INFECTION

3

Early target cells of measles virus after aerosol infection of non-human primates

Ken Lemon, Rory D. de Vries*, Annelies W. Mesman, Stephen McQuaid, Geert van Amerongen, Selma Yüksel, Martin Ludlow, Linda J. Rennick, Bert K. Rima, Teunis B.H. Geijtenbeek, Albert D.M.E. Osterhaus, W. Paul Duprex and Rik L. de Swart*

* both authors contributed equally

PLoS Pathogens 2011 Jan; 7(1): e1001263

Abstract

Measles virus (MV) is highly infectious, and has long been thought to enter the host by infecting epithelial cells of the respiratory tract. However, epithelial cells do not express signaling lymphocyte activation molecule (CD150), which is the high-affinity cellular receptor for wild-type MV strains. We have generated a new recombinant MV strain expressing enhanced green fluorescent protein (EGFP), based on a wild-type genotype B3 virus isolate from Khartoum, Sudan (KS). Cynomolgus macaques were infected with a high dose of $rMV^{KS}EGFP$ by aerosol inhalation to ensure that the virus could reach the full range of potential target cells throughout the entire respiratory tract. Animals were euthanized 2, 3, 4 or 5 days post-infection (d.p.i., n = 3 per time point) and infected ($EGFP^+$) cells were identified at all four time points, albeit at low levels 2 and 3 d.p.i. At these earliest time points, MV-infected cells were exclusively detected in the lungs by fluorescence microscopy, histopathology and/or virus isolation from broncho-alveolar lavage cells. On 2 d.p.i., $EGFP^+$ cells were phenotypically typed as large mononuclear cells present in the alveolar lumen or lining the alveolar epithelium. One to two days later, larger clusters of MV-infected cells were detected in bronchus-associated lymphoid tissue (BALT) and in the tracheo-bronchial lymph nodes. From 4 d.p.i. onward, MV-infected cells were detected in peripheral blood and various lymphoid tissues. In spite of the possibility for the aerosolized virus to infect cells and lymphoid tissues of the upper respiratory tract, MV-infected cells were not detected in either the tonsils or the adenoids until after onset of viremia. These data strongly suggest that in our model MV entered the host at the alveolar level by infecting macrophages or dendritic cells, which traffic the virus to BALT or regional lymph nodes, resulting in local amplification and subsequent systemic dissemination by viremia.

Author Summary

Measles remains an important vaccine-preventable cause of morbidity and mortality in developing countries. The causative agent, measles virus (MV), is one of the most contagious viruses known. Measles has an incubation time of approximately two weeks, and surprisingly little is known about the early events after MV infection. Epithelial cells in the upper respiratory tract have long been considered as early target cells, but more recently alveolar macrophages (AM) and dendritic cells (DC) have been proposed as alternatives. We have infected cynomolgus macaques with a high dose of a recombinant EGFP-expressing MV strain via aerosol inhalation, to ensure that the virus had access to the entire respiratory tract. At 2 days post-infection, MV-infected mononuclear cells were detectable in the alveolar lumen but not in the upper respiratory tract. These infected cells migrated through the bronchus-associated lymphoid tissue to the draining tracheo-bronchial lymph node at 3 days post-infection. Systemic infection was initiated from this point, as observed in macaques euthanized 4 or 5 days post infection. Thus, even though the aerosolized virus had access to epithelial cells and lymphoid tissues along the entire respiratory tract, AM and DC in the lungs were the first cells that sustained MV replication.

Introduction

Measles virus (MV) is one of the most contagious human viruses known, and is transmitted via aerosols or by direct contact with contaminated respiratory secretions. Clinical signs appear approximately two weeks after infection and include fever, rash, cough, coryza and conjunctivitis [16]. Measles is associated with a transient but profound immunosuppression, resulting in increased susceptibility to opportunistic infections. While significant progress has recently been made in global control programs, 164,000 deaths were still attributed to measles in 2008 [278].

It has been well established that MV infects cells via receptor-dependent fusion of the virion at the plasma membrane [279]. Two cellular receptors for MV have been identified. In 1993 the membrane cofactor protein CD46, expressed by virtually all nucleated human cells, was the first protein to be identified as MV receptor [110,111]. However, it soon became evident that only vaccine and laboratory-adapted MV strains were able to utilize this molecule as an entry receptor [112]. Signaling lymphocyte activation molecule (SLAM or CD150), a membrane glycoprotein expressed on subsets of immune cells, was identified as the receptor for wild-type MV strains in 2000 [113,114]. It is now generally accepted that pathogenic wild-type MV strains use CD150 as high affinity cellular receptor, whereas vaccine and laboratory-adapted strains can use either CD46 or CD150. Distribution of CD150 explains most, but not all aspects of measles pathogenesis and it may be possible that the utilization of additional low-affinity cellular receptors explains how wild-type viruses enter $CD150^-$ epithelial or neuronal cells [127,128,137].

Previously, we successfully infected macaques with a recombinant MV based on the pathogenic IC323 strain [52] that expresses enhanced green fluorescent protein (EGFP) from a promoter-proximal additional transcription unit (ATU); this wild-type recombinant virus (rMV^{IC323}EGFP) uses CD150 but not CD46 as a cellular entry receptor *in vitro* [53]. In macaques, rMV^{IC323}EGFP proved to be virulent and CD150-expressing lymphocytes and dendritic cells (DC) were identified as the predominant target cells for MV replication [54]. In a more recent study, macaques were infected with a rMV^{IC323} that inefficiently binds CD150, showing that this virus was attenuated and indicating that CD150-mediated entry is indeed essential for MV to be fully virulent *in vivo* [116].

In vitro studies have demonstrated that at a high multiplicity of infection (MOI) wild-type MV can infect cells that do not express CD150, although this process is inefficient and usually does not result in cell-to-cell spread or virus release [53]. However, a number of $CD150^-$ cell types of epithelial or neuronal origin have been identified in which wild-type MV infection at a low MOI results in cytopathic effects and virus release [127,128,137]. It is thought that entry into these $CD150^-$ cells is mediated by an unidentified cellular receptor for MV, which is often referred to as the epithelial cell receptor (epR). Even though the receptor has not been identified, epR-binding sites on the MV hemagglutinin protein have been mapped [127,137], and the receptor appears to be a protein expressed on the basolateral side of polarized epithelial cells associated with tight junctions [125,137,280]. In human tissues, cells within the

epithelium have historically been shown to be infected by wild-type MV. More recently, epithelial cell infection has been demonstrated with dual immunofluorescence, using the recombinant rMV^{IC323}EGFP strain in non-human primates [54,125]. However, the limited epithelial cell infection observed predominantly occurs in the presence of substantial infection of lymphoid and myeloid cells, which is consistent with the differential expression of CD150 on these cell types.

It has been postulated that MV infection starts from the luminal side of the upper respiratory epithelium [16]. However, there is no direct evidence for initial MV infection and replication in epithelial cells. Furthermore, the absence of CD150 or epR on the apical side of these cells makes it highly unlikely that respiratory epithelial cells are an initial target for MV. However, the respiratory epithelium contains many other cell types besides epithelial cells. Several research groups have postulated new strategies for MV to enter a host, namely via direct initial infection of CD150$^+$ immune cells present throughout the respiratory tract and interdigitated within the epithelium [54,117]. In 2006, the C-type lectin DC-SIGN was identified as an attachment receptor for MV [132]. *In vitro* DC-SIGN expressing DC could efficiently capture and transmit MV to CD4$^+$ and CD8$^+$ T-lymphocytes expressing CD150. This suggests a potential role for the DC as an initial target cell *in vivo*, where DC capture the virus from the luminal side of the respiratory tract and, with or without productive infection, transport the virus to draining lymph nodes (LN) containing many CD150$^+$ cells, thereby initiating the typical systemic infection [132,255].

In the present study, we have generated a rMV based on a genotype B3 wild-type MV isolate from Khartoum, Sudan. The open reading frame (ORF) encoding EGFP was introduced into the virus genome in the promoter-proximal position within an ATU using a similar approach as previously described for rMV^{IC323}EGFP [52]. In an attempt to identify the early target cells of MV in non-human primates, macaques were infected with rMV^{KS}EGFP and sacrificed 2, 3, 4 or 5 days post-infection (d.p.i). Infections were performed by inhalation of a high dose of virus formulated as small-particle size nebulized aerosol, thus exposing the entire upper and lower respiratory tract to the virus. MV-infected EGFP$^+$ cells were identified at all four time points, albeit at low levels 2 and 3 d.p.i. Infection is initiated in large mononuclear cells in the alveolar lumen, most likely either AM or DC.

Materials & Methods

Ethics statement

Animals were housed and experiments were conducted in strict compliance with European guidelines (EU directive on animal testing 86/609/EEC) and Dutch legislation (Experiments on Animals Act, 1997). The protocol was approved by the independent animal experimentation ethical review committee DCC in Driebergen, the Netherlands (Erasmus MC permit number EUR1664). Animal welfare was observed on a daily basis, and all animal handling was performed under light anesthesia using a mixture of ketamine and medetomidine to minimize animal suffering. After handling atipamezole was administered to antagonize the effect of medetomidine.

Generation of wild-type recombinant MV expressing EGFP

rMV^{KS}EGFP is based on a wild-type genotype B3 virus isolated from PBMC collected in 1997 from a severe measles case in Khartoum, Sudan [87]. The clinical isolate (MV^{KS}) was passaged exclusively in CD150^{+} human B-LCL and was previously shown to be highly pathogenic in macaques [281]. Total RNA was isolated from B-LCL infected with MV^{KS} and the complete consensus genomic sequence determined following RT-PCR (GenBank accession number HM439386). The sequences of the genomic termini were confirmed by 5' RACE. A full-length cDNA which expressed the MV^{KS} anti-genome (pMV^{KS}) was constructed based on a modified pBluescript vector [282]. A single silent mutation was introduced into the N ORF (T1245C) to act as a genetic tag to distinguish recombinant virus from the clinical isolate. The full-length plasmid was modified further by the introduction of an ATU expressing EGFP at the promoter proximal position to generate pMV^{KS}EGFP. Plasmid sequences are available on request. Recombinant viruses were recovered from MVA-T7-infected Vero-SLAM cells transfected with the full-length plasmids along with plasmids expressing MV N, P and L. Virus stocks were grown in B-LCL and tested negative for contamination with *Mycoplasma* species. Virus titers were determined by endpoint titration in Vero-SLAM cells, and expressed in 50% cell culture infectious dose ($CCID_{50}$).

Virus fitness of MV^{KS}, rMV^{KS}, rMV^{KS}EGFP and rMV^{IC323}EGFP was compared in a growth curve. Human B-LCL were infected in triplicate with MV^{KS}, rMV^{KS}, rMV^{KS}EGFP or rMV^{IC323}EGFP in 24-wells plates at MOI 0.1. At 24, 48, 72 and 96 hours post infection plates were freeze-thawed at –80°C, and cells and supernatant fluids were harvested. After sonification and clarification, the amounts of cell-free virus at different time-points were determined by endpoint titration in Vero-CD150 cells using ten-fold dilutions and testing eight wells per dilution, and expressed in $CCID_{50}$.

Early target cell animal study

Twelve juvenile, MV-seronegative cynomolgus macaques (*Macaca fascicularis*) were housed in negatively pressurized, HEPA-filtered BSL-3 isolator cages. Animals were infected with rMV^{KS}EGFP by aerosol inhalation using a pediatric face mask (ComfortSeal silicone mask assembly, small, Monaghan Medical Corp., Plattsburgh NY). Aerosol was generated using the Aerogen Aeroneb Lab nebulizer with an OnQ aerosol generator (kind gift of Dr. J. Fink, Aerogen) as previously described [265]. This nebulizer generates a small particle size aerosol (VMD 4–6 µm), which is deposited on epithelia throughout the entire respiratory tract upon inhalation [283]. A total dose of 10^6 $CCID_{50}$ was nebulized, but we previously found that a substantial part of nebulized virus is lost due to inactivation during nebulization, condensation in the nebulizer tubing or face mask, deposition on the skin of the animals or deposition in the mouth followed by swallowing. We therefore estimated that the delivered dose was approximately 10^5 $CCID_{50}$, of which based on previous studies approximately 10% is expected to reach epithelia in the lungs [283]. Animals were euthanized on 2, 3, 4 or 5 d.p.i. (n = 3 per time point).

Necropsy
Animals were euthanized by sedation with ketamine (20 mg/kg body weight) followed by exsanguination. Macroscopic detection of EGFP was performed at necropsy as described previously [54]. Briefly, fluorescence was detected with a custom-made lamp containing 6 LEDs (peak emission 490 – 495 nm); emitted fluorescence was detected through an amber cover of a UV transilluminator used for screening DNA gels. Photographs were made using a Nikon D80 SLR camera. Organs were collected in PBS, directly processed and screened for presence of EGFP by UV microscopy. From here, $EGFP^+$ samples were transferred to 4% (w/v) paraformaldehyde in PBS (to preserve EGFP autofluorescence) or to 10% neutral buffered formalin. The left lung lobe was inflated as described previously [284] using a solution of 4% (w/v) agarose in PBS mixed 1:1 with DMEM/Ham's F12 medium supplemented with L-glutamine (2 mM), 10% (v/v) heat-inactivated fetal bovine serum (FBS), penicillin (100 U/ml) and streptomycin (100 µg/ml). The inflated lung was allowed to solidify on ice, and ~1 mm slices were cut by hand. Slices were permeabilized with 0,1% (v/v) Triton-X100, counterstained with DAPI and directly analyzed for EGFP fluorescence by confocal laser scanning microscopy with a LSM700 system fitted on an Axio Observer Z1 inverted microscope (Zeiss). Images and videos were generated using Zen software.

Blood samples
Small volume blood samples were collected in Vacuette tubes containing K_3EDTA as an anticoagulant daily after infection. White blood cells (WBC) were obtained by treatment of EDTA blood with red blood cell lysis buffer (Roche diagnostics, Penzberg, Germany) and used directly for detection of EGFP by flow cytometry. During necropsy blood was collected in heparin to prevent coagulation, PBMC were isolated by density gradient centrifugation, washed, resuspended in complete RPMI-1640 medium (Gibco Invitrogen, Carlsbad, CA, USA) supplemented with L-glutamine (2 mM), 10% (v/v) heat-inactivated FBS, penicillin (100 U/ml) and streptomycin (100 µg/ml), counted using a haemocytometer and used directly for flow cytometry and virus isolation. Isolation of MV was performed on human B-LCL using an infectious center test as previously described [281]. Virus isolations were monitored by UV microscopy for EGFP fluorescence after co-cultivation with B-LCL for 3 – 6 days and results were expressed as number of virus-infected cells per 10^6 total cells.

Broncho-alveolar lavage
A BAL was performed post-mortem by direct infusion of 10 ml PBS into the right lung lobe. BAL cells were resuspended in culture medium with supplements as described above, counted and used directly virus isolation. Virus isolation was performed on B-LCL as described above. The remaining BAL cells were examined for EGFP expression by UV microscopy.

Throat and nose swabs
Throat and nose swabs were collected daily in transport medium (EMEM with Hanks' salts, supplemented with lactalbumine enzymatic hydrolysate, penicillin, streptomycin, polymyxine B sulphate, nystatin, gentamicin and glycerol) and frozen

at -80°C. After thawing samples were vortexed, the swab was removed and the remaining transport medium was used for virus isolation [285]. Isolation of MV was performed on Vero-SLAM cells using an infectious center test as previously described [281]. The isolations were screened for EGFP fluorescence at day 3 and 7 post titration and results are expressed as the number of $EGFP^+$ wells per 96 total wells.

Lymphoid organs
Lymphoid organs were collected during necropsy in PBS for direct preparation of single cell suspensions using cell strainers with a 100 µm pore size (BD Biosciences). Single cell suspensions were used directly for detection of EGFP by flow cytometry. From a selection of lymphoid organs (retropharyngeal LN, mandibular LN, tonsil and tracheobronchial LN) single cell suspensions were also used for virus isolation on Vero-SLAM cells as described above. The isolations were screened for EGFP fluorescence at day 3 and 7 post titration. The axillary and tracheobronchial LN were also collected in RNA later (Ambion) during necropsy for virus detection by real-time RT-PCR.

Flow cytometry
Freshly isolated WBC, PBMC and single cell suspensions prepared from lymphoid organs were analyzed unstained for EGFP expression by flow cytometry. EGFP was detected in the FITC channel on a FACS Canto II, approximately 10^6 events were obtained per sample to allow detection of low frequent $EGFP^+$ populations.

Immunohistochemical and immunofluorescence analysis of fixed tissues
Only lung slices which were scored positive on live UV fluorescent screening were processed to paraffin. At days 2 and 3, 8/49 and 16/95 slices were scored positive, respectively. Sections (7 µm) were cut and deparaffinized, antigen retrieval was performed in a pressure cooker at full power for 3 min in 0.01 M TRIS-EDTA buffer (pH 9.0). MV-infected cells were detected using a polyclonal rabbit antibody to EGFP (Invitrogen). Sections were incubated in primary antibody overnight at 4°C, and specific antibody-antigen binding sites were detected using an Envision-Peroxidase system with DAB (DAKO) as substrate. Dual labeling indirect immunofluorescence was performed using polyclonal rabbit anti-EGFP and monoclonal mouse antibodies to the macrophage/DC marker CD11c (Novocastra, clone 5D11), the T-lymphocyte marker CD3 (DAKO, clone F7.2.38), the B-lymphocyte marker CD20 (DAKO, clone L26), the epithelial cell marker cytokeratin (DAKO, clone AE1/AE3), the endothelial cell marker CD31 (DAKO, clone JC70A) and the macrophage marker Mac387 (Abcam). Further dual labeling to assess the organization of epithelia and different cell types within BALT were carried out with a polyclonal antibody to epithelial cytokeratin (DAKO, Cat. No. Z0622) in combination with the above monoclonal antibodies to CD3, CD20 or CD11c. In all cases antigen binding sites were detected with a mixture of anti-mouse Alexa 568 and anti-rabbit Alexa 488 (Invitrogen). Sections were counterstained with DAPI hardset mounting medium (Vector). All fluorescently stained slides were assessed and digital fluorescent images acquired with a Leica DFC350 FX digital camera and processed using Leica FW4000 software.

Results

Generation and characterization of rMV^{KS}EGFP

MVi/Khartoum.SUD/34.97/2 (MV^{KS}) was isolated from a measles case in Khartoum, Sudan in 1997 [48,87,286]. This virus was previously shown to be highly virulent in macaques [281]. A consensus sequence of the complete viral genome was derived *de novo*, including the 3' and 5' ends which were sequenced following rapid amplification of cDNA ends (RACE), and a full-length anti-genomic plasmid (pMV^{KS}) was constructed (Figure 1A). The plasmid was modified by the addition of an ATU encoding EGFP at the promoter proximal position (Figure 1A) to generate pMV^{KS}EGFP. Recombinant viruses rMV^{KS} and rMV^{KS}EGFP were recovered following transfection of Vero-SLAM cells, and were passaged exclusively on Epstein-Barr virus-transformed human B-lymphoblastic cells (B-LCL) (Figure 1B). Presence of a silent point mutation in the MV nucleocapsid (N) ORF (T1245C) acts as a genetic tag and its presence was confirmed by RT-PCR and sequencing of the ORF (data not shown). Observation of rMV^{KS}EGFP by fluorescence microscopy revealed a high level of EGFP expression associated with single infected cells and multinucleated syncytia. Growth analysis of MV^{KS}, rMV^{KS}, rMV^{KS}EGFP and rMV^{IC323}EGFP in B-LCL over a period of 4 days demonstrated that the viruses reached equivalent titers (Figure 1C).

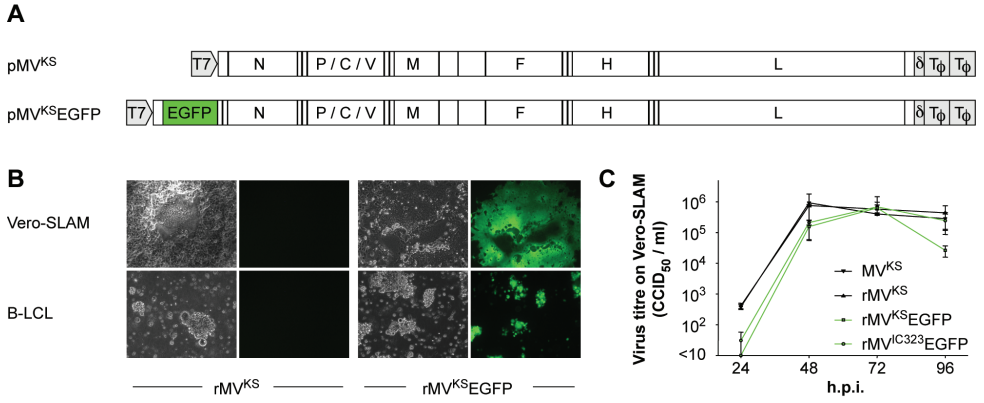

Figure 1. *Generation and growth of rMV^{KS}EGFP. (A) Plasmids generated after RT-PCR, cloning and sequencing of MV RNA isolated from MV^{KS}-infected PBMC. pMV^{KS} is a full-length plasmid containing the complete antigenome of MV^{KS} and pMV^{KS}EGFP was modified by the insertion of an ATU at the promoter proximal position containing the ORF encoding EGFP. (B) rMV^{KS} and rMV^{KS}EGFP were rescued from Vero-SLAM cells and passaged in B-LCL. Fluorescence microscopy confirmed high levels of EGFP expression in rMV^{KS}EGFP-infected cells. (C) Growth curves of MV^{KS}, rMV^{KS}, rMV^{KS}EGFP and rMV^{IC323}EGFP in human B-LCL. Virus was harvested 24, 48, 72 and 96 hours post infection, CCID$_{50}$ was determined in an endpoint titration test. Measurements shown are averages of triplicates ± SD. Key: h.p.i.: hours post infection.*

Early rMV^{KS}EGFP replication in the respiratory tract

Four groups of three cynomolgus macaques were infected with rMV^{KS}EGFP via the aerosol route as described previously [265]. Throat and nose swabs were collected daily and virus isolations were performed to determine the MV load in these clinical

samples. Necropsies were performed 2, 3, 4 and 5 d.p.i. BAL cells were collected for virus isolation and the entire respiratory tract was screened macroscopically and microscopically for fluorescence by live cell UV fluorescence and confocal scanning laser microscopy. At 2 and 3 d.p.i., no macroscopic fluorescence was detectable, probably because of low levels of viral replication. No virus could be isolated from the nose, whereas from throat swabs virus was only isolated at 4 (2/6 animals) and 5 (3/3 animals) d.p.i. (Figure 2A). However, MV was isolated from BAL cells as early as 2 d.p.i. (2/3 animals) and by 3, 4 and 5 d.p.i. virus was isolated from BAL cells of all animals with virus loads increasing over time (Figure 2A). Microscopic detection of MV replication in freshly collected tissues of the respiratory tract proved that as early as 2 d.p.i. the virus was consistently present in the lungs of all animals (Figure 2B). On 2 and 3 d.p.i. single infected mononuclear cells with the appearance, size and typical tissue distribution of AM and/or DC were detected attached to the alveolar wall or inside the alveolar lumen. At these time points no MV-infected epithelial cells were detected in the lungs of any animal, either phenotypically, following screening of lung slices for EGFP$^+$ cells or histologically, by dual staining of MV proteins and cytokeratin. MV-infected cells could not be detected in the nasal septum, nasal concha, nasal lining, trachea or primary bronchus 2 and 3 d.p.i. By 4 d.p.i. a fluorescent signal was detected in the nasal septum of a single animal, and by 5 d.p.i. the nose, trachea and primary bronchus were consistently positive (Table 1).

Table 1. *Dissemination of MV in tissues during early stage of infection. Numbers indicate the number of macaques with EGFP$^+$ cells in this tissue (n = 3). [1]LN: lymph node. [2]PBMC: peripheral blood mononuclear cells. [3]GALT: gut-associated lymphoid tissue. [4]-: no EGFP$^+$ cells detected.*

	Days post infection (d.p.i.)			
Tissue	**2**	**3**	**4**	**5**
Lung	3	3	3	3
Tracheobronchial LN[1]	1	3	3	3
PBMC[2]	-[4]	-	3	3
Adenoid	1	-	3	3
Retropharyngeal LN	-	-	1	3
Mandibular LN	-	-	-	3
GALT[3]	-	-	1	3
Spleen	-	-	1	2
Tonsil	-	-	1	1
Thymus	-	-	1	1
Nasal septum	-	-	1	1
Nasal concha	-	-	-	2
Trachea	-	-	-	2
Inguinal LN	-	-	-	2
Axillary LN	-	-	-	1
Mesenteric LN	-	-	-	1

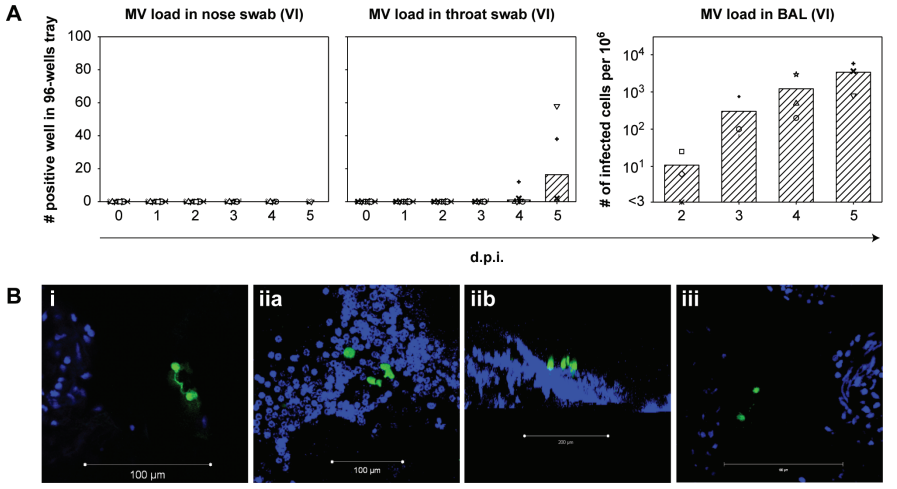

Figure 2. *Early rMV^{KS}EGFP replication in the respiratory tract. (A) Virus isolation performed from nose and throat swabs (left two panels), and from BAL cells (right panel). Each symbol represents an individual animal, bars indicate the geometric mean. Key: VI: virus isolation; d.p.i.: days post infection. (B) Live cell confocal microscopy performed on agarose-inflated lung slices from animals on 2 and 3 d.p.i. EGFP$^+$ cells are shown in green, DAPI was used to counter stain nuclei (blue). Three images were collected, labeled i, ii and iii. Panels iia and iib show infected cells in one image from different orientations.*

Systemic rMV^{KS}EGFP replication

Virus isolations were performed from peripheral blood mononuclear cells (PBMC) and single cell suspensions of four lymphoid organs (retropharyngeal LN, mandibular LN, tonsil and tracheo-bronchial LN). RNA isolations and virus detection by RT-PCR were performed on the axillary LN and tracheo-bronchial LN, which drain the arm and the lungs, respectively. Furthermore, PBMC and all lymphoid organs were analyzed directly by flow cytometry and UV microscopy for fluorescence. Viremia was detected in all animals on 4 and 5 d.p.i. but in none of the animals sampled 2 and 3 d.p.i. (Figure 3A, left panel, and Table 1). Virus was not isolated from any lymphoid organ 2 d.p.i. However, by 3 d.p.i. virus was isolated from the tracheo-bronchial LN of all animals (data not shown). RT-PCR and flow cytometry confirmed the early presence of MV in the tracheo-bronchial LN, but not in more distally located LN, for example the axillary and retropharyngeal LN (Figure 3A, right panel and Figure 3B). Flow cytometry confirmed that the number of EGFP$^+$ cells increased over time. Virus was detected by almost all methods in multiple lymphoid organs 4 and 5 d.p.i. by which time the MV was spreading systemically (Table 1). Macroscopic detection of EGFP proved possible only 4 and 5 d.p.i (Figure 3C). The tonsil of a single animal was positive 4 d.p.i . By 5 d.p.i. MV was detected macroscopically at multiple locations (adenoids, tonsil, retropharyngeal LN, trachea, tongue, tracheo-bronchial LN) in all animals indicating widespread dissemination. Phenotyping of the MV-infected cells in PBMC or single cell suspensions of lymphoid tissues collected on 4 and 5 d.p.i. showed that these were predominantly T- or B-lymphocytes (data not shown).

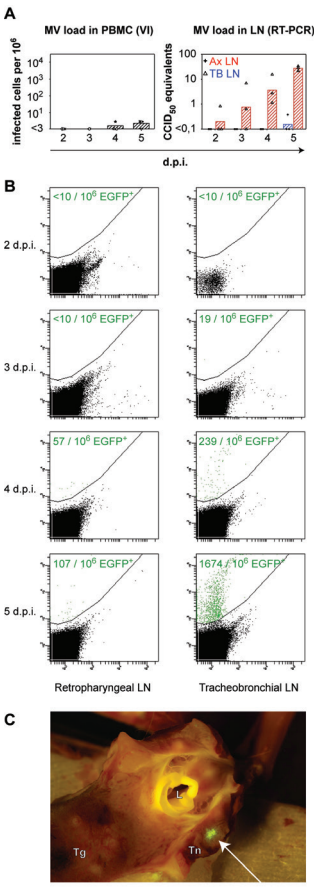

Figure 3. *Systemic rMV^{KS}EGFP replication. (A) MV load in PBMC and LN. The left panel shows virus isolations performed from PBMC, each symbol represents an individual animal, bars indicate the geometric means. The right panel shows the presence of MV genome in the axillary LN (crosshairs, geometric mean in blue) and in the tracheobronchial LN (triangles, geometric mean in red). Key: VI: virus isolation; RT-PCR: real-time reverse transcriptase PCR; d.p.i.: days post infection. (B) Detection of EGFP$^+$ cells by flow cytometry from the retropharyngeal LN (left) and the tracheobronchial LN (right) on 2, 3, 4 and 5 d.p.i. Data are shown as dot plots of FL-1 (EGFP) versus FL-2 (empty channel), generated with BD FACSDiva software. In these plots autofluorescent cells usually appear on a diagonal line as they cause comparable signals in both channels. The EGFP$^+$ events were gated as indicated by the curvilinear line. Data of a representative animal are shown on each time point. Numbers of EGFP$^+$ cells per million total cells are shown in each plot. (C) Representative example of macroscopic EGFP detection at 5 d.p.i. Arrow indicates the infected tonsillar tissue expressing EGFP. Key: Tg: tongue; Tn: tonsil; L: larynx.*

Phenotyping of early MV-infected cells in the lungs

Early after infection MV was consistently present in the lungs. In order to characterize the early target cells, live agarose-inflated lung slices containing EGFP$^+$ cells were formalin-fixed and paraffin-embedded. Serial sections were cut and used for immunohistochemistry and indirect immunofluorescence to determine the precise location of MV infection, identify the phenotype of the infected cells and gain an understanding of how such “seeding” of MV infection in the lungs might lead to the establishment of systemic infection. At 3 d.p.i., two foci of infection were identified in paraffin-embedded lung sections of one of the three infected animals, interestingly both in BALT (Figure 4A). These BALT structures were lined by a cytokeratin-positive epithelial cell layer and contained numerous immune cells (Figure 4B), that stained positive with CD11c for AM or DC, Mac387 for macrophages, CD20 for B-lymphocytes and/or CD3 for T-lymphocytes. Blood vessels, identified using the endothelial cell-specific marker CD31, were always present in BALT structures irrespective of the presence or absence of MV-infected cells. Since there were a limited number of foci of infection identified this early after infection, we were unable to quantify the levels of infection in different cell types. However, MV-infected B-lymphocytes, T-lymphocytes and DC could readily be detected by specific dual labeling at higher magnifications

(Figure 4C and Figure S2). Multiple foci of MV-infected cells were detected 4 and 5 d.p.i. in the alveolar lumina and walls of all animals and the majority of these infected cells were CD11c$^+$ (Figure S1), consistent with what had been observed previously in macaques euthanized 7 d.p.i. [265].

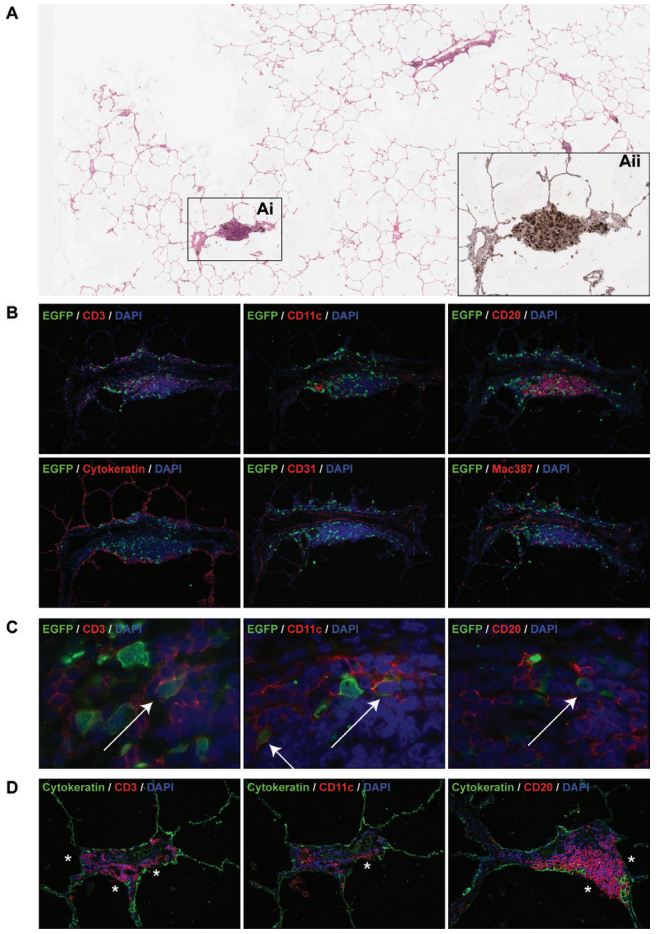

Figure 4. *Characterization of MV infection in BALT structures. (A) H&E staining on lung slice from an animal euthanized on 3 d.p.i.. The number of EGFP$^+$ foci was extremely low, the boxed area (Ai) is a BALT which was the only area on the section where EGFP$^+$ cells were present. (Aii) shows a serial section stained with anti-GFP (black) to detect the presence of virus. (B) Indirect dual immunofluorescence of the infected BALT structure, showing the presence of T-lymphocytes (CD3), DC or macrophages (CD11c, mac387) and B-lymphocytes (CD20) within the BALT. The BALT is lined by a layer of cytokeratin-positive epithelial cells, and has a blood vessel with CD31$^+$ endothelium running through it transversely. (C) Higher magnifications of dual immunofluorescence within the BALT indicates the presence of MV-infected T-lymphocytes (CD3), DC or macrophages (CD11c) and B-lymphocytes (CD20), Double positive cells are indicated by arrows. In panel (B) and (C), EGFP$^+$ cells are shown in green, cell-type specific staining is shown in red. DAPI was used to counter stain nuclei in blue. (D) Dual immunofluorescence performed on uninfected BALT region. Dual labelling with cytokeratin (green) and CD3, CD11c or CD20 (red) showed that T-lymphocytes, B-lymphocytes and DC or macrophages are present in very close proximity or in direct contact with the alveolar or bronchiolar lumen (asterisks). Single colour images for (C) are available as supporting data (Figure S2).*

Analysis of BALT structures in the lungs of non-infected macaques indicated that even though cytokeratin-positive epithelial cells lined these structures, cells of lymphoid and myeloid origin were present both within the epithelium and in direct contact with the adjacent lumen. Indirect immunofluorescence identified $CD11c^+$, $CD3^+$ and $CD20^+$ cells in direct contact with the lumen of alveoli, bronchioles or bronchi (Figure 4D, asterisks). This was also confirmed in virus-negative BALT structures from uninfected animals.

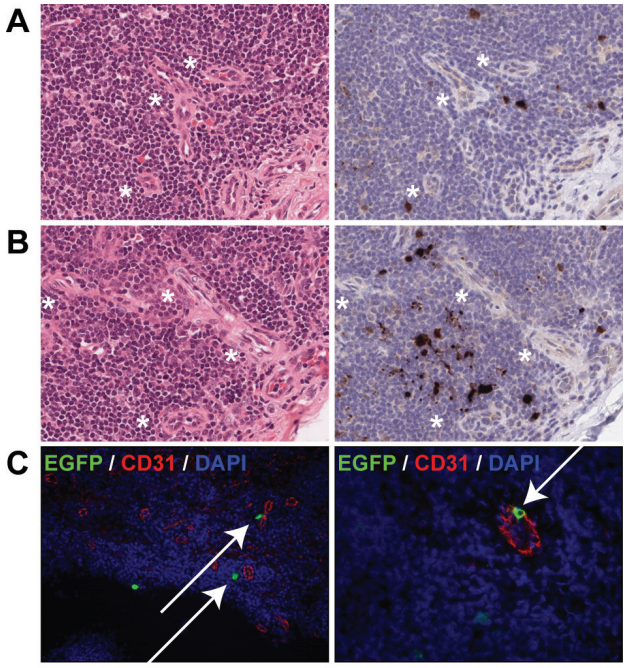

Figure 5. *Dissemination of MV into the lymphoid organs via blood vessels. (A,B) H&E staining (left panel) and EGFP staining (right panel) on serial sections of tonsils at 4 d.p.i. (A) and 5 d.p.i. (B). Asterisk denote the proximity of venules to MV-infected cells. (C) Dual labeling of EGFP (green) and the endothelial marker CD31 (red) performed on the tonsils from animals euthanized 5 d.p.i. The left panel shows MV-infected cells in close proximity to CD31+ endothelial cells of venules (arrows), the right panel shows an MV-infected cell migrating through the wall of the venule (arrow). DAPI was used to counter stain nuclei in blue. Single color images for (C) are available as supporting data (**Figure S2**).*

Early MV infection in lymphoid tissue is frequently associated with the presence of blood vessels

Within the infected BALT structures, MV-infected cells were readily detected in direct contact with or in close proximity to the endothelial wall of blood vessels. A similar distribution was observed in the tracheo-bronchial LN, tonsils and adenoids on 4 and 5 d.p.i., in which MV-infected cells were mostly detected in close proximity to venules (Figure 5). On rare occasions, MV-infected cells with the morphology of dendritic cells could be seen migrating through the endothelium (Figure 5, right panel and Figure S2).

Discussion

In the present study, we have generated and utilized a virulent rMV strain expressing EGFP, based on a wild-type genotype B3 MV isolate from Khartoum, Sudan. In growth curves in human B-LCL recombinant strains rMV^{KS} and rMV^{KS}EGFP reached equivalent titers, which were slightly higher than those reached by rMV^{IC323}EGFP. These data suggest that the addition of EGFP into the genome had no detectable effect on virus fitness as determined *in vitro*. Pathogenesis studies performed with molecular clones of wild-type MV have thus far exclusively been based on the Japanese strain IC323 [52]. Development of a second recombinant wild-type MV serves to complement ongoing studies of MV pathogenesis and ensures that observations are not strain-specific. Expression of EGFP from a promoter-proximal ATU leads to significant amounts of EGFP and, interestingly in the case of MV, has no or only a limited effect on the virulence *in vivo*. This was not the case for other morbilliviruses, for example canine distemper virus [105]. The new recombinant virus rMV^{KS}EGFP described here also proved to be virulent in cotton rats [284], and allowed sensitive microscopic detection of the virus *in vitro*, *ex vivo* and *in vivo*.

Macaques were infected with a high dose of rMV^{KS}EGFP via the aerosol route and early necropsies were performed to identify the initial target organs, tissues and cells. The nebulizer used was similar to the type that is used in ongoing clinical trials of measles aerosol vaccination, organized in India by the World Health Organization. The nebulizer produced a volume median diameter (VMD) of 4–6 µm, allowing the inoculum to deposit both in the upper respiratory and lower respiratory tract, and reach the alveolar lumina. A high infectious dose (10^6 $CCID_{50}$) was nebulized to ensure that all potential early target cells for MV infection in the respiratory tract were exposed to the virus. Such an approach is important in any study that aims to identify key cells targeted by a respiratory virus as it ensures the pathogen can access the broadest range of cell types and associated tissues throughout the respiratory tract. However, it is important to acknowledge our limited understanding of how MV is transmitted from human to human: in our current study we have infected animals with cell-free virus but transmission between humans could also involve excretion of cell-associated virus. Studies which examine the pathological consequences of MV infection in animals at later time points would greatly facilitate our understanding of virus transmission, both for MV and other respiratory viruses. The techniques and bank of tissues collected in this and other studies could be used to shed light on person to person transmission.

Our data strongly suggest the following sequence of events. At early time points (2 and 3 d.p.i.), MV infected large mononuclear cells with the phenotype and location of AM or DC. Targeting of these cells was followed by the establishment of localized MV replication in close proximity, lymphoid aggregates in the lungs (BALT). These BALT structures contained a large number of B-cells and memory $CD4^+$ T-cells [287], both cell types previously described as preferential targets for MV in lymphoid tissue at later time points [54]. Seeding and amplification of the infection in these microenvironments, which are well suited to a lymphotropic virus such as MV, is likely to be critical in the establishment of the infection. From the lungs, MV was

transported by infected cells to the draining tracheo-bronchial LN. After localized replication in the lungs and increased replication in the tracheo-bronchial LN, MV spread systemically through viremia to the majority of lymphoid organs by 4 or 5 d.p.i. MV-infected cells were always detected in close proximity to venules within lymphoid organs, suggesting that these were involved in spreading the virus.

It has been stated that MV initially targets the epithelium of the upper respiratory tract to establish infection [16]. However, all known wild-type MV receptors are absent on the luminal side of respiratory epithelial cells, making their initial infection by MV highly unlikely. Other potential entry strategies by which MV might enter a susceptible host have been described in the literature. For example, the Trojan horse strategy that has been described for HIV-1 has also been considered for MV [255]. DC could capture MV from the respiratory tract using dendrites protruding through the epithelium and transmit virus to $CD4^+$ and $CD8^+$ T-lymphocytes, leading to infection. *In vivo* in the macaque model, infection of DC has indeed been described in submucosal tissues [54]. Furthermore, in the present study we demonstrate that MV was detectable in the lungs 2 d.p.i., since MV-infected cells could be both isolated from BAL and imaged *in situ* by live cell confocal scanning laser microscopy. These data confirm that large mononuclear cells present in the alveolar lumen or lining the alveolar epithelium, most likely AM and/or DC, are among the earliest cells infected by MV in the macaque model. Even though the $Ifnar^{KO}$-SLAMGe mouse model does not recapitulate the whole spectrum of measles pathogenesis, initial infection of AM and DC was also shown in this model by flow cytometry [288].

We show here that, in the respiratory tract, BALT structures were the only MV-infected tissues at 3 d.p.i. BALT is normally lined by a continuous epithelial layer, making direct entry of MV unlikely. However, the epithelium of the BALT has previously been described to be a flattened respiratory epithelium, with common influx and efflux of lymphocytes, AM and DC [289]. Furthermore, the epithelium of BALT of many mammalian species contains M-cells [290], cells that are specialized for antigen uptake. In mouse models, it has been shown that BALT plays a role in the uptake of multiple bacteria (*Pseudomonas aeruginosa* [291], *Mycobacterium tuberculosis* [292]). Reoviruses have also been described to be taken up by M-cells, with subsequent spread to the regional lymph nodes [293]. In this study we did not observe antigen uptake by M-cells. Instead, we observed infected cells resembling AM or DC at 2 d.p.i. and suggest that they transported MV through the BALT epithelium into the underlying lymphoid tissue.

An alternative route for MV to enter a susceptible host would be via direct infection of $CD150^+$ cells in Waldeyer's tonsillar ring, consisting of tonsils and adenoids. Tonsils and adenoids are lined by $CD150^-$ epithelial cells, but at sites of damage or in tonsillar crypts direct infection of $CD150^+$ cells at the luminal surface might be possible. In our model, tonsils and adenoids were directly exposed to a high dose of nebulized virus, but a consistent level of infection was only detected 4 and 5 d.p.i., when the infection already was systemic. Only one out of six animals had MV-infected cells in the adenoid 2 d.p.i. and no infection was observed in the tonsils 2 and 3 d.p.i.

These data suggest that MV cannot easily penetrate the epithelial layer to initiate MV infection of $CD150^+$ cells in tonsillar tissue of the Waldeyer's ring.

Following the initial infection of cells in the lung, the draining TB-LN was the first lymphoid organ being consistently MV-positive 3 d.p.i. Since this LN drains the lungs, it is most likely that MV-infected cells are transported through lymphatic vessels to reach the TB-LN. In the BALT and TB-LN, MV-infected cells were often detected in close proximity of venules. We hypothesize that MV-infected cells are transported through these venules into the bloodstream, from where they reach the spleen and other lymphoid organs, initiating the systemic infection as observed 4 and 5 d.p.i. The proximity of MV-infected cells to venules in the tonsils and adenoids 4 and 5 d.p.i. substantiates this hypothesis.

In conclusion, aerosol exposure of the entire respiratory tract of macaques to a high dose of infectious MV leads to initial infection of mononuclear cells in the alveoli (2 d.p.i.), followed by MV replication in BALT (3 d.p.i.). Phenotypically and based on location it is likely that the initial target cells in the alveoli are AM or DC. In BALT, T-lymphocytes, B-lymphocytes and DCs are all productively infected. $CD11c^+$ cells are the major target cell population in the lungs 4 and 5 d.p.i. indicating an important role for AM and/or DC early in establishing the infection.

Funding

This work was supported by ZonMw (grant# 91208012), MRC (grant# G0801001) and the VIRGO consortium, an innovative cluster approved by the Netherlands Genomics Initiative and partially funded by the Dutch Government (grant# BSIK03012). The funders had no role in study design, data collection and analysis, decision to publish, or preparation of the manuscript.

Acknowledgments

The authors would like to thank Latoya Sarijoen, Tien Nguyen, Joyce Verburgh, Monique van Velzen and Robert Dias D'Ullois for practical assistance and are grateful to Yusuke Yanagi for providing the Vero-SLAM cell line. We would also like to thank the staff of the Tissue Core Technology Unit, QUB for their histological expertise. Furthermore, we are grateful to Zeiss for the "on loan use" of the LSM700 system fitted on an Axio Observer Z1 inverted microscope.

Author Contributions

Conceived and designed the experiments: RDdV WPD RLdS. Performed the experiments: KL RDdV AWM SM GvA SY ML LJR WPD RLdS. Analyzed the data: KL RDdV AWM SM TK BKR TBHG ADMEO WPD RLdS. Wrote the paper: KL RDdV TK WPD RLdS.

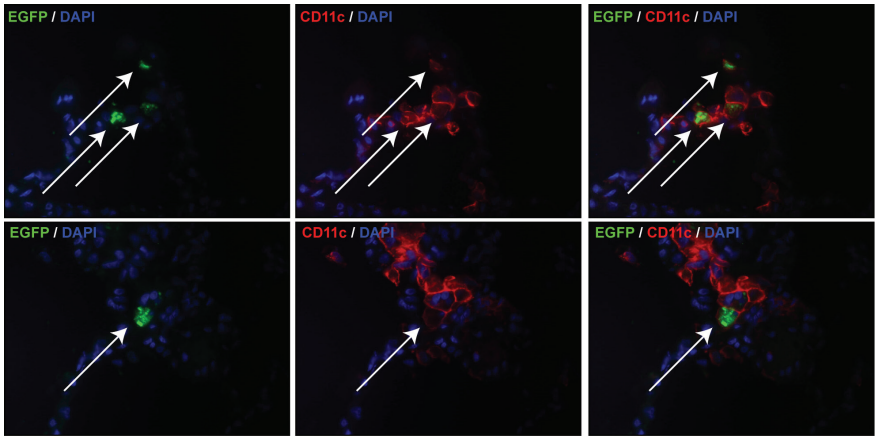

Figure S1. *CD11c⁺ DC and macrophages targeted in the lung at 4 and 5 d.p.i. At 4 and 5 d.p.i. the CD11c⁺ DC or macrophage population was the major cell type in the lung in which MV replicates. Dual labelling for EGFP (green) and CD11c (red), DAPI was used to counter stain nuclei in blue. Left panels show EGFP alone (green), centre panels show CD11c alone (red), right panels show overlay of EGFP and CD11c. The two rows are two representative examples of double positive cells as indicated by arrows.*

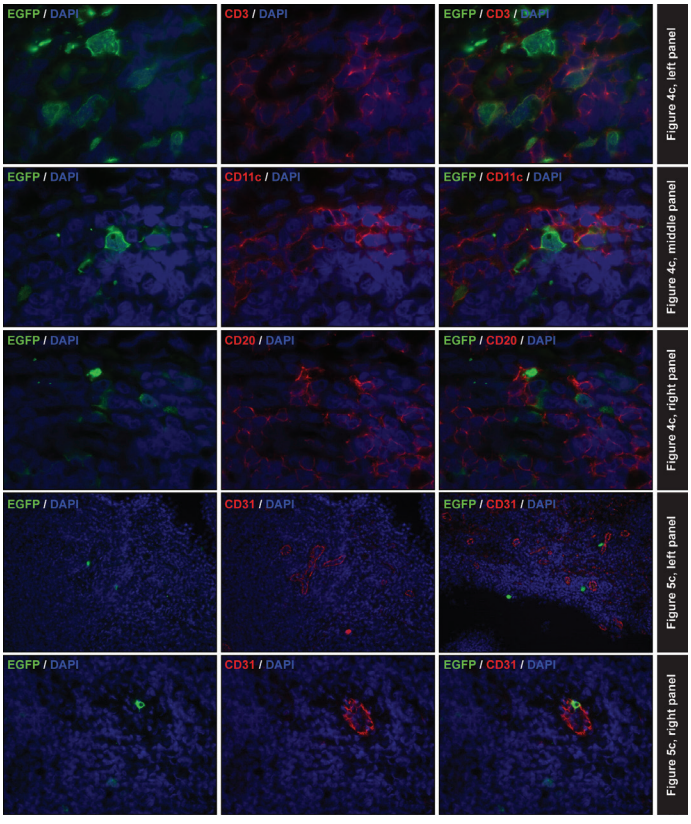

Figure S2. *Single color images for* ***Figure 4C*** *and* ***5C****.*

PATHOGENESIS OF DIFFERENT MV STRAINS

4

In vivo tropism of attenuated and pathogenic measles virus expressing green fluorescent protein in macaques

Rory D. de Vries, Ken Lemon, Martin Ludlow, Stephen McQuaid, Selma Yüksel, Geert van Amerongen, Linda J. Rennick, Bert K. Rima, Albert D.M.E. Osterhaus, W. Paul Duprex and Rik L. de Swart

Journal of Virology 2010 May; 84(9): 4714 - 4724

Abstract

The global increase in measles vaccination has resulted in a significant reduction of measles mortality. The standard route of administration for the live-attenuated measles virus (MV) vaccine is subcutaneous injection, although alternative needle-free routes, including aerosol delivery, are under investigation. *In vitro*, attenuated MV has a much wider tropism than clinical isolates, as it can use both CD46 and CD150 as cellular receptors. To compare the *in vivo* tropism of attenuated and pathogenic MV, we infected cynomolgus macaques with pathogenic or attenuated recombinant MV expressing enhanced green fluorescent protein (EGFP) (strains IC323 and Edmonston, respectively) via the intratracheal or aerosol route. Surprisingly, viral loads and cellular tropism in the lungs were similar for the two viruses regardless of the route of administration, and $CD11c^+$ cells were identified as the major target population. However, only the pathogenic MV caused significant viremia, which resulted in massive virus replication in B and T lymphocytes in lymphoid tissues and viral dissemination to the skin and the submucosa of respiratory epithelia. Attenuated MV was rarely detected in lymphoid tissues, and when it was, only in isolated infected cells. Following aerosol inhalation, attenuated MV was detected at early time points in the upper respiratory tract, suggesting local virus replication. This contrasts with pathogenic MV, which invaded the upper respiratory tract only after the onset of viremia. This study shows that despite *in vitro* differences, attenuated and pathogenic MV show highly similar *in vivo* tropism in the lungs. However, systemic spread of attenuated MV is restricted.

Introduction

Measles virus (MV) is one of the most contagious human viruses and is transmitted via aerosols or by direct contact with contaminated respiratory secretions. Clinical symptoms appear approximately 2 weeks after infection and include fever, rash, cough, coryza, and conjunctivitis [16]. Measles is associated with immune suppression, resulting in increased susceptibility to opportunistic infections. While significant progress has been made in global control programs, 164,000 deaths were attributed to measles in 2008 [278].

MV was first isolated in cell culture in 1954 [172]. This Edmonston wild-type MV strain was passaged multiple times in primary human kidney and amnion cells and adapted to eggs and chicken embryo fibroblasts to produce the live-attenuated Edmonston-B vaccine virus [294], which was later replaced by the more attenuated MV strains (Edmonston-Zagreb, Moraten, and Schwarz) [295]. These vaccines have been shown to be safe and effective, and high coverage in two-dose regimens has successfully interrupted endemic MV transmission in large geographic areas [296].

For many years, laboratory-adapted $MV^{Edmonston}$ strains were used as the prototype virus and were shown to display a wide cellular tropism *in vitro*. The virus efficiently infected epithelial cells, which were considered the target cells for primary MV infection *in vivo* [297]. In 1993, the cell surface glycoprotein CD46, expressed by virtually all nucleated human cells, was identified as a cellular receptor for MV [110,111]. However, it became evident that only vaccine and laboratory-adapted MV strains were able to utilize this molecule as a cellular receptor [112]. CD150, a membrane glycoprotein expressed on subsets of lymphoid and myeloid cells, was identified as the receptor for wild-type MV strains in 2000 [113,214].

Experimental infections of non-human primates with the Edmonston wild-type MV have given variable results: initial studies reported clinical signs, including rash [298], but later studies suggested that these viruses were in fact attenuated [98,102]. It is now known that most MV strains isolated in $CD150^-$ cells are attenuated *in vivo*, whereas non-cell-culture-passaged MV or wild-type strains isolated and passaged in $CD150^+$ cells retain pathogenicity [99]. We recently infected macaques with a recombinant MV based on the IC323 strain expressing a fluorescent protein [52,53], a virus that exclusively uses CD150 as a cellular receptor. This virus retained its pathogenicity in non-human primates, and CD150-expressing lymphocytes and dendritic cells (DC) were the predominant target cells for MV replication [54].

Although attenuated MV strains have been used successfully in large-scale vaccination campaigns, surprisingly little is known about the molecular mechanisms underlying this attenuation. In addition to having a wider tropism *in vitro*, attenuated MV strains have deficiencies in their capacity to antagonize innate immune responses [299]. Experimental infections in non-human primates demonstrated that attenuated MV may cause low-level viremia, although virus loads were 10- to 100-fold lower than those observed in animals infected with pathogenic MV [98,102] and in some cases were undetectable [300]. However, nothing is known about the cell

types and tissues targeted by attenuated MV strains *in vivo*. This subject has gained importance in recent years due to activities aimed at developing alternative needle-free routes of measles vaccination [301].

In the present study, we aimed to compare the *in vivo* tropism of attenuated and pathogenic MV using two recombinant MV strains expressing enhanced green fluorescent protein (EGFP): rMV^{rEdt}EGFP, a clone of the Edmonston-tag (Edtag) virus [51] that contains a repaired phosphoprotein (P) gene (L. J. Rennick *et al*, unpublished data), and rMV^{IC323}EGFP [53], which was previously used in pathogenesis studies of macaques [54]. rMV^{rEdt}EGFP can use both CD46 and CD150 as cellular receptors *in vitro*, whereas rMV^{IC323}EGFP exclusively uses CD150 as a cellular receptor. In the majority of previous experimental MV infections of macaques, we used intratracheal (i.t.) inoculation as the route of virus administration. The main advantage of this route is that it ensures delivery of the complete virus dose to the lungs. However, there is a clear disadvantage in that it does not mimic the natural route of MV transmission. In the present study, we compared i.t. inoculation and aerosol inhalation in order to overcome this limitation and better understand how the virus is able to establish a natural infection.

Materials & Methods

Cells and viruses

For the scope of this study, an attenuated and a pathogenic MV expressing EGFP were used. The attenuated MV was based on the first molecularly cloned MV strain, the Edtag virus [51]. The Edtag strain of MV has historically been used for *in vivo* MV studies [32,302,303]. The V protein of the Edtag strain has been shown to be defective in counteracting interferon (IFN) signaling pathways due to tyrosine-to-histidine and cysteine-to-arginine substitutions at amino acid positions 110 and 272, respectively [28,304,305]. The presence of a functional V protein is crucial for establishing a productive infection *in vivo* [304]. For this reason, the P gene of the recombinant Edtag virus was replaced with that of an early-passage Edmonston vaccine strain [306] (GenBank accession number GU327676). This gene encodes a V protein that is identical to that of the Moraten vaccine strain of MV, which has been shown to be competent for antagonizing the IFN signaling pathway [304]. Upon rescue, this virus was shown to have a normal V protein and stable EGFP expression and was designated rMV^{rEdt}EGFP (L. J. Rennick *et al*, unpublished data). As a pathogenic MV, we used rMV^{IC323}EGFP, the *in vivo* virulence of which has been previously validated in the macaque model [54]. Virus stocks were grown in an Epstein-Barr virus-transformed human B-lymphoblastic cell line (B-LCL) and tested negative for contamination with Mycoplasma species. Virus titers were determined by endpoint titration in Vero-CD150 cells and were expressed as 50% cell culture infectious doses ($CCID_{50}$).

In vitro infection of primary human cells

Peripheral blood mononuclear cells (PBMC) were isolated from human blood by density gradient centrifugation. T lymphocytes were expanded by stimulation of

PBMC with phytohemagglutinin (PHA-L) in the presence of interleukin 2 (IL-2) (50 IU/ml); B lymphocytes were isolated with CD19 magnetic beads and expanded by co-culture with gamma-irradiated murine L cells expressing human CD40L [307] in the presence of recombinant human IL-4 (40 IU/ml); monocytes were isolated by CD14 magnetic-bead separation and differentiated into immature DC and macrophages. Immature monocyte-derived DC were obtained by culturing monocytes for 5 days in the presence of IL-4 (300 IU/ml) and granulocyte-macrophage colony-stimulating factor (GM-CSF) (300 IU/ml), whereas to obtain macrophages, the monocytes were cultured in the presence GM-CSF only. Immature DC were differentiated by stimulation with a maturation mixture containing tumor necrosis factor alpha (TNFα), IL-6, IL-1β1, and prostaglandin E_2 (PGE_2), as described previously [308]. Different cell types were infected with either rMV^{rEdt}EGFP (attenuated) or rMV^{IC323}EGFP (pathogenic) MV at a multiplicity of infection (MOI) of 0.01 and cultured for 3 days. The percentages of MV-infected cells were measured by flow cytometry at 24, 48, and 72 h post infection (p.i.) by measuring the percentage of $EGFP^+$ cells on a FACS Canto II. Measurements were performed in triplicate on cells obtained from two different blood donors. Prior to infection, all cell types were analyzed for expression of the MV receptors CD46 and CD150 by flow cytometry with appropriate isotype controls performed in parallel.

***Ex vivo* infection of macaque spleen cells**

Spleens were collected from three rhesus macaques, which had been sacrificed in the framework of another study. The spleens were minced, and single-cell suspensions were prepared using cell strainers with a 100 µm pore size (BD Biosciences); mononuclear cells were obtained by density gradient centrifugation. The cells were infected with either attenuated or pathogenic MV at an MOI of 0.1 and cultured for 4 days. Infection percentages were measured in duplicate by flow cytometry at 24, 48, and 96 h p.i.

Animal study design

Juvenile MV-seronegative cynomolgus macaques were housed in negatively pressurized, HEPA-filtered biosafety level 3 (BSL-3) isolator cages. The animals were infected with either rMV^{IC323}EGFP (groups A and B; n = 8) or rMV^{rEdt}EGFP (groups C and D; n = 8). Within these two groups, four animals were infected with 10^4 $CCID_{50}$ by i.t. inoculation (groups A and C), and four animals were infected by aerosol inhalation (groups B and D). Aerosol was generated using the Aeroneb Lab nebulizer with an OnQ aerosol generator (kind gift of J. Fink, Nektar Therapeutics). Previous studies had shown that this combination efficiently delivers an aerosol to the airways of nonhuman primates, depositing over 10% of the generated aerosol into the lungs [283]. In order to optimize the infectious dose of virus, the virus was titrated on Vero-CD150 cells before and after bench nebulization. This showed an approximate 2-fold decrease in the amount of infectious virus (data not shown). Therefore, we hypothesized that exposing the macaques to a dose of 10^6 $CCID_{50}$ of nebulized virus corresponded to an approximate i.t. dose of 10^4 $CCID_{50}$. This corrected for the limited deposition into the lungs, virus loss by nebulization, loss of the aerosol into the environment, aerosol deposition on the skin and eyes, and

aerosol that was swallowed during nebulization. All animals were euthanized on day 7, which we estimated to be the peak of attenuated-MV replication and shortly before the peak of pathogenic-MV replication. This study was approved by the animal ethics committee and performed according to Dutch guidelines for animal experimentation.

Samples
Small-volume EDTA blood samples were collected in Vacuette tubes containing K_3EDTA as an anticoagulant 0, 2, 4, 5, 6, and 7 days p.i. Plasma was separated from the blood by centrifugation, heat inactivated (30 min; 56°C), and stored at -20°C. White blood cells (WBC) were obtained by direct treatment of EDTA blood with red blood cell lysis buffer (Roche Diagnostics, Penzberg, Germany). WBC were resuspended in complete RPMI 1640 medium (Gibco Invitrogen, Carlsbad, CA) supplemented with L-glutamine (2 mM), 10% (v/v) heat-inactivated fetal bovine serum (FBS), penicillin (100 U/ml), and streptomycin (100 µg/ml); counted using a hemocytometer and used directly for virus isolation and flow cytometry. PBMC were isolated from EDTA blood 0, 6, and 7 days p.i. by density gradient centrifugation; resuspended in culture medium as described above; and used for virus isolation and flow cytometry. A bronchoalveolar lavage (BAL) was performed 6 days p.i. by i.t. infusion of 10 ml phosphate-buffered saline (PBS) through a flexible catheter. On day 7 p.i., a BAL was performed postmortem by direct infusion of 10 ml PBS into the right lung lobe. BAL cells were resuspended in culture medium with supplements as described above, counted, and used directly for virus isolation. The remaining BAL cells were directly analyzed for EGFP expression by UV microscopy. Throat and nose swabs were collected 0, 2, 4, 5, 6, and 7 days p.i. for both virus isolation and virus detection by real-time reverse transcription (RT)-PCR [285].

Virus detection
Isolation of MV was performed on human B-LCL using an infectious-center test as previously described [281]. Virus isolations were monitored by UV microscopy for EGFP fluorescence after co-cultivation with B-LCL for 3 to 6 days. The results are expressed as the number of virus-infected cells per 10^6 total cells. Real-time RT-PCR on throat and nose swabs was performed as described previously [285].

Macroscopic detection of EGFP fluorescence
Macroscopic detection of EGFP was performed as described previously [54]. Briefly, fluorescence was detected with a custom-made lamp containing 6 LEDs (peak emission, 490 to 495 nm); the emitted fluorescence was detected through an amber cover of a UV transilluminator used for screening DNA gels. Photographs were made using a Nikon D80 SLR camera.

Necropsies
Animals were euthanized by sedation with ketamine (20 mg/kg body weight), followed by exsanguination. Samples were collected in 4% (w/v) paraformaldehyde (PFA) in PBS (to preserve EGFP autofluorescence) or in buffered formalin. Representative blocks from the upper, intermediate, and lower lung were sampled to provide maximum surface area. A selection of samples was also collected in PBS for direct

processing of tissues or was snap-frozen in liquid nitrogen and stored at -80°C.

Flow cytometry
Freshly isolated WBC and PBMC were stained with monoclonal antibodies raised against human antigens and cross-reactive with macaque cell surface markers. T lymphocytes were detected by staining them with CD3 (BD Pharmingen; clone SP34-2) and subdivided into CD4 (NIH; clone L200) and CD8 (Dako; clone DK25). B lymphocytes were identified using HLA-DR (BD Biosciences; clone L243) and CD20 (BD Biosciences; clone L27) monoclonal antibodies. EGFP was always detected in the fluorescein isothiocyanate (FITC) channel. Fluorescence was measured on a FACS Canto II, obtaining approximately 10^6 events to allow detection of low-frequency $EGFP^+$ populations. Lymphoid tissues, collected in PBS, were minced, and single-cell suspensions were prepared using cell strainers with a 100 µm pore size (BD Biosciences); the cells were directly used for flow cytometry, after being stained with CD3 and CD20.

Immunohistochemical and immunofluorescence analyses of formalin-fixed tissues
All formalin-fixed sections were deparaffinized, and antigen retrieval was performed in a pressure cooker at full power for 3 min in 0.01 M Tris-EDTA buffer (pH 9.0). MV-infected cells were detected using a polyclonal rabbit antibody to EGFP (Invitrogen). Sections were incubated in primary antibody overnight at 4°C, and specific antibody-antigen binding sites were detected using an Envision-Peroxidase system with DAB (Dako) as a substrate. Dual-labeling indirect immunofluorescence was performed using polyclonal rabbit anti-EGFP and monoclonal mouse antibodies to the myeloid (macrophage/DC) marker CD11c (Novocastra; clone 5D11), the T-lymphocyte marker CD3 (Dako; clone F7.2.38), the B-lymphocyte marker CD20 (Dako; clone L26), and an epithelial cytokeratin cell marker (Dako; clone AE1/AE3). Antigen binding sites were detected with a mixture of anti-mouse Alexa 568 and anti-rabbit Alexa 488 (Invitrogen). Sections were counterstained with DAPI (4',6'-diamidino-2-phenylindole) hard-set mounting medium (Vector). All fluorescently stained slides were examined at x200, x400, and x1,000 magnifications on a fluorescence imaging microscope (Leica Microsystems).

Results

***In vitro* infections of different cell types**
To compare the *in vitro* potential of the viruses to use CD150 as an entry receptor, Vero or Vero-CD150 cells were infected with $rMV^{rEdt}EGFP$ (attenuated) or $rMV^{IC323}EGFP$ (pathogenic). In Vero cells, pathogenic MV was able to infect single cells, but only at a high MOI and never associated with cytopathic effects (Figure 1A). Attenuated MV replicated well in Vero cells, resulting in large syncytia irrespective of the MOI. Both viruses efficiently infected Vero-CD150 cells both at high and at low MOIs, resulting in clear cytopathic effects (Figure 1A).

To compare the *in vitro* susceptibilities of primary human cells of lymphoid and myeloid origin, activated T and B lymphocytes, macrophages, immature DC, and mature DC were infected with either attenuated or pathogenic MV. At the time of infection, all cell types expressed CD46 at a high level, whereas CD150 expression was high on B lymphocytes, lower on T lymphocytes and mature DC, and virtually absent on immature DC and macrophages (Figure 1B). Infection with attenuated MV resulted in higher percentages of infected cells than infection with pathogenic MV (**Figure 1C**). Monocyte-derived macrophages and immature DC showed low infection percentages with pathogenic MV, corresponding to the absence of CD150, but despite the abundant expression of CD46, an analogous restriction in virus replication was also observed with attenuated MV (Figure 1C).

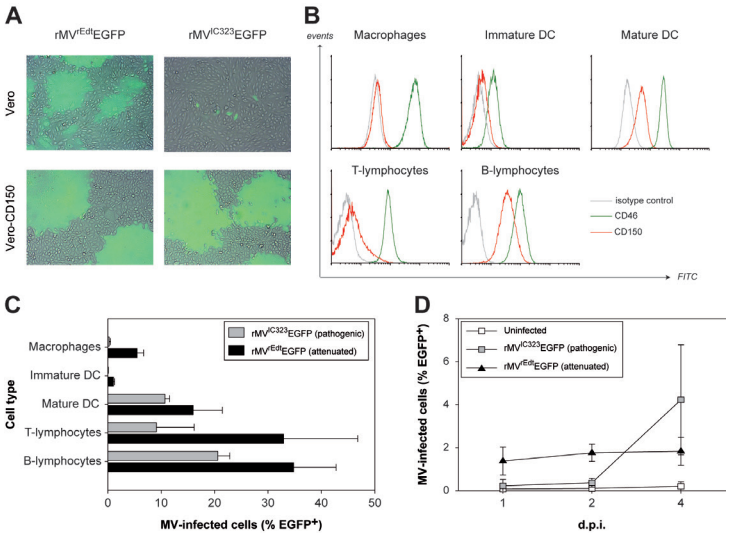

Figure 1. *(A) Infection of Vero and Vero-CD150 cells by attenuated and pathogenic MV. Attenuated MV was capable of infecting and causing cell-cell fusion in Vero and Vero-CD150 cells. Pathogenic MV infected and fused Vero-CD150 cells efficiently, but in Vero cells, only sparse single infected cells were detected. Overlays of normal light and fluorescence micrographs were created using Adobe Photoshop CS3 software. (B) CD46 and CD150 expression on primary human cells. Prior to infection of primary human cells, the levels of CD46 and CD150 surface expression were determined by flow cytometry. (C) Infection of primary human cells. Different cells of lymphoid or myeloid origin were infected in vitro with attenuated or pathogenic MV. Infection was measured by flow cytometry at 3 days p.i. The results are shown as means and standard deviations (SD) of triplicate measurements of two different donors. (D) Infection of macaque splenocytes. Macaque splenocytes were infected with attenuated or pathogenic MV, and infection was measured by flow cytometry at 1 to 4 days p.i. The results are shown as means ± SD of duplicate measurements of three different animals.*

In order to compare the infectivity of MV for macaque splenocytes, complete spleen cell populations were infected *ex vivo* with either attenuated or pathogenic MV. Using an MOI of 0.1, infection with attenuated MV resulted in 1 to 2% EGFP$^+$ cells 24 h p.i., which remained stable up to 4 days p.i. In contrast, pathogenic MV was barely detectable for the first 2 days p.i., but at day 4, the percentage of EGFP$^+$ cells increased up to 5 to 6% (Figure 1D).

MV replication after aerosol and i.t. delivery

Macaques were infected in four groups of four animals each with either pathogenic or attenuated MV, via either the i.t. or aerosol route. No clinical signs were observed during the course of the experiment. Virus isolations were performed from PBMC and BAL cells to compare viremia and local replication in the lower respiratory tract. Real-time RT-PCR on throat and nose swabs was performed to detect viral presence in the upper respiratory tract. Pathogenic MV was isolated from PBMC of all eight animals; the virus loads in these samples were comparable for both administration routes (Figure 2A, right). Clearly, the level of infection was still increasing to 7 days p.i., indicating that the animals were euthanized slightly before the peak of virus replication. Kinetics were similar to those described previously for pathogenic MV infections in macaques [54,1-2.281,309,310]. In contrast, attenuated MV was isolated only from PBMC of a single animal at a very low level in the aerosol-infected group (Figure 2A, right). The amounts of virus isolated from BAL cells were comparable after either i.t. or aerosol infection with pathogenic MV, and virus could be isolated from all animals. The BAL from all macaques infected with attenuated MV contained infectious MV at either 6 or 7 days p.i. The numbers of MV-infected cells were comparable after either i.t. or aerosol infection and were approximately 10-fold lower than those observed with pathogenic MV (Figure 2A, left). UV microscopy was used to confirm the presence of EGFP$^+$ cells in BAL in all cases (data not shown).

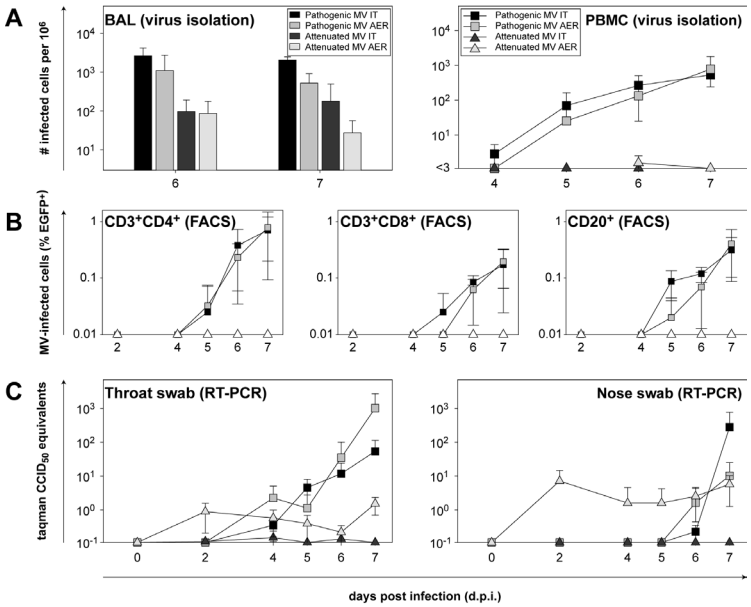

Figure 2. *Detection of MV in blood, lungs, throat, and nose. In all plots, the results are shown as means ± SD of the 4 animals within a group. (A) Virus isolations from BAL cells and PBMC. Virus was isolated in human B-LCL in an infectious-center assay, and the results are expressed as the number of infected cells per 10^6 total cells. AER, aerosol. (B) Flow cytometry of PBMC subpopulations. The data shown are the percentages EGFP$^+$ cells in the CD3$^+$ CD4$^+$, CD3$^+$ CD8$^+$, and CD20$^+$ subpopulations. FACS, fluorescence-activated cell sorter. (C) RT-PCR on throat and nose swabs. MV was detected by real-time RT-PCR on total RNA isolated from throat and nose swabs collected in transport medium.*

Flow cytometry of WBC and PBMC showed that $CD3^+$ $CD4^+$, $CD3^+$ $CD8^+$, and $CD20^+$ cells were infected with pathogenic MV to similar extents after i.t. or aerosol infection, with $CD3^+$ $CD4^+$ cells identified as the primary target cells. Attenuated MV could not be detected in PBMC by flow cytometry (Figure 2B).

Table 1. *Detection of MV antigen in different tissues by immunohistochemistry. a URT, upper respiratory tract; Nas., nasal; LRT, lower respiratory tract; 10 bronchus, primary bronchus; Up., upper; Int., intermediate; Low., lower; RP-LN, retropharyngeal lymph node; TB-LN, tracheobronchial lymph node. b MV infection in different cell types is indicated. EP, epithelium; SUB, submucosa; IM, immune cells. Scores for 2 animals per group are shown. -, absence of virus from all cell layers; +, sparse virus-infected cells; ++, moderate number of virus-infected cells with multinucleated giant cells (MNGC); +++, high numbers of virus-infected cells with MNGC; ND, not determined.*

Tissue[a]	Infection score[b]											
	Pathogenic ($rMV^{IC323}EGFP$)						Attenuated ($rMV^{rEdt}EGFP$)					
	i.t.			Aerosol			i.t.			Aerosol		
	EP	SUB	IM	EP	SUB	IM	EP	SUB	IM	EP	SUB	IM
URT												
Nas. septum	-/-	-/-		-/-	-/+		-/-	-/+		-/-	-/-	
Nas. concha	-/-	-/+		-/+	+/+		-/-	-/+		-/-	+/+	
Trachea	+/+	+/++		-/+	-/++		ND/-	ND/-		-/-	-/-	
LRT												
1^0 bronchus	-/-		-/-	-/+		+/+++	-/-		-/-	-/-		-/-
Up. lungs	-/-		-/-	-/-		+/+++	-/-		+/+	-/-		+/+
Int. lungd	-/-		-/+	-/-		+/++	-/-		-/+	-/-		+/+
Low. lungs	-/-		-/-	-/+		-/+	-/-		-/+	-/-		+/+
Lymphoid												
Tonsils			++/++			++/++			-/-			-/+
Adenoids			-/+			++/+++			ND/ND			ND/ND
RP-LN			ND/+++			++/+++			ND/-			-/+
TB-LN			+/+++			+/+++			-/-			-/+
Digestive												
Tongue	-/+	-/+		-/+	-/+++		-/-	-/-		-/-	-/-	
Stomach	-/-	++/++		-/-	++/++		-/-	-/-		-/-	-/-	

MV was detected by RT-PCR in the upper respiratory tract of all animals infected with $rMV^{IC323}EGFP$, but only after the onset of viremia (day 4 for throat swabs, and day 6 for nose swabs). Viral loads were again comparable for both routes of administration. In attenuated-MV-infected animals, there was a striking difference between the i.t. and aerosol infections. I.t. infection with attenuated MV did not lead to local replication in the nose and throat, whereas infection via the aerosol route led to immediate replication in the upper respiratory tract. Virus could already be

detected 2 days p.i. (Figure 2C). Virus isolations performed with cells from the throat and nose swabs showed similar results (data not shown), indicating that the virus detected by real-time RT-PCR was indeed live infectious virus. However, although pathogenic MV could never be detected in any nose or throat sample at these early time points, it should be noted that the absolute levels that were detected were relatively low compared to those detected at later time points in animals infected with pathogenic MV.

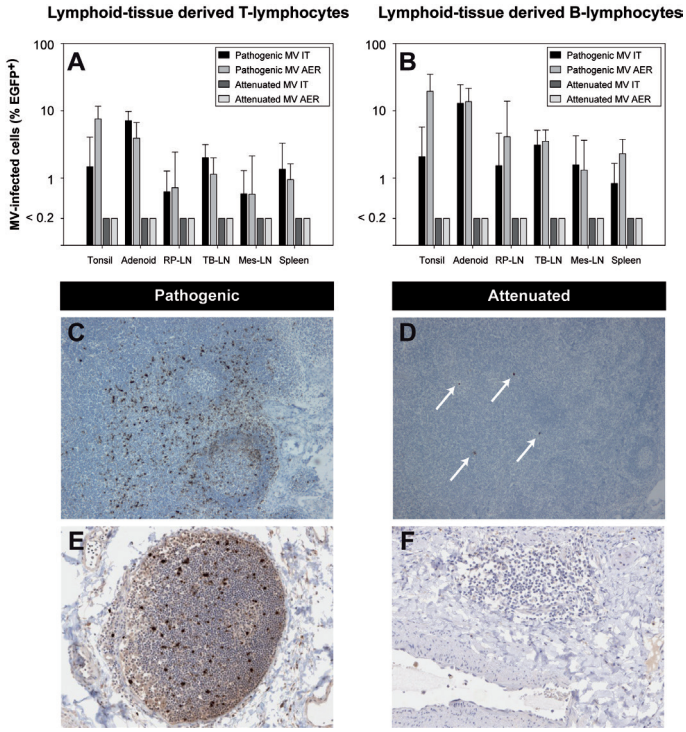

Figure 3. *Lymphoid infection by attenuated or pathogenic MV. (A,B) Percentages of EGFP⁺ cells in lymphoid organs. The percentages of MV-infected cells were determined in single-cell suspensions from lymphoid organs by flow cytometry and are shown as geometric means ± SD from the 4 animals within a group. AER, aerosol; RP-LN, retropharyngeal lymph node; TB-LN, tracheobronchial lymph node; Mes-LN, mesenteric lymph node. (C,D) Detection of EGFP⁺ cells in lymph nodes. Immunohistochemistry confirmed abundant MV-infected cells in lymphoid organs of pathogenic-MV-infected animals. Attenuated MV could be detected in only a few isolated cells from lymph nodes of two out of eight animals (see arrows in panel D). (E,F) Presence of lymphoid infiltrations in the lungs. In macaques infected with pathogenic MV, lymphoid infiltrations containing MV-infected cells were frequently observed in lung sections. In attenuated-MV-infected macaques, lymphoid infiltrations were less frequent and did not contain virus-positive cells.*

Infection of lymphoid tissues by pathogenic and attenuated MV

Macroscopic fluorescence was detected in all animals following either i.t. or aerosol infection with pathogenic MV. The affected tissues were similar in both groups and included the skin, gingiva, buccal mucosa, tongue, trachea, primary bronchus, lungs, and all lymphoid tissues (lymph nodes, spleen, thymus, tonsils, adenoids, and gut-

associated lymphoid tissue) (data not shown). These tissues correlate with affected tissues described previously [54]. Flow cytometry of single-cell suspensions from lymph nodes indicated that $CD20^+$ B lymphocytes were the primary target cells for pathogenic MV in these tissues and again showed no difference between infection via the i.t. or aerosol route (Figure 3A and B).

In attenuated-MV-infected macaques, macroscopic fluorescence was detected only in the upper and lower respiratory tract; all lymphoid tissues were negative. The absence of attenuated MV in these organs was confirmed by flow cytometry (Figure 3A and B). Immunohistochemistry revealed virus in lymph nodes from two attenuated-MV-infected macaques, but the numbers of infected cells were very limited in comparison to pathogenic-MV-infected lymph nodes (Table 1 and Figure 3C and D).

Local MV replication in the lungs

Macroscopically, EGFP was detected in all pathogenic-MV-infected lungs and in the lungs of 2 out of 4 attenuated-MV-infected animals from both the i.t. and aerosol-infected groups. Upon comparison to pathogenic MV, which formed large foci around the edges of the lung lobes, attenuated MV was observed to form smaller $EGFP^+$ foci of infection throughout the lungs (Figure 4). Microscopically, the presence of MV in the lungs was detected in all animals (Table 1). Little difference was observed between infected cells observed in the parenchyma of the lungs of pathogenic- and attenuated-MV-infected animals (Figure 5 and 6). However, in the lungs of animals infected with pathogenic MV, many $EGFP^+$ cells were found in infiltrating immune cells, whereas these cells were much less infected by attenuated MV (Figure 3E and F, respectively).

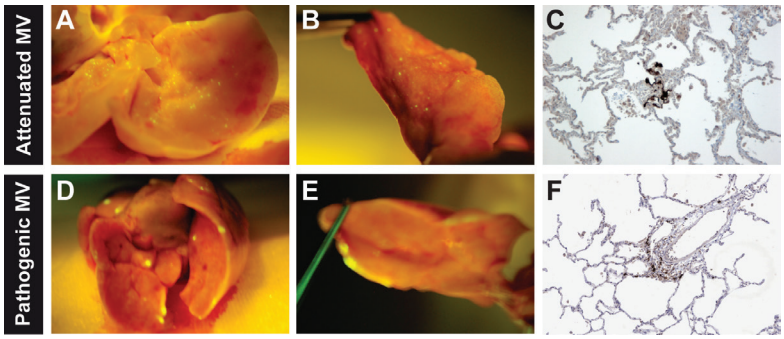

Figure 4. *Lung infection with attenuated or pathogenic MV. (A,B,D,E) Macroscopic detection of EGFP fluorescence. (C,F) Microscopic detection of MV-infected cells with anti-EGFP (counterstained with hematoxylin).*

Attenuated MV infects lymphoid, myeloid and epithelial cells in the lungs

Indirect-immunofluorescence dual labeling was performed on lung tissues from both i.t. and aerosol-infected macaques to identify which cell types were infected by attenuated MV. The vast majority of cells infected with attenuated MV were $CD11c^+$, and several $CD11c^+$ multinucleated giant cells were observed (Figure 5). While

MV infection of the epithelium surrounding the alveoli was detected, cytokeratin immunostaining (AE1/AE3) was disrupted within foci of infected cells (Figure 5). Furthermore, viral spread appeared to be predominantly mediated by cell-to-cell spread between intimately connected CD11c$^+$ cells. While CD3$^+$ T lymphocytes were abundantly present in the lungs, MV-infected T lymphocytes were rare and difficult to detect (Figure 5). Finally, only low numbers of CD20$^+$ B lymphocytes were detected in the lung parenchyma (although lymphoid infiltrations in the lung did contain B lymphocytes), and MV-infected B lymphocytes could not be observed (Figure 5).

Pathogenic MV infected similar cell types in general, although cytokeratin$^+$ infected epithelial cells were less frequently observed. Notably, more than 90% of EGFP$^+$ cells double stained with CD11c (Figure 6). An important difference with the lungs of animals infected with attenuated MV was that large numbers of MV-infected T and B lymphocytes were observed, mostly within large areas of lymphoid tissue but rarely around the alveoli (Figure 6).

Discussion

In this study, we performed a side-by-side comparison of the *in vivo* tropism of attenuated and pathogenic MV in non-human primates after i.t. or aerosol delivery. In the lungs, both viruses predominantly infected CD11c$^+$ myeloid cells, which include alveolar macrophages and DC. Although we have tried different surface molecules as specific markers, we have been unsuccessful in discriminating DC or macrophages in formalin-fixed tissues. Only the pathogenic MV also caused viremia and was disseminated to lymphoid tissues, the respiratory submucosa, and the skin.

The aerosol route of infection more closely mimics a natural MV infection than i.t. delivery. For the pathogenic MV strain (rMV^{IC323}EGFP), no differences were observed in the virus isolation profiles from BAL cells, blood, throat, or nose samples between the two routes of infection. In addition, no macroscopic or microscopic differences in distribution or intensity of fluorescent cells were observed in affected organs during necropsies 7 days p.i. Further analysis of the samples taken from macaques infected via either delivery route identified the same major target cells described previously [54], with CD3$^+$ CD4$^+$ T lymphocytes predominantly infected in blood and CD20$^+$ B lymphocytes predominantly infected in lymphoid organs. In all tissues, multifocal infection was detected, characterized by the presence of interconnected EGFP$^+$ cells, strongly suggesting that the virus spread in a cell-to-cell manner, as observed for several other viruses [143].

We used rMV^{rEdt}EGFP as an attenuated strain of MV. This virus is a recombinant EGFP-expressing virus based on the Edtag strain of MV. An important consideration in the use of Edtag for *in vivo* infections is previous studies that show that Edtag probably does not encode a functional V protein, due to many C-to-T transitions [304]. Therefore, we corrected the P gene sequence by site-directed mutagenesis and rescued a recombinant virus with normal V protein expression. To determine whether the attenuated rMV^{rEdt}EGFP behaved like other laboratory-adapted MV strains, *in vitro* infection experiments were performed with Vero and stably

transfected Vero-CD150 cells. As expected, Vero cells were efficiently infected by attenuated MV, but not by pathogenic MV, whereas Vero-CD150 cells were infected by both strains. This confirmed that the attenuated strain can use both CD46 and CD150 *in vitro*, whereas the pathogenic MV strain uses only CD150. Attenuated and pathogenic MV displayed similar tropism in primary human cells. Activated primary B and T lymphocytes and mature DC were efficiently infected, whereas only low levels of infection were observed in immature DC and macrophages. It is noteworthy that these cells all expressed CD46 at a high level but were infected inefficiently with the attenuated strain of MV. Strikingly, in these *in vitro* infections, attenuated MV reached higher infection percentages than pathogenic MV. This was not the case in primary macaque splenocytes, where pathogenic, but not attenuated, MV was able to spread and reached higher percentages at 4 days p.i. Overall, the percentages of infection were lower in the mixed splenocyte population than in the B and T lymphocytes and mature DC, probably due to the activation status of these cells. Previously, *ex vivo* infection of human tonsillar tissue with both recombinant pathogenic and attenuated MV strains also revealed that pathogenic MV infected most cell populations more efficiently [171].

It is important to note that rMV^{rEdt}EGFP is not completely identical to a live-attenuated MV vaccine strain. A sequence comparison was carried out between rMV^{rEdt}EGFP and the vaccine strains Moraten, Schwarz, Zagreb, Rubeovax, and AIK-C (GenBank accession numbers AF266287, AF266291, AF266290, AF266289 and AF266286 respectively). Analysis indicated that there were six amino acid changes in rMV^{rEdt}EGFP that were not present in at least one of the vaccine strains: M (R175G), F (M94V), H (E492G), and L (E429D, R1629Q, and N1805S). The mutations in M, F, and H have been investigated previously [311–313], on the basis of which it was decided not to change them to vaccine-identical amino acids. The changes in L either were outside the conserved domains (R1629Q) or the same changes were also retained in a previous study (E429D and N1805S) [304]. It was therefore decided that it was not necessary to change them to vaccine-identical amino acids either. However, the possibility that part of our results may reflect specific properties of the Edtag strain cannot be excluded.

In macaques, pathogenic MV was detected in PBMC from all animals from 4 days p.i., whereas attenuated MV was detected only in PBMC from a single animal at 6 days p.i. These data are in good agreement with previous studies of macaques using non-recombinant MV strains [98,102]. The most remarkable parallel between attenuated and pathogenic MV was observed in the lungs. Attenuated MV was readily isolated from BAL cells 6 and 7 days p.i., albeit at lower levels than pathogenic MV. Immunohistochemical staining of infected lung tissue showed similar levels of infection, and dual staining indicated that the target cells in the lungs for both viruses were also similar. Attenuated and pathogenic MV predominantly infected CD11c$^+$ cells in the lungs, while MV-infected cytokeratin$^+$ epithelial cells were detected only occasionally. Lymphoid infiltrations in pathogenic-MV-infected macaques contained high levels of infected T and B lymphocytes. Whether these are sites of primary virus replication or are a consequence of viremia remains to be determined. The

extent of infected epithelial cells in lung tissue has been previously described by Ludlow *et al*, with infection of the epithelium occurring only when MV was present in the underlying submucosa [125]. Our data indicate that MV-infected cells of a non-epithelial origin are often present in the BAL or located in the lumen of alveoli, indicating that infection of epithelial cells may not be required for transmission of MV, as has been previously suggested [137].

One difference governed by the route of infection was observed in animals infected with attenuated MV. In the upper respiratory tract, pathogenic MV was detected only after infiltration of MV-infected $CD150^+$ cells following the onset of systemic viremia in both i.t. and aerosol infections. This is probably because infection of the airway epithelium from the apical side is not possible, and only low numbers of $CD150^+$ target cells are available. Infection of $cytokeratin^+$ epithelial cells was observed, however, possibly via the recently described putative epithelial cell receptor present on the basolateral sides of these cells [127,137]. Early detection of attenuated MV in the throat and nose after aerosol inhalation indicates that, in contrast to pathogenic MV, attenuated MV may be capable of primary replication in the upper respiratory tract. Such early replication might be mediated by the use of CD46 as an entry receptor. However, the presence of MV-infected cells could not be confirmed by immunohistochemistry, suggesting that the numbers of infected cells in the upper respiratory tract were low.

Our study was not designed as a vaccination study but as a comparative study of two MV strains with important biological differences. For this reason, we did not include the standard route of administration of live-attenuated MV vaccines in our experimental design. We are currently preparing for a vaccination study in which $rMV^{Edmonston\text{-}Zagreb}$ expressing EGFP will be administered to macaques via four routes of inoculation: subcutaneous injection, i.t. inoculation, small-particle aerosol (for deep lung delivery), and large-particle aerosol (for upper respiratory tract delivery). In this study, animals will either be euthanized at early time points to assess virus tropism or be kept alive for monitoring of immune responses and assessment of protection from challenge infection.

In conclusion, we have shown that attenuated MV is capable of efficient replication in lymphoid cells *in vitro*, while replication in these cells is impaired *ex vivo* and *in vivo*. In addition, we show that even though attenuated MV is incapable of causing systemic infection, it causes a robust infection in the lungs of macaques. Most importantly, the cell types that are mainly targeted in the lungs are very similar to those targeted by pathogenic MV, and attenuated MV seems to prefer CD150 as a cellular entry receptor. It will be interesting to determine if this is the case in humans. There have been reports of progressive infection in vaccine recipients who have underlying immunological disorders [180,185]. Such tissues should be examined, as this would answer this question for the natural host and would also add to the weight of the macaque model as an ideal experimental-infection model for MV.

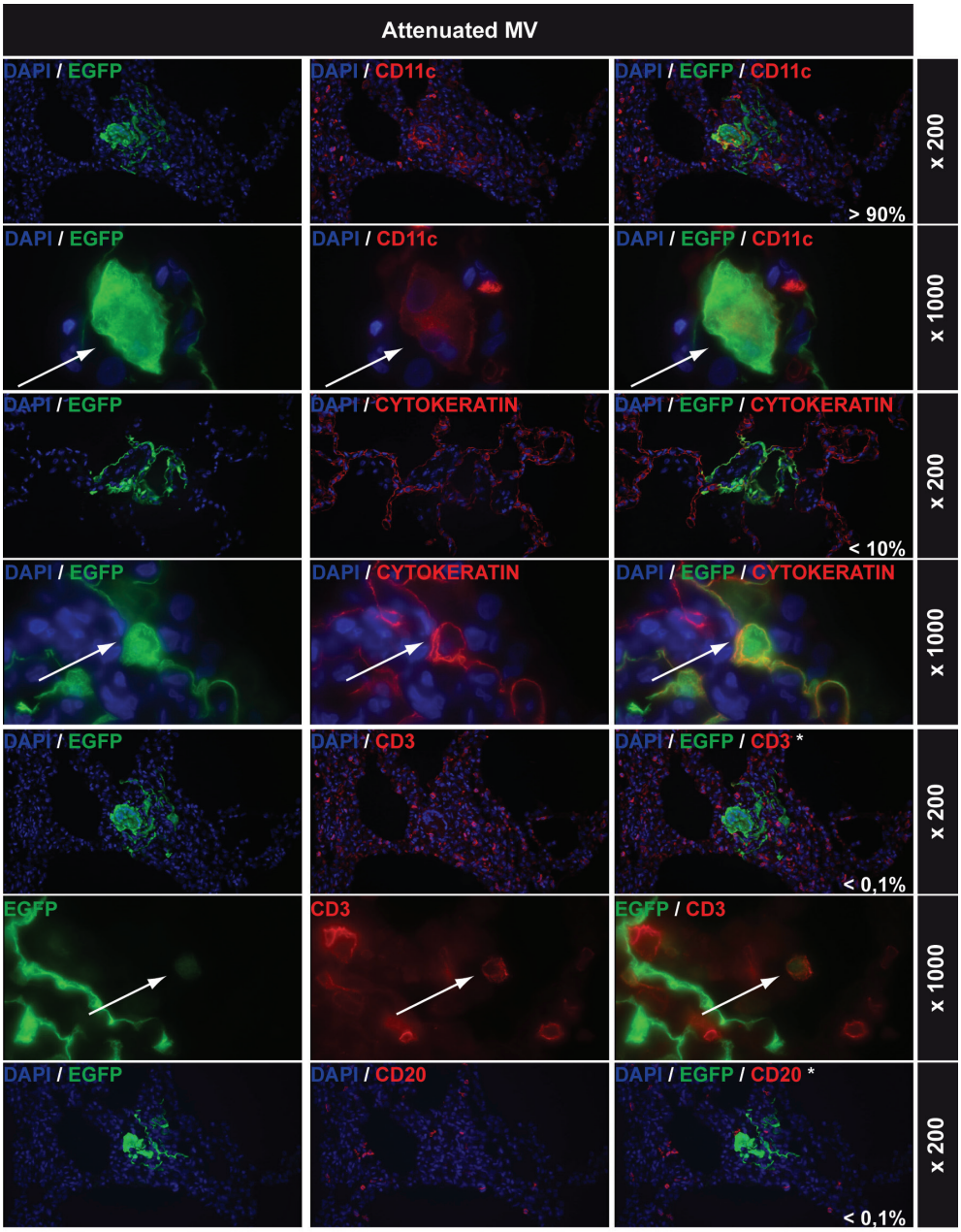

Figure 5. *Lung infections with attenuated MV: immunohistochemical double stainings. All rows show EGFP staining in green on the left, cell-type-specific staining in red in the middle (CD11c, cytokeratin, CD3, and CD20 for myeloid cells, epithelial cells, T lymphocytes, and B lymphocytes, respectively), and double staining on the right. DAPI counterstaining was used to identify nuclei. Magnifications are indicated on the right of each row. The percentages shown in white in the right-hand panels represent estimations of the relative contributions of these cell types to the total number of MV-infected cells in the lungs. Arrows indicate double-positive cells. Note that EGFP$^+$ cells shown in the CD3 and CD20 double stains are MV-infected CD11c$^+$ cells and that none of the CD3$^+$ or CD20$^+$ cells were EGFP$^+$.*

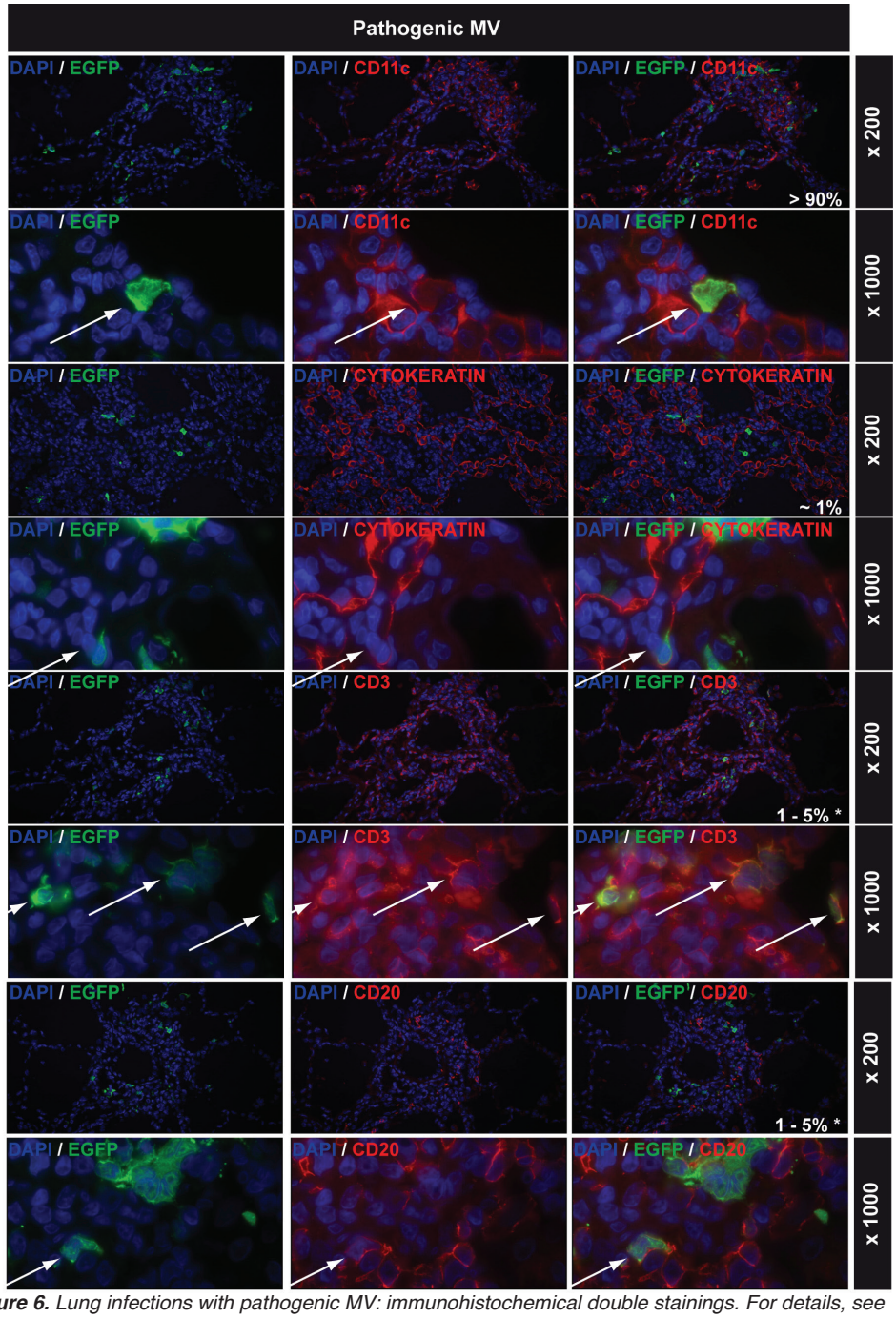

Figure 6. *Lung infections with pathogenic MV: immunohistochemical double stainings. For details, see the legend to* ***Figure 5****. Note that infected lymphocytes were mainly found in lymphoid infiltrations in the lungs.*

Funding

This work was supported by MRC (grant number G0801001), ZonMw (grant number 91208012), and the VIRGO Consortium, an innovative cluster approved by the Netherlands Genomics Initiative and partially funded by the Dutch government (grant number BSIK03012).

Acknowledgements

We thank Beverley Craig, Robert Dias D'Ullois, Joan van der Lubbe, Werner Ouwendijk, Marleen Reedijk, Monique van Velzen, Joyce Verburgh, Leon de Waal, and Lot de Witte for practical assistance. We are grateful to Yusuke Yanagi for providing the Vero-CD150 cell line and the plasmid from which the rMV^{IC323}EGFP virus was rescued. We thank Cees van Kooten for providing the CD40L-expressing cell line.

TRANSMISSION

5

TRANSMISSION

Infection of epithelial cells in the macaque nasopharynx and destruction of tonsillar epithelium is associated with high levels of transmissable measles virus

Martin Ludlow, Rory D. de Vries, Stephen McQuaid, Ken Lemon, Geert van Amerongen, Selma Yüksel, R. Joyce Verburgh, Emma Millar, Albert D.M.E. Osterhaus, Rik L. de Swart and W. Paul Duprex

Submitted

PUBLISHED AS:

- Measles virus infection of epithelial cells in the macaque upper respiratory tract is mediated by subepithelial immune cells. Ludlow M, Lemon K, de Vries RD, McQuaid S, Millar EL, van Amerongen G, Yüksel S, Verburgh RJ, Osterhaus AD, de Swart RL, Duprex WP. J Virol. 2013 Apr;87(7):4033-42. doi: 10.1128/JVI.03258-12. Epub 2013 Jan 30. PMID: 23365435 [PubMed - indexed for MEDLINE] Free PMC Article
- Infection of lymphoid tissues in the macaque upper respiratory tract contributes to the emergence of transmissible measles virus. Ludlow M, de Vries RD, Lemon K, McQuaid S, Millar E, van Amerongen G, Yüksel S, Verburgh RJ, Osterhaus AD, de Swart RL, Duprex WP. J Gen Virol. 2013 Sep;94(Pt 9):1933-44. doi: 10.1099/vir.0.054650-0. Epub 2013 Jun 19. PMID: 23784446 [PubMed - in process]

Abstract

Measles virus (MV) is one of the most contagious human infectious diseases, with an estimated R_0 of 12 – 18. However, the specific mechanism(s) responsible for the high transmissibility from infected to susceptible individuals are unknown. In this study, we have utilized the macaque model of measles to analyze virus distribution throughout the respiratory tract prior to and at the peak of virus replication. Analysis of tissues collected at early time-points, showed the presence of MV-infected lymphoid and myeloid cells in the absence of infected epithelial cells in both lower and upper respiratory tract (URT) epithelium. The crucial role of PVRL4, recently identified to mediate entry of MV into epithelial cells, in facilitating virus spread from immune cells to epithelial cells was confirmed by generating a PVRL4 'blind' recombinant wild-type MV and developing a novel *in vitro* B-cell/primary epithelial cell co-culture model. Previous analysis of PVRL4 mRNA levels has led to the proposal that MV transmission is facilitated by preferential targeting of epithelial cells of the trachea. However, we demonstrate widespread expression of PVRL4 in tissues throughout the respiratory tract and detected high infection levels in epithelial cells in the URT, particularly in the nasal cavity. This was accompanied by infiltration of MV-infected and uninfected immune cells, resulting in extensive disruption of the epithelial integrity throughout the respiratory tract. Tonsillar and adenoidal epithelia displaying the highest level of disruption, while this was absent or limited in the trachea and tongue. The epithelial damage resulted in large numbers of MV-infected lymphoid cells 'spilling' into the respiratory tract. Expulsion of cellular debris and cell free virus into the air following the induction of a coughing response likely explains the highly infectious nature of MV.

Introduction

Measles virus (MV), the prototype morbillivirus of the family *Paramyxoviridae,* remains a major cause of morbidity and mortality in the developing world and is highly transmissible [73]. An important consequence of this high rate of virus transmission is that vaccine coverage of >95% is required to eliminate endemic transmission [79], which increases the complexity and difficulty of MV eradication. Recent drops in vaccination rates in Europe have resulted in large-scale outbreaks of measles in a number of countries, with 30,567 cases, 8 deaths and 27 cases of acute encephalitis reported in 2011 [82]. However, whilst the epidemiology of measles has been extensively studied and is under constant surveillance by WHO reference laboratories, a paucity of data exists on the underlying lesions induced by MV in the respiratory tract of infected individuals that lead to such high rates of transmission.

The parameters of the contagious nature of MV and a postulated respiratory mode of transmission were first outlined by Peter Panum, following investigation of an epidemic in the Faro Islands in 1846 [75]. This enabled the incubation period of measles to be specified at 14 days, at which point the outbreak of the typical exanthem rash and catarrhal cough was associated with the time at which infected individuals were most infectious. Rapid resolution of the rash after 4 – 5 days was later shown to be associated with a strong immune response with cell-mediated rather than humoral immunity being predominantly responsible for clearance of MV [98,314]. Subsequent clinical studies demonstrated that MV is first detected in respiratory secretions during the preceding 2 – 4 day pro-dromal period [315,316], a feature of measles which complicates the management and control of outbreaks [63]. Thus MV-infected individuals are capable of transmitting virus to susceptible contacts for a total of 7-9 days. It is has been reported that <20% of cases are responsible for >80% of virus transmission [317], suggesting that differences in virus loads or degree of tissue damage during infection and/or host genetic differences have prominent roles in virus transmission.

In contrast to other paramyxoviruses such as respiratory syncytial virus and human metapneumovirus, which predominantly infect ciliated epithelial cells in the respiratory tract, MV is primarily a lymphotropic virus and causes systemic disease. Spread of virus to respiratory tract tissues following viremia is thought to be a mechanism responsible for the spread of MV to a new host. Studies showing that the apical side of ciliated epithelial cells is refractory to MV infection strongly indicate that these cells are not the initial target cells for MV infection in the respiratory tract [125,127]. However, the susceptibility of the basolateral side of epithelial cells to MV infection has led to the proposal that MV crosses the airway epithelium by directly infecting epithelial cells in the late stages of the disease [137]. Virus budding from the apical cell surface would then enable efficient transmission of virus via respiratory aerosols. The recent identification of PVRL4 as a cellular receptor for MV on some epithelial cell-lines [131] and subsequent confirmation and extension of this finding to primary differentiated epithelial cells grown on air-liquid interface [130] provides a mechanism through which MV infection of epithelial cells may occur *in vivo*.

We have previously investigated the early and viremic phases of measles in the macaque model, showing that alveolar macrophages and dendritic cells act as early targets of MV infection [54,256]. In addition, we demonstrated a prominent role for $CD150^+$ lymphocytes and myeloid cells in facilitating the spread of virus to lymphoid tissues throughout the body [54,256]. Moreover, we demonstrated that infection and subsequent depletion of memory T-lymphocytes and follicular B-lymphocytes may largely explain measles immune suppression [318]. Macaques provide an excellent natural model in which to investigate the late stages of measles and a number of outbreaks have been reported in primate colonies with extensive chains of transmission between animals [319–321]. In the present study we have examined the mechanism(s) through which MV is able to cross the epithelium and emerge into the respiratory tract of infected macaques at the peak of infection. We report a critical role for PVRL4 in mediating virus spread from immune to epithelial cells through a novel B-lymphocyte/epithelial cell model and show that disruption induced by immune cells infiltrating into the epithelium of respiratory tract and Waldeyer's ring tissues, concomitant with high levels of epithelial cell infection in the upper respiratory tract (URT), are key determinants governing MV transmission.

Materials & Methods

Ethics Statement

Animals were housed and experiments were conducted in compliance with European guidelines (EU directive on animal testing 86/609/EEC) and Dutch legislation (Experiments on Animals Act, 1997). The protocols were approved by the independent animal experimentation ethical review committee (DCC) in Driebergen, The Netherlands. Animal welfare was observed on daily basis, animal handling was performed under light anesthesia using ketamine and medetomidine. After handling atipamezole was administered to antagonize the effect of medetomidine.

Cells and viruses

Two molecular clones of wild-type MV expressing EGFP, rMV^{IC323}EGFP and rMV^{KS}EGFP, both validated in the macaque model previously [54,256,265], were used in this study to facilitate sensitive macroscopic and microscopic detection of foci of virus infection and the confirmation of pathological findings for different MV genotypes. rMV^{KS}EGFP was rescued from a molecular clone based on a wild-type genotype B3 virus isolated in 1997 from PBMCs taken from a measles case in Khartoum, Sudan [87,256] while rMV^{IC323}EGFP was based on the wild-type IC (Ichinose)-B strain of MV isolated from a throat swab taken from a patient in Japan in 1984 [53,322]. rMV^{KS}EGFP-PVRL4$^-$ was rescued in Vero-hCD150 cells following the insertion of two point mutations (P497S and P543A) into the H gene of pMV^{KS}EGFP (K. Lemon *et al*, in preparation). Virus stocks were generated in a human B-lymphoblastic cell line (B-LCL) and were tested to ensure the absence of *Mycoplasma* species prior to use in animal infections. Virus titres were obtained by endpoint titration in Vero-hCD150 cells and were expressed as 50% tissue culture infectious doses ($TCID_{50}$/ml).

Differentiation of NHBE cells

Normal human bronchial epithelial cells (NHBE) (Lonza, Walkersville Inc, MD, USA) were differentiated on type I collagen- and fibronectin-coated 6.5-mm transwell inserts with 0.4 µm pore size (Corning, Lowell, MA, USA) using an air-liquid interface as described previously [323]. Transepithelial electrical resistance measurement was measured using an STX3 electrode and EVOM meter device (World Precision Instruments). Cells were monitored using a DM IRBE UV microscope (Leica Microsystems) and images collected using a Leica DM600B microscope equipped with a Leica DFC350 FX digital camera and processed using Leica FW4000 software.

Animal study design

Cells and tissues were collected from MV-seronegative cynomolgus (n=35) and rhesus macaques (n=5) which were infected with rMV^{IC323}EGFP or rMV^{KS}EGFP (10^4 cell culture infectious dose-50 ($CCID_{50}$) by intra-tracheal inoculation or by aerosol inhalation. Animals were euthanized at 2 (n=3), 3 (n=3), 4 (n=3), 5 (n=4), 7 (n=9), 9 (n=8), 11 (n=6), 13 (n=2) or 15 (n=2) d.p.i. and represent animals infections reported previously (n=40) [54,256,265,318].

Virus detection in BAL, nose and throat swabs

Broncho-alveolar lavage (BAL) samples were collected by intra-tracheal infusion of PBS (10 ml) through a flexible catheter, followed by immediate recovery of 5 – 7 ml. After centrifugation (10 minutes, 300 g) the pellet was resuspended in PBS (3 ml) and BAL cells were counted using a hemocytometer. Nose- and throat swabs were collected using a polyester minitip urethral swab (Copan) or a cytobrush plus cell collector (Medsc and Medical), respectively. The swabs were collected in virus transport medium (2 ml), consisting of EMEM with Hanks' salts, supplemented with lactalbumine enzymatic hydrolysate (0.5 g/L), penicillin, streptomycin, polymyxine B sulphate, nystatin, gentamycin and glycerol (10% v/v). Swabs were frozen at -80°C within 2 hours after collection. Samples collected at different d.p.i. were thawed, vortexed, 200 µl was collected in lysis buffer for RNA isolation, and the remainder was used for serial two-fold titration (in eight rows) on Vero-hCD150 cells in 96-wells flat-bottom plates (Greiner Bio-One). Virus loads in BAL are expressed as the number of virus-infected cells per 10^6 total cells, virus loads in nose and throat swabs are expressed as the 50% endpoint dilution ($TCID_{50}$). In two experiments, including eight macaques, procedures were adapted to discriminate between cell-free and cell-associated virus. To this end, nose- and throat swabs were collected in RPMI-1640 medium supplemented with 10% (v/v) fetal bovine serum (FBS), and processed immediately after collection. The samples were briefly vortexed, and subsequently centrifuged for 10 minutes at 300 g. The supernatant was transferred to a new centrifuge tube, and the pellet was resuspended in an equivalent volume of RPMI + 10% (v/v) FBS to assess the level of cell-associated virus. The supernatant was centrifuged a second time for 15 minutes at 1000 g, and subsequently used to assess the level of cell-free virus.

Necropsies
Animals were euthanized by exsanguination under ketamine / medetomidine anesthesia, and macroscopic foci containing EGFP visualized and photographed as described previously [54,265]. Samples collected for direct detection of EGFP were collected in freshly prepared 4% (w/v) paraformaldehyde (PFA) in PBS, while samples required for histological, immunohistochemical or immunocytochemical analysis were collected in buffered formalin. Representative blocks from lung, multiple transverse cut blocks from trachea and primary bronchus, tonsil, adenoid, nasal septum, nasal concha, tongue, Koplik's spot and inner cheek were sampled. Tonsillar and adenoidal lymphoid tissues were bisected and embedded to provide full cross sections.

Immunohistochemical and immunofluorescence analysis of formalin fixed tissues
All formalin-fixed sections were deparaffinized, antigen retrieval performed and MV-infected cells detected as described previously [54] using polyclonal rabbit antibodies to EGFP (Invitrogen) or anti-measles N protein (Novus Biologicals) while PVRL4 present in adherent cell junctions in epithelia was detected using a polyclonal rabbit antibody (Sigma). An Envision-Peroxidase system with 3,3'-Diaminobenzidine (DAB) (DAKO) as substrate to detect antigen binding sites. Following assessment of histology and virus immunopathology in respiratory tract tissues, blocks were selected for dual labeling immunofluorescence performed using polyclonal rabbit antibodies to EGFP (Invitrogen), polyclonal rabbit and monoclonal mouse antibodies to measles N protein or human hyperimmune serum obtained from a patient with subacute sclerosing panencephalitis (SSPE) together with monoclonal mouse antibodies to the myeloid cell marker CD11c (Novocastra clone no. 5D11), T-lymphocyte marker CD3 (DAKO, clone F7.2.38), B-lymphocyte marker CD20 (DAKO, clone L26), macrophage marker Mac387 (Abcam) and an epithelial cytokeratin cell marker (DAKO, clone AE1/AE3) or a polyclonal rabbit antibody to PVRL4 (Sigma). Antigen binding sites were detected using antibodies anti-mouse/rabbit Alexa 488, anti-mouse/rabbit/human Alexa 568 and anti-human Alexa 488 (Invitrogen). Following washes to remove unbound antibody, sections were mounted on glass slides using DAPI (4',6-diamidino-2-phenylindole) hardset mounting medium (Vector). Selected hematoxylin and eosin (H&E) or immunohistochemically-stained sections were digitally scanned at high resolution and imaged using PathXL™ software package (i-Path Diagnostics Ltd.). Images from immunofluorescence stained slides were obtained using a fluorescent imaging microscope (Leica Microsystems).

Results

MV infection of respiratory tract tissues is widespread at the peak of MV infection
The spread of MV into respiratory tract tissues has been examined at different time-points in rhesus and cynomolgus macaques (n=40) [318] infected with recombinant (r) wild-type MV strains expressing EGFP. The expression of EGFP from an additional transcription unit facilitated sensitive macroscopic and microscopic detection of

MV-infected cells [54,104]. This targeted pathological assessment augmented the traditional use of 7 µm sections cut from selected blocks of formalin fixed paraffin-embedded tissues, which alone provide only a snapshot of the wider virus infection. Extensive EGFP fluorescence, indicative of MV infection, was visible throughout the respiratory tract at the peak of infection at 9 days post-infection (d.p.i.). Individual foci of MV infection were visible in the lung and trachea (Figure 1A and B), with more extensive fluorescence observed in the buccal mucosa, gingiva, tongue and Waldeyer's ring lymphoid tissues such as the tonsils (Figure 1C – E). Examination of transverse sections through the nose facilitated the detection of infected cells in the nasal concha and, more extensively, in the adjacent nasal mucosa (Figure 1F). Individual foci of infection were also present in the epithelium of the nasal septum (data not shown).

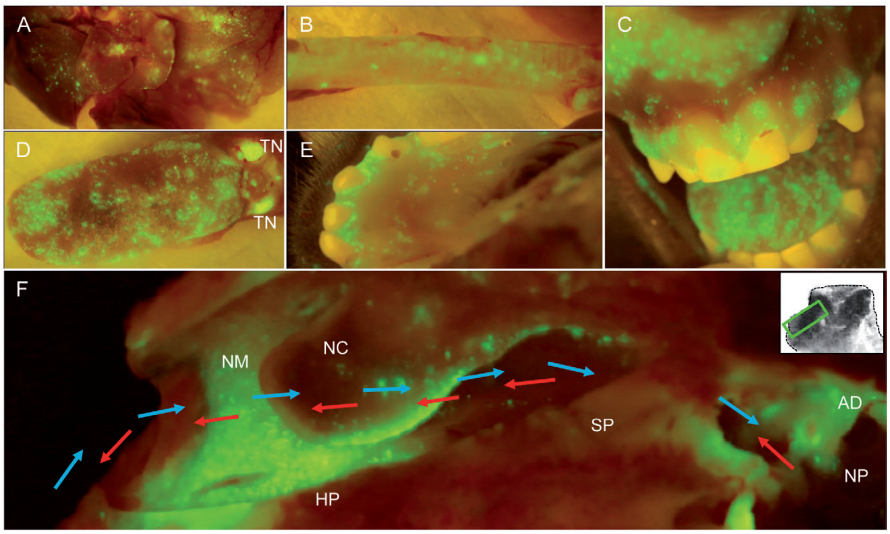

Figure 1. *Detection of macroscopic EGFP fluorescence in tissues from recombinant wild-type MV infected macaques. At the peak of infection (days 9 – 11) MV infection is present in (A) all lobes of the lung (B) trachea (C) buccal mucosa and gingiva (D) tongue and tonsils (E) gingiva (F) Transverse section through the nasal cavity. Direction of inhaled and exhaled airflow is indicated by blue and red arrows respectively and a schematic (inset) indicates the anatomical location of the transverse section. AD, adenoid; HP, hard palate; NC, Nasal Concha; NM, nasal mucosa; NP, nasopharynx; SP, soft palate; TN, tonsil.*

The release of virus into the respiratory tract lumen of infected macaques was examined between 0 and 13 d.p.i. through analysis of nose and throat swabs by virus isolation using Vero-hCD150 cells. Virus was neither isolated from nor detected in throat and nose samples until 3 and 5 d.p.i., respectively. Virus shedding reached a peak in the throat and nose at 9 – 11 d.p.i. (Figure 2A). Infectious virus was not isolated from throat or nose swabs at 13 d.p.i. or later. These results were confirmed by real-time reverse transcriptase PCR assays (data not shown). The widespread MV infection in respiratory tract tissues of infected macaques led us to hypothesize that virus-infected cells and/or cellular debris may be released into the lumen augmenting the budding of cell-free virus from the apical surface of epithelial

cells. This was examined by separating cell-associated and cell-free virus obtained from nose and throat swabs by repeated centrifugation. Isolation of virus from cell-associated or supernatant fractions showed equivalent levels of cell-associated and cell-free virus in throat- and nose samples, indicating either could be involved in transmission to susceptible hosts (Figure 2B).

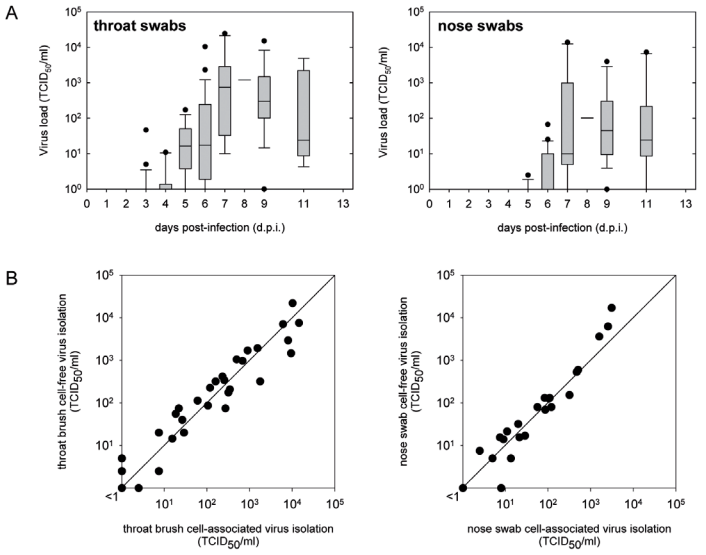

Figure 2. *Time course of MV replication in the respiratory tract of the macaque. (A) Isolation of MV from throat and nose swabs by assay on Vero-hCD150 cells. Median values are shown based on samples obtained from 38 wild-type MV infected animals between 0 and 13 d.p.i. (B) Taqman RT-PCR detection of cell-free and cell-associated MV from BAL, throat and nose swabs.*

PVRL4 is detected in epithelia in a large number of tissues in the LRT and URT

Primary normal human bronchial epithelial (NHBE) cells were cultured on transwell filters and differentiated at air-liquid interface, resulting in ciliated pseudostratified columnar epithelial cell cultures. Formalin-fixed and paraffin-embedded differentiated NHBE cells were used to test a number of commercial antibodies to PVRL4. Upon identification of a polyclonal antibody (Sigma) which met our criteria for acceptable levels of background staining and a staining pattern consistent with our understanding of spatial PVRL4 expression within epithelia (Figure 3A), this antibody was used to examine PVRL4 distribution in a large number of respiratory tract tissues from uninfected and MV-infected macaques. Prior to use, specificity of the antibody was verified by positive immunocytochemical staining of PVRL4 along the membrane of CHO-K1 cells transfected with a plasmid expressing human PVRL4, while negative staining was observed in cells transfected with an empty vector control plasmid (data not shown). High levels of PVRL4 expression were observed in the non-keratinized stratified squamous epithelia of the tonsil, with strong PVRL4 expression observed around the entire cell membrane of epithelial cells (Figure 3B). An analogous PVRL4 staining pattern was observed in focal areas of tongue epithelium (Figure 3C). In contrast, a more irregular polarized staining pattern was observed in nasal concha

epithelia in the URT and tracheal epithelia in the LRT, in which PVRL4 was mostly detected along the basolateral surface of pseudostratified columnar epithelial cells (Figure 3D and E). High levels of PVRL4 expression were also observed in the lung, especially in epithelial cells surrounding the lumen of bronchi (**Figure 3F**).

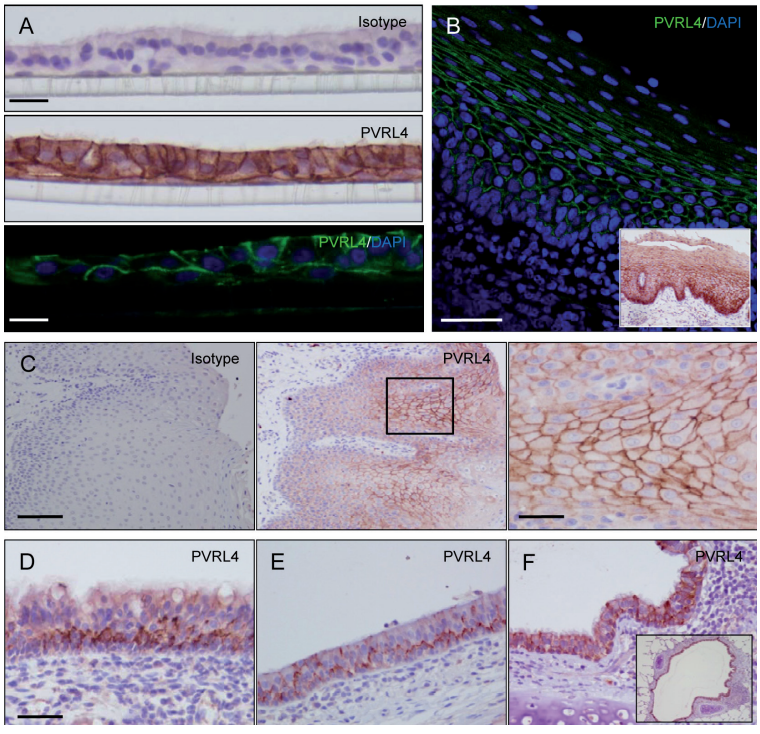

Figure 3. Distribution of PVRL4 within respiratory tract epithelia. *(A) Differentiated normal human bronchial epithelial (NHBE) cells grown on air-liquid interface. No positive staining is observed in control sections stained with an isotype antibody control (top). Immunohistochemical (middle, brown staining) and immunocytochemical (bottom, green staining) detection of PVRL4 present along the basolateral surface of epithelial cells and at cell junctions. Little positive staining is observed along the basolateral surface of basal cells in direct contact with the plastic membrane on which the cells are cultured. (B) Immunocytochemical detection of PVRL4 (green) at squamous epithelial cell boundaries within the epithelium of a tonsil obtained from an uninfected macaque. Nuclei were visualized using DAPI (blue). (C-F) Immunohistochemical staining of formalin fixed tissue sections taken from infected macaques at 9 d.p.i., at the peak of infection. (C) Tongue. Negative isotype control staining (left), high PVRL4 expression at cell boundaries of squamous epithelial cells in focal areas of the epithelium (middle), boxed area is shown at higher magnification (right). (D,E) PVRL4 expression is detected along the basolateral surface of pseudostratified ciliated epithelial cells in the nasal concha (D) and trachea (E). (F) Detection of PVRL4 at cell boundaries of bronchial epithelial cells in the lung. Strong expression of PVRL4 is observed throughout bronchial epithelium surrounding the lumen of the bronchus (inset).*

MV infection of epithelial cells occurs following contact with infected immune cells in respiratory tract epithelium

Respiratory tract tissue sections were examined at 7 d.p.i., one or two days prior to the peak of viremia, to assess how MV spreads into respiratory tract epithelia. While a low level of epithelial cell infection was observed in most respiratory tract

tissues (data not shown), an observation we have previously reported at this time point [54,284], large numbers of MV-infected leukocytes and myeloid cells were present beneath and within tonsillar epithelium (Figure 4A). Immune cells were the predominant MV-infected cell lineage present in respiratory tract epithelia at this time-point. Low levels of MV-infected immune cells were observed in close proximity to tracheal epithelium, with cellular processes interdigitating into the epithelium from underlying infected myeloid cells spanning the basement membrane, providing a route of virus entry into the epithelium (Figure 4B). The absence of MV-infected epithelial cells at many of these sites at this time point suggests that infiltration of infected immune cells or alternatively infection of resident immune cells in respiratory tract epithelium is an inherent pathological feature of MV infection and is not occurring in response to MV infection of epithelial cells.

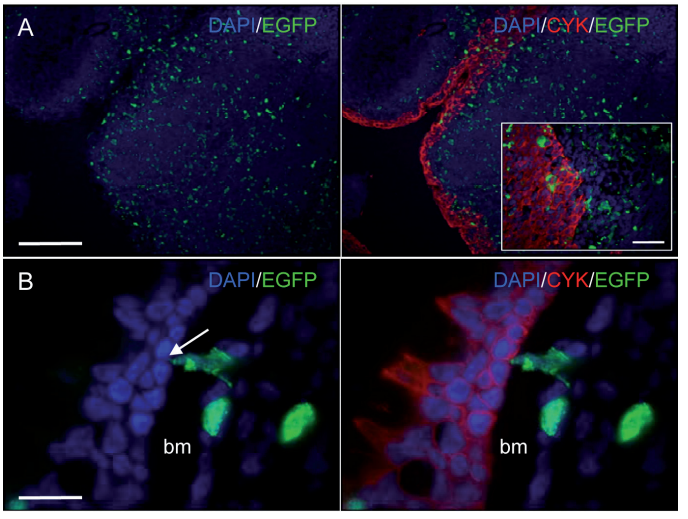

Figure 4. *Detection of MV-infected immune cells into respiratory tract epithelium. (A-C) Immunocytochemical staining of formalin-fixed tissue sections taken from infected macaques at 7 d.p.i., prior to the peak of infection. (A) Dual labeling of EGFP$^+$ immune cells (green) and epithelial cells (red) showing MV-infected cells in simple squamous epithelium of tonsillar crypts. Bar, 200 µm. Inset, Higher magnification of MV-infected immune cells present in tonsillar epithelium in the absence of adjacent epithelial cell infection. Bar, 50 µm. (B) A cellular process from a MV-infected myeloid cell (green) interdigitating between pseudostratified columnar epithelial cells (red) in the trachea. Bar, 20 µm. Nuclei were visualized using DAPI (blue).*

The role of MV-infected immune cells in the establishment of infection within respiratory tract epithelia was further investigated by establishing an *in vitro* co-culture model using human Epstein-Barr virus-transformed B-lymphoblastic cell lines (B-LCL) and differentiated NHBE cells. This model was used to monitor virus spread over time from rMV (rMV^{KS}EGFP) or PVRL4-'blind' MV (rMV^{KS}EGFP-PVRL4$^-$)-infected B-LCL to epithelial cells. PVRL4-'blind' MV contained two amino acid changes in the H gene (P497S and P543A), which have previously been shown to ablate virus-to-cell and cell-to-cell fusion in human epithelial cells [137]. Introducing these into the wild-type rMV^{KS} strain did not affect virus growth in B-LCL, but prevented MV cell-to-cell spread

in PVRL4^{+} NCI-H358 epithelial cells (K. Lemon *et al*, in preparation). Differentiated NHBE cultures containing beating cilia, mucus production and a transepithelial electrical resistance >800Ω/cm^2 contained multiple cytokeratin^{+} cell layers and cilia in immunohistochemically stained transverse sections of uninfected differentiated NHBE epithelium (Figure 5A). In order to model the seeding of immune cells directly into respiratory tract epithelium, 10^4 B-LCL infected with rMV^{KS}EGFP or rMV^{KS}EGFP-PVRL4^{-} at an MOI of 1 for 24 hours were overlaid onto the apical surface of intact NHBE cultures, or onto cultures in which the tight junctions had been scratched by drawing a pipette tip over the surface of the transwell. Prior to use in overlay experiments, MV-infected B-LCL were rinsed in DPBS to remove cell-free virus. This was confirmed by virus assay on Vero-hCD150 cells. As expected, no epithelial cell infection was observed at any time-point in transwells in which MV-infected B-LCL were overlaid onto the apical surface of an epithelium with intact tight junctions (data not shown). Fluorescent cells were observed to adhere equally to the scratched surface within twenty minutes of overlay of both rMV^{KS}EGFP and rMV^{KS}EGFP-PVRL4^{-} infected B-LCL onto wounded epithelium. (Figure 5B and C). Monitoring these infections over time revealed differences in the capacity of the viruses for cell-to-cell spread. Spread of rMV^{KS}EGFP into epithelial cells occurred from 12 hours post overlay (h.p.o.), and small foci of approximately 10-15 MV-infected epithelial cells were readily distinguished from adjacent fluorescent B-LCL at 24 h.p.o. (Figure 5D). At this time-point large aggregates of infected B-LCL were present at the sides of the transwell due to movement of cilia. Subsequent MV cell-to-cell spread resulted in progressively larger foci of >100 infected cells at 48 and 72 h.p.o (Figure 5D). In contrast, restricted cell-to-cell spread of MV from rMV^{KS}EGFP-PVRL4^{-}-infected B-LCL to adjacent epithelial cells was observed at 24 and 48 h.p.o., with foci of only 2 – 3 infected epithelial cells apparent at 72 h.p.o. (Figure 5E). Thus spread of MV from infiltrating immune cells within respiratory tract epithelium is dependent on the ability of the MV hemagglutinin glycoprotein to bind to PVRL4 on adjacent epithelial cells.

MV infection in the adenoid and tonsil is associated with extensive damage to the epithelium

We have previously shown that Waldeyer's ring lymphoepithelial tissues, including the adenoids (nasopharyngeal tonsils) and palatine tonsils, of macaques infected with pathogenic rMV contain large numbers of infected B- and T-lymphocytes and other mononuclear cells [54,265]. Although the role of these tissues in MV transmission has not been examined, disruption of adenoid or tonsillar epithelium would facilitate the release of both MV-infected cells and cell-free MV into the throat and nasal cavity. This hypothesis was examined in serial sections of Waldeyer's ring tissue from infected macaques. Epithelia showed extensive infection-associated lesions in comparison to uninfected tissue (Figure 6A). The adenoid and tonsillar epithelial architecture was disrupted with breakdown of the cytokeratin network observed, together with a reduction in the thickness of the epithelium and a concomitant infiltration of MV-infected and uninfected inflammatory immune cells. In a number of locations the epithelial cell barrier had been breached, with the lumen exposed to the underlying immune cells. Extensive disruption of the epithelium was also associated

with high levels of MV-infection of stratified squamous or pseudostratified ciliated columnar epithelial cells in the palatine tonsil or adenoid, respectively. Similar examples of epithelial disruption were observed in both the primary bronchus and lung (data not shown).

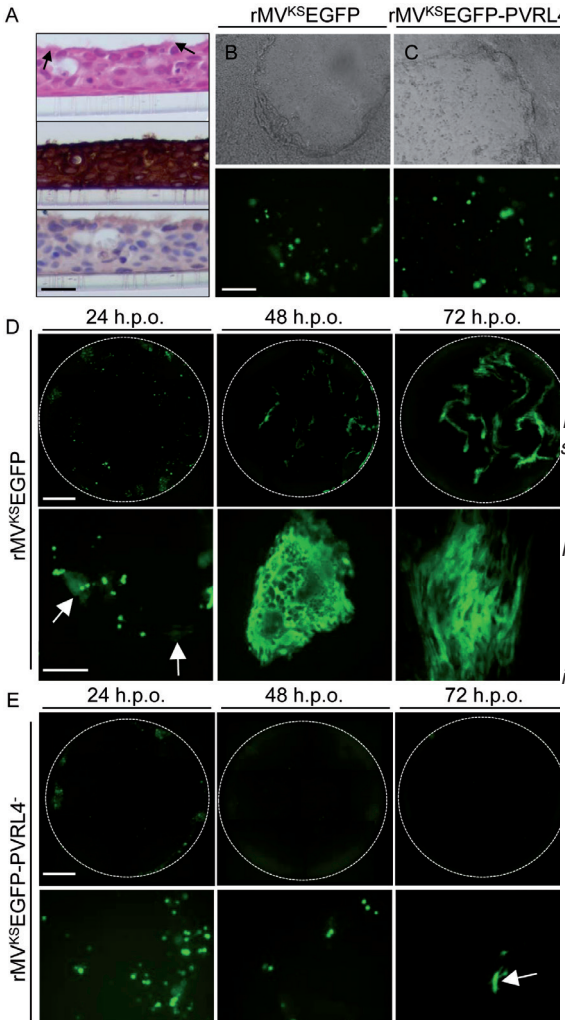

Figure 5. *PVRL4-blind MV does not spread from infected B-cells to epithelial cells. (A) Differentiated NHBE cells grown on air-liquid interface. Multiple cell layers and cilia (arrows) visible in an H&E stained section (top) stain positive for the cytokeratin cell marker AE1/AE3 (middle). No positive staining is observed in control sections in which the primary antibody is omitted (bottom). (B,C) Phase contrast and fluorescence photomicrographs 20 minutes after overlay of rMV^{KS}EGFP (B) or rMV^{KS}EGFP-PVRL4^{-} (C) infected B-LCL onto scratched monolayers of differentiated NHBE cells. (D) Time course of infection following overlay of rMV^{KS}EGFP infected B-LCL onto scratched monolayers of differentiated NHBE cells. Fluorescent images of the entire transwells at 24, 48 and 72 h.p.o are shown in the top panel while representative higher magnification images are shown in the bottom panel. Virus spread to epithelial cells is readily visualized at 24 h.p.o. (arrows) with increased cell-to-cell spread observed at 48 and 72 h.p.o. (E) Time course of infection following overlay of rMV^{KS}EGFP-PVRL4^{-} infected B-LCL onto scratched monolayers of differentiated NHBE cells. Only infected B-LCL are visible at 24 and 48 h.p.o with isolated examples of limited epithelial cell present at 72 h.p.o. (arrow).*

The availability of formalin-fixed samples of tonsillar tissue from a large number of animals enabled a retrospective temporal histopathological analysis to be performed on serial sections of tonsillar crypts (Figure 6B). These invaginated structures increase the surface area of tonsillar epithelium exposed to the environment and as such represent attractive targets in the investigation of routes of MV egress from the body. MV-infected cells and associated epithelial disruption were not evident in uninfected tonsillar crypt epithelium, but large numbers of MV-infected cells were present in underlying lymphoid tissue and within the stratified squamous epithelium

by 11 d.p.i. This was associated with epithelial disruption and the presence of large amounts of cellular debris containing mononuclear cells in the crypts. While MV-infected cells were no longer detected and some degree of epithelium repair was evident at 15 d.p.i., analysis of H&E-stained serial sections showed cellular debris consisting predominantly of mononuclear cells still trapped within the lumen of the crypts.

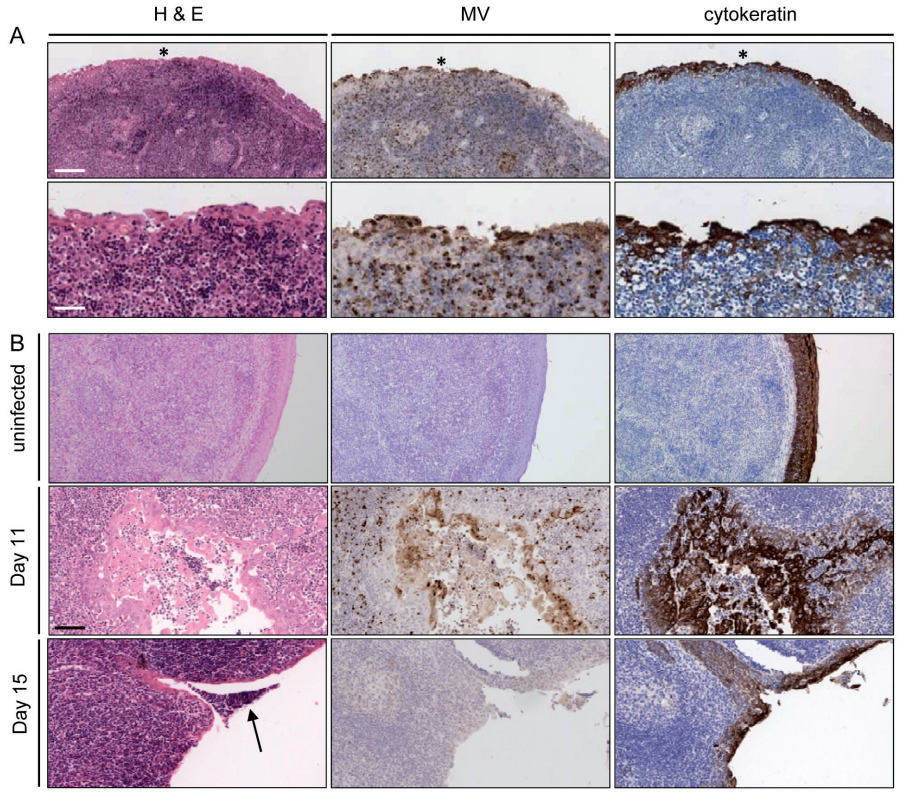

***Figure 6**. Disruption of tonsillar epithelium in MV-infected macaques due to infiltration of immune cells. (A,B) Serial H&E stained (left) and immunohistochemically stained sections (MV-N, centre; Cytokeratin, right) of tonsillar tissue from MV-infected macaques. (A) Extensive MV infection of epithelial cells and infiltration of infected and uninfected lymphoid/myeloid cells is associated with damage to the integrity of adenoidal epithelium at the peak of infection at 9 d.p.i. Bar (top), 160 µm; Bar (bottom), 40 µm. (B) Progressive infection and disruption is observed in tonsillar crypt epithelium. No infection is observed in uninfected epithelium, but extensive infection and disruption is evident at 11 d.p.i. MV infected cells are not observed in the epithelium at 15 d.p.i but aggregates of cellular debris remain in the lumen of the crypt (arrow). Bar (uninfected), 160 µm; Bar (days 11 – 15), 80 µm.*

Epithelial disruption in the respiratory tract is associated with immune cell infiltration

Extensive infiltration of immune cells into respiratory tract epithelium was a prominent feature of MV infection at the peak of infection (9 d.p.i.), a pathology not observed in uninfected tissues. Dual labeling of bronchial epithelium with antibodies against EGFP and cytokeratin showed the presence of exfoliated epithelial cells and EGFP$^+$

cells which did not contain cytokeratin (Figure 7A). Cytokeratin^{-} EGFP^{+} cells were commonly observed in the lumen of the respiratory tract. Examination of serial H&E and immunohistochemically stained sections of primary bronchus revealed extensive infiltration of mononuclear cells into the epithelium including locations which did not contain prominent MV infection, suggesting that both uninfected and infected immune cells infiltrate into the epithelium from underlying aggregates of lymphoid cells (Figure 7B). Epithelium disruption was more extensive than the observed level of epithelial cell infection and thus cannot be attributed to epithelial cell infection alone. Analogous lesions were readily observed in sections of the lung, in which the normal architecture of the simple squamous and cuboidal epithelium lining bronchioles was disrupted due to extensive infiltration of underlying immune cells, resulting in the formation of giant cells within the epithelium (data not shown).

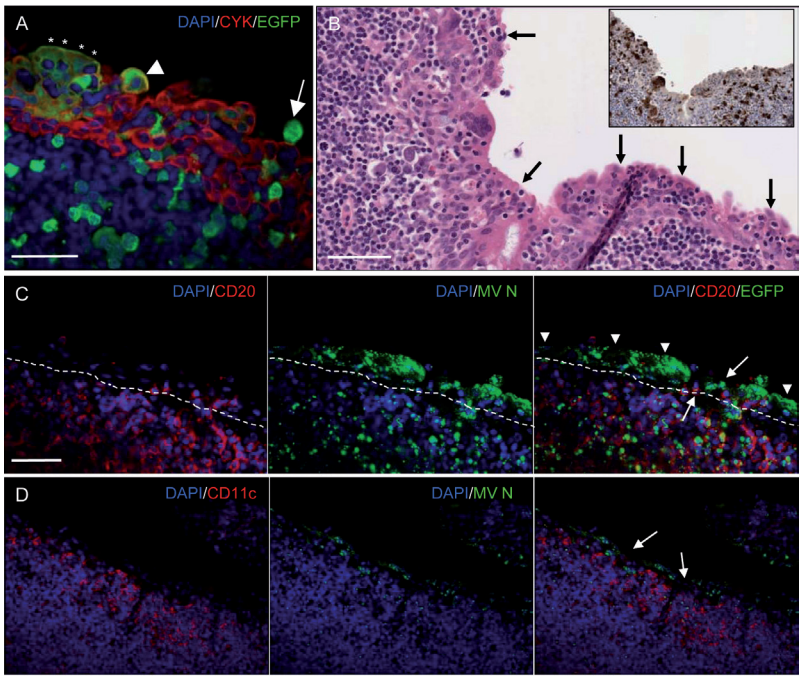

Figure 7. *Characterization of pathology in epithelium of MV-infected macaques. (A) Disruption of bronchial epithelium architecture due to extensive immune cell infiltration. Cytokeratin^{+} epithelial cells (red) at the luminal surface contain EGFP (green) (asterisks) and in some instances are exfoliated into the lumen (arrowhead). A single MV-infected cell on the apical surface of the epithelium does not contain cytokeratin (arrow). Bar, 50 µm. (B) Extensive infiltration of leukocytes (arrows) into primary bronchus epithelium is present in an H&E stained section of primary bronchus. Bar, 80 µm. Inset. MV-infected cells observed in an immunohistochemically stained serial section showing focal infection of the epithelium. (C) Dual labeling of MV antigen (green) and CD20^{+} B cells (red) in adenoid tissue showing B-cells infiltrating through a break in the epithelium (arrows). Contiguous MV infection of pseudostratified ciliated columnar adenoidal epithelial cells is observed adjacent to this area (arrowheads). The approximate location of the demarcation boundary of the epithelium from underlying tissue is indicated by a dashed line. (D) Dual labeling of MV infected cell (green) and CD11c-expressing myeloid cells (red) beneath and within tonsillar epithelium. MV-infected simple squamous epithelial cells are present adjacent to 'breaks' in the integrity of the epithelium (arrows). Bar (C,D), 100 µm. DAPI was used to counterstain nuclei (blue).*

Epithelial cell disruption was much more prominent in adenoid and tonsillar epithelium than in the bronchi and lung. Breaks in the integrity of adenoid epithelium facilitated the release of MV-infected CD20$^+$ B cells into the nasopharynx (Figure 7C), and large numbers of CD11c$^+$ myeloid cells were present beneath and within disrupted tonsillar epithelium (Figure 7D). The degree of epithelium disruption in the respiratory tract correlated with the amount of lymphoid tissue present with the more extensive infection and disruption of tonsillar and adenoid epithelium associated with high levels of underlying immune cell infection.

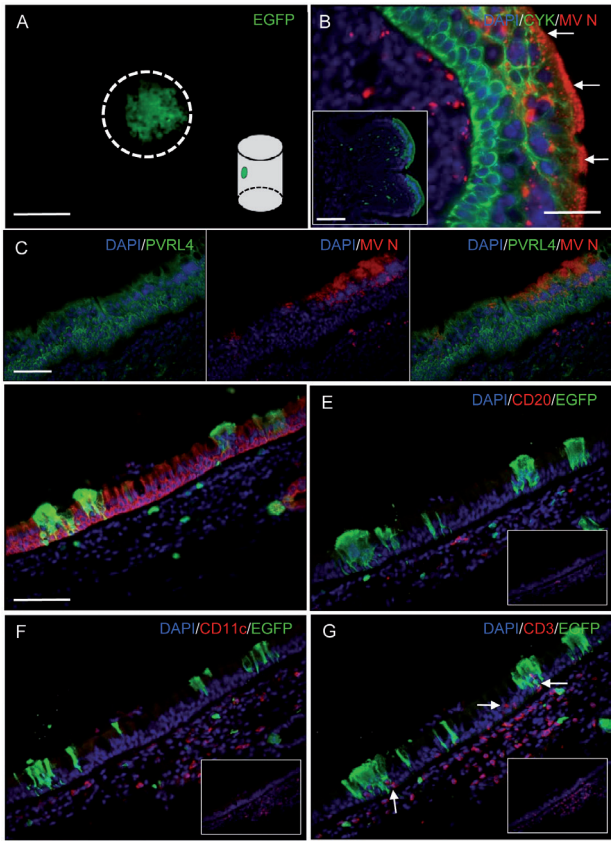

Figure 8. *Detection of MV-infected cells in the trachea. (A) Direct detection of a focus of MV-infected epithelial cells on the luminal surface of the trachea. No cell-to-cell fusion is observed within the focus of infection. A schematic diagram illustrates the presence of the circular EGFP$^+$ focus on the inside wall of the trachea. Bar, 250 µm. (B) Dual labeling of cytokeratin (green) and MV-N (red) showing MV infection of the luminal epithelial cell layers. MV-N was observed to accumulate beneath the apical cell membrane (arrows). Bar, 50 µm. Inset. A lower magnification image taken of the same region in an immunofluorescence stained serial section showing contiguous EGFP$^+$ epithelial cells (green). Bar, 200 µm. (C) No alteration of PVRL4 expression (green) is visible within a large focus of MV-infected cells (red). Bar, 80 µm. (D) Co-localization is observed between EGFP (green) and cytokeratin$^+$ epithelial cells (red). (E,F) No infiltration of CD20$^+$ B cells (red) (E) or CD11c$^+$ myeloid cells (red) (F) is observed into epithelium containing EGFP$^+$ epithelial cells. (G) Infiltration of CD3-expressing T-cells (red) into regions of epithelium containing foci of MV-infected epithelial cells (green). Bar (D-G), 100 µm. DAPI was used to counterstain cell nuclei (blue).*

MV infection of oral epithelium was investigated by targeted histopathological analysis of EGFP$^+$ foci taken from the inner cheek, tongue and buccal mucosa, which were readily identified macroscopically in the oral cavity (Figure 1). MV infection of the inner cheek was predominantly associated with infection of aggregates of lymphoid tissue adjacent to minor salivary gland ducts (Figure S1A). Non-keratinized stratified squamous epithelial cells lining the ducts were infected and this was associated with exfoliation of infected cells into the lumen of the duct and disruption of the epithelium (Figure S1B). Foci of MV infection in the buccal mucosa consisted of aggregates of infected lymphocytes and myeloid cells in the oral mucosa, with spread to adjacent non-keratinized stratified squamous epithelial cells (Figure S1C). Examination of intact foci of MV infection from the buccal mucosa by live cell confocal microscopy showed loosely connected aggregates of infected cells, with focal areas of cell-to-cell fusion visible in areas containing the highest density of MV-infected cells (Figure S1D). Importantly, no disruption of the oral epithelium adjacent to the lumen of the oral cavity was apparent, suggesting that these MV-infected cells present within the parenchyma of the tissue were unlikely to contribute to transmission. Similarly, analysis of serial histological and immunostained sections showed that MV-infected cells in the tongue were surrounded by uninfected keratinocytes and the overlying keratin layer, with little evidence of immune cell infiltration and no disruption of the integrity of the tongue epithelium (Figure S1E). Dual labeling with cytokeratin showed that infected cells within tongue epithelium consisted of non-keratinized stratified squamous epithelial cells (Figure S1F).

MV infection in the trachea is focal and does not result in damage to epithelium integrity

Microscopic examination of the inner surface of intact trachea rings obtained from animals at the peak of infection revealed circular foci of MV infected epithelial cells (Figure 8A). These may arise via the lateral spread of virus within the epithelium following initial infection of an epithelial cell, akin to virus cell-to-cell spread *in vitro* (compare with Figure 5D), albeit without apparent fusion of adjacent cell membranes. Spread of virus into the epithelium resulted in MV infection of ciliated pseudostratified columnar epithelial cells (Figure 8B, inset). Dual labeling for MV nucleoprotein (N) and cytokeratin showed accumulation of N protein underneath the apical membrane of MV-infected epithelial cells and an absence of infection in cytokeratin$^+$ cells present within lower layers of the epithelium (Figure 8B). Analysis of PVRL4 distribution showed that highest expression levels were present at the cell boundaries of basal tracheal epithelial cells, with no discernible modulation of PVRL4 expression visible within large foci of MV-infected cells (Figure 8C). Further analysis of the differential susceptibility of tracheal epithelial cells to MV infection by dual labelling with EGFP and Ki67, a marker of cellular proliferation, demonstrated that MV-negative epithelial cells present in basal cell layers of the epithelium stain positive for Ki67 and thus represent a population of uninfected proliferating epithelial cells (Figure S2A). The integrity of the tracheal epithelium was largely unaffected in areas of MV infection, apart from a low level of exfoliation of MV-infected epithelial cells from the cell surface (Figure 8D). Although no infiltration of CD20$^+$ B-cells or CD11c$^+$ myeloid cells into the epithelium was observed (Figure 8E and F), CD3$^+$

T-cells were observed in close proximity to MV-infected epithelial cells within the epithelium (Figure 8G). Absence of epithelial breakdown in foci of MV infection was occasionally observed in other tissues, including the primary bronchus (Figure S2B) and adenoids (data not shown). These rare foci were typically observed in the absence of underlying lymphoid infection and were characterized by fusion of adjacent pseudostratified columnar epithelial cells leading to large giant cells within the epithelium. Exfoliation and shedding of MV-infected epithelial cells was the predominant pathological response within such foci.

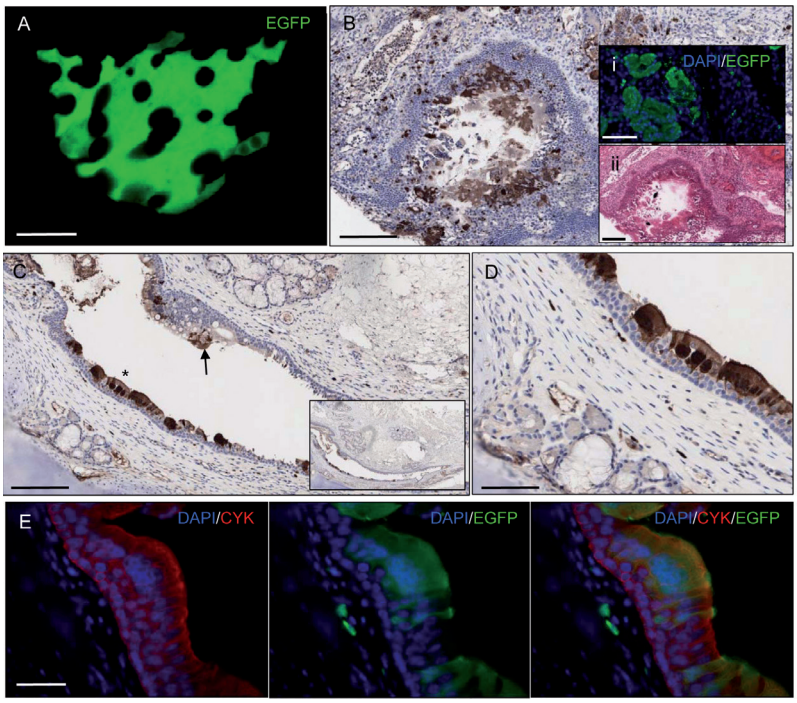

Figure 9. *MV infection of nasal epithelium. (A) Direct detection of a focus of EGFP⁺ cells on the surface of the nasal concha. No cell-to-cell fusion was observed between MV-infected cells. Bar, 100 µm. (B) Large numbers of MV-infected epithelial cells are present in an immunohistochemically stained section of nasal concha. Bar, 160 µm. (Inset i) Serial section of nasal concha showing immunofluorescence detection of EGFP in adjacent epithelial cells. Bar, 100 µm. (Inset ii) A H&E stained serial section of nasal concha showing shedding of epithelial cells into the lumen. Bar, 160 µm. (C) Immunohistochemical detection of EGFP in URT epithelium. Extensive infection of epithelial cells is apparent in the absence of underlying MV-infected immune cells. Bar, 160 µm. (D) Higher magnification of MV-infected epithelial cells indicated by the asterisk in (C). Little infection is apparent in the basal epithelial cell layers of the epithelium. Bar, 80 µm. (E) Dual labeling of EGFP (green) and cytokeratin⁺ pseudostratified columnar epithelial cells (red). Bar, 50 µm.*

Prominent MV infection of ciliated epithelial cells in the upper respiratory tract

High levels of MV-infected cells were present in the nasal cavity of MV-infected macaques at and immediately after the peak of infection (9 and 11 d.p.i., see Figure 1F), which suggested a role for nasal epithelium in MV transmission. Live cell confocal analysis of the nasal concha collected from infected animals using UV microscopy

revealed irregularly shaped foci of morphologically identifiable infected epithelial cells on the surface of the tissue (Figure 9A), illustrating the lateral spread of MV between epithelial cells once infection in the epithelium is established via contact with MV-infected immune cells. Examination of a transverse section through the nasal concha revealed high levels of epithelial cell infection and epithelial damage due to shedding of these cells into the lumen (Figure 9B). In the nasal mucosa MV mainly infected ciliated pseudostratified columnar epithelial cells, with contiguous epithelial cell infection and exfoliation of MV-infected epithelial cells into the nasal cavity observed as characteristic features of the infection in the URT (Figure 9C and D). In common with the distribution of MV-infected cells in tracheal epithelium, no positive immunostaining was observed in non-ciliated basal epithelial cells present in lower levels of the epithelium. Although cell-to-cell fusion was observed in large foci of MV-infected cytokeratin$^+$ epithelial cells, as evidenced by some degree of nuclei clustering, limited immune cell infiltration or disruption of the cytokeratin cytoskeleton was apparent (Figure 9E).

Cell-associated MV in the respiratory tract may contribute to MV transmission. In addition to the presence of MV-infected cells in the lumen of the respiratory tract, non-cellular EGFP$^+$ debris was readily detected adjacent to tracheal epithelium (Figure S3A and B). Dual labeling of EGFP and cytokeratin in nasal concha epithelium confirmed that this debris was present in the lumen and did not represent sub-cellular structures within infected cells (Figure S3C). Positive immunostaining observed using hyperimmune serum from an SSPE patient showed that MV antigen was present within these EGFP$^+$ structures on the surface of tracheal epithelium (Figure S3D). Transport of cellular debris and infectious virus released from MV-infected cells by the mucociliary escalator would represent an efficient mechanism through which MV infected cells/debris are removed from the body.

Discussion

Measles is characterized by a number of unique pathological and epidemiological features which slow progress towards controlling and eradicating the disease, such as a long incubation period prior to the onset of clinical symptoms, the fact that individuals in the prodromal stage are highly infectious and the requirement of vaccine coverage of greater than 95% in order to prevent endemic transmission. Furthermore, in contrast to infections caused by other respiratory pathogens such as human respiratory syncytial virus (HRSV), seasonal influenza strains and rhinoviruses, MV spreads systemically and infection of respiratory tract tissues occurs only in the latter stages of the disease. The identification of MV-infected cells or tissues in the lower and upper respiratory tract (LRT/URT) of infected individuals contributing to MV transmission has historically proven difficult to assess, due to a paucity of published pathological studies from human measles cases which made use of a set of diverse tissue blocks free of complications caused by underlying disease or secondary bacterial infections. With the macaque being an established natural model of measles, we undertook a comprehensive analysis of the respiratory tract of MV-infected macaques to analyze the pathology associated with the late stages of measles complementing our studies into early events in measles pathogenesis

[256]. The availability of tissue blocks from the respiratory tract of a large number of MV-infected animals (n=40) strengthens the pathological observations made in this study.

Analysis of respiratory tract tissues from MV-infected macaques highlighted the crucial role of MV-infected immune cells in the spread of virus to epithelial cells. Although long assumed, this is the first direct evidence of immune cells having a direct role in the spread of MV into epithelia *in vivo* and thus completes a missing link in our understanding of measles pathogenesis. MV spread into epithelia is most likely mediated via the interaction of MV glycoprotein complexes on the surface of immune cells with PVRL4, which we show to be present in epithelial cell adherent junctions in a wide array of tissues including lung, bronchi, trachea, tonsils, adenoids, nasal concha and tongue. This provides a mechanism through which MV can access a cellular receptor that is inaccessible to virus present in the lumen of the respiratory tract, due to its spatial localization within epithelia, and allow MV infection of epithelial cells in tissues of both the LRT and URT. Interestingly, PVRL4 was present around the entire cell membrane of squamous epithelial cells in the tonsils and focal areas of the tongue, whereas more polarized expression was observed along the basolateral surface of pseudostratified ciliated epithelial cells in the trachea and nasal concha. The observation that MV infection is primarily restricted to non-dividing ($Ki67^-$) pseudostratified columnar ciliated epithelial cells in tracheal epithelium, despite high levels of PVRL4 expression in dividing ($Ki67^+$) basal epithelial cells, suggests that additional host factors or the context through which such cells are contacted by MV-infected immune cells may influence the susceptibility of tracheal epithelial cells to MV infection.

We have previously reported the efficacy of using fluorescent MV to sensitively monitor virus cell-to-cell spread *in vitro* in neural and primary epithelial cells [125,324]. In this study we have applied these techniques to a novel *in vitro* co-culture model and show rapid virus spread from MV-infected B-cells to adjacent primary differentiated bronchial epithelial cells in which the adherent junctions were rendered accessible by cell wounding. This demonstrated that immune cells are capable of transferring MV infectivity into respiratory epithelium. The key role of PVRL4 in governing MV cell-to-cell spread from immune cells to epithelial cells in this model is highlighted by the observation that an rMV strain unable to bind to PVRL4 was restricted to B-LCL. The location of PVRL4 at adherent cell junctions within epithelia means that this molecule is inaccessible to cell-free virus, demonstrating that MV spread primarily occurs via cell-to-cell fusion rather than virus-cell fusion. Further research is required using model systems in which PVRL4 is expressed in its normal architectural location rather than over-expression in continuous cell-lines in order to gain a more complete understanding of the differences between these two modes of virus spread and ultimately their relevance to virus spread *in vivo*.

Recently, the trachea has been proposed as the primary site from which MV emerges into the airways of the respiratory tract prior to transmission to a susceptible host [130,158]. However, our extensive analysis of MV infection and related epithelial

disruption of respiratory tract epithelia and lymphoid tissues presents a more complex picture. While we detected large circular foci of MV-infected ciliated epithelial cells along the inner surface of the trachea, the overall burden of MV infection and associated lesions were lower than those of the nasal concha and mucosa in the nasal cavity and lymphoid tissues such as the palatine tonsils and adenoids, in which strong PVRL4 expression in epithelia was also observed. The anatomical location of these tissues means that virus shed from these sites is inherently more likely to be expelled into the environment by air flow and coughing than virus emerging lower in the airways, which has to survive neutralization for a longer time period by host factors present in mucus and saliva. A number of other viruses transmitted via the respiratory route are known to infect the URT including HRSV, coronaviruses and rhinoviruses [325–327]. In the case of Sendai virus, transmission of virus from infected animals was directly associated with infection of the URT and was independent of infection in the lung [328]. Conversely, H5N1 strains of influenza cause significant disease in humans with high case-fatality rates, but usually remain restricted to the initial index patient due to the fact that the virus replicates mostly in the LRT [329,330]. While the cough reflex typically associated with measles is triggered by stimulation of sensory nerves at or below the level of the larynx, URT infections can also trigger a productive cough due to non-specific effects of inflammatory mediators and increased mucus production on sensory nerve endings in the bronchi and trachea in the LRT [325].

Virus present in aerosol droplets expelled from MV-infected individuals by coughing is suspected of being the primary route of virus transmission to susceptible hosts [16] and is assumed to augment virus spread through fomites and/or close contact with bodily secretions. Conversely, while titers obtained from *in vitro* cultivation of MV are moderate (usually $<10^7$ $TCID_{50}$/ml) and comparable to many other respiratory pathogens, virus shedding into the airways of the respiratory tract of MV-infected individuals results in measles being the most infectious of all currently circulating human viruses. Indeed, the transmissibility of MV has been extensively documented with infected individuals in schools, sports stadiums, airplanes and offices responsible for triggering outbreaks [331–334]. In many of these cases, aerosol transmission of MV was suspected due to the absence of direct contact between many of the secondary cases with the index case.

The extreme infectiousness of some MV-infected individuals has resulted in the use of the term ‘superspreader’. In a well documented case from April 1951 a large measles outbreak was initiated in Qaqortoq (formerly Julianehåb), Greenland, when an asymptomatic sailor infected approximately 250 people in a dancehall in a single evening [335]. The fact that this event occurred when the index case was still in the prodromal stage of measles, three days before the onset of rash, demonstrated the difficulty in controlling outbreaks of measles. This provides a prime example of the complexity and heterogeneity of virus transmission as modeling has shown that approximately 20% of measles cases are responsible for 80% of virus transmission [317], thus adhering to the general ‘20/80’ rule governing individual variation in virus transmission [336]. It remains to be determined if such variation is linked to either

differences in the extent of epithelial disruption or the virus burden in the epithelium of the URT. Although *in vitro* studies have shown that epithelial cells can be infected by MV and produce new virus particles by budding from the apical membrane [127,129,337], MV cell-to-cell spread is relatively slow and results in the release of low virus titers [125,130,137]. In contrast, the MV replication cycle in lymphocytes is usually more rapid, and results in higher levels of viral shedding [256,265]. Therefore, the high MV infection levels in the lymphoid tissues of the URT should be considered more seriously as potential source of transmissible MV, especially when taking into account the amount of epithelial disruption we observed in these tissues.

Our long term studies in MV cell-to-cell spread led us to hypothesize that cell-associated virus may also contribute to virus transmission, especially in the spread of virus via close contact. This is supported by the fact that the release of giant cells into the lumen of the respiratory tract is a consistent pathological feature of measles [315,338,339]. Such cells obtained from nasopharyngeal or conjunctival swabs can be detected during the prodrome and have proven valuable as an additional diagnostic feature of measles in resource-limited areas [340]. Similarly, we also detected MV-infected cells and associated sub-cellular debris in the lumen of the respiratory tract together with cell-associated virus in nose and throat swabs taken from infected macaques. Such debris may be readily expelled into the air by coughing. Although there is a paucity of research into aerosol transmission of MV, it has been reported that cell-free MV survives for longer in the air than influenza virus [341], but shows increased rates of virus decay at humidity levels of 50-70%. It could be postulated that MV released into the environment in a cell-associated form would be better protected against environmental hazards such as humidity, temperature and UV radiation, and may be more infectious than cell-free virions due to the greater efficacy and speed of cell-to-cell fusion in comparison to virus-to-cell fusion. Future studies focused on aerosolized transmission of fluorescent morbilliviruses in the ferret, a model used extensively for virus transmission studies [342,343], would help to illuminate natural routes of virus transmission and provide the basis for more challenging studies into natural transmission of MV in the macaque.

In summary, we propose a mechanism for the introduction of MV into the respiratory epithelium following viremia, via the infiltration of MV-infected immune cells and subsequent spread to PVRL4-positive pseudostratified columnar and non-keratinized squamous epithelium (Figure S4), and demonstrate an analogous mode of cell-to-cell spread in a novel *in vitro* co-culture model of respiratory epithelium. Differential levels of MV infection were observed in epithelium from different respiratory tract tissues with tonsillar and nasal epithelium in the URT consistently displaying the highest levels of infection. In many instances this was associated with the infiltration of large numbers of uninfected immune cells leading to breakdown of the epithelium and sloughing of debris into the lumen of the respiratory tract. This complex emerging view of the late stages of measles pathogenesis should inform further experiments focused on the aerosolized transmission of morbilliviruses.

Acknowledgements

We would like to thank the staff of the Tissue Core Technology Unit and the Bioimaging Unit, QUB for expert technical assistance, Yusuke Yanagi for providing the Vero-hCD150 cell line and the plasmid from which the rMV^{IC323}EGFP virus was rescued and Thijs Kuiken and Bert Rima for helpful discussions. In addition, we thank Robert Dias D'Ullois, Tien Nguyen and Linda Rennick for their contributions to these studies. This work was funded by MRC (grant number G0801001) and ZonMW (grant number 91208012). The funders had no role in study design, data collection and analysis, decision to publish, or preparation of the manuscript.

Author contributions

Conceived and designed the experiments: ML, RDdV, AO, WPD, RLdS. Performed the experiments: ML, RDdV, SMcQ, JV, KL, EM, GvA, SY, RLdS. Analyzed the data: ML, RDdV, SMcQ, ADMEO, WPD, RLdS. Wrote the paper: ML, WPD, RLdS.

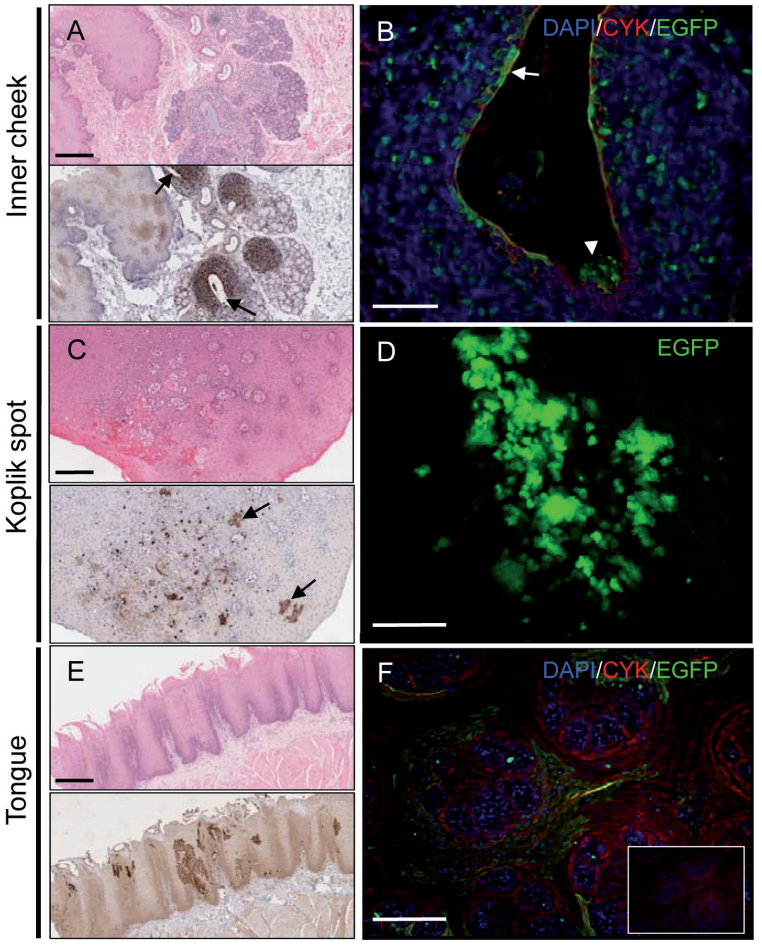

Figure S1. *MV infection of oral epithelium. (A) Serial H&E (top) and IHC stained (bottom) sections of the inner cheek. Heavy MV-infection of lymphoid tissue is observed adjacent to epithelial-cell lined minor salivary gland ducts (arrows). Bar, 320 µm. (B) Dual labeling of EGFP (green) and cytokeratin (red) showing MV infected epithelial cells (arrow) lining a duct located in the inner cheek. Disruption of the normal cytokeratin architecture and exfoliation of MV-infected cells is visible at the base of the duct (arrowhead). Bar, 100 µm. (C) Serial H&E (top) and IHC stained (bottom) sections of a focus of infection present in the buccal mucosa. MV infection is predominately observed in infiltrates of immune cells but a few foci of infected epithelial cells are present (arrows). Bar, 160 µm. (D) Three-dimensional reconstruction of a focus of infection in the buccal mucosa obtained from a 50 µm vibratome-cut section showing interconnected MV-infected immune cells (green). Bar, 60 µm. (E) Serial H&E (top) and IHC stained (bottom) sections of tongue. No infiltration of immune cells or disruption of epithelium is observed. Foci of MV-infected stratified squamous epithelial cells are visible in tongue epithelium. Bar, 320 µm. (F) Indirect dual immunofluorescence on a transverse tongue section. Large foci of MV-infected (EGFP, green) cells dual label with the epithelial cell marker cytokeratin (red). Bar, 200 µm. DAPI was used as a nuclei counterstain (blue) in (B and F).*

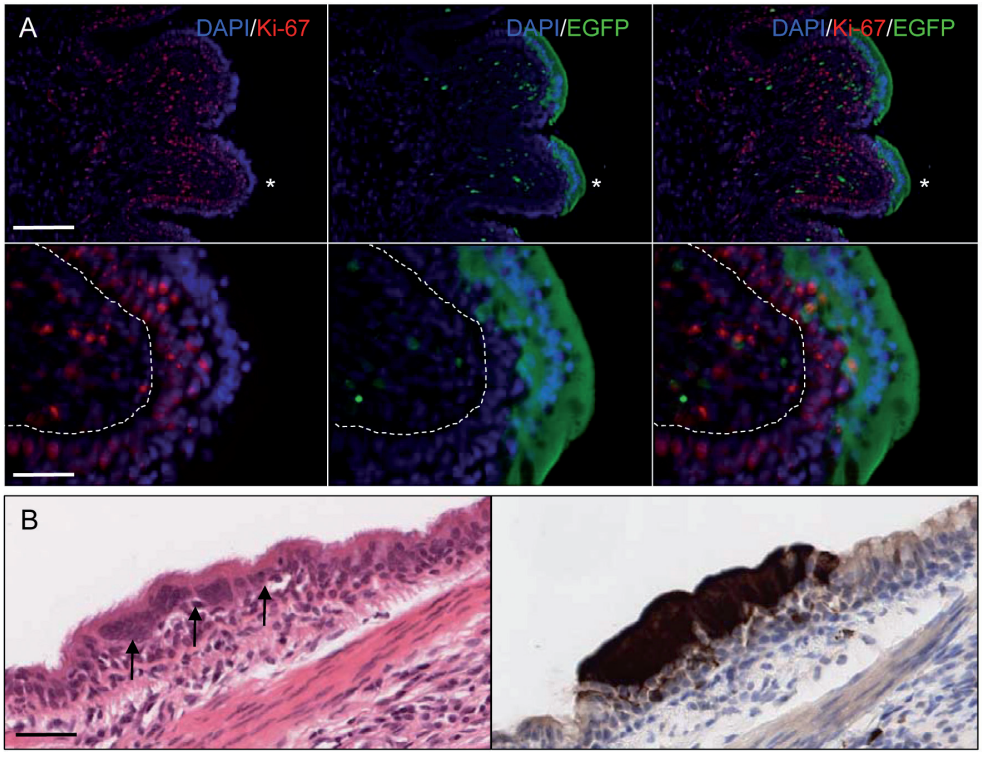

Figure S2. *MV does not infect proliferating basal epithelial cells in the trachea. (A) Little co-localization is observed between EGFP and Ki67, a marker of cell proliferation. The approximate location of the images shown at higher magnification in the bottom panel is indicated by an asterisk. The approximate location of the division between the epithelium and the sub-epithelial cell layers is shown by a dashed line. Bar (top), 200 µm; Bar (bottom), 50 µm. (B) Serial sections of primary bronchus. Multinucleated giant cells (arrows) present in the epithelium of an H&E stained section (left) are positive for EGFP in a serial immunohistochemically stained section (right). Bar, 40 µm.*

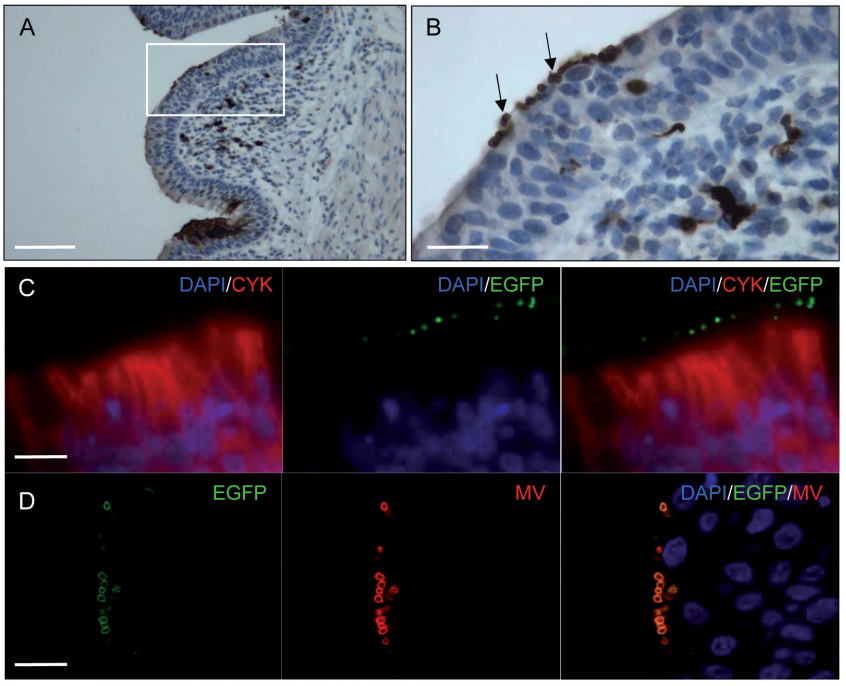

Figure S3. *Visualization of cell-associated virus in the lumen of the respiratory tract. (A) Detection of EGFP⁺ sub-cellular debris from MV-infected cells on the surface of trachea epithelium. Bar, 160 µm. (B) Higher magnification image of boxed area in (A). Bar, 20 µm. (C) EGFP⁺ sub-cellular debris (green) is present adjacent to cytokeratin⁺ nasal concha epithelial cells (red). Bar, 25 µm. (D) Detection of MV antigen using SSPE serum in EGFP⁺ sub-cellular structures in the tracheal lumen. Bar, 12 µm. DAPI was used as a nuclear counterstain in (C,D).*

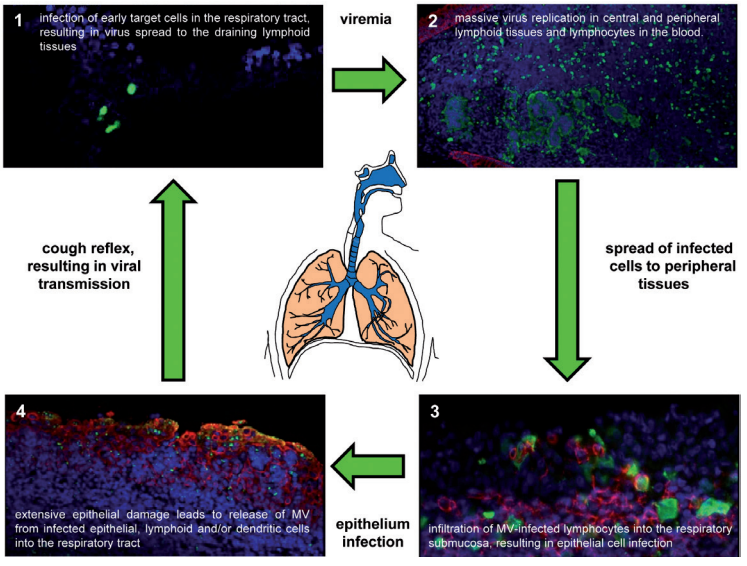

Figure S4. *A unified model of measles pathogenesis based on pathological analysis of tissues taken from wild-type MV infected macaques between 2 and 15 d.p.i.*

Immune suppression

IMMUNE SUPPRESSION

Specific CD8$^+$ lymphocytes control dissemination of measles virus

Rory D. de Vries, Selma Yüksel, Albert D.M.E. Osterhaus and Rik L. de Swart

European Journal of Immunology 2010 Feb; 40(2): 388 - 395

Abstract

Measles continues to be an important cause of childhood mortality in developing countries. Measles virus (MV) is lymphotropic and infects high percentages of B- and T-lymphocytes in lymphoid tissues. Cellular immunity is considered crucial for viral clearance; however, MV-specific T-lymphocytes generated during primary infection also constitute a potential target for MV infection. We therefore aimed to identify T-lymphocyte subsets that can clear MV infection without becoming infected. To this end, we infected human EBV transformed B-lymphoblastic cell lines (B-LCL) with a recombinant MV strain expressing enhanced GFP, and co-cultured these with non-infected B-LCL resulting in rapid viral spread. MV-specific $CD8^+$ T-cell clones efficiently suppressed MV dissemination in autologous and HLA-matched, but not in HLA-mismatched B-LCL. In contrast, $CD4^+$ T-cell clones could not control MV dissemination but became a target for MV infection themselves. Furthermore, PBMC collected 6 – 9 months after acute measles and stimulated with autologous MV-infected B-LCL also efficiently suppressed MV dissemination; this was mediated by the fraction containing $CD8^+$ T-lymphocytes. In conclusion, we have developed a powerful tool to study cellular immunity against measles, and demonstrate that control of MV dissemination is mediated by virus-specific $CD8^+$ rather than by $CD4^+$ T-lymphocytes.

In this issue

Measles virus-specific T cells: Kill or be killed

Measles is a highly contagious viral disease, killing approximately 200,000 children each year. The virus is lymphotropic and infects high percentages of B and T cells via its cellular receptor CD150. Paradoxically, virus-specific T cells can be either viral targets or effector cells mediating viral clearance. In this issue, de Vries *et al* examine whether specific $CD4^+$ or $CD8^+$ T cells can inhibit measles virus replication. The authors infected B cells with a recombinant measles virus expressing GFP, added specific T cells and monitored virus dissemination. Using this model, the authors demonstrate that measles virus-specific $CD8^+$ T-cell clones and primary $CD8^+$ T cells isolated from convalescent measles patients suppressed virus replication in autologous or HLA-matched B cells. Specific $CD4^+$ T cells not only were incapable of inhibiting virus replication, but were also more readily infected by the virus. The authors speculate that a similar approach may be used to study functional T-cell responses as potential correlates of protection in vaccine trials.

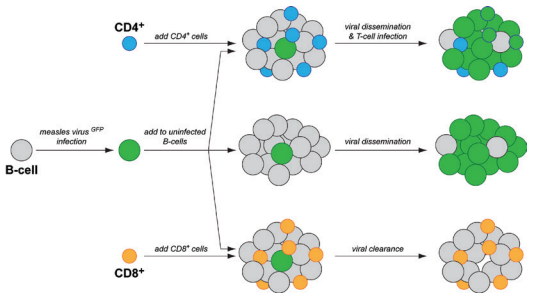

Introduction

Despite significant progress of global control programs, measles continues to be an important cause of morbidity and mortality in developing countries. Measles virus (MV) is a highly contagious agent that is transmitted by aerosols or direct contact with contaminated respiratory secretions. Measles starts with a prodromal phase of fever, cough and coryza, followed by a generalized maculopapular skin rash and conjunctivitis [16]. This phase is associated with a transient but profound immune suppression that can persist for months after convalescence, resulting in an increased susceptibility to opportunistic infections. Paradoxically, measles also induces strong MV-specific humoral and cellular immune responses, resulting in lifelong immunity [68].

Virus neutralizing serum antibodies are considered the main correlate of protection against MV infection [155]. However, viral clearance is predominantly mediated by cellular immune responses. This is illustrated by the fact that hypogammaglobulinemic children recover normally from MV infection [144,145], whereas children with deficits in cellular immunity develop severe disease and display prolonged viral shedding [144,146,344]. This could be partly due to the spread of MV via cell-cell fusion, thus potentially avoiding neutralizing antibodies in the bloodstream. *Ex vivo* experiments have shown that $CD8^+$ MV-specific T-lymphocytes predominate shortly after acute measles [148], indicating that these cells play a role in viral clearance. However, in classical ^{51}Cr-release assays both $CD4^+$ and $CD8^+$ MV-specific T-cell clones (TCC) had cytolytic activity against MV-infected autologous target cells [148–150], indicating that both subsets are capable of killing MV-infected cells.

Recent *in vivo* experiments in non-human primates have corroborated the importance of cellular immunity in MV clearance. MV-infected macaques depleted of B-lymphocytes were able to normally clear virus [153], whereas $CD8^+$ T-lymphocyte-depleted macaques presented with a more extensive rash, higher viral loads and a longer duration of viremia [314]. Depletion experiments for $CD4^+$ T-lymphocytes have not been performed in macaques, but studies in cotton rats showed that depletion did not have an effect on viral titres in the lung or on viral clearance [154]. More recently it was shown in a mouse model for respiratory syncytial virus, a related member of the family *Paramyxoviridae*, that both $CD4^+$ and $CD8^+$ T-lymphocytes independently contributed to virus elimination [151].

Currently, most studies on antiviral cellular immunity focus on quantification of virus-specific T cells rather than on the functional capacity of these cells. These assays either assess lymphoproliferation (*e.g.* CFSE dilution assays) [345], production of cytokines (*e.g.* ELISPOT or intracellular staining) [346–348], expression of cell surface markers (*e.g.* CD69 and CD107a) [349] or expression of a specific T-cell receptor (*e.g.* tetramer staining) [350]. Recently, a functional assay to assess virus-specific T-lymphocyte-mediated killing was developed based on transfection of autologous target cells with a viral gene linked to GFP. This assay was referred to as the fluorescent antigen-transfected target cell-CTL assay [351]. We adapted this set-up to a more dynamic system, in which autologous target cells were infected with a

recombinant MV strain expressing enhanced GFP (EGFP) [53] and co-cultured with MV-specific TCC. Using this assay, we determined the role of different T-lymphocyte subsets in the suppression of MV dissemination. We show that $CD8^+$ TCC efficiently clear an ongoing MV infection in B-lymphocytes, while $CD4^+$ TCC could not control spread of infection but instead became infected themselves. PBMC collected during measles convalescence could also control MV infection in autologous B cells, which was again predominantly mediated by $CD8^+$ T lymphocytes.

Materials & Methods

EBV transformation and susceptibility of B-LCL to MV infection

B-LCL from six donors were used as APC in these studies and were prepared as described previously [150], and cultured in RPMI-1640 supplemented with 10% FBS, 2 mM L-glutamine, penicillin (100 U/mL) and streptomycin (100 µg/mL). Susceptibility to WT recombinant MV expressing EGFP ($rMV^{IC323}EGFP$ [53], a kind gift of Dr. Y. Yanagi) infection was determined in a time-course experiment. Non-infected B-LCL were seeded into a 96-wells round-bottom plate at 2×10^4 cells per well, 50 MV-infected cells expressing EGFP as determined by flow cytometry were added to the cell pellet. Subsequently, the percentage of EGFP-expressing $CD19^+$ cells was determined in triplicate by flow cytometry after 6, 12, 24, 48 and 72 h of co-cultivation. To validate EGFP expression as a marker for MV infection, an intracellular counterstaining for MV-N with an unconjugated primary antibody (KK2, Chemicon) followed by a PE-conjugated goat anti-mouse secondary antibody (DAKO) was performed after fixation and permeabilization using cytofix/cytoperm buffers (BD Biosciences) containing 5% normal goat serum. Pictures of cell pellets were taken under an inverted light fluorescence microscope.

TCC

TCC (Table 1) were described previously (WH2.5, JP323, JP70 and Maja-F94) [148,219,234,352], or generated for the scope of this study (LB6 MV4, LB6 MV8, LB6 non-MV4 and LB6 non-MV8) as described previously [150]. Expression of CD4 or CD8 was assessed by flow cytometry using mAb SK3 (BD Biosciences) and DK25 (DAKO). Specificity of TCC was analyzed by IFNγ ELISPOT (Mabtech AB) in duplicate as described previously [353]. Briefly, 5×10^3 TCC and 2×10^4 autologous B-LCL infected with $MV^{Edmonston}$ or $rMV^{IC323}EGFP$ were co-cultured for 1.5 h at 37°C in a 96-wells V-bottom plate. Cells were transferred to nylon membrane bottom ELISPOT plates (Millipore) coated with a mAb against IFNγ and incubated for 4 h at 37°C. Spots were stained with a secondary mAb against IFNγ, and counted using an automated ELISPOT reader. One $CD4^+$ and one $CD8^+$ TCC that did not respond to MV in any assay were selected as non-specific controls.

PBMC bulk stimulations

PBMC from eight human donors (LB1 – 8) collected 6 – 9 months after acute measles were thawed and cultured in 96-well round-bottom plates at 2×10^5 cells per well. IL-7 was added at 3.5 ng/mL once after thawing and 5,000 autologous UV-irradiated non-infected or $MV^{Edmonston}$ infected B-LCL were added per well. Cultures

were maintained, and IL-2 was added 7 and 10 days after thawing. After 14 days, the bulk cultures were separated into a $CD4^+$ and $CD8^+$ fraction by magnetic separation with CD4 and CD8 microbeads (BD Biosciences). Purity and viability of subsets was confirmed by flow cytometry (data not shown). Written informed consent was obtained from all donors. The study was approved by the Medical Ethical Committee of the University Hospital Rotterdam-Dijkzigt (MEC 00.822).

Table 1. *TCC used in virus suppression assays. Four $CD4^+$ and four $CD8^+$ TCC were used to determine the contribution of these subsets to viral suppression. From both subtypes one non-MV-specific TCC was used as a negative control. Four of the selected clones were specific for MV-F, specificities of the other TCC was unknown. Autologous B-LCL were prepared for all donors and used as target cells in different assays.*

TCC	CD4/8	Specificity	Alternative names	References
Maja-F94	$CD4^+$	MV-F	Maja 94, JG-F94, 3-F94	[219,234,352]
JP70	$CD4^+$	MV	---	[148]
LB6 MV4	$CD4^+$	MV-F	---	---
LB6 non-MV4	$CD4^+$	non-MV	---	---
WH2.5	$CD8^+$	MV-F	WH 25, WH-F40, 2-F40	[148,219,352]
JP323	$CD8^+$	MV-F	JP-F20, 1-F20	[219,352]
LB6 MV8	$CD8^+$	MV	---	---
LB6 non-MV8	$CD8^+$	non-MV	---	---

In vitro virus suppression assay

TCC and PBMC bulk cultures, or PBMC $CD4^+/CD8^+$ subpopulations, were evaluated for their ability to control dissemination of MV infection in human B-LCL. In 96-well round-bottom plates (Greiner), a twofold dilution series of TCC or PBMC was prepared in RPMI-1640 supplemented with 10% FBS starting at 2×10^4 or 4×10^4 cells per well, respectively. To each well, a mixture of 2×10^4 non-infected and 50 rMV^{IC323}EGFP infected autologous, HLA-matched or HLA-mismatched B-LCL was added (cell number based on EGFP-expressing cells identified by flow cytometry). After 48 h of co-culture, cell pellets were examined for EGFP under an inverted light fluorescence microscope to assess the presence of MV-infected cells. In the absence of virus-specific T cells these conditions always resulted in massive MV infection of the complete culture. Since TCC and PBMC were added as a twofold dilution series, the minimal amount of cells required to control spread of MV infection could be determined. All TCC virus suppression assays were performed in duplicate as three independent experiments; all PBMC bulk virus suppression assays were performed in duplicate with the total bulk, the $CD4^+$ and the $CD8^+$ fraction.

Susceptibility of T-cell subsets for MV infection

Four clones were selected to determine susceptibility of T-cell subsets for infection with MV. A non-specific and MV-specific $CD4^+$ and $CD8^+$ TCC from a single donor (LB6 MV4, non-MV4, MV8 and non-MV8) were stimulated with anti-CD3 (Orthoclone, clone OKT3) and γ-irradiated allogeneic PBMC and B-LCL. Seven days after stimulation, 4×10^4 TCC were co-cultured with 1×10^4 MV-infected B-LCL.

At that moment, expression of the MV receptor CD150 on TCC was determined by flow cytometry by staining with mAb A12 (BD Pharmingen). As a negative control for CD150 expression, TCC were stained with an IgG1k^{PE} isotype control (CLB, clone CLB-203). After 24 h, cells were stained with mAb to CD3 (BD Pharmingen, clone SP34-2) and CD45RO (BD Pharmingen, clone UCHL-1). CD3^{+}CD45RO^{+} cells, representing the TCC, were selected and analyzed for EGFP expression by flow cytometry. CD45RO was used as a marker since in some cultures CD3 was downregulated due to specific stimulation; CD45RO was not expressed on any of the B-LCL used in this study. Infection percentages and geometric mean fluorescence levels of the positive populations were compared by Student's t-test.

Results

MV spreads rapidly in human EBV transformed B-lymphoblastic cell line cultures

We previously demonstrated that CD150^{+} B-lymphocytes are a major target cell for MV infection in lymphoid tissues of macaques [54]. To mimic MV spread in lymphoid tissues, we added small numbers of MV-infected human EBV transformed B-lymphoblastic cell line (B-LCL) to non-infected B-LCL cultures. The percentage of MV-infected cells was determined by flow cytometry at time points 0, 6, 12, 24, 48 and 72 h (Figure 1A). At time point 0, the 50 EGFP-expressing MV-infected cells were readily detectable by both flow cytometry and fluorescence microscopy (data not shown). After 48 h the percentage of MV-infected B-LCL of six different donors varied between 30 and 80%. MV infection could easily be assessed by screening for EGFP fluorescence under an inverted fluorescence microscope (Figure 1B). These experiments demonstrate that rMV^{IC323}EGFP infection spreads rapidly in human B-LCL, resulting in productive infection of the majority of the cells within 48h. In order to confirm that EGFP expression could be used as a reliable marker of MV infection, we performed intracellular staining of MV-infected B-LCL for expression of MV-nucleoprotein (N) at the different time-points. The data shown in Figure 1C demonstrate that expression of N strongly correlates with EGFP positivity, validating that EGFP can indeed be used as a reliable indicator of MV infection in this system.

MV-specific TCC recognize autologous target cells infected with MV

Six MV-specific and two non-specific TCC were used in this study (Table 1). Specificity of all TCC for MV was re-evaluated in an IFNγ ELISPOT assay (Figure 2A and B). All MV-specific TCC produced IFNγ when stimulated with autologous B-LCL infected with either MV^{Edmonston} or rMV^{IC323}EGFP. TCC LB6 non-MV4 and non-MV8 did not recognize MV-infected autologous cells, and were used as non-specific controls. In subsequent experiments with the selected TCC, IFNγ ELISPOT assays were always performed in parallel to confirm specificity of the TCC and their capacity to recognize their autologous B-LCL.

MV-specific CD8^{+} TCC suppress dissemination of MV infection

To determine the ability of TCC to suppress spread of an ongoing MV infection, we co-cultured MV-infected and non-infected B-LCL as described in Figure 1, and

added serial dilutions of TCC. After 48 h the minimal numbers of TCC necessary to control infection were determined by screening for EGFP fluorescence. For TCC of which the restriction element was known, autologous, HLA-matched and HLA-mismatched B-LCL were used, to confirm that suppression was HLA-restricted. All three MV-specific CD8$^+$ TCC were capable of controlling spread of MV infection, whereas the non-specific CD8$^+$ TCC could not (Figure 3A). In cultures in which infection was controlled the original 50 MV-infected B-LCL had also disappeared, demonstrating TCC-mediated clearance. Virus suppression in HLA-matched target cells was similar to that in autologous B-LCL, whereas MV infection could never be controlled in HLA-mismatched B-LCL. Similar experiments were performed with CD4$^+$ TCC, which displayed limited or no suppression capacity: only TCC Maja-F94 was capable of clearing MV-infected cells, but less efficient than any of the CD8$^+$ TCC tested (Figure 3A).

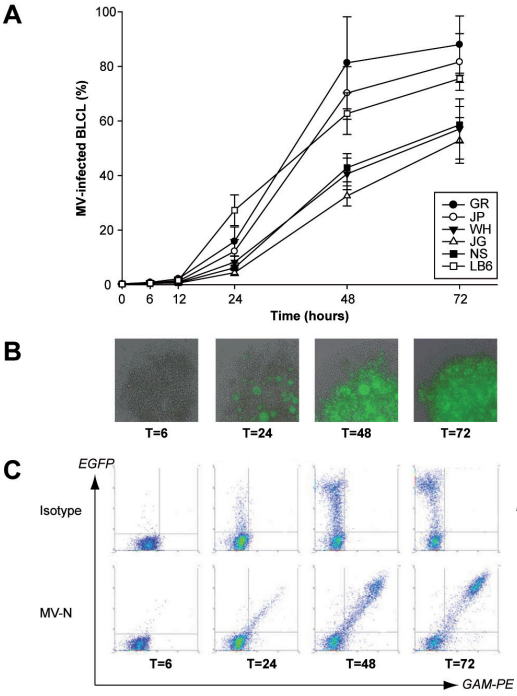

Figure 1. *MV spread in human B-LCL. (A) 50 rMV^{IC323}EGFP-infected B-LCL were added to 2 x 10^4 non-infected B-LCL in 96-well round-bottom plates. Percentages of EGFP-expressing cells were determined by flow cytometry after 0, 6, 12, 24, 48 and 72 h. Data show mean ± SD (n = 3) and are representative of six independent experiments. Symbols represent B-LCL from different human donors. (B) Representative images of cell pellets at 6, 24, 48 or 72 h after co-culture. (C) Counter staining for MV-N validated the use of EGFP expression as a marker for MV infection. All EGFP$^+$ cells also stained positive for MV-N by intracellular staining using mAb KK2 followed by secondary staining with goat anti-mouse^{PE} (DAKO), while EGFP$^+$ cells remained negative after staining with an isotype control. Data shown were obtained with B-LCL from donor WH (same experiment as shown in (A)), at least three independent repeats were performed for different B-LCL with comparable results.*

CD8$^+$ fractions of specifically stimulated PBMC control MV infection

Instead of using MV-specific TCC, mock- or MV-stimulated bulk cultures of PBMC collected from eight human donors (LB1 – 8) 6 – 9 months after acute measles were tested for their clearance capacity. After a single round of stimulation with autologous MV-infected or mock-infected UV-irradiated B-LCL, two-fold dilutions of the PBMC bulk cultures were co-cultured with rMV^{IC323}EGFP infected autologous B-LCL similar as described above for TCC. PBMC stimulated with mock-infected B-LCL displayed limited clearance capacity, but PBMC from six out of eight donors stimulated with MV-infected BLCL specifically controlled MV spread (Figure 3B, left panel). Interestingly, we were unable to detect MV-specific T cells by IFNγ ELISPOT assays in any of

these bulk cultures, due to high background responses after stimulation with mock-infected APC (data not shown). CD4+ fractions of these PBMC bulk cultures showed no suppressive capacity (Figure 3B, middle panel). In contrast, the CD8+ fraction inhibited MV dissemination to a comparable level as the complete bulk culture (Figure 3B, right panel), demonstrating that also in PBMC bulk cultures clearance was mediated by CD8+ T-lymphocytes.

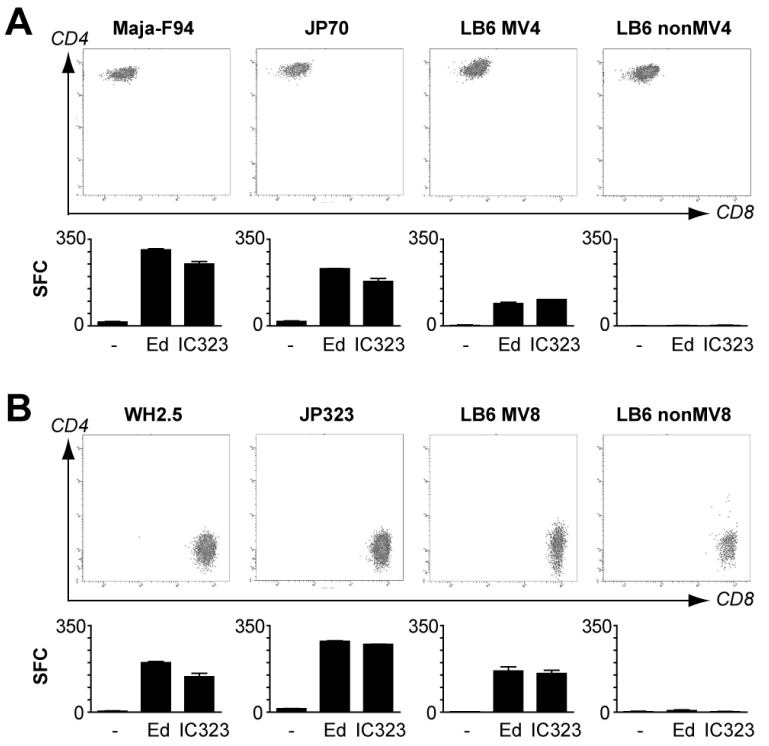

Figure 2. *Phenotype and MV specificity of TCC. Specificity of TCC was determined by IFNγ ELISPOT (bottom panels), and CD4/CD8 surface expression by flow cytometry (top panels). (A) CD4+ TCC Maja-F94, JP70 and LB6 MV4 are MV-specific; LB6 non-MV4 is a non-specific negative control. (B) CD8+ TCC WH2.5, JP323, LB6 MV8 are MV-specific; LB6 non-MV8 is a non-specific negative control. IFNγ ELISPOT was performed by co-culture of 2 x 10⁴ autologous B-LCL (mock infected, MV^{Edmonston} infected, rMV^{IC323}EGFP infected) with 5 x 10³ TCC. IFNγ ELISPOT results show spot forming cells (SFC), mean ± SD of duplicates. Data are representative of three independent experiments.*

MV-specific CD8+ TCC are less susceptible to MV infection

While performing virus suppression assays we often observed MV infection of CD4+ TCC. Since MV-specific CD8+ TCC efficiently cleared MV infection, the susceptibility of CD4+ and CD8+ TCC to MV infection was difficult to compare in that system. We therefore selected non-specific and MV-specific CD4+ and CD8+ TCC for co-cultivation with MV-infected HLA-mismatched B-LCL to exclude an influence of specific killing. At the time-point of infection, all TCC expressed the MV receptor CD150 at comparable levels on their cell surface (Figure 4A). Susceptibility of the two non-specific and the CD4+ MV-specific TCC was comparable, but the MV-specific CD8+ TCC was

significantly less susceptible to MV infection ($p < 0.05$ for LB6 MV8 compared with all other TCC by Student's t-test, Figure 4B, left panel). Flow cytometry showed that in MV-specific CD8+ TCC not only the percentage EGFP-expressing cells, but also the absolute EGFP expression levels were significantly lower than those in the other three TCC, suggesting that virus replication was suppressed ($p < 0.05$ for LB6 MV8 compared with all other TCC by Student's t-test, Figure 4B, right panel).

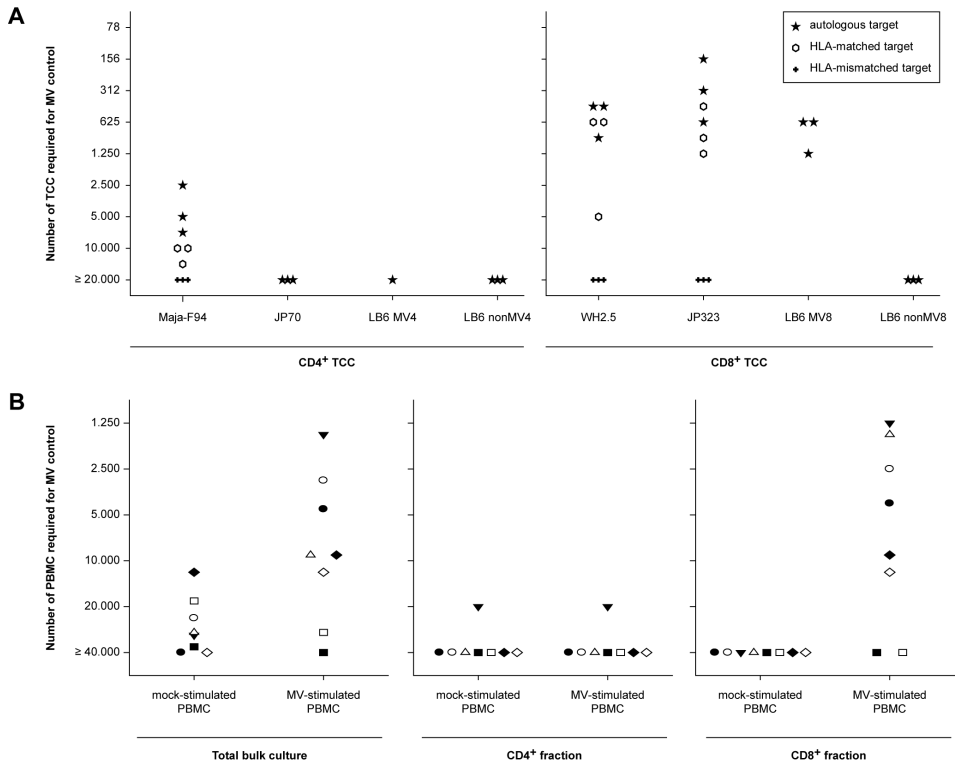

Figure 3. *(A) Suppression of MV dissemination by CD4+ and CD8+ TCC. Data show the minimal number of TCC required to suppress MV spread in autologous B-LCL. Virus suppression assays with TCC Maja-F94, WH2.5, and JP323 were also performed with HLA-matched and mismatched target cells. Each symbol represents the mean of duplicate measurements in one assay, the three identical symbols represent the results of three independent experiments. IFNγ ELISPOT assays were performed in parallel to confirm the TCC specificity (data not shown). Data are representative of three independent experiments. These experiments were also repeated under different conditions and with different CD4+ and CD8+ TCC, always resulting in similar results. (B) Suppression of MV dissemination by PBMC bulk cultures. PBMC from eight donors collected 6 – 9 months after natural measles infection were stimulated with UV-inactivated mock- or MV-infected autologous B-LCL and expanded for 2 wk. Data show the minimal number of PBMC required for suppression of MV spread in autologous B-LCL (means of duplicate measurements). Each symbol represents an individual donor. The left panel shows suppression with total PBMC bulk cultures; the middle and right panels show suppression mediated by CD4+ and CD8+ fractions, respectively.*

Discussion

Here we have demonstrated that control of MV dissemination *in vitro* is predominantly mediated by HLA class I-restricted CD8+ T-lymphocytes. Both the use of virus-specific TCC and PBMC bulk cultures confirmed that CD4+ T-lymphocytes have limited effector capacity, but that CD8+ T-lymphocytes efficiently cleared an ongoing MV infection. Furthermore we have shown that MV-specific CD4+ T-lymphocytes are targets for MV infection. MV-specific CD8+ T-lymphocytes could also be infected by the virus, but displayed a lower sensitivity and sustained lower levels of virus replication.

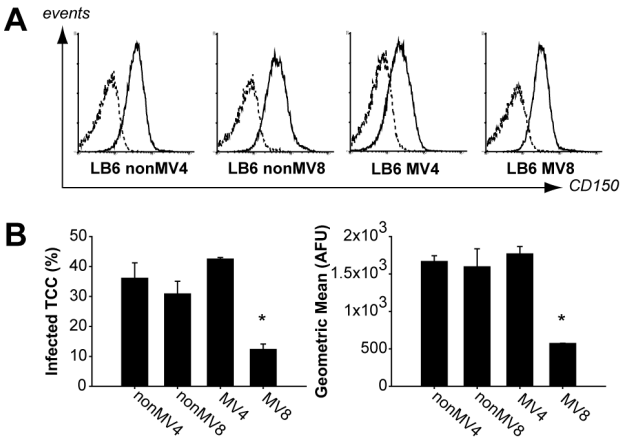

Figure 4. *Susceptibility of TCC to MV infection. Four TCC isolated from a single donor were stimulated with mAb to human CD3 and irradiated feeder cells, IL-2 was added on days 1 and 4. After 7 days cells were washed and used for infection by co-culture with HLA-mismatched MV-infected B-LCL. (A) Staining of TCC with mAb to CD150 (solid line) or isotype control (dotted line). (B) Percentages MV-infected TCC after 24 h co-culture of 4 x 10^4 TCC with 1 x 10^4 MV-infected mismatched B-LCL (left panel), and the geometric mean fluorescence signal of the EGFP+ population (in arbitrary fluorescence units, AFU, right panel). Data show mean ± SD of triplicate measurements, *p < 0.05 as determined by Student's t-test for TCC MV8 compared with all other TCC. This experiment was repeated twice with similar results under the conditions described here, and several times under other conditions (e.g. different number of infected cells, or direct infection of TCC with cell-free virus).*

Our study design is based on the use of MV-specific TCC or PBMC bulk cultures, in combination with autologous or HLA-matched B-LCL infected with an EGFP-expressing virus. IFNγ ELISPOT was performed in parallel with the suppression assays to confirm the specificity of the TCC in each experiment. We have previously used the same B-LCL as APC for these TCC, and demonstrated that CD8+ TCC recognize MV-infected B-LCL whereas CD4+ TCC can recognize either MV-infected or antigen-pulsed B-LCL [234]. The virus suppression assay as described here has several advantages over the more traditional methods to study cellular immunity: it directly assesses antiviral activity rather than parameters that are associated with the antiviral capacity, like IFNγ production or cytolytic activity. Compared to the fluorescent antigen-transfected target cell-CTL described by Van Baalen *et al* [351] this assay is closer to the natural situation, since it is based on infection rather than transfection of APC. Consequently, viral antigens are processed and presented as

they would be during natural measles *in vivo*, and antiviral capacity is measured against the entire virus instead of single proteins or peptides.

Previously, $CD4^+$ MV-specific TCC were described to have cytolytic activity in classic ^{51}Cr-release assays, albeit at lower levels than $CD8^+$ TCC [148–150]. In this study, we show that most $CD4^+$ MV-specific TCC could not kill MV-infected cells, and that the $CD4^+$ fraction from PBMC by itself had no viral suppression capacity. Apparently, the requirements for suppression of virus spread are more stringent than those for chromium release. Since our virus suppression assay more closely resembles the *in vivo* situation than a ^{51}Cr release assay performed over a period of 4 – 6 h, our data suggest that $CD4^+$ T-lymphocytes play a limited role in viral clearance during natural measles.

We also assessed suppression of MV dissemination by PBMC collected 6 – 9 months after recovery from measles, after stimulation with either MV- or mock-infected autologous B-LCL and expansion for 2 wk in the presence of IL-2. Specifically stimulated bulk cultures of the majority of the donors were capable of clearing the virus. When testing $CD4^+$ and $CD8^+$ fractions separately, MV clearance proved to be exclusively mediated by the $CD8^+$ fraction. In conclusion, these data confirm that clearance of MV infection is predominantly mediated by $CD8^+$ T-lymphocytes, and that $CD4^+$ T-lymphocytes only have a limited contribution as effector cells.

It remains difficult to determine if MV control as determined in our assays is predominantly mediated by clearance of infected cells or by suppression of production of progeny virus. Theoretically, MV-specific T-lymphocytes could rapidly kill the 50 MV-infected B-LCL that were used as input. However, it is likely that by that time the input cells have already started to infect the 2×10^4 uninfected B-LCL. Whether the outcome is mediated by killing of infected cells or suppression of MV replication before production of progeny virus, the outcome of our experiments is that control of MV dissemination is mediated by $CD8^+$ T-lymphocytes.

Our studies indicated that the TCC themselves could become a target for MV infection. When comparing antigen-specific and non-specific $CD4^+$ and $CD8^+$ TCC from a single donor, the antigen-specific $CD8^+$ TCC proved least susceptible. After co-culture of TCC with HLA-mismatched MV-infected cells, both the percentage of EGFP-expressing cells and the absolute levels of EGFP within the positive population were lower than those in the other three TCC. These experiments were performed with HLA-mismatched MV-infected cells to prevent specific killing of B-LCL by the MV-specific $CD8^+$ TCC. Once a fraction of the MV-specific $CD8^+$ TCC becomes infected with MV these cells can serve as APC for the uninfected TCC in the same culture. Although we have not been able to experimentally prove auto-killing in the context of our assay, we hypothesize that the interaction between infected and uninfected MV-specific $CD8^+$ TCC may result in suppression of MV replication. Future experiments will focus on potential mechanisms of virus suppression, by studying the release of cytolytic effector molecules (*e.g.* granzyme, perforin), cytokines (*e.g.* TNFα and IFNγ) and the interaction between Fas and Fas-ligand [354].

Like for HIV and other lymphotropic viruses, the cellular immune response to MV is characterized by a fierce battle between virus and host immune response: virus-specific T-lymphocytes can either kill or be killed. However, whereas HIV establishes a chronic infection and slowly exhausts the immune system, MV causes an acute and usually self-limiting infection. In experimentally infected macaques levels of MV-infected lymphocytes increase exponentially during the first 7 – 9 days but decrease rapidly during the subsequent week [54]. Our data suggest that viral clearance *in vivo* coincides with the appearance of MV-specific $CD8^+$ T-lymphocytes.

In conclusion, the new approach towards measuring antiviral cellular immunity described here offers opportunities for specific and sensitive analysis of functional aspects of T-lymphocyte-mediated cytotoxicity. We have shown that we can determine the ability of TCC or PBMC bulks to suppress MV dissemination in autologous B-lymphocytes. In the future this approach could allow functional studies of the role of cellular immunity as a correlate of protection in virus infections and/or vaccine trials.

Acknowledgements

The authors thank A. M. Bohnen, W. P. Duprex, H. W. Vos, Y. Yanagi and the Municipal Health Services Zuid Holland Zuid for their contributions to this study, and L. D. de Witte, C. A. Van Baalen and R. S. van Binnendijk for critical comments to the manuscript. The study was funded by ZonMW (RDdV, grant# 91208012) and by the VIRGO consortium, an innovative cluster approved by the Netherlands Genomics Initiative and partially funded by the Dutch Government (SY and RLdS, BSIK 03012).

IMMUNE SUPPRESSION

Measles immune suppression: lessons from the macaque model

Rory D. de Vries, Stephen McQuaid, Geert van Amerongen, Selma Yüksel, R. Joyce Verburgh, Albert D.M.E. Osterhaus, W. Paul Duprex and Rik L. de Swart

PLoS Pathogens 2012 Aug; 8(8): e1002885

Abstract

Measles remains a significant childhood disease, and is associated with a transient immune suppression. Paradoxically, measles virus (MV) infection also induces robust MV-specific immune responses. Current hypotheses for the mechanism underlying measles immune suppression focus on functional impairment of lymphocytes or antigen-presenting cells, caused by infection with or exposure to MV. We have generated stable recombinant MVs that express enhanced green fluorescent protein, and remain virulent in non-human primates. By performing a comprehensive study of virological, immunological, hematological and histopathological observations made in animals euthanized at different time points after MV infection, we developed a model explaining measles immune suppression which fits with the "measles paradox". Here we show that MV preferentially infects CD45RA$^-$ memory T-lymphocytes and follicular B-lymphocytes, resulting in high infection levels in these populations. After the peak of viremia MV-infected lymphocytes were cleared within days, followed by immune activation and lymph node enlargement. During this period tuberculin-specific T-lymphocyte responses disappeared, whilst strong MV-specific T-lymphocyte responses emerged. Histopathological analysis of lymphoid tissues showed lymphocyte depletion in the B- and T-cell areas in the absence of apoptotic cells, paralleled by infiltration of T-lymphocytes into B-cell follicles and reappearance of proliferating cells. Our findings indicate an immune-mediated clearance of MV-infected CD45RA$^-$ memory T-lymphocytes and follicular B-lymphocytes, which causes temporary immunological amnesia. The rapid oligoclonal expansion of MV-specific lymphocytes and bystander cells masks this depletion, explaining the short duration of measles lymphopenia yet long duration of immune suppression.

Author Summary

Measles is associated with a transient immune suppression, resulting in increased susceptibility to opportunistic infections. Indeed, the main causes of measles mortality are secondary infections in the respiratory and digestive tract. Although measles is associated with lymphopenia, depletion of lymphocytes has often been dismissed as a cause of immune suppression. Lymphocyte counts rapidly return to normal after clearance of the virus, while immune suppression lasts several weeks to months. Many studies have focused on suppression of lymphocyte proliferation as an *in vitro* correlate of immune suppression. However, experimental infections of non-human primates show that *in vivo* lymphocyte proliferation is not impaired after measles. Instead, we hypothesize that massive expansion of MV-specific and bystander lymphocytes masks the fact that pre-existing memory lymphocytes have been depleted. We conclude that measles virus infection wipes out immunological memory, leaving individuals susceptible to opportunistic infectious agents that would normally be controlled by the immune system.

Introduction

Measles is associated with a transient but profound immune suppression, which may last for several weeks to months after the acute stage of the disease. The clinical importance of this immune suppression is illustrated by the observation that measles mortality is typically caused by secondary infections in the respiratory or digestive tract [64–66]. However, the mechanism by which measles virus (MV) infection causes immune suppression is not completely understood. Multiple *in vivo* correlates of immune suppression have been described, including disappearance of Mantoux responses [156,160], lymphopenia [161,355] and impaired responses to vaccination [162,163]. Decreased lymphoproliferative responses [165,166], altered cytokine response profiles [167] and impairment of antigen-presenting cell function [168,169,356] have been described *in vitro*. The relevance of these observations to immune suppression and enhanced susceptibility to opportunistic infections remains unclear. The paradox of measles is that the acute phase of the disease is not only associated with immune suppression, but also with immune activation [170] and induction of robust MV-specific humoral and cellular immune responses that result in lifelong immunity.

MV infection is initiated in the respiratory tract. It has long been thought that the initial target cells of the virus were epithelial cells of the upper respiratory tract, but recent studies have demonstrated a major role for alveolar macrophages and dendritic cells (DC) in this process [256,288]. These first MV-infected cells transmit the virus to the bronchus-associated lymphoid tissue (BALT) and/or the draining lymph nodes, where the infection is further amplified in lymphocytes and viremia is initiated [256,357]. MV infects both T- and B-lymphocytes by binding of the MV-hemagglutinin (H) glycoprotein to the cellular receptor CD150 [115]. Recently, the adherens junction protein PVRL4 was identified as cellular receptor on epithelial cells [130,131]. However, as this receptor is exclusively expressed on the basolateral surface of epithelial cells, it does not facilitate MV infection of epithelial cells during the early stages of the disease, but instead is thought to play a role in transmission during the late stages of measles pathogenesis [158].

It has been proposed that direct infection of lymphocytes and the subsequent lymphopenia could explain measles-associated immune suppression [358,359]. However, this hypothesis has often been dismissed based on the observation that lymphopenia only lasts about a week, whilst immune suppression persists for several weeks to months. In addition, during the peak of viremia no more than 1 to 5% of the total lymphocyte population in peripheral blood is infected [54,360]. Recent observations that MV infects high percentages of cells in lymphoid tissues [54] and preferentially targets $CD45RA^-$ or $CD45R0^+$ memory T-lymphocytes [54,171] led us to revisit the lymphocyte depletion hypothesis for immune suppression using the macaque model. Analysis of virological, immunological and histopathological parameters has demonstrated a remarkable similarity between measles in macaques and humans [99]. Here we present a comprehensive overview of a number of *in vivo* studies performed in macaques which provides a unifying model for the etiology of measles immune suppression.

Materials & Methods

Ethics statement

Animal experiments were conducted in compliance with European guidelines (EU directive on animal testing 86/609/EEC) and Dutch legislation (Experiments on Animals Act, 1997). The protocols were approved by the independent animal experimentation ethical review committee DCC in Driebergen, The Netherlands. Animal welfare was observed on daily basis, animal handling was performed under light anesthesia using ketamine and medetomidine. After handling atipamezole was administered to antagonize the effect of medetomidine. For experiments involving PBMC from human donors, written informed consent for research use was obtained by the Sanquin blood bank.

Animal study design

PBMC and tissues were collected from cynomolgus (*Macaca fascicularis*) (n = 35) or rhesus (*Macaca mulatta*) (n = 5) macaques included in previously published studies [54,256,265] (n = 26) or from unpublished infection experiments with $rMV^{IC323}EGFP$ or $rMV^{KS}EGFP$ (n = 14). Macaques were infected by intra-tracheal inoculation or aerosol inhalation and euthanized at 2 (n = 3), 3 (n = 3), 4 (n = 3), 5 (n = 4), 7 (n = 9), 9 (n = 8), 11 (n = 6), 13 (n = 2) or 15 (n = 2) d.p.i. Although some of the experiments had been designed to address different research questions, the accumulated samples effectively covered all stages of MV infection in macaques.

Mantoux tests

Four macaques received intra-dermal vaccinations with 4 x 0.1 ml of live BCG (NVI, Bilthoven, Netherlands). The animals received an intra-dermal Mantoux test with old tuberculin (0.1 ml, 25,000 IU/ml, Statens Serum Institut) [361] 3 months post-vaccination at 7 days pre-MV-infection, or 3 days prior to necropsy. Skin reactivity was assessed for three consecutive days. Skin samples from both Mantoux tests (pre- and post-MV infection) were collected into formalin.

Tuberculin- and MV-specific T-lymphocyte responses

PBMC obtained 7 days pre-infection and during necropsy were thawed and plated into 96-wells round-bottom plates at 2 x 10^5 cells per well. Cells were stimulated with either PPD (10 µg/ml), UV-inactivated MV (10 µg/ml) or live $rMV^{rEdt}EGFP$ [265] (5 x 10^4 $CCID_{50}$ in the presence of 10 µg/ml infection-enhancing lipopeptide $PHCSK_4$ [362]) for 48 hours in triplicate. IFNγ concentrations were measured in supernatants by ELISA (U-CyTech Biosciences).

Leukopenia

After each blood collection, total WBC counts were obtained using an automated counter (Sysmex pocH-100iV). To address measles-induced leukopenia in these animals, mean WBC counts were determined on 0 (n = 31), 1 (n = 6), 2 (n = 20), 3 (n = 17), 4 (n = 18), 5 (n = 11), 6 (n = 20), 7 (n = 10), 8 (n = 6), 9 (n = 12), 11 (n = 8) and 13 (n = 2) d.p.i. Different animals were included at each time-point.

Necropsy
Animals were euthanized by exsanguination under ketamine anesthesia. For the purpose of detecting EGFP fluorescence, a lamp was custom-made containing six 5-volt LEDs (Luxeon Lumileds, lambertian, cyan, peak emission 490 – 495 nm) mounted with D480/40 bandpass filters (Chroma) in a frame that allowed decontamination with 70% (v/v) alcohol or fumigation with formaldehyde. Emitted fluorescence was visualized through the amber cover of a UV transilluminator normally used for screening DNA gels. Photographs were made using a Nikon D80 digital SLR camera. Lymphoid tissues were collected in buffered formalin for immunohistochemistry or PBS for preparation of single cell suspensions, which were used directly for flow cytometry.

Flow cytometry
T-lymphocytes were subdivided into T^{n}, T^{CM} and T^{EM} populations (Figure S1) by staining with $CD3^{PerCP}$ (BD Biosciences, clone SP34-2), $CD4^{V450}$ (BD Biosciences, clone L200), $CD8^{AmCyan}$ (BD Biosciences, clone SK1), $CD45RA^{PE\text{-}Cy7}$ (BD Biosciences, clone L48) and $CCR7^{APC}$ (R&D Systems, clone 150503). The APC signal was enhanced using an APC-FASER Kit (Miltenyi Biotec). B-lymphocytes were subdivided into B^{n} and B^{M} populations (Figure S1) by staining with $CD20^{PE\text{-}Cy7}$ (BD Biosciences, clone L27), $HLA\text{-}DR^{Pacific\ Blue}$ (Biolegend, clone L243), $CD27^{APC}$ (eBioscience, clone O323) and a combination of IgD^{Biotin} (Southern Biotech, goat polyclonal) and $streptavidin^{PerCP}$ (BD Biosciences). CD150 expression was determined by staining with $CD150^{FITC}$ (AbD Serotec, clone A12). The infection percentages within the populations were determined by detection of EGFP. All flow cytometry was performed on a FACS Canto II (BD Biosciences).

Histological and immunohistochemical analysis
H&E staining was performed to evaluate histological changes. Immunohistochemical staining was performed using a fully automated BondMax immunostainer with a polymer-based peroxidase detection system. MV-infected cells were detected using a polyclonal rabbit antibody to EGFP (Invitrogen). Similar stainings were performed with the following monoclonal antibodies: T-lymphocyte marker CD3 (DAKO, clone F7.2.38), B-lymphocyte marker CD20 (DAKO, clone L26), proliferation marker Ki67 (DAKO, clone MIB1) and apoptosis marker cleaved caspase 3 (Cell Signaling, clone 5A1E). Glass slides were scanned with a 40x/0.75 Olympus UPlan FLN objective on an Aperio Scanscope CS-O SS5200 equipped with Spectrum Plus. An Aperio Positive Pixel Count Algorithm was applied to quantify and therefore standardize the intensity of stains present to produce optimal discrimination between immunoperoxidase diaminobenzidine (DAB) tetrahydrochloride reactions and hematoxylin stained nuclei. Scanners are kept at ambient temperature in a temperature-controlled area to eliminate loss of performance due to overheating.

Susceptibility of lymphocyte subsets to infection
PBMC from healthy human or macaque donors were sorted into pure $CD4^{+}$ or $CD8^{+}$ naive ($CD45RA^{+}$) and memory ($CD45RA^{-}$) T-lymphocyte populations on basis of CD45RA expression. Unsorted or sorted PBMC from humans or macaques were

infected by co-culture with low numbers (1:1000) of autologous MV-infected B-LCL or BAL cells (infected with cell-free rMV^{KS}EGFP at an MOI of 1 for 48 hours), respectively. After two days of co-culture infection percentages in the different subsets were determined by flow cytometry.

Statistical analysis

Differences between percentages infected cells or CD150 expression were tested by the non-parametric Wilcoxon rank test using SPSS software.

Results

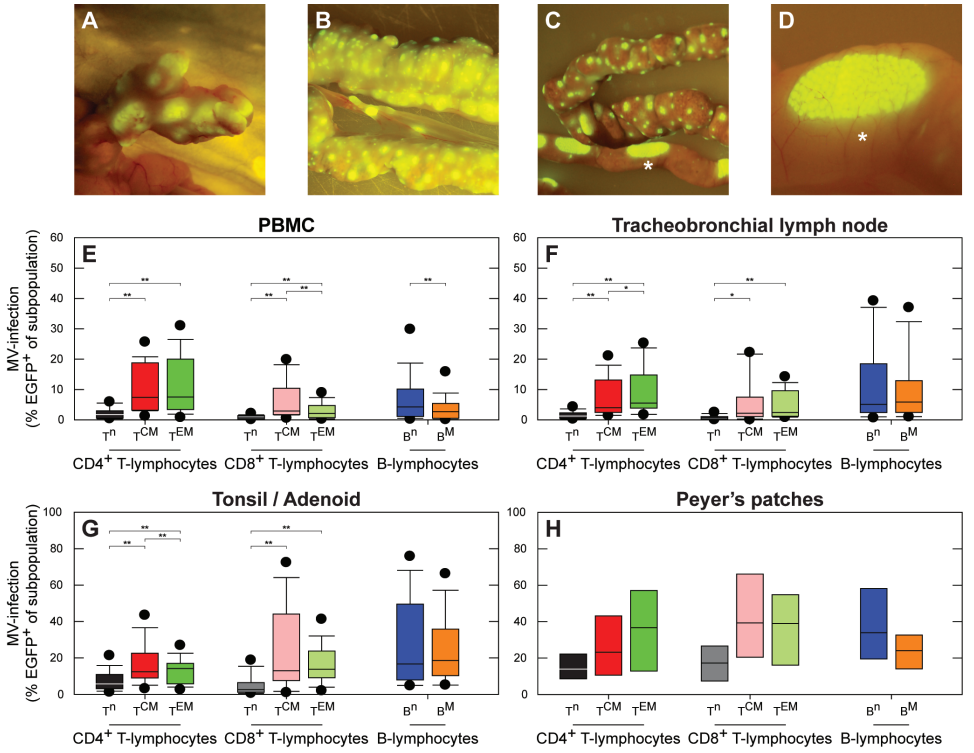

Figure 1. *MV infects high percentages of B-lymphocytes and CD45RA$^-$ memory T-lymphocytes. (A – D) Macroscopic detection of EGFP in lymphoid tissues of the gastro-intestinal tract in three different macaques: mesenteric lymph nodes (A), gut-associated lymphoid tissue (GALT) (B,C), including the Peyer's patches (C,D). Panel D is an enlargement of panel C (indicated by asterisk); (E – H) MV infection percentages in lymphocyte subsets during the approximate peak viremia. T-lymphocyte subpopulations were identified as T^n (CD45RA$^+$), T^{CM} (CD45RA$^-$CCR7$^+$) or T^{EM} (CD45RA$^-$CCR7$^-$), B-lymphocytes were identified as B^n (CD27$^-$IgD$^+$) or B^M (CD27$^+$IgD$^-$). Box plots were chosen since the data were not normally distributed, and show the median infection percentages with the 25th – 75th percentiles, error bars indicate the 10th – 90th percentiles, dots the 5th – 95th percentiles. The 10th – 90th percentiles and 5th – 95th percentiles are only shown if the number of observations is at least ten; **, P < 0.01. *, P < 0.05. In panel E, F and G 14 animals were included; in panel H 3 animals were included.*

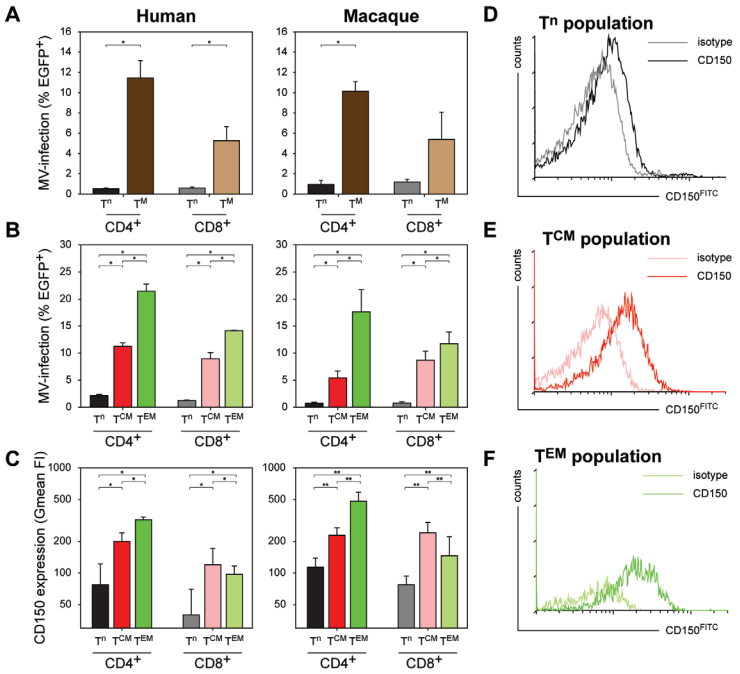

Figure 2. *Susceptibility of human or macaque T-lymphocyte subsets to in vitro MV infection. (A) Human or macaque PBMC were sorted into naive (CD45RA$^+$, T^n) or memory (CD45RA$^-$, T^M) CD4$^+$ or CD8$^+$ T-lymphocytes, and infected with MV in vitro. Percentages MV-infected T-lymphocytes were determined 2 d.p.i. by measuring EGFP fluorescence by flow cytometry. CD4$^+$ (human and macaque) and CD8$^+$ (human only) T^M were significantly more susceptible to MV infection than the corresponding T^n. For macaque CD8$^+$ T-lymphocytes the difference was significant in two out of three experiments; (B) Unsorted human and macaque PBMC were infected, MV infection percentages in the different T-lymphocyte subsets were determined 2 d.p.i. by flow cytometry. Both in human and macaque PBMC the CD4$^+$ and CD8$^+$ T^{CM} and T^{EM} were significantly more susceptible to MV infection than the corresponding T^n subpopulations. In addition, CD4$^+$ T^{EM} and, to a lesser extent, CD8$^+$ T^{EM} proved more susceptible to MV infection than T^{CM}. (C – F) Levels of CD150 expression on the different T-lymphocyte subsets in human and macaque PBMC. (C) PBMC collected from human or macaque donors were stained for memory markers as described in Figure S1, in combination with an IgG1 isotype control or CD150^{FITC} staining. CD150 expression on the different subsets is shown as geometric mean fluorescence intensity (Gmean FI) ± SD. Both for humans and macaques CD150 expression on CD4$^+$ and CD8$^+$ T^{CM} and T^{EM} was significantly higher than on T^n. Interestingly, in CD4$^+$ T-lymphocytes CD150 expression was significantly higher on T^{EM} than on T^{CM}, whereas in CD8$^+$ T-lymphocytes an inverse pattern was observed. (D – F) An IgG1 isotype control was used to determine the level of background staining, and is shown in combination with the CD150 staining for each subset. **, P < 0.01. *, P < 0.05. Experiments were performed with sorted cells from 3 macaque and 2 human donors, and unsorted cells from 4 macaque and 5 human donors. Data are shown as means ± standard deviation (SD) of representative donors.*

MV targets lymphoid tissues and preferentially infects CD45RA$^-$ memory T-lymphocytes

We have analyzed data from rhesus or cynomolgus macaques (n = 40) infected with recombinant (r) MV strains (rMV^{IC323} or rMV^{KS}) expressing enhanced green fluorescent protein (EGFP), spanning the early, intermediate and late stages of MV infection. Data from previous studies [54,256,265] and from additional experimentally

infected macaques (n = 14) were combined. The rMVs expressed EGFP from an additional transcription unit, and MV replication results in the host cell becoming $EGFP^+$. At the peak of viremia, EGFP fluorescence was macroscopically detected in all lymphoid tissues (Figure 1A – D). The percentages MV-infected cells in lymphocyte subsets in PBMC or lymphoid tissues collected 9 or 11 days post-infection (d.p.i.) were determined by flow cytometry. Lymphocytes were subtyped as $CD4^+$ or $CD8^+$ naive ($CD45RA^+$, T^n), central memory ($CD45RA^-CCR7^+$, T^{CM}) or effector memory ($CD45RA^-CCR7^-$, T^{EM}) T-lymphocytes or as naive (IgD^+CD27^-, B^n) or memory (IgD^-CD27^+, B^M) $CD20^+HLA\text{-}DR^+$ B-lymphocytes (Figure S1). T^{CM} and T^{EM} were infected at a significantly higher level than T^n. In contrast, B^M were not preferentially infected (Figure 1E – H).

To determine whether the increased susceptibility of $CD45RA^-$ memory T-lymphocytes (T^M) to MV infection is an inherent property of these cells, and comparable between humans and macaques, we sorted naive and memory $CD4^+$ and $CD8^+$ T-lymphocyte populations from human or macaque PBMC on basis of CD45A expression. *In vitro* co-culture of these populations with MV-infected autologous cells showed that both human and macaque $CD45RA^-$ T^M were preferentially infected by MV (Figure 2A). In an alternative approach, unsorted human or macaque PBMC were co-cultured with autologous MV-infected cells, and infection percentages in T^n, T^{CM} and T^{EM} were determined by flow cytometry, resulting in similar differences in the susceptibility of T-lymphocyte subpopulations (Figure 2B). This not only corroborated the *in vivo* results from the experimentally infected macaques, but also demonstrated a virtually identical trend for human and macaque subpopulations.

The MV receptor CD150 is expressed at high levels by activated human $CD45RO^{high}$ memory T-lymphocytes [118]. We determined the expression levels of CD150 on the different human and macaque T-lymphocyte subsets. This confirmed the higher level of CD150 expression by human $CD45RA^-$ T^{CM} and T^{EM} when compared to $CD45RA^+$ T^n, and showed that the expression levels of CD150 on human and macaque T-lymphocyte subsets are comparable, which likely explains the increased susceptibility of $CD45RA^-$ T^M to MV infection (Figure 2C – F). Although we were unsuccessful in further subtyping B-lymphocyte subsets on basis of expression patterns of different surface markers, the observed efficient infection of both B^n and B^M lymphocytes seems in accordance with recent studies demonstrating CD150 expression on virtually all human B-lymphocyte subpopulations [363].

MV causes lymphocyte depletion in lymphoid tissues

To address the impact of MV infection *in situ*, immunohistochemical analyses of serial sections of lymphoid tissues collected at different d.p.i. were performed. This demonstrated that MV mainly replicated in B-cell follicles (Figure 3; 7 and 9 d.p.i.), as previously described [54,101]. Multiple syncytia were observed 9 d.p.i., and dual immunofluorescence showed these were of B-lymphocyte origin (Figure S2). Strikingly similar to classic observations in humans [142], lymphoid exhaustion of the centers of the B-cell follicles was observed during and shortly after the peak of viremia (Figure 3; 9 and 11 d.p.i.).

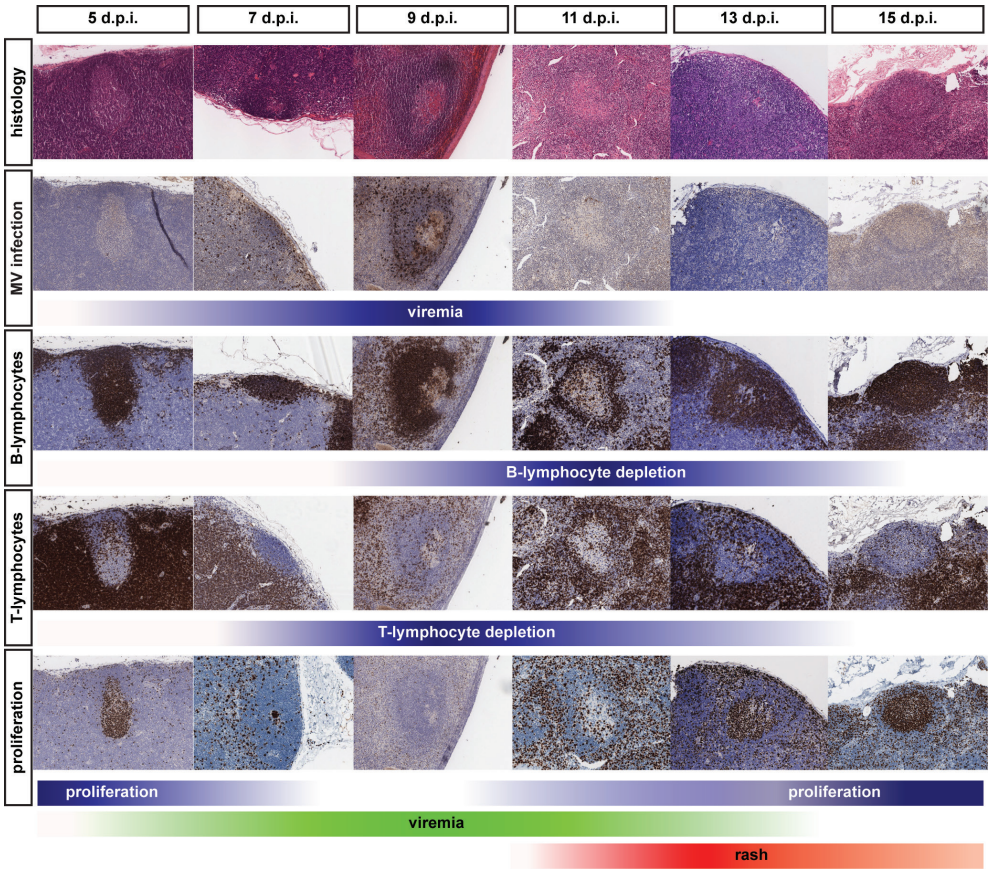

Figure 3. *Histology and immunohistochemistry of lymphoid tissues obtained from macaques euthanized between 5 and 15 d.p.i. Serial sections were stained for histological changes (H&E), MV infection (EGFP), B-lymphocytes (CD20), T-lymphocytes (CD3) or proliferating cells (Ki67). Multiple lymphoid tissues from multiple animals collected at each time-point were analyzed, panels shown are representative for the tissues that have been examined. The color intensity of the blue bars below the photomicrographs indicates the relative levels of viremia, lymphocyte depletion or proliferation. The green and red bars at the bottom indicate the appearance and disappearance of viremia and rash and correspond to the bars in Figure 5B.*

MV infection suppresses tuberculin-specific T-lymphocyte responses

In vitro and *in vivo* recall T-lymphocyte responses to tuberculin were measured in Bacille Calmette-Guérin (BCG)-vaccinated macaques, prior to and 11 or 13 d.p.i. IFNγ production of PBMC in response to purified-protein derivative (PPD) stimulation was reduced after MV infection. Notably, an MV-specific IFNγ response was detected in PBMC collected from macaques sacrificed 13 d.p.i. (Figure 4A). The *in vivo* recall response was determined by Mantoux testing. Before MV infection a characteristic delayed-type hypersensitivity response developed on the site of intra-dermal tuberculin injection, characterized by a well-delineated soft swelling of the cutus, corresponding with an influx of $CD3^+$ T-lymphocytes (Figure 4B). In line with classical observations [159,160], Mantoux responses were suppressed after MV infection,

with a much smaller and harder swelling in the cutus, potentially corresponding with epidermal repair, skin-infiltrating CD3$^+$ T-lymphocytes were absent (Figure 4B). Interestingly, we also observed macroscopically detectable EGFP expression in the skin at the sites where the animals had been vaccinated intra-cutaneously with BCG three months prior to MV infection (Figure S3), suggesting infection of tissue-resident memory lymphocytes in the skin.

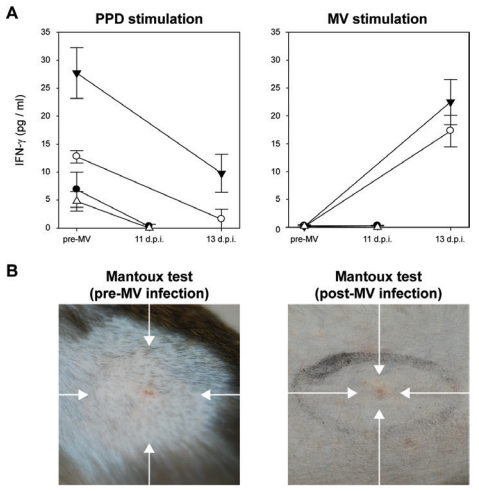

Figure 4. *MV infection causes temporary immunological amnesia. (A) T-lymphocyte responses to PPD and MV were measured by IFNγ production after in vitro stimulation of PBMC collected from 4 BCG-vaccinated macaques. Measurements were performed in triplicate, graphs shows means ± SD; (B) Mantoux tests were performed 7 days before (n = 4) and 8 (n = 2) or 10 (n = 2) days after MV infection. Images were collected 3 days after intra-dermal injection with tuberculin. Before MV infection classical delayed-type hypersensitivity responses were observed, associated with diffuse swelling and redness (indicated by arrows), after MV only a small localized papule was observed (indicated by arrow). Representative images from 4 animals are shown.*

MV infection causes leukopenia followed by massive lymphocyte expansion

Analysis of macaque white blood cell (WBC) counts during the acute infection demonstrated a profound but transient leukopenia (Figure 5B, circles), which coincided with the peak of viremia. There was a relative decrease in size of the CD45RA$^-$ CD4$^+$ and CD8$^+$ T^{CM} and T^{EM} populations between 0 and 9 d.p.i. (Figure 5A), suggesting that leukopenia was related to depletion of MV-infected cells. WBC counts rapidly returned to pre-infection levels between 9 and 15 d.p.i. (Figure 5B), paralleled by a restoration of the relative CD45RA$^-$ T^{CM} and T^{EM} population sizes (Figure 5A). Lymph nodes were enlarged in all animals euthanized between 11 and 15 d.p.i., which was paralleled by the clearance of EGFP$^+$ lymphocytes from lymphoid tissues. During this period large numbers of Ki67$^+$ proliferating cells repopulated the B-cell follicles in the germinal centers of lymphoid tissues (Figure 3; 13 and 15 d.p.i.). Numbers of apoptotic lymphocytes, as detected by staining for cleaved caspase 3 (CC3), remained low at all time-points (Figure S4). Infiltration of CD3$^+$ T-lymphocytes into the B-cell follicles suggests that MV-infected cells were cleared by cytotoxic T-lymphocyte-mediated killing, rather than undergoing apoptosis [364].

A unified model for measles immune suppression

Based on the observations described above we propose a model for the events leading to measles immune suppression. Infection and subsequent immune-mediated clearance of $CD150^+$ lymphocytes results in specific depletion of memory T-lymphocytes and follicular B-lymphocytes, whilst the naive T-lymphocyte population remains relatively unaffected (Figure 5B, populations shown in red and blue, respectively). However, this leaves the question how such a short duration of measles lymphopenia can be reconciled with the long-lasting immune suppression. We hypothesize that the lymphocyte depletion is masked by the massive expansion of MV-specific and bystander lymphocytes (Figure 5B, population shown in green), which has also been observed in humans by a massive expansion of $CD8^+$ T-lymphocytes [148] and by demonstrating skewing of the T-cell receptor repertoire after measles [365]. As a consequence, the qualitative composition of the lymphocyte population immediately after recovery from lymphopenia is dramatically different from that before MV infection, as pre-existing memory lymphocytes have been depleted and replaced by MV-specific and bystander lymphocytes. The net result is a temporary immunological amnesia, and restoration of immunological memory may take several weeks. Thus this model explains why measles-associated immune suppression extends well beyond the transient lymphopenia.

Discussion

Based on our observations, we conclude that measles immune suppression can, at least in part, be explained by massive infection and subsequent immune-mediated clearance of $CD150^+$ memory T-lymphocytes and follicular B-lymphocytes. Depletion of T- and B-lymphocytes has also been described in the BALT of measles patients [366]. We show that MV preferentially infects $CD45RA^-$ T^{CM} and T^{EM}, which during secondary immune responses are the primary source of T-lymphocyte expansion or generation of effector T-lymphocytes, respectively [367]. Infection and subsequent immune-mediated depletion of memory T-lymphocyte subsets fits with the first description of measles-induced immune suppression, namely the disappearance of Mantoux responses in measles patients [160].

Several hypotheses for the underlying mechanism of measles immune suppression have been described previously. However, none of these adequately explain the "measles paradox": the disease is associated with immune suppression but also with induction of strong MV-specific immune responses. Our observations not only explain the measles paradox, but also shed light on many of the *in vivo* and *in vitro* correlates of measles immune suppression described in literature [368–370]. Unresponsiveness of PBMC to mitogens and altered cytokine profiles during and after the acute phase of measles have been demonstrated *in vitro* in several studies [165,166]. These observations are not disputed, but we consider it difficult to extrapolate unresponsiveness of PBMC to mitogens *in vitro* to immune suppression *in vivo*. In parallel with the clearance of MV-infected cells we observed high numbers of proliferating $Ki67^+$ cells in B-cell follicles. This fits well with classical observations of immune activation following measles [170], suggesting that lymphoproliferation is not impaired *in vivo* during the convalescent phase. The observed *in vitro*

suppression of mitogen-induced lymphoproliferation could also be explained by the altered qualitative composition of lymphocyte populations in convalescent measles patients, compared to healthy controls. Our model and previously published observations [170] show that a large proportion of the lymphocytes that circulate during the first weeks after measles infection have been recently activated *in vivo*, potentially making these cells less susceptible to re-stimulation *in vitro*.

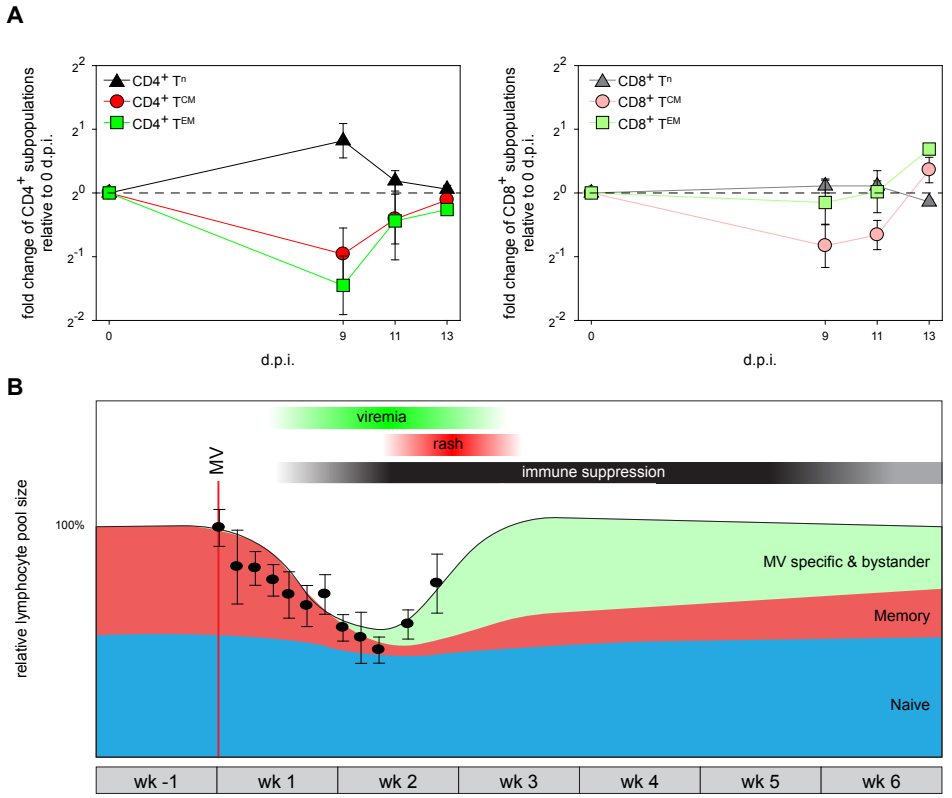

Figure 5. *A model for measles immune suppression. (A) Relative population sizes of CD4⁺ or CD8⁺ T^n, T^{CM} and T^{EM} in PBMC at different d.p.i., expressed as fold changes relative to 0 d.p.i. Means ± SEM of 9 animals are shown. (B). A model describing the changes in the relative size of pre-existing naive lymphocytes (blue), pre-existing memory lymphocytes (red, sum of T^M and follicular B-lymphocytes) and newly induced MV-specific (and bystander) lymphocytes (green) before, during and after measles. The relative WBC counts obtained from the macaques included in this study have been overlaid (black circles, means ± SEM). Thirty-four animals were included to obtain the WBC count graph. The red line indicates the time-point of MV-infection, bars above the graph indicate the approximate period of MV viremia (green), rash (red) and immune suppression (black).*

We do not exclude that a functional impairment of lymphocytes or DC contributes to immune suppression and thus may augment the extent of immune suppression. Actually, it is likely that there are many factors that contribute to immune suppression *in vivo*. To date, direct evidence of DC infection by MV in humans has not been obtained. However, it has been demonstrated *in vitro* that MV is capable of infecting

mature DC and Langerhans cells (LC) [123,168,169,255,257,371,372]. *In vivo* in experimentally MV-infected macaques there was strong evidence for infection of DC in the skin and secondary lymphoid tissues [54]. The role of DC in immune suppression has not been extensively studied *in vivo*, but it is possible that they play a role either by directly being targeted and depleted by MV or indirectly by interaction with and silencing of T-lymphocytes. Furthermore, the capacity to function as antigen presenting cells might be affected [164,370].

Our study covers a time period of two weeks after MV infection, and as such does not provide experimental proof of what happens during resolution of measles immune suppression. The strength of our model using recombinant EGFP-expressing MV mainly lies in the sensitive detection of MV-infected cells, which is limited to the first two weeks after MV infection. Clearly, the memory lymphocyte populations specific for previously encountered pathogens are not completely depleted, and are largely restored during the weeks to months after measles. For instance, previously positive Mantoux responses disappear after onset of rash [159,160], but eventually reappear. We have indicated this in our model (Figure 5B) by showing a gradual increase of the memory lymphocyte population after clearance of MV. Although we cannot fully explain the drivers of the resolution of immune suppression, it is possible that expansion of non-depleted T^{CM} upon renewed antigen encounter may play an important role. However, homeostatic restoration by the immune system itself could be an alternative explanation.

Some of the individual observations described here have been reported earlier in relationship to animal morbillivirus-related immune suppression [106,373,374]. The novelty of our model lies in the immune-mediated lymphodepletion being masked by the massive expansion of MV-specific and bystander lymphocytes. Although effective MV-specific $CD8^+$ T-lymphocyte responses as well as immune activation and lymph node enlargement have been described earlier [148,170,365,373], they have not been associated with immune suppression in this way.

The most important consequence of our model is that the qualitative composition of lymphocyte populations changes dramatically upon MV infection. Although lymphocyte numbers in peripheral blood and lymphoid organs appear normal, depletion of pre-existing specific T- and B-lymphocytes subpopulations provides a direct explanation for the suppression of recall responses to other pathogens during and after measles. This allows such pathogens to cause severe disease and in the developing world leads to the high level of MV-associated mortality. In addition, MV efficiently replicates in B-lymphocytes, resulting in follicular exhaustion and disorganization of the germinal centers, which are essential in actively ongoing humoral immune responses.

We observed comparable levels of MV-infected cells in T^{CM}, T^{EM} and B^n, and in parallel observed lymphocyte depletion and disorganization in B-cell follicles during the acute phase of MV infection (Figure 3, 9–11 d.p.i.). However, we have also shown that proliferating cells can be detected in lymphoid tissues as early as

11 d.p.i., after which time the follicle structure is being restored. This matches the kinetics of antibody responses in the macaque model, in that MV-specific IgM and IgG responses are first detected around 11 d.p.i. and peak at 17 (IgM) and 24 (IgG) d.p.i. [54,375]. These kinetics fit well with our conclusions from the data and map well onto the immune suppression model.

It has been described that MV infection can result in transient remissions of certain autoimmune diseases [376–378]. Our observations suggest that this can be explained by direct MV infection of $CD150^+$ lymphocytes, followed by immune-mediated depletion. Similarly, this mechanism could also explain reductions in HIV-1 loads during acute measles [379,380]: MV infection of memory $CD4^+$ T-lymphocytes could result in depletion of HIV-1-infected cells. In certain auto-immune diseases, and in animal studies in which lymphocyte populations were experimentally depleted, commensal or opportunistic infectious agents that would normally be controlled by the immune system have been shown to cause severe disease [381]. The high incidence of respiratory and gastro-intestinal complications following measles [64–66] may therefore be directly related to the observed high percentages of MV-infection and subsequent lymphocyte depletion in the adenoids, tonsils and gut-associated lymphoid tissue, which form a first line of defense against inhaled or ingested pathogens. We conclude that MV infection wipes immunological memory, resulting in increased susceptibility to commensal or opportunistic infections.

Funding
This work was financially supported by ZonMW (grant number 91208012) and MRC (grant number G0801001). The funders had no role in study design, data collection and analysis, decision to publish, or preparation of the manuscript.

Acknowledgements
The authors would like to thank Theo Geijtenbeek, Thijs Kuiken, Ken Lemon, Martin Ludlow, Annelies Mesman, Tien Nguyen, Werner Ouwendijk, Linda Rennick, Bert Rima, Sibylle Schneider-Schaulies, Wenda Schoordijk, Edwin Veldhuis Kroeze, Lot de Witte and Yusuke Yanagi for their contributions to these studies.

Author Contributions
Conceived and designed the experiments: RDdV WPD RLdS. Performed the experiments: RDdV SMQ GvA SY RJV WPD RLS. Analyzed the data: RDdV SMQ WPD RLdS. Wrote the paper: RDdV ADMEO WPD RLdS.

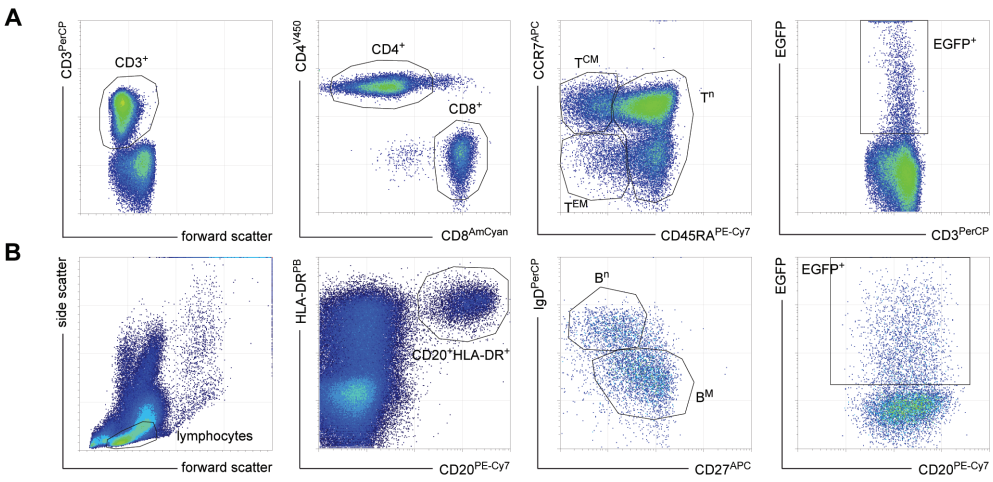

Figure S1. *Gating strategy used to distinguish between different T- and B-lymphocyte subsets. As a first step, the lymphocyte population was gated on basis of forward and side scatter (FSC and SSC, respectively). (A) T-lymphocyte subpopulations were subsequently detected on basis of expression of CD3 and CD4 or CD8, and identified as naive T-lymphocytes (T^n, CD45RA$^+$), central memory T-lymphocytes (T^{CM}, CD45RA$^-$CCR7$^+$) or effector memory T-lymphocytes (T^{EM}, CD45RA$^-$CCR7$^-$). The monoclonal antibodies used (see materials and methods for clone numbers) cross-react with rhesus and cynomolgus macaque antigens (nhpreagentsbidmc.harvard.edu/), and identified similar lymphocyte populations as previously described for human T-lymphocytes. (B) B-lymphocytes were detected on basis of expression of CD20 and HLA-DR, and identified as naive B-lymphocytes (B^n, CD27$^-$IgD$^+$) or memory B-lymphocytes (B^M, CD27$^+$IgD$^-$) as previously described. EGFP$^+$ cells were gated to determine the level of MV infection within each lymphocyte subset. In some cases cells expressing high levels of EGFP were found to run "off-scale" (see upper right plot), but these events could be included in the analysis of the percentage EGFP$^+$ cells.*

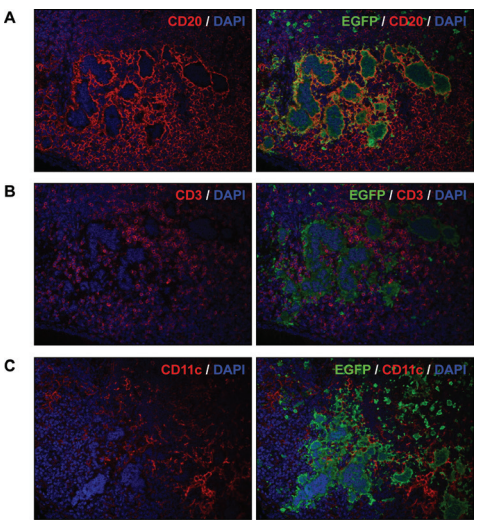

Figure S2. *Dual immunofluorescence staining of lymphoid tissues obtained from macaques euthanized 7 d.p.i. (A – C) Large numbers of multinucleated syncytia were observed in the B-cell follicles and were stained for EGFP (green) as a marker of MV infection. Double stains were performed with a B-lymphocyte marker (CD20, red, A), a T-lymphocyte marker (CD3, red, B) or a macrophage/DC marker (CD11c, red, C) and DAPI was used to counterstain the nuclei (blue). Left panels only show the red and blue channels, right panels show the combined red, blue and green channels. Multi-nucleated giant cells were mainly of B-lymphocyte origin (panel A), and the infection was associated with significant cytopathic effects in lymphoid tissues.*

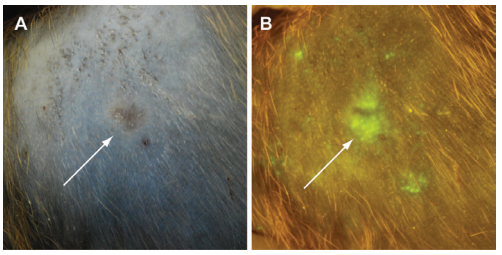

Figure S3. *Macroscopic detection of EGFP at BCG intra-dermal injection sites (indicated by arrows). (A) Corresponding normal and (B) fluorescent macroscopic photographs of BGC-injection sites. To study MV infection of pre-existing specific memory lymphocytes, four macaques were vaccinated intra-dermally with BCG three months prior to MV infection. Vaccination with this live-attenuated bacterial vaccine resulted in macroscopically detectable local inflammatory responses, which remained detectable for several weeks post-vaccination. After MV infection, EGFP fluorescence was observed macroscopically in the skin at the BCG vaccination sites 9 d.p.i. This was due to the presence of EGFP^{+} lymphocytes (not shown), suggesting that the virus targeted the BCG-specific tissue-resident memory T-lymphocytes. We have previously described the presence of MV-infected aggregates of lymphoid cells in the skin of macaques [54], but were unable to determine the answer to the "chicken or egg" question: were these cells present in the skin before MV infection and subsequently targeted by the virus, or did they infiltrate into the skin after MV infection? The observed infection of lymphocytes in the skin at the location where the animals had been intra-dermally immunized with BCG three months earlier strongly suggests that these lymphocytes were present in the skin and subsequently targeted by the virus.*

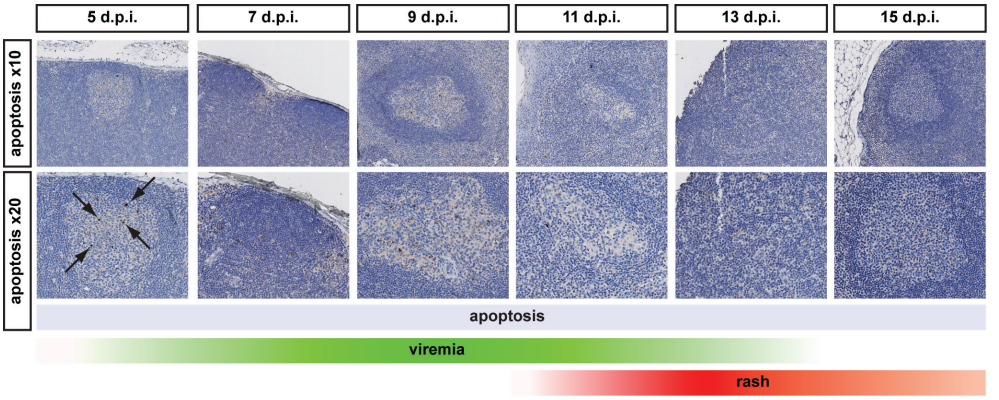

Figure S4. *Immunohistochemical staining of lymphoid tissues obtained from macaques euthanized between 5 and 15 d.p.i. Apoptotic cells were visualized indirectly using monoclonal antibody against CC3 and DAB-detection. The same animals and lymphoid tissues used in* ***Figure 4*** *were analyzed and panels shown are representative for the tissues that have been examined. The same B-cell follicle is shown at ×10 and ×20 magnification. The bar below the photomicrographs of the CC3 staining indicates the relative level of apoptosis, as was done for MV-infection, B-cell depletion, T-cell depletion and proliferation in* ***Figure 4****. Note that there was no change in the numbers of apoptotic cells within B-cell follicles during the time-course of MV infection. The green and red bars at the bottom indicate viremia and rash, and correspond to the bars in* ***Figure 5B****. Examples of CC3^{+} cells are indicated by arrows in the lower left panel at 5 d.p.i. These stainings show that the depletion of B-cell follicles is not caused by apoptosis of infected cells.*

POST MV ERADICATION

7

POST MV ERADICATION

Virulence and tropism of recombinant EGFP-expressing canine distemper virus in naive and measles-vaccinated non-human primates

Rory D. de Vries, Martin Ludlow, R. Joyce Verburgh, Geert van Amerongen, Selma Yüksel, D. Tien Nguyen, Stephen McQuaid, Albert D.M.E. Osterhaus, W. Paul Duprex and Rik L. de Swart

Submitted

Abstract

Measles virus (MV) is being considered for global eradication, which will result in reduced compliance to MV vaccination. As a result, children will grow up without MV-specific immunity, creating a niche for animal morbilliviruses. Recent outbreaks in captive macaques have shown that canine distemper virus (CDV) crosses the species barrier causing disease in non-human primates, but the potential primate-adaptation of these viruses has not been assessed. We studied the virulence and tropism of recombinant (r) CDV in non-human primates. Two rCDV strains were used, based on the well-characterized wild-type strains Snyder-Hill (SH) and Ohio R252 (R252). Both rCDV strains expressed enhanced green fluorescent protein (EGFP) from an additional transcription unit (ATU) and were virulent in ferrets. In naive macaques rCDV caused viremia and fever, and predominantly infected lymphocytes and dendritic cells (DC). Percentages of peripheral blood lymphocytes infected with rCDV^{SH}EGFP were higher than those with rCDV^{R252}EGFP, and exceeded those previously observed after experimental MV infection. However, neither rCDV strain spread to epithelial cells or the CNS at the time points examined and the infections were self-limiting. rCDV^{SH}EGFP infection of MV-vaccinated animals also resulted in viremia, but the virus was cleared more rapidly than in naive animals and virus shedding from the upper respiratory tract was virtually abolished. Neither CDV infection nor MV vaccination induced detectable cross-reactive morbillivirus neutralizing (VN) antibodies. However, MV-specific VN antibody levels of vaccinated macaques were boosted by rCDV^{SH}EGFP infection, suggesting that cross-reactive VN epitopes do exist. In conclusion, this study demonstrates that wild-type strains of CDV readily infect non-human primates, but as yet unidentified mutations are apparently required to achieve full virulence in non-natural hosts. Understanding the mechanism underlying this adaptation is crucial, as it will offer the basis for surveillance of animal morbilliviruses that may emerge in humans after measles eradication.

Introduction

Canine distemper has been described as an infectious disease of dogs since the 17th century [382]. The causative agent, canine distemper virus (CDV), is a member of the family *Paramyxoviridae*, genus *Morbillivirus,* and was first isolated in 1957 [383]. In common with the closely related measles virus (MV), CDV initially replicates in the lymphoid tissues [384]. Further spread and amplification of CDV infection in immune cells throughout the body results in profound lymphopenia and immune suppression, often leading to secondary opportunistic infections [374,385,386]. However, CDV readily infects cells of the central nervous system (CNS), which is rarer for MV [373,387]. This difference, together with the massive amount of lymphoid infection and problems with mounting a proper CDV-specific immune response, may explain the high case-fatality rates observed in canine distemper, which are substantially lower for measles [373].

The spectrum of CDV-induced disease is modeled well in ferrets that recapitulate many aspects of the disease in dogs. A recombinant (r) ferret-adapted CDV strain expressing enhanced green fluorescent protein (EGFP) has been used previously to examine the cellular tropism of CDV [105]. CDV initially replicated in T- and B-lymphocytes in lymphoid organs and the animals developed fever, rash and viremia. After the initial lymphoid phase, epithelial cell infection was readily observed around 12 days post-infection (d.p.i.). Furthermore, infected ferrets were severely immune suppressed and generally died 2 – 3 weeks post infection. Disease outcome in the ferret model is strain-dependent, with 100% mortality observed for strains that spread systemically and to the CNS [105,106].

CD150 or signaling lymphocyte activation molecule (SLAM) is the primary entry receptor for wild-type morbilliviruses on immune cells [113,115,388,389]. A rCDV unable to recognize CD150 was severely attenuated in ferrets, demonstrating infection of $CD150^+$ lymphocytes and DC is vital for entry and virulence [117]. Similar to MV in non-human primates, CDV infects epithelial cells in ferrets, but to a much larger extent and mainly in the late stages of disease [105]. Poliovirus receptor-related 4 (PVRL4) was recently described as a cellular receptor for MV expressed by epithelial cells [130,131]. PVRL4 is expressed in the adherens junctions at the basolateral surface of differentiated epithelial cells, explaining why morbilliviruses usually do not infect epithelial cells apically. Analogous residues to those on the MV hemagglutinin (H) glycoprotein involved in binding to PVRL4 have also been shown to be important for epithelial cell entry by CDV [390,391], and canine PVRL4 was recently demonstrated to be an entry receptor for CDV in the latter stages of the disease [392]. When ferrets were infected with a rCDV unable to infect epithelial cells, the virus replicated in lymphocytes and caused lymphopenia. However, the ferrets did not display fever or rash, CDV could not be isolated from the throat and epithelial cell infection was not detected by immunohistochemistry [391]. This suggests that epithelial cell infection is important for clinical disease and virus transmission, as was previously hypothesized for measles virus [137].

Even though CDV was originally described as an infectious disease of dogs, it naturally infects a wide range of carnivores and has a relatively high propensity to cross species barriers. The virus has been reported to cause disease in a wide range of carnivores, including members of the families of *Ailuridae*, *Felidae*, *Hyaenidae*, *Mustelidae*, *Procyonidae*, *Ursidae*, *Viverridae* [393–405] and *Phocidae* [406–408]. Outside these carnivore families, CDV has also been reported to infect javelinas [409].

CDV infection of non-human primates, which are naturally susceptible to MV infection [99], was first reported in 1989 when 22 Japanese macaques (*Macaca fuscata*) kept in an animal research facility seroconverted to CDV, but not to MV [410]. More recently, related outbreaks in breeding colonies of rhesus macaques (*Macaca mulatta*) in China and cynomolgus macaques (*Macaca fascicularis*) in Japan were described [200,411,412]. Collectively the outbreaks included more than 10,000 animals, and resulted in case-fatality rates of 5-30%. The main causes of death were pneumonia and few animals displayed neurological signs. The frequent detection of secondary pathogens suggests that the high case-fatality rates were related to opportunistic infections resulting from CDV-induced immune suppression. It remains unclear whether or not the virus had adapted to primates.

In April 2012, the WHO published the 'Global Measles and Rubella Strategic Plan 2012-2020'. One of the milestones of this plan is to establish a target date for the global eradication of measles. Although measles eradication would save many lives, it will result in reduced compliance in MV vaccination across the world. In this scenario children would grow up without MV-specific immunity, possibly creating a niche for animal morbilliviruses that might cross the species barrier to infect humans. Morbillivirus infections induce partial cross-protection, as illustrated by the use of live-attenuated MV vaccines to protect dogs from CDV [11,413,414]. Thus, cessation of MV vaccination may facilitate cross-species infection and adaptation of animal morbilliviruses to humans. Although it has been claimed that this risk is low [199], the large CDV outbreaks in non-human primates accompanied by high levels of morbidity and mortality suggest that animal morbilliviruses represent more than a theoretical risk for humans lacking morbillivirus immunity. Furthermore, new paramyxoviruses are still being discovered on a regular basis, emphasizing the need for surveillance [4].

We have previously used rMV expressing EGFP in conjunction with macroscopic and microscopic imaging techniques to sensitively detect virus-infected cells and study measles pathogenesis in the macaque model [54,125,256,265]. Here we show that cynomolgus macaques are susceptible to infection with wild-type strains of CDV via the respiratory route, and that MV vaccination cross-protects from CDV infection and disease. In addition, we show that the viruses mainly replicated in $CD150^+$ lymphocytes and DC, but can adapt to efficient lateral spread in epithelial cells.

Materials and Methods

Ethics statement

Animal experiments were conducted in compliance with European guidelines (EU directive on animal testing 86/609/EEC) and Dutch legislation (Experiments on Animals Act, 1997). The protocols were approved by the independent animal experimentation ethical review committee DCC in Driebergen, The Netherlands. This committee is not affiliated to the Erasmus MC, where the experiments were performed. During the period before CDV challenge, animals were housed in groups, received standard primate feed and fresh fruit on a daily basis and had access to water *ad libitum*. In addition, their cages contained several sources of environmental enrichment in the shape of hiding places, hanging ropes, tires and other toys. During the infection study animals were housed in HEPA-filtered negatively pressurized BSL-3 isolator cages. Animal welfare was observed on daily basis, and all animal handling was performed under light anesthesia using ketamine and medetomidine. After handling atipamezole was administered to antagonize the effect of medetomidine.

Animal study design

Nine juvenile CDV- and MV-seronegative and six MV-vaccinated cynomolgus macaques (*Macaca fascicularis*) were used for the CDV infection studies. A temperature probe was implanted intra-peritoneally two weeks before the beginning of the experiments to monitor body temperature non-invasively. CDV- and MV-seronegative animals were infected with either a high dose rCDV^{SH}EGFP (n=3), low dose rCDV^{SH}EGFP (n=3) or a high dose rCDV^{R252}EGFP (n=3). MV^{EZ}-vaccinated animals were challenged at 10 months post vaccination with either a high (n=3) or low (n=3) dose rCDV^{SH}EGFP. Animals receiving a high viral dose were infected with 10^6 cell culture infectious dose-50 ($CCID_{50}$) of CDV, of which 50% was administered IT, 40% intra-nasal (IN) and 10% onto the eyes. Animals receiving a low dose were infected with 10^5 $CCID_{50}$ of CDV exclusively via IT inoculation. Animals were euthanized on 6, 10 or 14 d.p.i. (n=1 per group per time point).

Necropsy

Animals were euthanized by exsanguination under deep ketamine anesthesia. Macroscopic detection of EGFP was performed as described previously [54,256,265]. During necropsy, tissues from the upper and lower respiratory tract, including the nasal concha, nasal septum, trachea, primary bronchus and lungs were harvested and directly screened for EGFP expression. The lungs were pre-inflated with 2% (w/v) low-melting point agarose before screening as described previously [256]. After screening the tissues were transferred to buffered formalin (FA). Non-lymphoid tissues were collected directly in FA, lymphoid tissues were either collected in FA for immunohistochemistry or phosphate buffered saline (PBS) for preparation of single cell suspensions using cell strainers with a 100 μm pore size (BD Biosciences), which were used directly for flow cytometry.

Blood samples
Small volume blood samples were collected in Vacuette tubes containing K_3EDTA as an anticoagulant 3, 6, 8, 10, 12 and 14 d.p.i. During necropsy blood was collected in heparin to prevent coagulation. After collection of blood, total WBC counts were obtained using an automated counter (Sysmex pocH-100iV). On all time-points, plasma was separated by centrifugation, heat inactivated (30 min 56°C) and stored at –20°C. PBMC were isolated by density gradient centrifugation, washed, resuspended in complete RPMI-1640 medium (Gibco Invitrogen, Carlsbad, CA, USA) supplemented with L-glutamine (2 mM), 10% (v/v) heat-inactivated fetal bovine serum (FBS), penicillin (100 U/ml) and streptomycin (100 μg/ml), counted using a haemocytometer and used directly for flow cytometry and virus isolation. Isolation of CDV was performed on VDS cells [389] using an infectious center test as previously described [281]. Virus isolations were monitored by UV microscopy for EGFP fluorescence after co-cultivation with VDS for 3 – 6 days and results were expressed as number of virus-infected cells per 10^6 total cells.

Broncho-alveolar lavage
A BAL was performed 3, 6, 8, 10, 12 and 14 d.p.i., by IT infusion of 10 ml PBS through a flexible catheter. In animals that were sacrificed, a BAL was performed post-mortem by direct infusion of 10 ml PBS into the righthand side of the lung. BAL cells were resuspended in culture medium with supplements as described above, counted and used directly for flow cytometry and virus isolation. Virus isolation was performed on VDS as described for MV on vero-CD150 [54].

Throat, nose and eye swabs
Throat, nose and eye swabs were collected 3, 6, 8, 10, 12 and 14 d.p.i. in transport medium (EMEM with Hanks' salts, supplemented with lactalbumin enzymatic hydrolysate, penicillin, streptomycin, polymyxine B sulphate, nystatin, gentamicin and glycerol) and frozen at –80°C. After thawing samples were vortexed, the swab was removed and the remaining transport medium was used for virus isolation. Isolation of CDV was performed on VDS using an infectious center test as previously described [281]. The isolations were screened for EGFP fluorescence at day 3 and 7 post-titration and results are expressed as $TCID_{50}$ / ml.

CDV and MV serology
VN antibody responses were measured by an endpoint neutralization assay. Briefly, serial 2-log dilutions (starting at 2^{-2}) of heat-inactivated plasma samples were incubated in triplicate with $rCDV^{SH}$EGFP, $rCDV^{R252}$EGFP or MV strain Edmonston (MV^{Ed}) for 1 h at 37°C in 96-well flat-bottom plates (Greiner Bio-One). Subsequently, trypsinized VDS (for CDV) or Vero (for MV) cells were added at a concentration of 1 x 10^4 cells / well. Plates were incubated for 5-7 days at 37°C and visually monitored for CPE. VN titers were calculated as the 50% endpoint of triplicate measurements using the Reed & Muench method [349,428]. MV-F and MV-H glycoprotein–specific serum IgG antibody levels were determined by flow cytometry as described previously [375].

Flow cytometry
Phenotyping of CDV-infected cells in PBMC was performed by flow cytometry. PBMC were stained with CD3$^{APC\text{-}Cy7}$ (BD, clone SP34-2), CD4^{V450} (BD, clone L200), CD8^{AmCyan} (BD, clone SK1), CD20$^{PE\text{-}Cy7}$ (BD, clone L27), CD14^{PerCP} (BD, clone M5E2) and CD150^{PE} (BD, clone A12). Lymphoid organs were stained with the same set of monoclonal antibodies, with the exception of CD14^{PerCP}. The infection percentages within the populations were determined by detection of EGFP. All flow cytometry was performed on a FACS Canto II (BD). The amount of proliferation in naive and memory T-lymphocyte subsets was determined for the rCDV^{SH}EGFP high dose group only, by staining with Ki67^{V450} (BD, clone B56) CD3^{PE} (BD, clone SP34-2), CD4^{PerCP} (BD, clone SK3), CD8^{AmCyan} (BD, clone SK1), CD45RA$^{PE\text{-}Cy7}$ (BD, clone L48) and CCR7^{APC} (R&D Systems, clone 150503). The APC signal was enhanced using an APC-FASER Kit (Miltenyi Biotec).

Histological and immunohistochemical analysis
H&E staining was performed to evaluate histological changes. Immunohistochemical staining was performed using a fully automated BondMax immunostainer with a polymer-based peroxidase detection system. CDV-infected cells were detected using a polyclonal rabbit antibody to EGFP (Invitrogen), specific antibody-antigen binding sites were detected using an Envision-Peroxidase system with diaminobenzidin (DAB, DAKO) as substrate. Dual labeling indirect immunofluorescence was performed using polyclonal rabbit anti-EGFP and monoclonal mouse antibodies to the macrophage/DC marker CD11c (Novocastra, clone 5D11), the T-lymphocyte marker CD3 (DAKO, clone F7.2.38), the B-lymphocyte marker CD20 (DAKO, clone L26) and the epithelial cell marker cytokeratin (DAKO, clone AE1/AE3). In all cases antigen binding sites were detected with a mixture of anti-mouse Alexa 568 and anti-rabbit Alexa 488 (Invitrogen). Sections were counterstained with DAPI hardset mounting medium (Vector). All fluorescently stained slides were assessed and digital fluorescent images acquired with a Leica DFC350 FX digital camera and processed using Leica FW4000 software.

***In vitro* rCDV^{R252}EGFP adaptation to human cells**
To adapt rCDV^{R252}EGFP to human cells, the virus was passaged 28 times through human cells. To this end both H358, a human bronchio-alveolar lung carcinoma epithelial cell line expressing PVRL4, and maturated human moDC expressing CD150 were used. P1 – P8 were performed on H358, P9 – P18 alternatively on H358 and moDC, P19 – P28 on H358. During P19 – P28, the most fusogenic viruses were selected every passage, and three rounds of plaque purification were performed. DC were infected by overlaying them onto the rCDV^{R252}EGFP-infected monolayer. For this plaque-purified virus, the H gene was completely sequenced at P17, P20 and P25 and screened for mutations compared to P0. The plaque-purified virus obtained at P28 was named rCDV^{R252}EGFP(C5) and was grown on H358, and the complete H, F and P genes were sequenced and screened for mutations.

Growth curve of non-adapted and primate-adapted CDV
Growth curves were performed on both VDS and H358 with the original rCDV^{R252}EGFP and the adapted rCDV^{R252}EGFP(C5). Briefly, 6 wells plates with either VDS or H358 were infected at multiplicity of infection (MOI) 0.01 or 0.1 respectively, in triplicate. At 24, 48 and 72 hours post infection (h.p.i.) infections were snap-frozen. Subsequently all samples were thawed, sonicated and clarified, before titration on VDS.

Infection of primary normal monkey bronchial epithelial cells
Primary macaque bronchial epithelial cells or NMBE were obtained directly from bronchi of euthanized macaques (n=3), as described previously for humans [429]. Undifferentiated NMBE were grown in type 1 collagen and fibronectin-coated T75 flasks, trypsinized at 60 – 80 % confluence and subsequently seeded into 6.5-mm transwell inserts with 0.4 µm pore size at 5 x 10^4 cells per insert as described previously [323]. After the NMBE had polarized and developed cilia, the monolayers on filters were scratched and subsequently infected apically with 2 x 10^5 $CCID_{50}$ of either rMV^{KS}EGFP (3), rCDV^{SH}EGFP, rCDV^{R252}EGFP or rCDV^{R252}EGFP(C5). After 90 minutes, the virus was removed. At 72 h.p.i. the filters were screened for infection, fixed, permeabilized and counterstained for cilia with anti-human β tubulin IV. Stained filters were analyzed by confocal laser scanning microscopy with a LSM700 system fitted on an Axio Observer Z1 inverted microscope (Zeiss). Images and videos were generated using Zen software.

Results

rCDV^{SH}EGFP and rCDV^{R252}EGFP efficiently replicate in macaques
Six morbillivirus-naive cynomolgus macaques were infected intra-nasally (IN), intra-tracheally (IT) and onto the eyes with a high dose (10^6 $TCID_{50}$) rCDV^{SH}EGFP (n=3) or rCDV^{R252}EGFP (n=3). Within each group, one animal was euthanized 6, 10 or 14 d.p.i. Blood and broncho-alveolar lavage (BAL) samples were obtained 3, 6, 8, 10, 12 and 14 d.p.i., and directly used for detection of EGFP by flow cytometry. EGFP$^+$ cells were detected in the BAL (Figure 1A) and peripheral blood mononuclear cells (PBMC) (Figure 1B) of all animals. Infection levels in BAL were comparable for rCDV^{SH}EGFP and rCDV^{R252}EGFP (Figure 1A). In PBMC, rCDV^{SH}EGFP infected approximately 10 times more cells than rCDV^{R252}EGFP (Figure 1B). Subsequently, three additional animals were infected with a tenfold lower dose of rCDV^{SH}EGFP, delivered exclusively by IT inoculation. This route was chosen as it was previously shown to be a highly reproducible way for experimental MV infection of macaques. Similar CDV infection percentages were detected in BAL and PBMC as compared to the animals inoculated with the high dose of rCDV^{SH}EGFP, although virus replication peaked approximately one or two days later (Figure 1A and B). Macroscopic detection of EGFP during the necropsies of the high and low dose rCDV^{SH}EGFP-infected macaques at 6 d.p.i. showed EGFP fluorescence in the lymphoid tissues (Figure 1C – 1G).

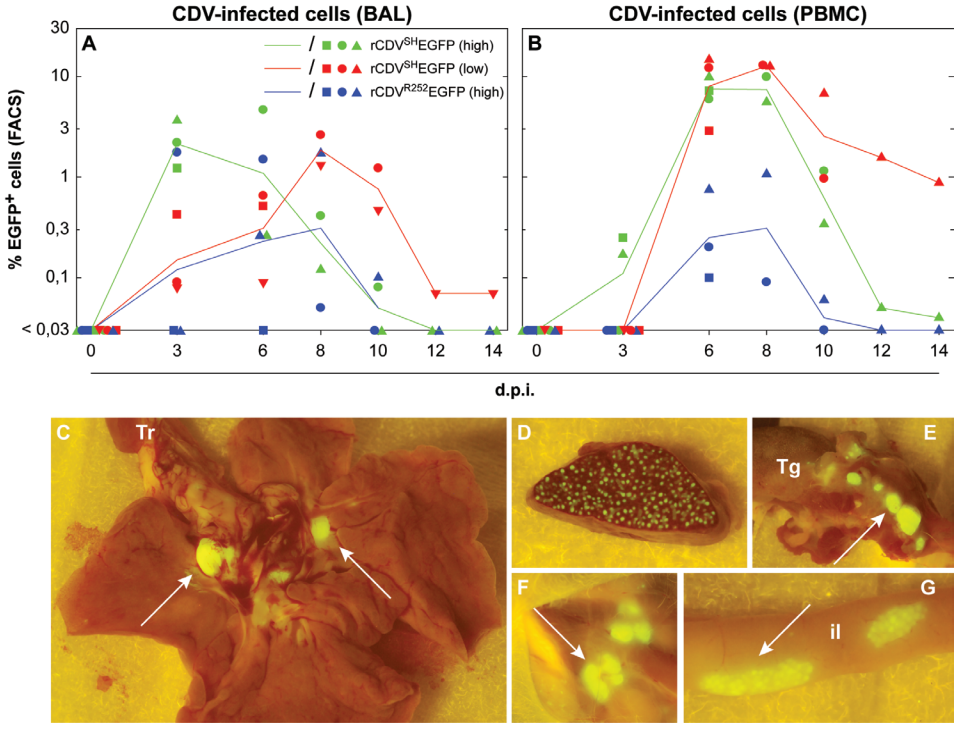

Figure 1. *rCDV^{SH}EGFP and rCDV^{R252}EGFP replication in macaques. Nine morbillivirus-naive cynomolgus macaques were infected with either a low dose rCDV^{SH}EGFP (red), a high dose rCDV^{SH}EGFP (green) or a high dose rCDV^{R252}EGFP (blue). PBMC and BAL were obtained 3, 6, 8, 10, 12 and 14 d.p.i., and used for detection of EGFP$^+$ cells by flow cytometry. Tissues were screened for macroscopic EGFP fluorescence during necropsy. (A,B) Detection of EGFP$^+$ cells in BAL or PBMC. All plots show means ± SEM per group, symbols show the data of individual animals. (C-G) Macroscopic detection of EGFP during the necropsies of the high and low dose rCDV^{SH}EGFP-infected macaques at 6 d.p.i. showed EGFP fluorescence in the lungs and tracheobronchial lymph node (C), spleen (D), tonsils (E), mandibular lymph node (F) and the Peyer's patches (G). Tr: trachea; Tg: tongue; Il: ileum.*

rCDV^{SH}EGFP and rCDV^{R252}EGFP are virulent in the macaque and cause lymphopenia and fever

To confirm the pathogenicity of CDV in macaques and demonstrate that the EGFP$^+$ cells produced infectious virus, virus isolations were performed from eye, nose and throat swabs, from BAL cells and from PBMC. With both strains, peak virus replication was reached around 6 – 8 d.p.i., especially in PBMC (Figure 2A – E). rCDV^{SH}EGFP replicated to higher levels than rCDV^{R252}EGFP. White blood cell (WBC) counts and body temperature were recorded. All groups developed leukopenia, which was most pronounced in the two rCDV^{SH}EGFP groups (Figure 2F). In general, WBC returned to normal levels from day 8 onwards. All animals developed fever, which peaked earlier in animals infected with rCDV^{SH}EGFP (Figure 2G). CDV-specific virus neutralizing (VN) antibodies were detected from 8 d.p.i. onward (Figure 2H – I), but no MV-specific VN antibodies were detected in these animals (Figure 2J).

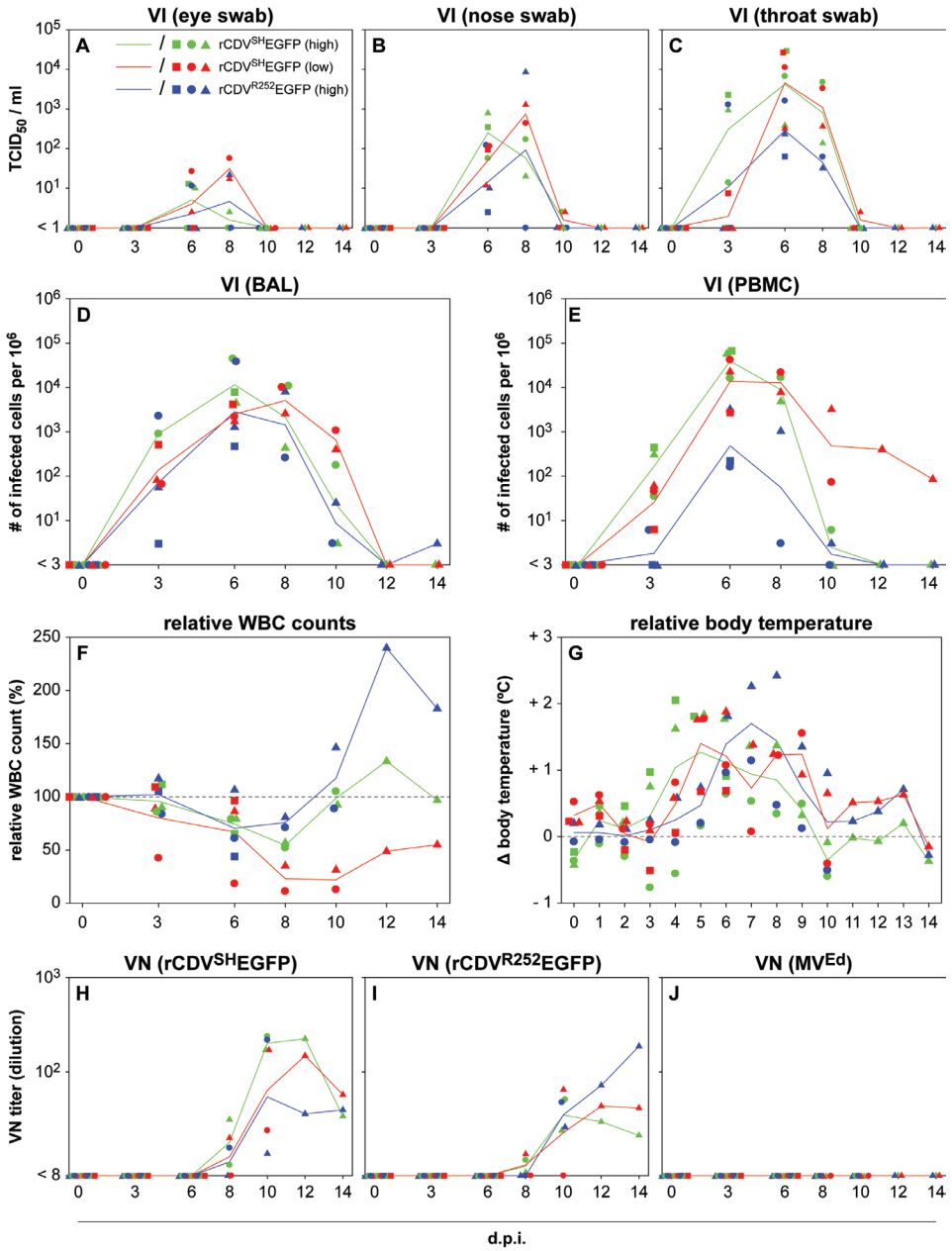

Figure 2. *rCDV^{SH}EGFP and rCDV^{R252}EGFP are virulent in macaques and result in lymphopenia, fever and VN antibody responses. The animals and legend correspond to the data shown in figure 1. (A-E) Virus was isolated in Vero-dogSLAM cells, and results are expressed in TCID$_{50}$ / ml transportmedium (eye-, nose- and throat swabs) or as numbers of infected cells / 10^6 total cells (BAL, PBMC). (F,G) White blood cell (WBC) counts and body temperature are shown relative to the starting values of the individual animals. All groups showed leukopenia and fever. (H-J) Virus neutralizing (VN) antibody responses to CDV strain SH (H) and R252 (I) were detected from 8 d.p.i. onwards, but MV-specific VN antibodies were not detected (J).*

Tropism of rCDV in lymphoid tissues

The phenotype of CDV-infected cells in lymphoid tissues was assessed by immunohistochemistry and flow cytometry. In PBMC, $CD3^+CD4^+$ T-lymphocytes and $CD20^+$ B-lymphocytes were the predominant CDV-infected cell types, and infection percentages in these subpopulations exceeded those observed previously in experimental MV infection [54,265,318]. $CD8^+$ T-lymphocytes were also infected, whereas virtually no $CD14^+$ monocytes or $CD3^-CD8^+$ NK cells were infected by CDV (Figure 3A). These results were mirrored when five key lymphoid tissues were examined and $CD20^+$ B-lymphocytes were predominantly infected, followed by $CD4^+$ and $CD8^+$ T-lymphocytes. Macaques infected with the high dose of $rCDV^{SH}EGFP$ reached higher infection percentages in all populations on 6 d.p.i. than low dose infected macaques. In contrast, macaques receiving a low dose had higher levels of infection on 10 d.p.i. compared to the high dose (Figure 3B). This indicates an earlier peak of replication in animals receiving a high dose of CDV than was previously described for MV [102]. Flow cytometric staining with CD150 indicated, as expected, that the CDV-infected $EGFP^+$ cells were $CD150^+$ (Figure 3C).

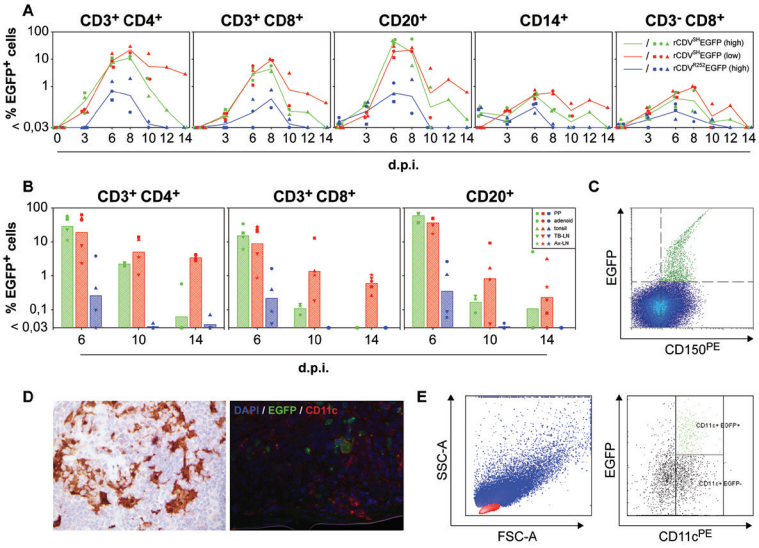

Figure 3. *Tropism of rCDV in PBMC and lymphoid tissues. The phenotype of CDV-infected cells in PBMC and lymphoid tissues was assessed by flow cytometry and immunohistochemistry. (A) Percentages $EGFP^+$ cells in $CD3^+CD4^+$ helper T-lymphocytes, $CD3^+CD8^+$ cytotoxic T-lymphocytes, $CD20^+$ B-lymphocytes, $CD14^+$ monocytes or $CD3^-CD8^+$ NK cells in PBMC. Legends and symbols correspond with those of figure 1. (B) Percentages $EGFP^+$ cells in $CD3^+CD4^+$ helper T-lymphocytes, $CD3^+CD8^+$ cytotoxic T-lymphocytes, $CD20^+$ B-lymphocytes in five key lymphoid tissues. Results are shown as mean percentages $EGFP^+$ cells of the 5 lymph nodes combined, and individual percentages per lymph node. (C) Flow cytometric staining with CD150 indicated that the CDV-infected $EGFP^+$ cells were $CD150^+$. (D) Many $EGFP^+$ cells with the phenotype of DC were detected in the lymphoid tissues. Dual indirect immunofluorescence using anti-EGFP and anti-CD11c monoclonal antibodies showed that $EGFP^+CD11c^+$ cells were present in these tissues. (E) Flow cytometry of single cells suspensions prepared from lymphoid tissues showed CDV-infected DC. After excluding lymphocytes on basis of forward and side scatter (red plot in left panel), large cells were gated as non-clustering cells being $CD3^-$, $CD20^-$ and HLA-DR high. CDV-infected DC were shown as $CD11c^+EGFP^+$ cells within this population (right panel).*

Many EGFP$^+$ cells with the phenotype of DC were detected in the lymphoid tissues (Figure 3D, left panel). Dual indirect immunofluorescence using anti-EGFP and anti-CD11c monoclonal antibodies showed that EGFP$^+$CD11c$^+$ cells were present in these tissues (Figure 3D, right panel). Flow cytometry of single cells suspensions prepared from lymphoid tissues also showed CDV-infected DC. After excluding lymphocytes on basis of forward and side scatter (red plot, Figure 3E, left panel), large cells were gated as non-clustering cells being CD3$^-$, CD20$^-$ and HLA-DR high. CDV-infected DC were shown as CD11c$^+$EGFP$^+$ cells within this population (Figure 3E, right panel).

MV vaccination induces partial protection against CDV challenge infection

Based on the high levels of virulence of rCDV^{SH}EGFP in macaques, this virus was used to evaluate the virulence of CDV in MV-vaccinated animals. Six macaques vaccinated by intra-tracheal (IT) inoculation with MV^{EZ} in the framework of another study 10 months earlier were infected with either a high (n=3) or low (n=3) dose of rCDV^{SH}EGFP. Prior to challenge we confirmed that vaccinated macaques had MV-specific VN antibody levels that are considered protective against measles (mean 2.4 IU/ml, range 0.84 – 6.7). Infections were performed in parallel with the low-dose rCDV^{SH}EGFP infection of naive macaques, using identical methods. To compare virus loads in vaccinated and unvaccinated macaques, virus was isolated from nose (Figure 4A) and throat (Figure 4B) swabs, from BAL cells (Figure 4C) and from PBMC (Figure 4D). Results obtained from six animals infected with high (n=3) or low (n=3) doses were pooled, and are presented as means ± SEM. All MV-vaccinated macaques were productively infected by rCDV^{SH}EGFP independent of the dose, however virus replication levels were significantly reduced and the infection was more rapidly cleared in all samples tested from the vaccinated macaques (Figure 4A – D). Interestingly, virus loads detected in the upper respiratory tract of vaccinated macaques were substantially reduced compared to unvaccinated animals, suggesting that MV vaccination reduces transmission of CDV between macaques.

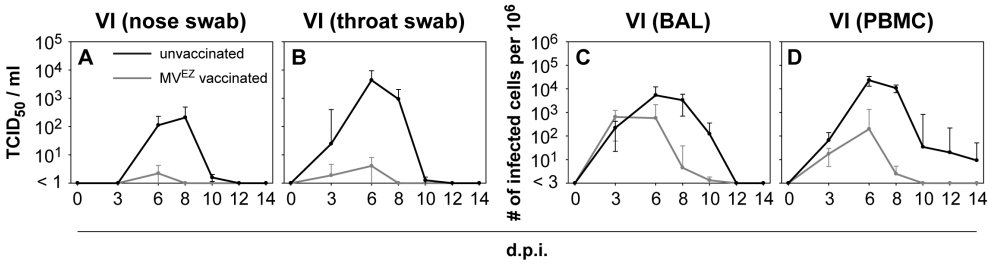

Figure 4. *MV vaccination induces partial protection against CDV. The six unvaccinated and the six MV-vaccinated rCDV^{SH}EGFP-infected macaques were pooled into two groups to compare virus loads, expressed as means ± SEM. All macaques became productively infected by rCDV^{SH}EGFP, but virus replication levels were significantly reduced in the nose (A), throat (B), BAL (C) and PBMC (D) of MV-vaccinated macaques.*

Immune responses in unvaccinated and vaccinated macaques

In agreement with the finding that experimental CDV infection of macaques failed to induce MV-specific VN antibodies (Figure 2J), MV vaccination did not induce CDV-specific VN antibodies (Figure 5A – C). CDV-specific VN antibodies appeared approximately 8 d.p.i. in both vaccinated and unvaccinated macaques, although antibody levels were higher in vaccinated than in unvaccinated animals (Figure 5A and B). Interestingly, MV-specific VN antibody levels of vaccinated macaques were boosted by the CDV infection (Figure 5C), suggesting the existence of cross-neutralizing B-cell epitopes. Subsequently, serum IgG antibody levels to the MV fusion (F) or H glycoproteins were measured to determine the specificity of the antibodies mediating this secondary immune response. Although both curves showed a slight increase, boosting of MV-F-specific IgG antibodies was more pronounced (Figure 5D). At 10 d.p.i. all vaccinated animals showed a more than 4-fold increase in MV-F-specific IgG antibody levels, which was the case for only 2 out of 4 animals for MV-H specific IgG (data not shown). However, accelerated clearance of CDV in MV-vaccinated macaques may also have resulted from cross-specific cellular immune responses. Whereas CDV infection of unvaccinated macaques resulted in severe leukopenia with lowest WBC counts measured 8 d.p.i., leukopenia in MV-vaccinated animals was less pronounced and followed by a rapid increase of WBC counts from 6 d.p.i. onwards (Figure 5E).

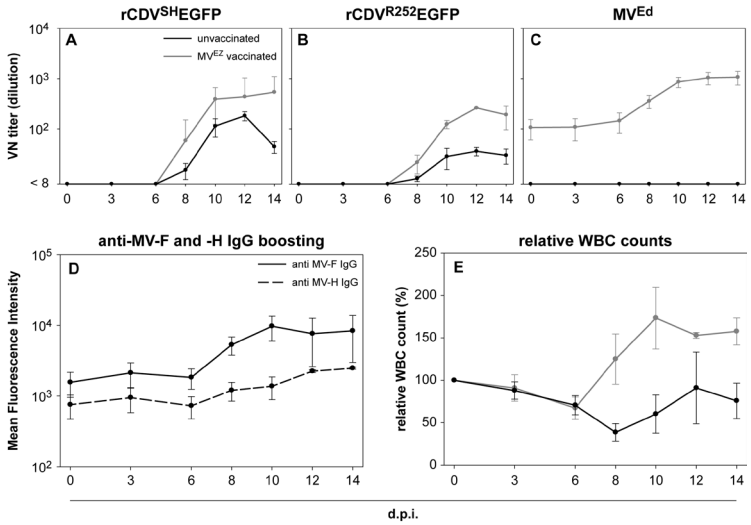

Figure 5. *Immune responses in unvaccinated and vaccinated macaques. (A-C) VN titers against rCDV^{SH}EGFP (A), rCDV^{R252}EGFP (B) and MV^{Ed} (C) were determined in MV-vaccinated and unvaccinated macaques before and after infection with rCDV^{SH}EGFP. MV vaccination did not induce detectable CDV-specific VN antibodies (A,B). CDV-specific VN antibodies appeared approximately 8 d.p.i. in both vaccinated and unvaccinated macaques (A,B). MV-specific VN antibody levels of vaccinated macaques were boosted by the CDV infection (C). (D) Serum IgG antibody levels to the MV-F or -H glycoproteins were measured by a flow cytometric assay [375], demonstrating a more pronounced boosting of antibodies specific to MV-F than to MV-H. (E) WBC counts showed severe leukopenia in unvaccinated macaques, whereas leukopenia in MV-vaccinated animals was less pronounced and followed by a rapid increase of WBC counts from 6 d.p.i. onwards. All plots show means ± SEM. Animals and legend correspond to those of figure 4.*

rCDV-infected epithelial cells are not observed in macaques

In unvaccinated rCDV^{SH}EGFP-infected macaques, macroscopic fluorescence was detected in all lymphoid organs on 6 d.p.i. (Figure 1C – G). During necropsy, the upper and lower respiratory tract were sampled extensively, samples were processed, paraffin embedded and sections were analyzed by EGFP staining. In all tissues, including the adenoids, tonsil, nasal septum, trachea, primary bronchus and lung, submucosal infection of lymphoid and myeloid cells was detected (Figure 6A – F). Notably, epithelial cell infection was not detected in any of the tissues at the time points examined. Although in several cases CDV-infected cells were detected within the epithelial layer, dual immune fluorescence consistently identified these as CD3$^+$, CD11c$^+$ or CD20$^+$ (Figure 6G – I, indicated by arrows) and not cytokeratin$^+$.

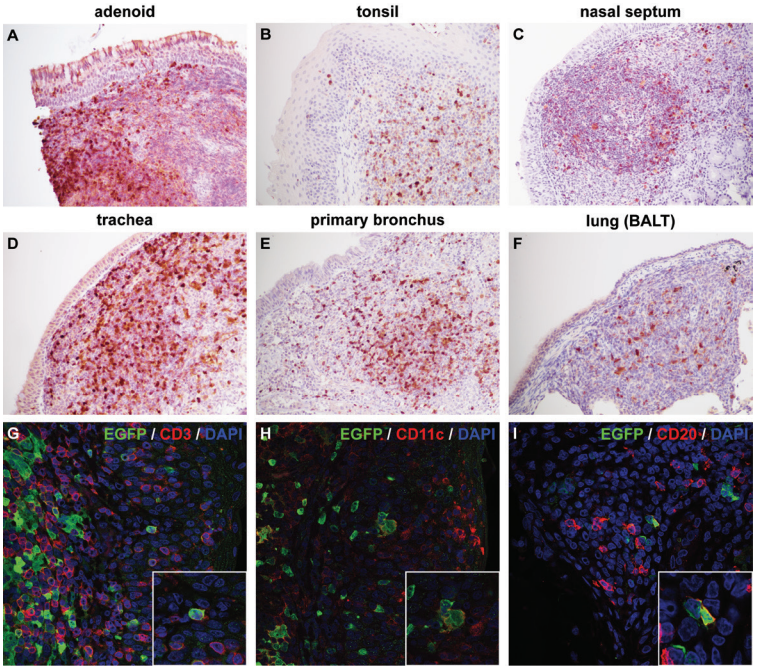

Figure 6. *rCDV-infected epithelial cells are not observed in macaques. During necropsy, the upper and lower respiratory tract were sampled extensively, samples were fixed in buffered formalin, paraffin embedded and sections were analyzed by EGFP staining. (A-F) In all tissues, including the adenoid (A), tonsil (B), nasal septum (C), trachea (D), primary bronchus (E) and lung (F), submucosal infection of lymphoid and myeloid cells was detected (EGFP$^+$ cells shown in brown). Notably, epithelial cell infection was not detected in any of these tissues at the time points examined. (G-I) CDV-infected cells (green) detected within the epithelial layer were identified as CD3$^+$ (G, red), CD11c$^+$ (H, red) or CD20$^+$ (I, red) by dual immune fluorescence consistently. Nuclei were counterstained with DAPI (blue).*

rCDV^{R252}EGFP adaptation to primate epithelial cells

Since no epithelial cell infection was observed *in vivo*, we attempted *in vitro* rCDV infection of human H358 cells, which express PVRL4 but not CD150. These cells are susceptible to infection with wild-type MV [128]. However, rCDV^{SH}EGFP was not able to infect these cells, whereas rCDV^{R252}EGFP infected single cells and was able to spread, but did not cause cell-cell fusion. To try and adapt rCDV^{R252}EGFP to

epithelial cells, the virus was passaged *in vitro* alternating between H358 and human monocyte-derived dendritic cells (moDC). After 18 passages a virus was obtained that caused syncytium formation in H358 cells. This virus was passaged ten more times in H358, including 3 rounds of plaque purification. The P28 virus was named rCDV^{R252}EGFP(C5). Both rCDV^{R252}EGFP and rCDV^{R252}EGFP(C5) grew efficiently on Vero-dogSLAM (VDS) (Figure 7A), but only the adapted virus was able to cause fusion in H358 cells (Figure 7B). This was confirmed in a growth curve, where the non-adapted virus replicated to a level of approximately 10^6 tissue culture infectious dose-50 ($TCID_{50}$) / ml on VDS but on H358 titers remained $<10^2$. The adapted virus replicated to similar titers on VDS, but also replicated efficiently on H358 to a titer of $>10^4$ $TCID_{50}$ / ml (Figure 7C).

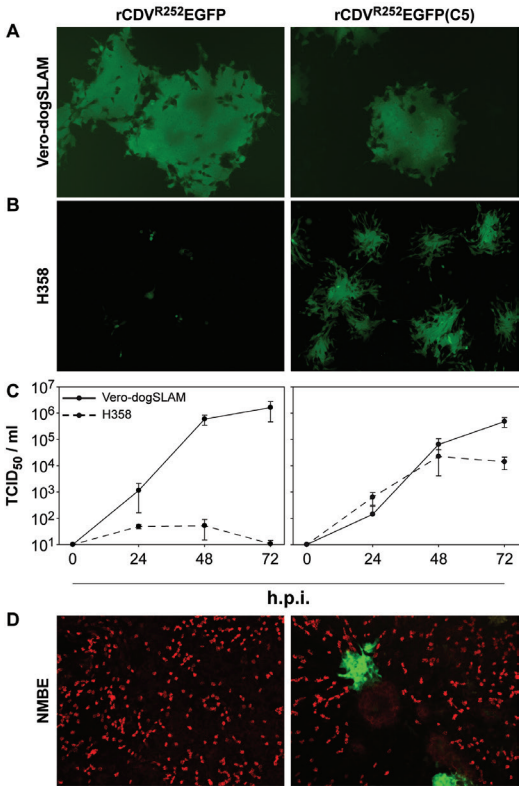

Figure 7. *rCDV^{R252}EGFP adaptation to primate epithelial cells. (A,B) Both rCDV^{R252}EGFP and rCDV^{R252}EGFP(C5) grew efficiently on Vero-dogSLAM (A), but only the adapted virus was able to cause fusion in H358 cells (B). (C) In a growth curve the non-adapted virus replicated to a level of approximately 10^6 $TCID_{50}$ / ml on Vero-dogSLAM but on H358 titers remained $<10^2$. The adapted virus replicated to similar titers on Vero-dogSLAM, but also replicated efficiently on H358 to a titer of $>10^4$ $TCID_{50}$ / ml. (D) rCDV^{R252}EGFP infection of scratched differentiated normal macaque bronchial epithelial cells. The non-adapted rCDV^{R252}EGFP infected only few single cells in the NMBE cultures, whereas the H358-adapted rCDV^{R252}EGFP(C5) spread from cell-to-cell and caused foci of infection around the scratch.*

Infection of differentiated macaque bronchial epithelial cells

Primary normal macaque bronchial epithelial cells (NMBE) were obtained from the bronchus of a euthanized macaque and differentiated on air-liquid interface [323]. The monolayer of differentiated epithelial cells was scratched and infected with rMV^{KS}EGFP, rCDV^{SH}EGFP, rCDV^{R252}EGFP or rCDV^{R252}EGFP(C5). rMV^{KS}EGFP, which served as a positive control, caused extensive infection around the scratch (data not shown). rCDV^{SH}EGFP (data not shown) and the non-adapted rCDV^{R252}EGFP (**Figure 7D**) infected single cells in the NMBE cultures, but the viruses were unable to spread. In contrast, the H358-adapted rCDV^{R252}EGFP(C5) readily spread from

cell-to-cell and caused foci of infection around the scratch (**Figure 7D**). Sequence analysis revealed no mutations in phosphoprotein (P), an N574S mutation in the F glycoprotein, and a T544A mutation in the H glycoprotein.

Discussion

In the present study we show that wild-type CDV strains can readily infect cynomolgus macaques, causing fever and lymphopenia. The viruses predominantly replicated in $CD150^+$ macaque lymphocytes and DC. In PBMC, $rCDV^{SH}EGFP$ replicated faster and to higher levels than MV. MV-vaccinated macaques were partially protected from CDV challenge, resulting in highly restricted virus shedding from the upper respiratory tract.

Both MV and CDV are members of the family *Paramyxoviridae*, genus *Morbillivirus*. In recent years, we have studied the tropism of MV in macaques [54,256,265]. The predominant infection of $CD150^+$ lymphocytes and DC in macaques we report here for CDV corresponds well with the reported tropism of MV in macaques [54]. In addition to being lymphotropic, in its natural host species CDV readily infects epithelial and neuronal cells [105,373]. This has also been described for MV in non-human primates [54,125], although CDV normally infects higher percentages of epithelial cells in carnivores than MV does in primates, and is therefore regarded as more epitheliotropic. Recently, it has been demonstrated that entry into epithelial cells for both CDV and MV is not CD150-mediated, but dependent on another cellular receptor, PVRL4. This receptor is present in the adherens junction on the basolateral side of epithelial cells and postulated to be important for viral shedding, in that it allows a predominantly lymphotropic virus to break through epithelial barriers [130,131].

At the time-points examined, we were not able to demonstrate spread of CDV infection into either macaque epithelial cells or the CNS. *In vitro* infection studies in primary well-differentiated NMBE showed that $rCDV^{SH}EGFP$ or $rCDV^{R252}EGFP$ could infect single NMBE when the monolayer was scratched to expose the basolaterally-expressed PVRL4, but were unable to spread to the neighboring cells. In contrast, these cultures were readily infected with wild-type MV. *In vivo* large numbers of CDV-infected cells were seen within the respiratory epithelium or in the respiratory submucosa, demonstrating that epithelial cells were exposed to CDV. However, CDV-infected epithelial cells were not observed in these macaques. Interestingly, by consecutive passaging of $rCDV^{R252}EGFP$ in H358, a human cell line expressing PVRL4, the virus could be adapted to efficiently cause cell-cell fusion in human $PVRL4^+$ cells. In a recent report Sakai *et al.* described experimental infections of macaques with a CDV strain isolated during an outbreak amongst cynomolgus macaques. The authors not only showed that this virus could efficiently use both macaque CD150 and PVRL4 *in vitro*, but also infected both lymphocytes and epithelial cells *in vivo* [412]. These observations suggest that the continuing chain of CDV transmissions in macaques has resulted in adaptation of the virus enabling cell-to-cell spread in macaque $PVRL4^+$ epithelial cells.

In contrast to previously reported experimental infections with rMV or rCDV modified to prevent PVRL4 binding [137,391], we isolated significant amounts of CDV from BAL cells, throat swabs and nasopharyngeal swabs, demonstrating shedding of CDV in the absence of detectable infection of epithelial cells. This observation suggests that recently proposed hypotheses explaining transmission of morbilliviruses [158] may not tell the complete story.

In previous experimental morbillivirus cross-species infection studies, these viruses often proved less pathogenic than in their natural host. Experimental infection of pigs with CDV showed that these were susceptible to infection. However, the virus replicated exclusively in the lymphoid tissues without causing clinical signs of disease [396]. In a controversial inoculation of a probably MV-seropositive human with CDV described in 1931, subclinical infection was observed [415], which may have been comparable to what we observe in non-human primates. In a reciprocal experiment, it has been reported that experimental infection of dogs with MV also resulted in subclinical infection [416,417].

Experimental infection of cats with CDV resulted in subclinical infection [396]. However, large outbreaks among felids in Africa and North America caused by CDV have been reported in the 1990s [393,395,398]. Strikingly similar to these observations, experimental infection of seals with wild-type CDV^{SH} led to an exclusively lymphoid and not epithelial infection, which did not transmit to sentinel hosts [408]. However, in 1987 and 2002 CDV caused massive lethal outbreaks in Baikal and Caspian seals [406,407,418,419]. Taken together these observations are reminiscent of what we observe as a self-limiting non-lethal infection in macaques in our experimental infections, and the currently ongoing lethal CDV outbreaks in macaques in China [200,411].

Immunological relationships between morbilliviruses have long been reported [420–422]. However, the cross-neutralizing capacity of specific antibodies is not fully understood. Örvell *et al.* reported that convalescent sera from CDV-infected dogs could not cross-neutralize MV [423]. Furthermore, it was shown that MV monospecific antibodies against H and F could not cross-neutralize CDV [424]. Surprisingly, it is known that vaccination with attenuated morbilliviruses does cross-protect from infection with heterologous morbilliviruses. In fact, live-attenuated and recombinant MV vaccines have been used to immunize dogs, even in the presence of maternal antibodies, against CDV [414,417,425], resulting in partial protection from CDV even though CDV-specific antibodies could not be detected. This indicates that cellular rather than humoral immunity could play an important role in cross-protection [426]. These results correspond well with our observations.

One of the milestones of the WHO is to establish a target date for the global eradication of measles, which would save many lives but may also result in reduced compliance to MV vaccination, resulting in many children growing up without MV-specific immunity and potentially opening a niche for animal morbilliviruses. Even though CDV infection of humans has rarely been described [415,427], some humans

have CDV-specific virus neutralizing antibodies [420]. Whether these are high titer MV-specific antibodies cross-reactive with CDV, or whether these individuals have actually experienced CDV infection is unknown.

In conclusion, we have demonstrated that non-human primates are susceptible to infection with wild-type CDV strains, and that measles immunity provides partial protection and limits viral shedding. Thus, morbillivirus cross-specific immunity of the human population restricts the possibilities of CDV and other animal morbilliviruses to replicate in and adapt to humans. However, if measles eradication would be followed by significant drops in MV vaccination coverage, such adaptation cannot be excluded. Although this should not be used to argue against measles eradication, it reinforces the general idea that sustained MV vaccination and serological and virological surveillance of morbillivirus infections will remain essential. Potentially, the use of recombinant MV strains as vectors for vaccination against heterologous pathogens could provide the necessary incentive to sustain compliance to MV vaccination.

Acknowledgements

The authors would like to thank Ken Lemon and Linda Rennick for their contributions to these studies. Vero-dogSLAM cells were a kind gift of Yusuke Yanagi.

SUMMARIZING DISCUSSION

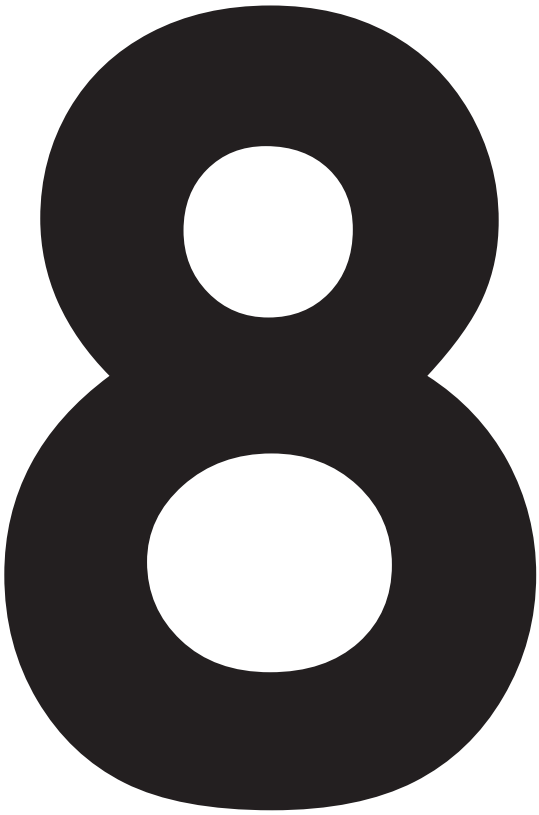

SUMMARIZING DISCUSSION

Based on:

Measles vaccination: new strategies and formulations
Rory D. de Vries, Koert J. Stittelaar, Albert D.M.E. Osterhaus and Rik L. de Swart
Expert Reviews of Vaccines 2008 Oct; 7(8):1215 - 1223 (review)

The pathogenesis of measles
Rory D. de Vries, Annelies W. Mesman, Teunis B.H. Geijtenbeek, W. Paul Duprex and Rik L. de Swart
Current Opinion in Virology 2012 Jun; 2(3): 248 - 255 (review)

Evaluating measles vaccines: can we assess cellular immunity?
Rory D. de Vries and Rik L. de Swart
Expert Reviews of Vaccines 2012 Jul; 11(7): 779 - 782 (key paper evaluation)

Introduction

Despite the availability of safe and effective MV vaccines, measles still caused an estimated 140,000 deaths in 2010 [62]. The disease is characterized by fever and maculopapular rash, often in combination with cough, coryza and conjunctivitis. MV is efficiently transmitted by aerosols entering the respiratory tract or by direct contact with respiratory secretions. Upon transmission it causes a systemic infection. However, the cell types involved in primary infection or human-to-human transmission have long been poorly understood. These events were studied in detail in the macaque model, as described in chapters 2, 3, 4 and 5 of this thesis. Measles mortality mainly results from the transient but profound measles-associated immune suppression that lasts for several weeks to months. Paradoxically, measles is also associated with the induction of strong MV-specific humoral and cellular immune responses, resulting in lifelong immunity. The studies described in chapter 6 contributed to a new model for the underlying cause of measles-associated immune suppression and this apparent 'paradox'. Since measles is considered for global eradication, the potential of other animal morbilliviruses to cross the species barrier into primates was studied in chapter 7. Here, macaques were infected with rCDV and the tropism of CDV in macaques was elucidated.

Macaque model

Even though multiple animal models have been developed for the study of measles pathogenesis over the past decades [94–96], the *in vivo* experiments described in this thesis have all been performed in non-human primates. This model has been shown to be the optimal animal model for measles [430]. Both rhesus and cynomolgus macaques are highly susceptible to infection with wild-type MV and develop clinical signs and pathologic lesions similar to those described in humans [99–102]. Moreover, natural infections following contact with MV-infected humans have been frequently reported [99,103].

Fluorescent reporter proteins

Throughout the chapters of this thesis rMV or rCDV strains expressing fluorescent reporter proteins were used. In chapter 3 the generation of a new rMV expressing EGFP, based on a wild-type genotype B3 MV isolate from Khartoum, Sudan, is described. Before the generation of that virus, pathogenesis studies performed with molecular clones of wild-type MV were mainly based on the Japanese strain IC323 [52]. Development of a new recombinant wild-type MV as described in this thesis serves to complement ongoing studies of MV pathogenesis and ensures that observations are not strain-specific. Altogether, the EGFP-expressing viruses have made sensitive detection of virus-infected cells possible, and greatly facilitated pathogenesis studies *in vitro*, *ex vivo* and *in vivo* [104].

Early target cells for MV

Since MV is often described as a respiratory virus, it is evident that MV initiates infection in the respiratory tract. As such the initial target cells were originally thought to be respiratory epithelial cells [16]. However, since these cells do not express the

MV receptors CD150 or PVRL4 on their apical cell surface, they are an unlikely primary target. Viruses unable to bind CD150 were severely attenuated in macaques [116], whereas viruses unable to bind PVRL4 caused a normal systemic infection [137]. The initial infection of cells in the respiratory tract is therefore most likely a CD150-dependent event. DC-SIGN could play an additional role, by capturing MV from the lumen of the respiratory tract, as discussed in chapter 2 and below.

With the macaque model and rMV strains expressing EGFP in hand, the studies described in chapter 3 were designed to investigate which cell types were initially infected by MV in macaques. Furthermore, the locations of early amplification of MV within the host were elucidated, before the virus disseminated throughout the body. In the experiments described in chapter 3, MV-naive macaques were exposed to a high virus dose by inhalation of a small particle size aerosol to ensure that the entire upper and lower respiratory tract was exposed [256,265]. Animals were sacrificed at early time-points post infection to further elucidate the route of entry.

MV attachment receptors

Before hypothesizing on the route of entry, it is important to discuss which attachment receptors could potentially be involved in 'capturing' MV from the airways. In chapter 2 of this thesis the role of two attachment receptors DC-SIGN [255] and Langerin [123] in measles pathogenesis and antigen presentation is discussed. In this chapter, it is shown that a subset of DC, the DC-SIGN$^+$ DC, mediate both transmission and MV antigen presentation to T-lymphocytes. The role of LC in the pathogenesis of measles is currently less clear.

Role of DC-SIGN in transmission of MV from DC to T-lymphocytes

Since measles is highly contagious and infection results in strong MV-specific immune responses, both viral transmission and antigen presentation should occur through efficient and robust processes. DC-SIGN$^+$ DC have previously been reported to be important antigen presenting cells. In chapter 2 of this thesis it is shown that they are present in the sub-epithelial tissues of the mouth, pharynx, trachea and bronchi, and that there are scattered DC-SIGN$^+$ cells throughout the lung (Figure 1). Since MV enters in the respiratory tract and DC-SIGN can function as an attachment receptor for MV [132], these DC-SIGN$^+$ DC are likely targets for MV entry into the host.

In addition to the role DC-SIGN$^+$ DC may play in the entry of MV into its host and transmission of infectious virus to T-lymphocytes, it is described in chapter 2 that DC-SIGN$^+$ DC are also capable of MV antigen presentation. Both DC-SIGN and CD150 are involved in MV processing and presentation of MV-derived peptides to a specific CD4$^+$ T-cell clone, but antibodies against DC-SIGN inhibited antigen presentation to a larger extent than antibodies against CD150. Thus, although both DC-SIGN and CD150 are involved, DC-SIGN appeared more important for antigen presentation of MV by DC.

LC capture MV through Langerin and present antigen to CD4⁺ T-lymphocytes
Next to DC-SIGN⁺ DC, other DC subsets may have distinct functions in MV pathogenesis and antigen presentation. In chapter 2, the role of LC and Langerin was investigated. A C-type lectin present on LC, Langerin, was identified as an attachment receptor for MV [123]. LC were observed in the tongue, buccal cavity, tonsil, pharynx and bronchi (Figure 1). The density of LC was high in the upper respiratory tract and decreased while descending toward the lungs, where LC were only scarcely detected. *In vitro*, immature LC were not susceptible to MV infection but mature LC could readily be infected, resulting in activation of CD8⁺ T-lymphocytes through antigen presentation in the context of HLA class I.

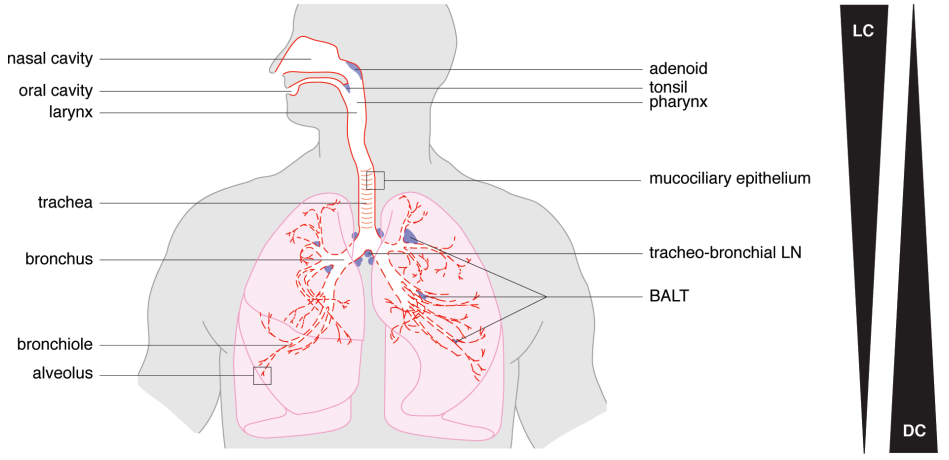

Figure 1. *Schematic representation of the different compartments of the human respiratory tract. Next to the respiratory tract, the adjacent lymphoid tissues are indicated in blue (figure adapted from [357]). LC are abundant in the upper respiratory tract, but scarcely detected in the lower respiratory tract, where for DC this distribution is inversed.*

Classically, exogenous antigens are presented in the context of HLA class II, whereas endogenous-derived peptides are presented in the context of HLA class I molecules. However, several DC subsets have the capacity to cross-present exogenous antigens in the context of HLA class I molecules [240]. The data in chapter 2 shows that where human monocyte-derived DC (moDC) were capable of efficient cross-presentation, human primary LC were not capable of cross-presenting inactivated or apoptic MV particles to CD8⁺ T-lymphocytes *in vitro*. However, capture of virus through Langerin resulted in normal antigen processing and presentation to CD4⁺ T-lymphocytes. Anti-Langerin as well as mannan partly inhibited this, suggesting that other receptors or other uptake mechanisms also contribute to antigen uptake.

In vivo tropism of attenuated MV strains

In chapter 4 the development of an aerosol infection model for macaques is described and compared with intra-tracheal (IT) administration. Furthermore, the *in vivo* tropism of an attenuated and a pathogenic strain of MV was compared in animals euthanized close to the peak of virus replication (7 d.p.i.).

rMV^{rEdt}EGFP was used as an attenuated MV strain in this study. This virus is a "repaired" recombinant EGFP-expressing virus based on the Edtag strain of MV. An important consideration in the use of Edtag for *in vivo* infections is that Edtag does not encode a functional V protein, due to many C-to-T transitions [304]. Therefore, the studies described in chapter 4 were performed with a virus in which the P gene sequence was corrected by site-directed mutagenesis. The rescued recombinant virus was shown to have a normal V protein expression and *in vitro*, rMV^{rEdt}EGFP could use both CD46 and CD150 as entry receptors. However, despite efficient replication in lymphoid cells *in vitro*, rMV^{rEdt}EGFP replication was impaired *ex vivo* and *in vivo*.

Chapter 4 also shows that even though attenuated MV is incapable of causing systemic infection, it causes a robust infection in the lungs of macaques upon IT or aerosol administration. Both the attenuated and pathogenic viruses predominantly infected CD11c$^+$ myeloid cells, which include alveolar macrophages and DC. Therefore it was hypothesized that attenuated MV prefers CD150 over CD46 as a cellular entry receptor in macaques. However, only pathogenic MV also caused viremia and was disseminated to lymphoid tissues, the respiratory submucosa and the skin.

The aerosol infection model proved highly comparable to the standard IT route of pathogenic MV infection of macaques. Few differences were observed between the two routes in the virus isolation profiles from broncho-alveolar lavage (BAL), blood, throat, or nose samples. In addition, no macroscopic or microscopic differences in distribution or intensity of fluorescent cells were observed in affected organs during necropsies 7 d.p.i. Further analysis of the samples collected from macaques infected via either delivery route identified the same major target cells described previously [54].

One difference governed by the route of infection was observed in animals infected with attenuated MV. In the upper respiratory tract, pathogenic MV was detected only after infiltration of MV-infected CD150$^+$ cells following the onset of systemic viremia in both IT and aerosol infections. This is probably because infection of the airway epithelium from the apical side is not possible, and only low numbers of CD150$^+$ target cells are available. Early detection of attenuated MV in the throat and nose after aerosol inhalation indicated that, in contrast to pathogenic MV, attenuated MV may be capable of primary replication in the upper respiratory tract. Such early replication might be mediated by the use of CD46 as an entry receptor. However, the presence of MV-infected cells could not be confirmed by immunohistochemistry, suggesting that the numbers of infected cells in the upper respiratory tract were low.

MV strategy of host entry

With the results from chapter 2 and 3 in hand, two potential strategies on how MV enters its host were developed: the first strategy was based on infecting CD150$^+$ cells in the alveoli (Figure 2A), the second strategy was based on being captured from the respiratory tract lumen by DC-SIGN$^+$ DC (Figure 2B). Chapter 3 shows

that in macaques at early time points (2 and 3 d.p.i.) after inhalation of an aerosol containing a high MV dose, MV-infected large mononuclear cells with the phenotype of AM or DC were observed in the alveolar spaces or attached to alveolar walls (Figure 3A). Targeting of these cells was followed by the establishment of localized MV replication in organized lymphoid structures in the lungs. These BALT contain a large number of susceptible B-lymphocytes and memory CD4$^+$ T-lymphocytes [287], both cell types previously described as target cells for MV in lymphoid tissue at later time points [54,318]. Seeding and amplification of the infection in these microenvironments, which are well suited to a lymphotropic virus such as MV, is likely to be critical in the establishment of the infection. The next location where MV-infected cells were observed was in the tracheo-bronchial lymph node (LN), the draining lymph node of the lungs, whereafter viremia was initiated and MV-infected cells could be detected in peripheral lymphoid tissues. This suggested that from the lungs, MV was transported by infected cells to the draining tracheo-bronchial LN. After localized replication in the lungs and increased replication in the tracheo-bronchial LN, MV spread systemically through viremia to the majority of lymphoid organs by 4 or 5 d.p.i. At these relatively early time points MV-infected cells were mostly detected in close proximity to venules within lymphoid organs, suggesting that these were involved in spreading the virus.

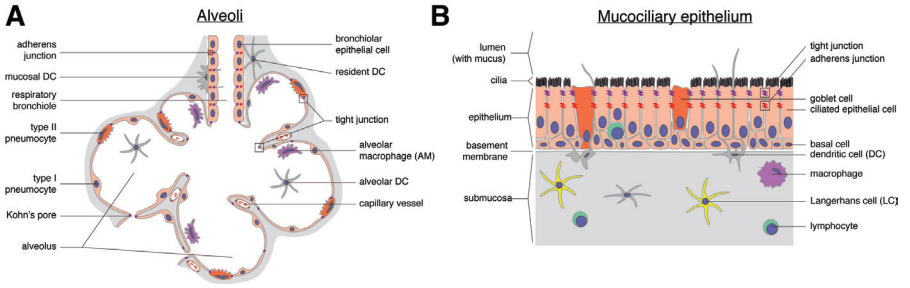

Figure 2. *Schematic representation of the different compartments of the human respiratory tract. (A) Enlargement of a bronchiole ending in multiple alveoli containing alveolar macrophages and dendritic cells. (B) Enlargement of the pseudo-stratified columnar epithelium present in the upper respiratory tract, trachea, bronchi and bronchioles, with intra-epithelial and sub-epithelial immune cells. (figure adapted from [357]).*

A “Trojan horse” strategy has been described for HIV-1, in which DC allow HIV-1 to enter the body and transport the virus to susceptible CD4$^+$ T-lymphocytes [135,216]. The abundant presence of DC-SIGN$^+$ DC in the respiratory tract makes them potential targets for initial infection with MV. After binding of MV to a DC-SIGN$^+$ DC in the respiratory tract (Figure 3B), the DC maturates and migrates to the draining LN, bringing the virus into close proximity of its favored target cells, CD150$^+$ B-lymphocytes and memory T-lymphocytes [54,318]. However, *in vitro* studies have indicated that interaction of DC with MV can also result in physical and functional paralysis [431]. The *in vivo* relevance of this observation remains to be determined. Indeed, *in vivo* in the macaque model, infection of MHC class II$^+$ CD11c$^+$ DC has been described in the lungs, respiratory submucosa and the skin, but also in lymphoid tissues [54,265]. The close contact between CD150$^+$ and DC-SIGN$^+$

cells in lymphoid tissues likely contributes to the massive level of MV replication in these tissues. In chapter 2 it is shown *in vitro* that DC-SIGN$^+$ DC can transmit MV to both CD4$^+$ and CD8$^+$ T-lymphocytes and DC-SIGN$^+$ DC enhance infection of T-lymphocytes in co-cultures. This *trans*-infection was shown to be dependent on DC-SIGN, not CD150.

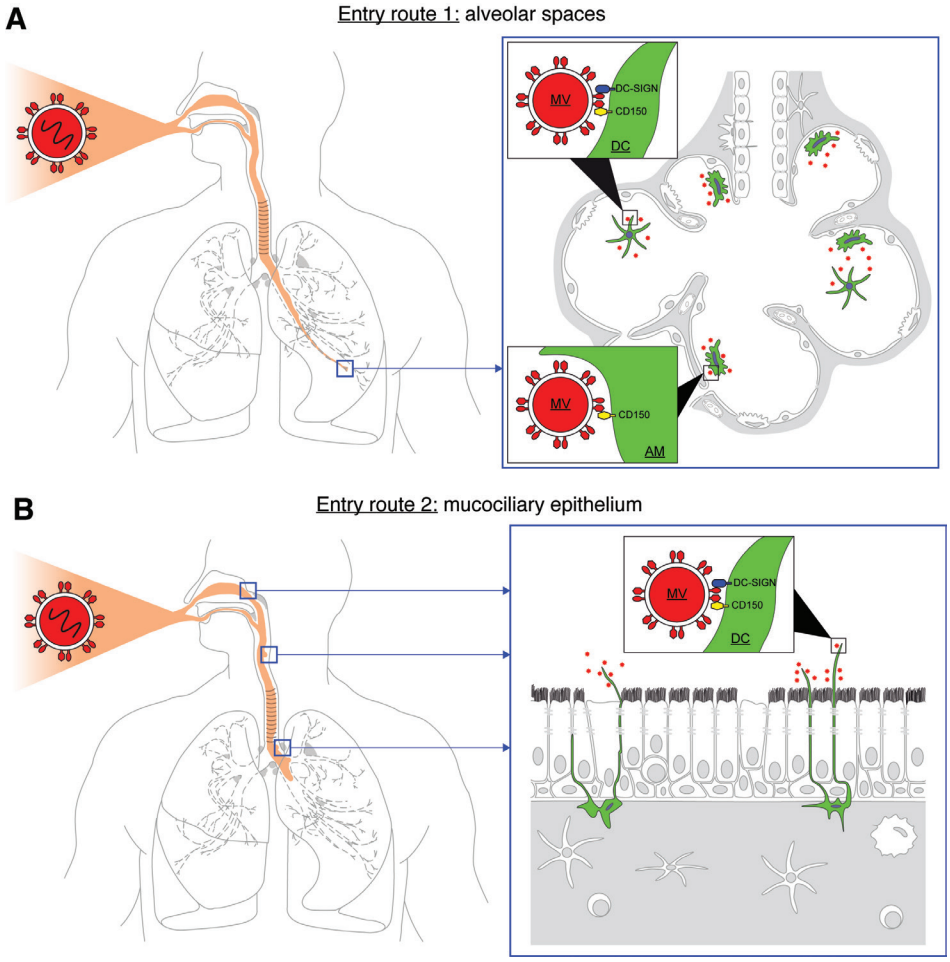

Figure 3. *Two possible entry strategies for described for MV. MV particles are shown in red, potential target cells for MV infection are shown in green. (A) In entry route 1, MV is inhaled and reaches the alveoli, where it can infect CD150$^+$ and/or DC-SIGN$^+$ AM or DC. (B) In entry route 2. MV binds to DC-SIGN$^+$ DC with dendrites protruding into the mucus covering the lumen of the mucociliary epithelium. In both cases, the DC or AM carrying MV will travel to the draining lymphoid tissues, where the virus is transmitted to the CD150$^+$ lymphocytes (figure adapted from [357]).*

An alternative route for MV to enter a susceptible host would be via direct infection of CD150$^+$ cells in Waldeyer's tonsillar ring, consisting of tonsils and adenoids. Tonsils and adenoids are lined by CD150$^-$ epithelial cells, but at sites of damage or in tonsillar crypts direct infection of CD150$^+$ cells at the luminal surface might be

possible. In the aerosol infection model, tonsils and adenoids were directly exposed to a high dose of nebulized virus, but a consistent level of infection was only detected at 4 and 5 d.p.i., after onset of viremia. These data suggest that MV cannot easily penetrate the epithelial barrier to initiate MV infection of $CD150^+$ cells in Waldeyer's ring lymphoid tissues.

Finally, the results described in chapter 2 and 3 suggest that LC have a specialized function in MV infection. Immature LC, mainly present in the upper respiratory tract [123], are refractory to MV infection and do not induce MV-specific $CD8^+$ T-lymphocytes. These data suggest that other DC subsets, like the DC-$SIGN^+$ DC, are probably involved in initial entry into the host, and dissemination to the lymphoid tissues.

MV host-to-host transmission

MV is mainly transmitted from host-to-host by aerosols, either in the form of cell-free virions or as debris from MV-infected cells. It has been speculated that infection of epithelial cells during the late stage of measles pathogenesis may contribute to MV transmission [130,131]. MV-infected lymphocytes or DC present in the respiratory submucosa [125] transmit the virus to epithelial cells via PVRL4. This may cause apical shedding of MV, resulting in transmission to the next host [130,131,158].

In chapter 5 a comprehensive analysis of the respiratory tract of MV-infected macaques was described to analyze the distribution of MV-infected cells and the associated lesions during the late stages of measles, between 9 and 13 d.p.i. Based on these observations, an alternative hypothesis of MV transmission was developed, in which epithelial damage plays a crucial role. This analysis of respiratory tract tissues from MV-infected macaques highlighted the importance of MV-infected immune cells infiltrating into epithelia in the spread of virus to epithelial cells. The study described in chapter 5 provides evidence of immune cells having a direct role in the spread of virus into epithelia *in vivo* and thus completes a missing link in our understanding of measles pathogenesis. MV spread into epithelia is most likely mediated via the interaction of MV-H on the surface of infiltrating immune cells with PVRL4 present in epithelial cell adherens junctions.

Recently, the trachea has been proposed as the primary site from which MV emerges into the airways of the respiratory tract prior to transmission to a susceptible host [130]. However, while isolated small circular foci of MV-infected ciliated epithelial cells along the inner surface of the trachea have been shown, the overall burden of virus infection and pathology was much less compared to the nasal concha and mucosa in the nasal cavity and lymphoid tissues such as the palatine tonsils and adenoids. The anatomical location of these tissues higher in the respiratory tract (Figure 1) means that virus shed from these sites is inherently more likely to be expelled into the environment than virus emerging lower down the airways which has to survive neutralization by host factors present in mucus and saliva for a longer time period.

In chapter 5, potential alternative strategies of MV transmission are described. First of all, a high level of MV-infected epithelial cells was detected in the nose of macaques. Furthermore, MV-infected cells and associated sub-cellular debris in the lumen of the respiratory tract was detected, together with cell-free and cell-associated virus in nose and throat swabs taken from infected macaques. Virus particles and subcellular debris may be readily expelled into the air by coughing and sneezing. It could be postulated that MV released into the environment in a cell-associated form would be better protected against environmental hazards such as humidity and high temperatures and may be more infectious than cell-free virions due to the greater efficacy and speed of cell-to-cell fusion in comparison to virus-to-cell fusion.

In summary, a mechanism for the introduction of MV into the respiratory epithelium following viremia via the infiltration of infected immune cells and subsequent spread to pseudostratified columnar and non-keratinized squamous epithelium was described. Differential levels of infection were observed in epithelium from respiratory tract tissues, with tonsillar and nasal epithelium in the upper respiratory tract consistently displaying the highest levels of infection. In many instances this was associated with the infiltration of large numbers of uninfected immune cells leading to breakdown of the epithelium and sloughing of debris into the lumen of the respiratory tract.

Immune suppression

Measles is associated with a transient but profound immune suppression, of which the clinical importance is illustrated by the observation that measles mortality is typically caused by secondary infections of the respiratory and digestive tracts [64–66]. Based on the observations described in chapter 6, measles immune suppression can, at least in part, be explained by massive infection and subsequent immune-mediated clearance of $CD150^+$ memory T-lymphocytes and follicular B-lymphocytes. MV preferentially infected $CD45RA^-$ T^{CM} and T^{EM}, which during secondary immune responses are the primary source of T-lymphocyte expansion or generation of effector T-lymphocytes, respectively [367]. Infection and subsequent immune-mediated depletion of memory T-lymphocyte subsets fits with the first description of measles-induced immune suppression, namely the disappearance of Mantoux responses in measles patients [160].

Since none of the current hypotheses for the underlying mechanism of measles-associated immune suppression adequately explain the measles paradox, chapter 6 discusses a novel model that fits the current observations on immune suppression and MV-specific immune responses. The novelty of this model lies in an immune-mediated lymphodepletion being masked by the massive expansion of MV-specific and bystander lymphocytes. Although effective MV-specific $CD8^+$ T-lymphocyte responses as well as immune activation and lymph node enlargement have been described earlier [148,170,365,373], they have not been associated with immune suppression in this way. The experiments described in chapter 6 illustrate the importance of $CD8^+$ T-lymphocytes in the control of MV dissemination and *in vitro* clearance of MV-infected lymphocytes. Both the use of virus-specific TCC and PBMC bulk cultures confirmed that $CD4^+$ T-lymphocytes have limited effector capacity, but

that CD8+ T-lymphocytes efficiently cleared an ongoing MV infection. Like described for HIV and other lymphotropic viruses, the cellular immune response to MV is characterized by a fierce battle between virus and host immune response: virus-specific T-lymphocytes can either kill or be killed. However, whereas HIV establishes a chronic infection and slowly exhausts the immune system, MV causes an acute and usually self-limiting infection.

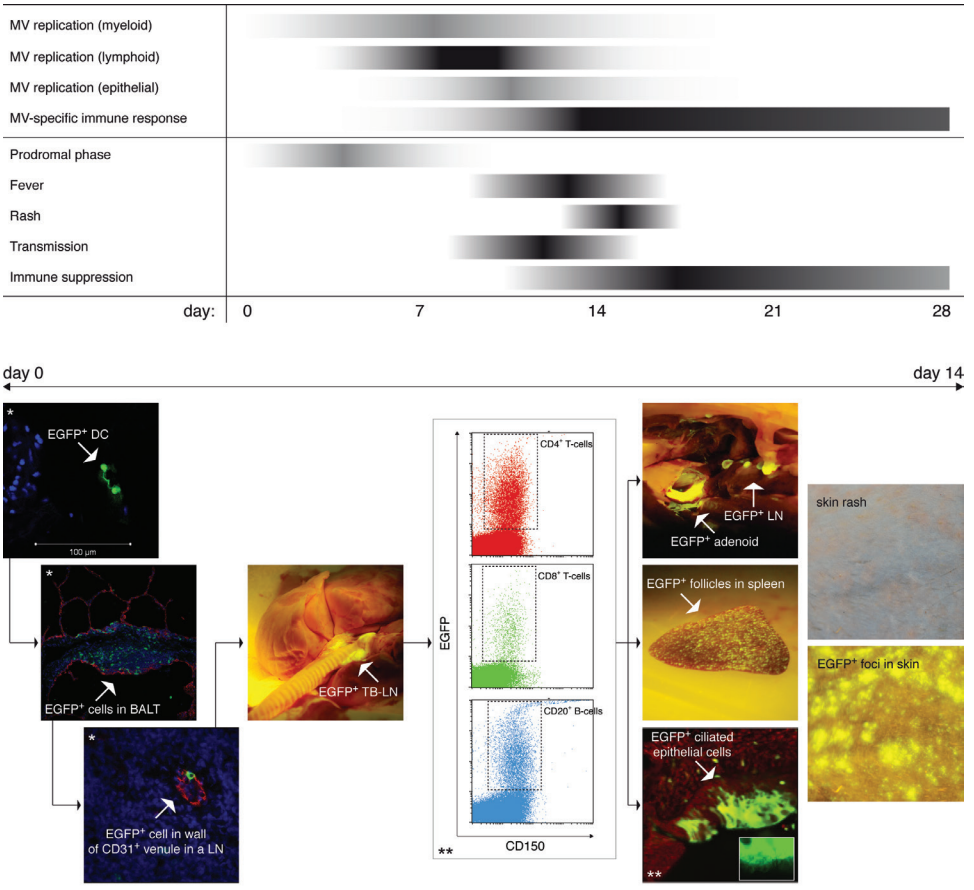

Figure 4. *Schematic representation of MV pathogenesis. In the upper panel, the color intensity of the black bars indicates the approximate timing of MV replication in myeloid, lymphoid and epithelial cells, MV-specific immune responses, fever, rash, transmission and immune suppression based on observations in the macaque model. In the lower panel, major events in MV pathogenesis are illustrated with images taken from macaques infected with rMV expressing EGFP. Viremia is illustrated by FACS plots, showing EGFP+ CD150+ cells in peripheral blood (figure adapted from [357]). * taken from [256]; ** taken from [54].*

In certain auto-immune diseases, and in animal studies in which lymphocyte populations were experimentally depleted, commensal or opportunistic infectious agents that would normally be controlled by the immune system have been shown to cause severe disease [381]. The high incidence of respiratory and gastro-intestinal

complications following measles [64–66] is therefore directly related to measles-associated lymphocyte depletion in the adenoids, tonsils and gut-associated lymphoid tissue, tissues which form a first line of defense against inhaled or ingested pathogens. In line with the developed model, chapter 5 concludes that MV infection wipes immunological memory, resulting in immunological amnesia leading to increased susceptibility to commensal or opportunistic infections.

MV pathogenesis

Combining the results obtained in macaques described in chapters 2 – 6, a schematic representation of the sequence of events observed in measles pathogenesis in macaques has been proposed (Figure 4). After the initial infection of DC or AM in the alveoli (myeloid infection), MV seeds into the BALT where it is amplified (start of lymphoid infection). Next, MV-infected cells are first observed in the tracheo-bronchial LN (3 d.p.i.), the draining LN of the lungs. The infection becomes systemic from ± 4 d.p.i., with T-lymphocytes being the preferential target in PBMC and B-lymphocytes the preferential target in LN. Around the peak of replication ± 7 – 9 d.p.i., all lymphoid organs were MV-infected, and infected epithelial cells start appearing. This is the time-point where the MV-specific immune response is detected, which inhibits MV replication. The start of the immune response goes hand-in-hand with the appearance of clinical symptoms.

The infection and destruction of epithelial cells in the respiratory tract sets the stage for viral excretion and host-to-host transmission. At the same time, MV-infected cells are rapidly cleared by MV-specific $CD8^+$ T-lymphocytes, leading to a depletion of central and effector memory T-lymphocytes and depletion of B-cell follicles, and a subsequent period of immune suppression.

Assessing MV immunity

Measles infection or vaccination induces both humoral and cellular immunity, and high vaccination coverage in two-dose regimens has successfully interrupted endemic MV transmission in many geographic regions. MV-specific VN antibodies have been identified as a correlate of protection from disease. However, several studies have suggested that cellular immune responses may also confer protection from measles in the absence of VN antibodies. VN antibody levels above 120–200 mIU / ml have been identified as a correlate of protection from measles in two independent studies [155,432].

Indeed, passive immunization with antibody preparations results in protection against measles, and maternal antibodies protect infants during the first months of life. In this respect, it is important to discriminate between protection from and clearance of MV: it is generally accepted that for the latter, cytotoxic T-cell responses are of crucial importance [314,344,364], as also illustrated by the fact that subjects with cellular immunodeficiency usually develop severe and often fatal disease after MV infection [433].

It has been demonstrated that some MV-vaccinated subjects with low VN antibody titers have detectable MV-specific T lymphocytes in their peripheral blood [434,435]. In addition, it was shown that MV-vaccinated subjects with undetectable MV-specific VN antibodies are still significantly protected from measles as compared with non-vaccinated subjects [432]. The incubation time of measles is relatively long, allowing the immune system to develop a secondary immune response. This may limit MV replication and restrict or completely prevent subsequent clinical disease [155,436,437].

Recent studies have indicated a lack of correlation between MV-specific antibody levels and T-cell responses detected in the peripheral blood of vaccinated subjects [438]. The large number of subjects included in the study, the statistical evaluation based on median rather than mean responses and the fact that the subjects resided in an area where virtually no measles cases were observed during the study period strongly suggest that their conclusions are justified. Therefore, the authors of this paper concluded that in future measles vaccination studies both humoral and cellular immune responses should be measured to demonstrate non-inferiority of candidate new vaccines or vaccination routes in comparison with the existing measles vaccines and vaccinations.

Although seemingly justified, some problems are associated with this statement. As described above, VN antibodies have clearly been identified as a correlate of protection against measles. Moreover, it is thought that VN assays measure the actual biological function of MV-specific antibodies: in subjects who carry protective levels of VN antibodies the virus is neutralized *in vivo* in a similar way as measured in the VN assay *in vitro*. Although it is generally accepted that cellular immunity indeed contributes to protection from measles [439], two crucial problems need to be solved: can biological function of MV-specific memory T-lymphocytes be measured and Is it possible to use PBMC for this purpose? One fundamental problem is that it is becoming increasingly clear that virus-specific memory lymphocytes do not circulate but rather reside in mucosal or peripheral tissues [440]. If these are the cells that confer protection in subjects vaccinated against measles with non-detectable VN antibody levels, it may be hard to design functional assays using human or animal MV-specific memory lymphocytes as correlates of protection.

Measles eradication

In April 2012 the WHO published the 'Global Measles and Rubella Strategic Plan 2012-2020' (http://www.who.int/immunization/documents/control/ISBN_978_92_4_150339_6/en/index.html), prepared with the CDC, American Red Cross, UN Foundation and UNICEF in the framework of the Measles and Rubella Initiative (www.measlesrubellainitiative.org). The objective of this strategic plan is to describe how countries may achieve a world without measles, rubella and congenital rubella syndrome. One of the milestones is to establish a target date for the global eradication of measles.

Although measles eradication would save many lives, it will likely result in reduced compliance to MV vaccination. As a result, children may grow up without MV-specific immunity. Morbillivirus infections induce (partial) cross-protection from other morbilliviruses [11,413,414], illustrated by the use of live-attenuated measles vaccine to protect dogs from CDV. Thus, cessation of MV vaccination may facilitate cross-species infection and subsequent adaptation of animal morbilliviruses to humans. Indeed, CDV infection of humans has been described [415,427], and some humans have CDV-specific virus neutralizing antibodies [420]. Whether these are high titer MV-specific antibodies cross-reactive with CDV, or whether these individuals have actually experienced CDV infection is unknown.

Crossing the species barrier
Although it has been claimed this risk is low [199], adaptation of CDV to cause disease in humans could have disastrous consequences after immunity against MV wanes. When comparing CDV with MV of humans, it appears that the case-fatality rate of CDV in its natural host species may be higher than that of measles in humans. The main factor determining severe and fatal measles is the virus-induced immune suppression that results in increased susceptibility to opportunistic infections. Indeed, the direct cause of death is more often a severe complication such as bacterial pneumonia or gastroenteritis than direct virus-induced lesions [16,318,357]. However, whereas MV rarely infects the CNS, this is much more common for animal morbilliviruses, and often results in fatalities [373]. Thus, an animal morbillivirus adapted to humans could potentially cause more serious disease than the disease caused by MV.

CDV in macaques
The experiments described in chapter 7 were designed to determine whether prototypic CDV strains are capable of infecting macaques, and whether measles vaccination cross-protects from CDV challenge. The results show that macaques are susceptible to primary CDV infection, and that the virus causes fever and lymphopenia. Furthermore, CDV predominantly replicated in $CD150^{+}$ macaque lymphocytes and DC. In the second part of the experiment, it was shown that MV-vaccinated macaques were partially protected from CDV challenge, with cross-specific cellular immune responses as the most likely correlate of protection.

Interestingly, CDV followed a different disease course in macaques when compared to its natural hosts. For example, *in vivo* spread of CDV infection into either macaque epithelial cells or the CNS was not detected, even though large numbers of $rCDV^{SH}$EGFP-infected cells were present within the respiratory epithelium and submucosa. Corroborating this result, *in vitro* infection studies in primary well-differentiated normal macaque bronchial epithelial cells (NMBE) showed that none of the CDV strains could spread in NMBE, even when the monolayer was scratched to expose the basolaterally-expressed receptor PVRL4. However, an *in vitro* human PVRL4 adapted strain of CDV, could easily infect and spread in NMBE. Together, these experiments indicate that initially prototypic CDV is able to directly use macaque CD150 and infect lymphocytes and DC, however the infection of

epithelial and neuronal cells is not yet possible. Surprisingly, the description of CDV outbreaks in captive macaque colonies included observations of skin rash and CNS signs [200,411], suggesting that adaptations to infect these cell types had already occurred *in vivo*. The viruses causing these outbreaks must have taken the initial steps to becoming fully 'primate-adapted'.

Continuing measles vaccination

The experiments described in chapter 7 have shown that CDV is able to cause infections in non-human primates, but also that measles immunity offers partial protection from CDV challenge. Thus, morbillivirus cross-specific immunity of the human population restricts the possibilities of CDV to replicate in and adapt to humans. However, if the envisaged measles eradication would be followed by significant drops in MV vaccination coverage, such adaptation cannot be excluded. Although this should not be used to argue against measles eradication, sustained MV vaccination and serological and virological surveillance of morbillivirus infections should be enforced. The use of rMV strains as vectors for vaccination against heterologous pathogens could provide the necessary incentive to sustain compliance to MV vaccination.

Conclusions

In contrast to many respiratory viruses, MV infection of immunologically naive humans always results in systemic disease. Whereas some respiratory viruses have developed strategies to enable repeated infections during the lifetime of an individual host, such as genetic drift or suppression of virus-specific immune responses, MV has specialized in targeting naive hosts, by virtue of evolving its high R_0 of 12 – 18 [16]. Since MV infection induces lifelong immunity, the virus can only establish endemic circulation if the population is of sufficient size, usually estimated at 250,000 – 500,000 [16]. The experiments described in this thesis have resulted in a better understanding of measles pathogenesis, the methods of viral transmission and the underlying causes of immune suppression, which may in turn contribute to the development of novel intervention strategies.

NEDERLANDSE SAMENVATTING

Ondanks de beschikbaarheid van een veilig en werkzaam mazelenvaccin, veroorzaakt mazelen virus (MV) nog steeds ruim honderdduizend sterfgevallen per jaar. De ziekte mazelen wordt gekenmerkt door hoge koorts en een rode huiduitslag. Mazelen is zeer besmettelijk en wordt overgedragen door aanhoesten van kleine vochtdruppels, ook wel bekend als aerosolen. Al vroeg in de 20e eeuw is aangetoond dat mazelen veroorzaakt wordt door een virus. Echter, het is nog steeds onduidelijk welke cellen het eerst worden geïnfecteerd, hoe het virus daarna wordt verspreid in het lichaam en hoe het van mens op mens wordt overgedragen.

Meerdere kleine proefdiermodellen zijn beschreven voor mazelenonderzoek [94–96], maar in geen van deze modellen wordt de ziekte mazelen echt gereproduceerd. De experimenten beschreven in dit proefschrift zijn grotendeels uitgevoerd met makaken, een diermodel dat is beschreven als het optimale model voor onderzoek aan mazelen. Daarin worden de symptomen en pathologie die in mensen gezien worden grotendeels gereproduceerd [54,100–102]. In dit proefschrift worden experimenten in dit diermodel gecombineerd met het gebruik van recombinante virussen die fluorescerende eiwitten tot expressie brengen. Wanneer deze virussen cellen infecteren worden de cellen fluorescerend en kunnen daarmee *in vitro*, *ex vivo* en *in vivo* gevoelig worden gedetecteerd.

In proefdierstudies met makaken worden de dieren vaak geïnfecteerd door middel van intratracheale inoculatie (IT). Aangezien deze toedieningsroute ver van de natuurlijke infectieroute van MV af staat, is in hoofdstuk 4 van dit proefschrift een nieuwe toedieningswijze beschreven. De gestandaardiseerde IT toediening is hiertoe vergeleken met een aerosol toediening, waarbij makaken gedurende een korte periode aerosolen met MV inademen. De twee toedieningsmethoden resulteerden in vergelijkbare resultaten: het virus vermenigvuldigde zich in dezelfde tijdsduur en dezelfde mate, en dezelfde celtypes bleken geïnfecteerd op de piek van infectie. Dit maakte vervolgonderzoek mogelijk naar de route die het MV volgt na binnenkomst in het lichaam.

Aangezien MV wordt verspreid door de lucht is het waarschijnlijk dat de infectie begint in de luchtwegen. Daarom werd lange tijd gedacht dat epitheelcellen van de luchtwegen de eerste doelwitcellen voor MV waren [16]. Echter de receptor voor MV, CD150, is niet aanwezig op het oppervlak van deze epitheelcellen. Met de resultaten van de studies in hoofdstuk 2 en 3 zijn er twee hypotheses geformuleerd voor binnenkomst van MV (Figuur 2A en B van “summarizing discussion”). Toen makaken korte tijd na infectie met MV werden geëuthanaseerd, werden geïnfecteerde cellen met de morfologie van dendritische cellen (DC) en alveolaire macrofagen (AM) gevonden in de alveoli (Figuur 3A van “summarizing discussion”). Dit geeft aan dat MV na inademing tot diep in de longen is doorgedrongen, waar het virus $CD150^+$ cellen infecteert.

De tweede hypothese voor binnenkomst van MV in de gastheer lijkt meer op de wijze waarop HIV het lichaam binnenkomt. In hoofdstuk 2 wordt beschreven dat DC en Langerhans’ cellen (LC) receptoren op hun oppervlak hebben die MV kunnen

binden. Dit zijn DC-SIGN op DC en Langerin op LC. Met name de DC-SIGN$^+$ DC zijn overvloedig aanwezig in de luchtwegen, en deze DC hebben lange uitlopers die kunnen doordringen tot het lumen van de luchtwegen (Figuur 2B van "summarizing discussion"). In dit proefschrift wordt aangetoond dat DC het MV kunnen binden en gemakkelijk geïnfecteerd kunnen worden en dat DC MV over kunnen dragen aan de T-lymfocyten. In deze tweede strategie voor binnenkomst in het lichaam wordt MV dan ook weggevangen uit de luchtwegen door DC-SIGN$^+$ en CD150$^+$ DC (Figuur 3B van "summarizing discussion"). Echter, in de proefdierstudies in dit proefschrift hebben we voor deze route geen onweerlegbaar bewijs kunnen vinden.

Na elk van deze twee gepostuleerde strategieën van binnenkomst verloopt de verdere verspreiding van infectie het zelfde. De geïnfecteerde DC of AM migreren na infectie naar de luchtweg-geassocieerde lymfoïde organen, waar het virus zich lokaal kan vermenigvuldigen in T- en B-lymfocyten. Deze geïnfecteerde cellen worden vervolgens via het bloed verspreid naar alle andere lymfoïde organen (Figuur 4 van "summarizing discussion"), maar ook naar de submucosa van de luchtwegen en de huid. Tenslotte infecteert MV ook CD150$^-$ epitheelcellen via de receptor PVRL4 [130,131].

In tegenstelling tot echte luchtweginfecties leidt infectie met MV altijd tot een systemische infectie. Waar sommige virussen een strategie hebben ontwikkeld om een gastheer meerdere malen te infecteren, heeft MV zich 'gespecialiseerd' in het infecteren van volledig onbeschermde gastheren. Om deze reden is het virus zo infectieus, met een zeer hoge "reproductive rate" (R_0) van 12 – 18 [16]. Omdat mazelen leidt tot een levenslange immuniteit kan het virus alleen endemisch worden als er een populatie vatbare individuen is van minimaal 250,000 – 500,000 personen [16]. De experimenten beschreven in dit proefschrift hebben geleid tot een beter begrip van de mazelen-pathogenese, de methode van mazelen-transmissie en de onderliggende oorzaak van mazelen-geassocieerde immuunsuppressie.

Zoals gesteld wordt MV zeer waarschijnlijk vooral van mens op mens overgedragen via aerosolen. Of deze transmissie via losse viruspartikels in druppeltjes of via afbraakprodukten van MV-geïnfecteerde cellen gaat is onbekend. Echter, de literatuur beschrijft dat infectie van epitheelcellen, gevolgd door het produceren van viruspartikels in het lumen van de luchtwegen, noodzakelijk is voor de transmissie van mens op mens [158]. In hoofdstuk 5 wordt gespeculeerd over een methode van transmissie die onafhankelijk zou zijn van geïnfecteerde epitheelcelcellen, maar afhankelijk is van resten van beschadigde epitheelcellen. In deze studie is een uitgebreide analyse van weefsels in de luchtwegen en lymfoïde organen van makaken tijdens de latere stadia van MV infectie uitgevoerd. Met name in de keel- en neusamandelen werd grote epitheelschade gezien en werd een grote hoeveelheid MV-geïnfecteerde cellen en afval van geïnfecteerde cellen gevonden. De conclusie van deze studie was dat dit waarschijnlijk een belangrijke bijdrage aan de transmissie van MV levert. Tevens leidt deze schade een hoestprikkel, waardoor efficiënt aerosolen geproduceerd worden.

Mazelen resulteert met name in een hoge sterfte doordat het virus het afweersysteem verzwakt. Hierdoor kunnen mazelenpatiënten gemakkelijk longontsteking of ernstige diarree oplopen [64–66]. Het wekt dan ook verwondering dat, ondanks deze immuunsuppressie, MV infectie leidt tot een sterke virus-specifieke immuunrespons en levenslange bescherming. Deze tegenstelling wordt vaak aangeduid als de “mazelen paradox”. De studies in hoofdstuk 6 van dit proefschrift beschrijven een model voor de onderliggende oorzaken van mazelen geassocieerde immuunsuppressie die deze paradox kunnen verklaren. Het ontwikkelde model is gebaseerd op de studies aan weefsels van een groot aantal makaken op verschillende tijdspunten na MV infectie. Zoals beschreven in hoofdstuk 6 kan mazelen geassocieerde immuunsuppressie voor een groot deel verklaard worden door de massale infectie en depletie van $CD150^+$ geheugen T- en B-lymfocyten. Het nieuwe inzicht dat dit model verschaft is dat deze depletie met name het gevolg is van de eigen mazelen-specifieke immuunrespons, met MV-specifieke $CD8^+$ T-lymfocyten als belangrijke effectorcellen. De depletie wordt gemaskeerd doordat op hetzelfde moment de MV-specifieke lymfocyten massaal prolifereren, waardoor het totaal aantal lymfocyten binnen enkele dagen weer op peil is. Echter, de immunologische geheugencellen die voorafgaand aan MV infectie aanwezig waren zijn grotendeels verdwenen, waardoor het immunologisch geheugen is ‘gewist’. Dit leidt tot een verhoogde vatbaarheid voor opportunistische infecties met ziekteverwekkers die mogelijk al in het lichaam aanwezig waren, maar voorheen onder controle werden gehouden.

Omdat mazelen niet alleen een belangrijke kinderziekte in ontwikkelingslanden is, maar ook weer bezig is aan een opmars in Europa, wordt er overwogen om de ziekte wereldwijd uit te roeien door middel van massale vaccinatiecampagnes. Hiermee zouden veel ziekte- en sterfgevallen voorkomen kunnen worden. Echter, het zal het moeilijk zijn om na deze campagnes de vaccinatiegraad tegen mazelen op peil te houden. Op het eerste gezicht lijkt dit misschien onbelangrijk, maar de mazelenvaccinatie beschermt ons ook tegen infectie met dierlijke morbillivirussen. Wanneer een grote groep mensen geen afweer heeft tegen MV, bestaat het risico dat deze nauw verwante virussen zich kunnen aanpassen aan de mens en ‘het gat gaan opvullen’. Het zou hierbij bijvoorbeeld om morbillivirussen van honden, fretten, zeezoogdieren, geiten en schapen kunnen gaan. Het morbillivirus dat hondenziekte veroorzaakt, canine distemper virus (CDV), lijkt veel op mazelen van de mens maar veroorzaakt doorgaans een veel hogere mortaliteit. Dit komt met name door de frequente infectie van het centrale zenuwstelsel, iets dat veel minder voorkomt bij MV infecties van mensen.

De studies in hoofdstuk 7 van dit proefschrift beschrijven de infectie van makaken met CDV. De belangrijkste doelstelling van deze studie was om te onderzoeken of mazelenvaccinatie primaten daadwerkelijk beschermt tegen CDV-infectie. De studie toont aan dat makaken vatbaar zijn voor infectie met CDV en dat de infectie hoge koorts en daling van de hoeveelheid witte bloedcellen veroorzaakt. Daarnaast werden, vergelijkbaar met MV, met name $CD150^+$ T- en B-lymfocyten en DC geïnfecteerd. Mazelenvaccinatie leidde inderdaad tot een gedeeltelijke bescherming tegen CDV infectie, gemedieerd door kruis-reagerende T-cel responsen. Er waren

echter ook belangrijke verschillen tussen MV en CDV infectie van makaken. Het belangrijkste verschil was dat waar MV zich op late tijdspunten naar het epitheel verspreidt, dit niet werd gezien met CDV. Ook de ongevaccineerde apen herstelden daarom snel van de CDV infectie. Onlangs is in de literatuur een grote uitbraak van CDV in een kolonie makaken in China beschreven [200]. Interessant genoeg werd in deze apen wel infectie van epitheelcellen en van het centraal zenuwstelsel gezien, hetgeen aangeeft dat adaptatie van CDV in makaken mogelijk is en in dit geval reeds heeft plaatsgevonden. Om deze reden is beschreven in hoofdstuk 7 en de “summarizing discussion” van dit proefschrift dat het noodzakelijk is om door te gaan met mazelenvaccinatie, ook als MV zou zijn uitgeroeid, met name om mensen te beschermen tegen geadapteerde dierlijke morbillivirussen.

Het gebruik van proefdieren voor wetenschappelijk onderzoek staat maatschappelijk veelvuldig ter discussie, zeker wanneer de experimenten worden uitgevoerd met apen. In dit proefschrift zijn experimentele infecties met MV in apen uitgevoerd, met als doel om ons begrip van de manier waarop MV ziekte veroorzaakt beter te begrijpen. Alle studies voldeden aan de Nederlandse wet op de dierproeven, die voorschrijft dat protocollen voorafgaand door een dier-ethische commissie beoordeeld moeten worden om vast te stellen of de doelstelling van het experiment het gebruik van proefdieren rechtvaardigt. Ik vind het belangrijk om hier ook zelf dit belang te rechtvaardigen.

De ziekte mazelen kent in mensen een lange incubatietijd (ongeveer twee weken), waardoor het moeilijk is om de pathogenese van deze ziekte in mensen te bestuderen. Het is in dit stadium vrijwel onmogelijk om een MV-geïnfecteerd persoon te herkennen. Het is dan ook begrijpelijk dat meer dan honderd jaar na de ontdekking van MV ons begrip van deze ziekte nog steeds zo beperkt is. In ons laboratorium was de kennis van en ervaring met het werken met apen als proefdiermodel voor mazelen reeds aanwezig, maar mede door de samenwerking met de onderzoeksgroepen van Theo Geijtenbeek in Amsterdam en Paul Duprex in Belfast (later Boston), en het beschikbaar komen van stabiele recombinant MV stammen die fluorescente eiwitten tot expressie brengen, ontstond een unieke gelegenheid om het volledige verloop van een infectie met MV te bestuderen. Hiervoor is in een periode van enkele jaren een aanzienlijk aantal apen opgeofferd, maar dit aantal staat in schril contrast met de meer dan 300 kinderen die wereldwijd nog steeds iedere dag overlijden als gevolg van mazelen. De in dit proefschrift beschreven studies dragen er hopelijk toe bij dat meer mensen begrijpen dat mazelen geen ‘onschuldige kinderziekte’ is, maar een gevaarlijke infectieziekte die niet onderschat mag worden. Daarnaast zijn de studies naar de pathogenese van mazelen zoals beschreven in dit proefschrift een opstapje voor vervolgstudies, waarin er veel aandacht wordt besteed aan de ontwikkeling van nieuwe en meer efficiënte methodes van toediening van mazelen vaccin.

Reference list

1. Lamb RA, Parks GD (2007) Paramyxoviridae: the viruses and their replication. In: Knipe DM, Howley PM, editors. Fields Virology. Philadelphia: Lippincott Williams & Wilkins. pp. 1449-1496.
2. Choppin PW, Compans RW (1975) Reproduction of paramyxoviruses. In: Fraenkel-Conrat H, Wagner RR, editors. Comprehensive virology: reproduction, large RNA viruses. New York: Plenum Press. pp. 95-178.
3. Briand FX, Henry A, Massin P, Jestin V (2012) Complete genome sequence of a novel avian paramyxovirus. J Virol 86: 7710.
4. Drexler JF, Corman VM, Muller MA, Maganga GD, Vallo P, Binger T, Gloza-Rausch F, Rasche A, Yordanov S, Seebens A, Oppong S, Sarkodie YA, Pongombo C, Lukashev AN, Schmidt-Chanasit J, Stocker A, Carneiro AJ, Erbar S, Maisner A, Fronhoffs F, Buettner R, Kalko EK, Kruppa T, Franke CR, Kallies R, Yandoko ER, Herrler G, Reusken C, Hassanin A, Kruger DH, Matthee S, Ulrich RG, Leroy EM, Drosten C (2012) Bats host major mammalian paramyxoviruses. Nat Commun 3: 796.
5. Hyndman TH, Marschang RE, Wellehan JF, Jr., Nicholls PK (2012) Isolation and molecular identification of Sunshine virus, a novel paramyxovirus found in Australian snakes. Infect Genet Evol 12: 1436-1446.
6. Kurth A, Kohl C, Brinkmann A, Ebinger A, Harper JA, Wang LF, Muhldorfer K, Wibbelt G (2012) Novel paramyxoviruses in free-ranging European bats. PLoS One 7: e38688.
7. Marsh GA, de JC, Barr JA, Tachedjian M, Smith C, Middleton D, Yu M, Todd S, Foord AJ, Haring V, Payne J, Robinson R, Broz I, Crameri G, Field HE, Wang LF (2012) Cedar virus: a novel henipavirus isolated from Australian bats. PLoS Pathog 8: e1002836.
8. Woo PC, Lau SK, Wong BH, Fan RY, Wong AY, Zhang AJ, Wu Y, Choi GK, Li KS, Hui J, Wang M, Zheng BJ, Chan KH, Yuen KY (2012) Feline morbillivirus, a previously undescribed paramyxovirus associated with tubulointerstitial nephritis in domestic cats. Proc Natl Acad Sci USA 109: 5435-5440.
9. van den Hoogen BG, de Jong JC, Groen J, Kuiken T, de Groot R, Fouchier RAM, Osterhaus ADME (2001) A newly discovered human pneumovirus isolated from young children with respiratory tract disease. Nat Med 7: 719-724.
10. Collins PL, Crowe Jr. JE (2007) Respiratory syncytial virus and metapneumovirus. In: Knipe DM, Howley PM, editors. Fields Virology. Philadelphia: Lippincott Williams & Wilkins. pp. 1601-1646.
11. Barrett T (1999) Morbillivirus infections, with special emphasis on morbilliviruses of carnivores. Vet Microbiol 69: 3-13.
12. Normile D (2008) Rinderpest. Driven to extinction. Science 319: 1606-1609.
13. Roeder PL (2011) Rinderpest: the end of cattle plague. Prev Vet Med 102: 98-106.
14. Morens DM, Holmes EC, Davis AS, Taubenberger JK (2011) Global rinderpest eradication: lessons learned and why humans should celebrate too. J Infect Dis 204: 502-505.
15. Visser IKG, Van Bressem MF, Barrett T, Osterhaus ADME (1993) Morbillivirus infections in aquatic mammals. Vet Res 24: 169-178.
16. Griffin DE (2007) Measles virus. In: Knipe DM, Howley PM, editors. Fields Virology. Philadelphia: Lippincott Williams & Wilkins. pp. 1551-1585.
17. Rima BK, Duprex WP (2011) New concepts in measles virus replication: Getting in and out in vivo and modulating the host cell environment. Virus Res 162: 47-62.
18. Rima BK, Duprex WP (2009) The measles virus replication cycle. Curr Top Microbiol Immunol 329: 77-102.
19. Sidhu MS, Chan J, Kaelin K, Spielhofer P, Radecke F, Schneider H, Masurekar M, Dowling PC, Billeter MA, Udem SA (1995) Rescue of synthetic measles virus minireplicons: measles genomic termini direct efficient expression and propagation of a reporter gene. Virology 208: 800-807.
20. Hamaguchi M, Yoshida T, Nishikawa K, Naruse H, Nagai Y (1983) Transcriptive complex of Newcastle disease virus. I. Both L and P proteins are required to constitute an active complex. Virology 128: 105-117.
21. Bellini WJ, Englund G, Rozenblatt S, Arnheiter H, Richardson CD (1985) Measles virus P gene codes for two proteins. J Virol 53: 908-919.
22. Curran J, Kolakofsky D (1988) Ribosomal initiation from an ACG codon in the Sendai virus P/C mRNA. EMBO J 7: 245-251.
23. Palosaari H, Parisien JP, Rodriguez JJ, Ulane CM, Horvath CM (2003) STAT protein interference and suppression of cytokine signal transduction by measles virus V protein. J Virol 77: 7635-7644.
24. Rothlisberger A, Wiener D, Schweizer M, Peterhans E, Zurbriggen A, Plattet P (2010) Two domains of the V protein of virulent canine distemper virus selectively inhibit STAT1 and STAT2 nuclear import. J Virol 84: 6328-6343.
25. Li T, Chen X, Garbutt KC, Zhou P, Zheng N (2006) Structure of DDB1 in complex with a paramyxovirus V protein: viral hijack of a propeller cluster in ubiquitin ligase. Cell 124: 105-117.
26. Andrejeva J, Young DF, Goodbourn S, Randall RE (2002) Degradation of STAT1 and STAT2 by the V proteins of simian virus 5 and human parainfluenza virus type 2, respectively: consequences for virus replication in the presence of alpha/beta and gamma interferons. J Virol 76: 2159-2167.
27. Lin GY, Paterson RG, Richardson CD, Lamb RA (1998) The V protein of the paramyxovirus SV5 interacts with damage-specific DNA binding protein. Virology 249: 189-200.
28. Ohno S, Ono N, Takeda M, Takeuchi K, Yanagi Y (2004) Dissection of measles virus V protein in relation to its ability to block alpha/beta interferon signal transduction. J Gen Virol 85: 2991-2999.
29. Devaux P, Hudacek AW, Hodge G, Reyes del Valle J, McChesney MB, Cattaneo R (2011) A recombinant measles virus unable to antagonize STAT1 function cannot control inflammation and is attenuated in rhesus monkeys. J Virol 85: 348-356.
30. Bankamp B, Wilson J, Bellini WJ, Rota PA (2005) Identification of naturally occurring amino acid variations that affect the ability of the measles virus C protein to regulate genome replication and transcription. Virology 336: 120-129.
31. Escoffier C, Manie S, Vincent S, Muller CP, Billeter M, Gerlier D (1999) Nonstructural C protein is required for efficient measles virus replication in human peripheral blood cells. J Virol 73: 1695-1698.
32. Patterson JB, Thomas D, Lewicki H, Billeter MA, Oldstone MBA (2000) V and C proteins of measles virus function as virulence factors in vivo. Virology 267: 80-89.
33. Bellini WJ, Englund G, Richardson CD, Rozenblatt S, Lazzarini RA (1986) Matrix genes of measles virus and canine distemper virus: cloning, nucleotide sequences, and deduced amino acid sequences. J Virol 58: 408-416.
34. Hirano A, Wang AH, Gombart AF, Wong TC (1992) The matrix proteins of neurovirulent subacute sclerosing panencephalitis virus and its acute measles virus progenitor are functionally different. Proc Natl Acad Sci U S A 89: 8745-8749.
35. Liljeroos L, Huiskonen JT, Ora A, Susi P, Butcher SJ (2011) Electron cryotomography of measles virus reveals how matrix protein coats the ribonucleocapsid within intact virions. Proc Natl Acad Sci U S A 108: 18085-18090.
36. Cathomen T, Mrkic B, Spehner D, Drillien R, Naef R, Pavlovic J, Aguzzi A, Billeter M, Cattaneo R (1998) A matrix-less measles virus

is infectious and elicits extensive cell fusion: consequences for propagation. EMBO J 17: 3899-3908.
37. Stricker R, Mottet G, Roux L (1994) The Sendai virus matrix protein appears to be recruited in the cytoplasm by the viral nucleocapsid to function in viral assembly and budding. J Gen Virol 75: 1031-1042.
38. Tahara M, Takeda M, Yanagi Y (2007) Altered interaction of the matrix protein with the cytoplasmic tail of hemagglutinin modulates measles virus growth by affecting virus assembly and cell-cell fusion. J Virol 81: 6827-6836.
39. Sanderson CM, McQueen NL, Nayak DP (1993) Sendai virus assembly: M protein binds to viral glycoproteins in transit through the secretory pathway. J Virol 67: 651-663.
40. Apte-Sengupta S, Negi S, Leonard VHJ, Oezguen N, Navaratnarajah CK, Braun W, Cattaneo R (2012) Base of the measles virus fusion trimer head receives the signal that triggers membrane fusion. J Biol Chem .
41. Zhang P, Li L, Hu C, Xu Q, Liu X, Qi Y (2005) Interactions among measles virus hemagglutinin, fusion protein and cell receptor signaling lymphocyte activation molecule (SLAM) indicating a new fusion-trimer model. J Biochem Mol Biol 38: 373-380.
42. Plemper RK, Brindley MA, Iorio RM (2011) Structural and mechanistic studies of measles virus illuminate paramyxovirus entry. PLoS Pathog 7: e1002058.
43. Portner A, Murti KG, Morgan EM, Kingsbury DW (1988) Antibodies against Sendai virus L protein: distribution of the protein in nucleocapsids revealed by immunoelectron microscopy. Virology 163: 236-239.
44. Horikami SM, Curran J, Kolakofsky D, Moyer SA (1992) Complexes of Sendai virus NP-P and P-L proteins are required for defective interfering particle genome replication in vitro. J Virol 66: 4901-4908.
45. Gupta AK, Shaji D, Banerjee AK (2003) Identification of a novel tripartite complex involved in replication of vesicular stomatitis virus genome RNA. J Virol 77: 732-738.
46. Schneider-Schaulies S, Duprex WP (2011) Measles virus. In: Samal SK, editors. The biology of paramyxoviruses. Norfolk, UK: Caister Academic Press. pp. 245-274.
47. Rota PA, Featherstone DF, Bellini WJ (2009) Molecular epidemiology of measles virus. Curr Top Microbiol Immunol 330: 129-150.
48. El Mubarak HS, Van de Bildt MWG, Mustafa OA, Vos HW, Mukhtar MM, Ibrahim SA, Andeweg AC, El Hassan AM, Osterhaus ADME, De Swart RL (2002) Genetic characterisation of wild type measles viruses circulating in suburban Khartoum, 1997-2000. J Gen Virol 83: 1437-1443.
49. Rima BK, Earle JAP, Baczko K, Ter Meulen V, Liebert UG, Carstens C, Carabana J, Caballero M, Celma ML, Fernandez-Munoz R (1997) Sequence divergence of measles virus haemagglutinin during natural evolution and adaptation to cell culture. J Gen Virol 78: 97-106.
50. Rota PA, Rota JS, Bellini WJ (1995) Molecular epidemiology of measles virus. Semin Virol 6: 379-386.
51. Radecke F, Spielhofer P, Schneider H, Kaelin K, Huber M, Dotsch C, Christiansen G, Billeter MA (1995) Rescue of measles viruses from cloned DNA. EMBO J 14: 5773-5784.
52. Takeda M, Takeuchi K, Miyajima N, Kobune F, Ami Y, Nagata N, Suzaki Y, Nagai Y, Tashiro M (2000) Recovery of pathogenic measles virus from cloned cDNA. J Virol 74: 6643-6647.
53. Hashimoto K, Ono N, Tatsuo H, Minagawa H, Takeda M, Takeuchi K, Yanagi Y (2002) SLAM (CD150)-independent measles virus entry as revealed by recombinant virus expressing green fluorescent protein. J Virol 76: 6743-6749.
54. De Swart RL, Ludlow M, De Witte L, Yanagi Y, Van Amerongen G, McQuaid S, Yüksel S, Geijtenbeek TBH, Duprex WP, Osterhaus ADME (2007) Predominant infection of CD150+ lymphocytes and dendritic cells during measles virus infection of macaques. PLoS Pathog 3: e178.
55. Duprex WP, Duffy I, McQuaid S, Hamill L, Cosby SL, Billeter MA, Schneider-Schaulies J, Ter Meulen V, Rima BK (1999) The H gene of rodent brain-adapted measles virus confers neurovirulence to the Edmonston vaccine strain. J Virol 73: 6916-6922.
56. Vongpunsawad S, Oezgun N, Braun W, Cattaneo R (2004) Selectively receptor-blind measles viruses: Identification of residues necessary for SLAM- or CD46-induced fusion and their localization on a new hemagglutinin structural model. J Virol 78: 302-313.
57. Takeda M, Nakatsu Y, Ohno S, Seki F, Tahara M, Hashiguchi T, Yanagi Y (2006) Generation of measles virus with a segmented RNA genome. J Virol 80: 4242-4248.
58. Billeter MA, Naim HY, Udem SA (2009) Reverse genetics of measles virus and resulting multivalent recombinant vaccines: applications of recombinant measles viruses. Curr Top Microbiol Immunol 329: 129-162.
59. Yaiw KC, Miest TS, Frenzke M, Timm M, Johnston PB, Cattaneo R (2010) CD20-targeted measles virus shows high oncolytic specificity in clinical samples from lymphoma patients independent of prior rituximab therapy. Gene Ther 18: 313-317.
60. Furuse Y, Suzuki A, Oshitani H (2010) Origin of measles virus: divergence from rinderpest virus between the 11th and 12th centuries. Virol J 7: 52.
61. McNeill WH (1976) Plagues and Peoples. Garden City, NY: Anchor Books. 340 p.
62. Simons E, Ferrari M, Fricks J, Wannemuehler K, Anand A, Burton A, Strebel P (2012) Assessment of the 2010 global measles mortality reduction goal: results from a model of surveillance data. Lancet 379: 2173-2178.
63. Moss WJ, Griffin DE (2012) Measles. Lancet 379: 153-164.
64. Akramuzzaman SM, Cutts FT, Wheeler JG, Hossain MJ (2000) Increased childhood morbidity after measles is short-term in urban Bangladesh. Am J Epidemiol 151: 723-735.
65. Beckford AP, Kaschula RO, Stephen C (1985) Factors associated with fatal cases of measles. A retrospective autopsy study. S Afr Med J 68: 858-863.
66. Shanks GD, Lee SE, Howard A, Brundage JF (2011) Extreme mortality after first introduction of measles virus to the polynesian island of Rotuma, 1911. Am J Epidemiol 173: 1211-1222.
67. Van den Hof S, Conyn-van Spaendonck MAE, van Steenbergen JE (2002) Measles epidemic in the Netherlands, 1999-2000. J Infect Dis 186: 1483-1486.
68. Duke T, Mgone CS (2003) Measles: not just another viral exanthem. Lancet 361: 763-773.
69. Gutierrez J, Issacson RS, Koppel BS (2010) Subacute sclerosing panencephalitis: an update. Dev Med Child Neurol 52: 901-907.
70. Liebert UG (1997) Measles virus infections of the central nervous system. Intervirology 40: 176-184.
71. Kipps A, Dick G, Moodie JW (1983) Measles and the central nervous system. Lancet 2: 1406-1410.
72. Buchanan R, Bonthius DJ (2012) Measles virus and associated central nervous system sequelae. Semin Pediatr Neurol 19: 107-114.
73. Moss WJ, Griffin DE (2006) Global measles elimination. Nat Rev Microbiol 4: 900-908.

74. Moss WJ (2007) Measles still has a devastating impact in unvaccinated populations. PLoS Med 4: e24.
75. Panum PL (1939) Observations made during the epidempic of measles on the Faroe Islands in the year 1846. Med Classics 3: 839-886.
76. Black FL (1975) Infectious diseases in primitive societies. Science 187: 515-518.
77. Keeling MJ, Grenfell BT (1997) Disease extinction and community size: modeling the persistence of measles. Science 275: 65-67.
78. Leuridan E, Hens N, Hutse V, Ieven M, Aerts M, Van DP (2010) Early waning of maternal measles antibodies in era of measles elimination: longitudinal study. BMJ 340: c1626.
79. Anderson RM, May RM (1982) Directly transmitted infections diseases: control by vaccination. Science 215: 1053-1060.
80. Gay NJ (2004) The theory of measles elimination: implications for the design of elimination strategies. J Infect Dis 189: S27-S35.
81. Cutts FT, Markowitz LE (1994) Successes and failures in measles control. J Infect Dis 170 (Suppl. 1): S32-S41.
82. ECDC (2012) European Monthly Measles Monitoring (EMMO). EMMO 7: 1-9.
83. Rota PA, Brown K, Mankertz A, Santibanez S, Shulga S, Muller CP, Hubschen JM, Siqueira M, Beirnes J, Ahmed H, Triki H, Al-Busaidy S, Dosseh A, Byabamazima C, Smit S, koua-Koffi C, Bwogi J, Bukenya H, Wairagkar N, Ramamurty N, Incomserb P, Pattamadilok S, Jee Y, Lim W, Xu W, Komase K, Takeda M, Tran T, Castillo-Solorzano C, Chenoweth P, Brown D, Mulders MN, Bellini WJ, Featherstone D (2011) Global distribution of measles genotypes and measles molecular epidemiology. J Infect Dis 204 Suppl 1: S514-S523.
84. Rota JS, Wang Z-D, Rota PA, Bellini WJ (1994) Comparison of sequences of the H, F, and N coding genes of measles virus vaccine strains. Virus Res 31: 317-330.
85. WHO (2006) Global distribution of measles and rubella genotypes-update. Wkly Epidemiol Rec 81: 474-479.
86. Rota PA, Liffick SL, Rota JS, Katz RS, Redd S, Papania M, Bellini WJ (2002) Molecular epidemiology of measles viruses in the United States, 1997-2001. Emerg Infect Dis 8: 902-908.
87. El Mubarak HS, Van de Bildt MWG, Mustafa OA, Vos HW, Mukhtar MM, Groen J, El Hassan AM, Niesters HGM, Ibrahim SA, Zijlstra EE, Wild TF, Osterhaus ADME, De Swart RL (2000) Serological and virological characterization of clinically diagnosed cases of measles in suburban Khartoum. J Clin Microbiol 38: 987-991.
88. Ramsay M, Reacher M, O'Flynn C, Buttery R, Hadden F, Cohen B, Knowles W, Wreghitt T, Brown D (2002) Causes of morbilliform rash in a highly immunised English population. Arch Dis Child 87: 202-206.
89. De Swart RL, Wertheim-van Dillen PME, Van Binnendijk RS, Muller CP, Frenkel J, Osterhaus ADME (2000) Measles in a Dutch hospital introduced by an immunocompromised infant from Indonesia infected with a new genotype virus. Lancet 355: 201-202.
90. Featherstone D, Brown D, Sanders R (2003) Development of the Global Measles Laboratory Network. J Infect Dis 187(Suppl.1): S264-S269.
91. Bellini WJ, Helfand RF (2003) The challenges and strategies for laboratory diagnosis of measles in an international setting. J Infect Dis 187(Suppl.1): S283-S290.
92. Brown DW, Ramsay ME, Richards AF, Miller E (1994) Salivary diagnosis of measles: a study of notified cases in the United Kingdom, 1991-3. B M J 308: 1015-1017.
93. De Swart RL, Nur Y, Abdallah A, Kruining H, El Mubarak HS, Ibrahim SA, van den Hoogen BG, Groen J, Osterhaus ADME (2001) Combination of reverse transcriptase PCR analysis and immunoglobulin M detection on filter paper blood samples allows diagnostic and epidemiological studies of measles. J Clin Microbiol 39: 270-273.
94. Niewiesk S (2009) Current animal models: cotton rat animal model. Curr Top Microbiol Immunol 330: 89-110.
95. Pillet S, Svitek N, von Messling V (2009) Ferrets as a model for morbillivirus pathogenesis, complications, and vaccines. Curr Top Microbiol Immunol 330: 73-87.
96. Sellin CI, Horvat B (2009) Current animal models: transgenic animal models for the study of measles pathogenesis. Curr Top Microbiol Immunol 330: 111-127.
97. Anderson JF (1911) Experimental measles in the monkey: a preliminary note. Public Health Reports 26: 847-848.
98. Auwaerter PG, Rota PA, Elkins WR, Adams RJ, DeLozier T, Shi Y, Bellini WJ, Murphy BR, Griffin DE (1999) Measles virus infection in rhesus macaques: altered immune responses and comparison of the virulence of six different virus strains. J Infect Dis 180: 950-958.
99. De Swart RL (2009) Measles studies in the macaque model. Curr Top Microbiol Immunol 330: 55-72.
100. Kobune F, Takahashi H, Terao K, Ohkawa T, Ami Y, Suzaki Y, Nagata N, Sakata H, Yamanouchi K, Kai C (1996) Nonhuman primate models of measles. Lab Anim Sci 46: 315-320.
101. McChesney MB, Miller CJ, Rota PA, Zhu Y, Antipa L, Lerche NW, Ahmed R, Bellini WJ (1997) Experimental measles I. Pathogenesis in the normal and the immunized host. Virology 233: 74-84.
102. Van Binnendijk RS, van der Heijden RWJ, Van Amerongen G, UytdeHaag FGCM, Osterhaus ADME (1994) Viral replication and development of specific immunity in macaques after infection with different measles virus strains. J Infect Dis 170: 443-448.
103. Remfry J (1976) A measles epizootic with 5 deaths in newly-imported rhesus monkeys (Macaca Mulatta). Lab Anim 10: 49-57.
104. Ludlow M, Duprex WP, Cosby SL, Allen IV, McQuaid S (2008) Advantages of using recombinant measles viruses expressing a fluorescent reporter gene with vibratome slice technology in experimental measles neuropathogenesis. Neuropathol Appl Neurobiol 34: 424-434.
105. von Messling V, Milosevic D, Cattaneo R (2004) Tropism illuminated: lymphocyte-based pathways blazed by lethal morbillivirus through the host immune system. Proc Natl Acad Sci USA 101: 14216-14421.
106. von Messling V, Springfeld C, Devaux P, Cattaneo R (2003) A ferret model of canine distemper virus virulence and immunosuppression. J Virol 77: 12579-12591.
107. Rudd PA, Bastien-Hamel LE, von Messling V (2010) Acute canine distemper encephalitis is associated with rapid neuronal loss and local immune activation. J Gen Virol 91: 980-989.
108. Stephensen CB, Welter J, Thaker SR, Taylor J, Tartaglia J, Paoletti E (1997) Canine distemper virus infection of ferrets as a model for testing morbillivirus vaccine strategies: NYVAC-and ALVAC-based CDV recombinants protect against symptomatic infection. J Virol 71: 1506-1513.
109. Rima BK, Duprex WP (2006) Morbilliviruses and human disease. J Pathol 208: 199-214.
110. Dörig RE, Marcil A, Chopra A, Richardson CD (1993) The human CD46 molecule is a receptor for measles virus (Edmonston strain). Cell 75: 295-305.

111. Naniche D, Varior-Krishnan G, Cervoni F, Wild TF, Rossi B, Rabourdin-Combe C, Gerlier D (1993) Human membrane cofactor protein (CD46) acts as a cellular receptor for measles virus. J Virol 67: 6025-6032.
112. Buckland R, Wild TF (1997) Is CD46 the cellular receptor for measles virus? Virus Res 48: 1-9.
113. Tatsuo H, Ono N, Tanaka K, Yanagi Y (2000) SLAM (CDw150) is a cellular receptor for measles virus. Nature 406: 893-897.
114. Yanagi Y, Takeda M, Ohno S, Seki F (2006) Measles virus receptors and tropism. Jpn J Infect Dis 59: 1-5.
115. Tatsuo H, Ono N, Yanagi Y (2001) Morbilliviruses use signaling lymphocyte activation molecules (CD150) as cellular receptors. J Virol 75: 5842-5850.
116. Leonard VHJ, Hodge G, Reyes del Valle J, McChesney MB, Cattaneo R (2010) Measles virus selectively blind to signaling lymphocytic activation molecule (SLAM; CD150) is attenuated and induces strong adaptive immune responses in rhesus monkeys. J Virol 84: 3413-3420.
117. von Messling V, Svitek N, Cattaneo R (2006) Receptor (SLAM [CD150]) recognition and the V protein sustain swift lymphocyte-based invasion of mucosal tissue and lymphatic organs by a morbillivirus. J Virol 80: 6084-6092.
118. Cocks BG, Chang CC, Carballido JM, Yssel H, De Vries JE, Aversa G (1995) A novel receptor involved in T-cell activation. Nature 376: 260-263.
119. Kruse M, Meinl E, Henning G, Kuhnt C, Berchtold S, Berger T, Schuler G, Steinkasserer A (2001) Signaling lymphocytic activation molecule is expressed on mature CD83+ dendritic cells and is up-regulated by IL-1beta. J Immunol 167: 1989-1995.
120. McQuaid S, Cosby SL (2002) An immunohistochemical study of the distribution of the measles virus receptors, CD46 and SLAM, in normal human tissues and subacute sclerosing panencephalitis. Lab Invest 82: 403-409.
121. Sidorenko SP, Clark EA (2003) The dual-function CD150 receptor subfamily: the viral attraction. Nat Immunol 4: 19-24.
122. Veillette A (2006) NK cell regulation by SLAM family receptors and SAP-related adapters. Immunol Rev 214: 22-34.
123. Van der Vlist M, De Witte L, De Vries RD, Litjens M, De Jong MAWP, Fluitsma D, De Swart RL, Geijtenbeek TBH (2011) Human Langerhans cells capture measles virus through Langerin and present viral antigens to CD4(+) T-cells but are incapable of cross-presentation. Eur J Immunol 41: 2619-2631.
124. Andres O, Obojes K, Kim KS, Ter Meulen V, Schneider-Schaulies J (2003) CD46- and CD150-independent endothelial cell infection with wild-type measles viruses. J Gen Virol 84: 1189-1197.
125. Ludlow M, Rennick L, Sarlang S, Skibinski G, McQuaid S, Moore T, De Swart RL, Duprex WP (2010) Wild-type measles virus infection of primary epithelial cells occurs via the basolateral surface without syncytium formation or release of infectious virus. J Gen Virol 91: 971-979.
126. Moench TR, Griffin DE, Obriecht CR, Vaisberg AJ, Johnson RT (1988) Acute measles in patients with and without neurological involvement: distribution of measles virus antigen and RNA. J Infect Dis 158: 433-442.
127. Tahara M, Takeda M, Shirogane Y, Hashiguchi T, Ohno S, Yanagi Y (2008) Measles virus infects both polarized epithelial and immune cells using distinctive receptor-binding sites on its hemagglutinin. J Virol 82: 4630-4637.
128. Takeda M, Tahara M, Hashiguchi T, Sato TA, Jinnouchi F, Ueki S, Ohno S, Yanagi Y (2007) A human lung carcinoma cell line supports efficient measles virus growth and syncytium formation via SLAM- and CD46-independent mechanism. J Virol 81: 12091-12096.
129. Takeuchi K, Miyajima N, Nagata N, Takeda M, Tashiro M (2003) Wild-type measles virus induces large syncytium formation in primary human small airway epithelial cells by a SLAM(CD150)-independent mechanism. Virus Res 94: 11-16.
130. Mühlebach MD, Mateo M, Sinn PL, Prufer S, Uhlig KM, Leonard VH, Navaratnarajah CK, Frenzke M, Wong XX, Sawatsky B, Ramachandran S, McCray Jr. PB, Cichutek K, von Messling V, Lopez M, Cattaneo R (2011) Adherens junction protein nectin-4 is the epithelial receptor for measles virus. Nature 480: 530-533.
131. Noyce RS, Bondre DG, Ha MN, Lin LT, Sisson G, Tsao MS, Richardson CD (2011) Tumor cell marker PVRL4 (nectin 4) is an epithelial cell receptor for measles virus. PLoS Pathog 7: e1002240.
132. De Witte L, Abt M, Schneider-Schaulies S, van Kooyk Y., Geijtenbeek TBH (2006) Measles virus targets DC-SIGN to enhance dendritic cell infection. J Virol 80: 3477-3486.
133. De Jong MAWP, Geijtenbeek TBH (2010) Langerhans cells in innate defense against pathogens. Trends Immunol 31: 452-459.
134. De Witte L, Nabatov A, Pion M, Fluitsma D, De Jong MAWP, de Gruijl T, Piguet V, van Kooyk Y, Geijtenbeek TBH (2007) Langerin is a natural barrier to HIV-1 transmission by Langerhans cells. Nat Med 13: 367-371.
135. Geijtenbeek TBH, Kwon DS, Torensma R, van Vliet SJ, van Duijnhoven GC, Middel J, Cornelissen IL, Nottet HS, KewalRamani VN, Littman DR, Figdor CG, van Kooyk Y (2000) DC-SIGN, a dendritic cell-specific HIV-1-binding protein that enhances trans-infection of T cells. Cell 100: 587-597.
136. Gringhuis SI, Van der Vlist M, van den Berg LM, Den Dunnen J, Litjens M, Geijtenbeek TBH (2010) HIV-1 exploits innate signaling by TLR8 and DC-SIGN for productive infection of dendritic cells. Nat Immunol 11: 419-426.
137. Leonard VHJ, Sinn PL, Hodge G, Miest T, Devaux P, Oezguen N, Braun W, McCray PB, McChesney MB, Cattaneo R (2008) Measles virus blind to its epithelial cell receptor remains virulent in rhesus monkeys but cannot cross the airway epithelium and is not shed. J Clin Invest 118: 2448-2458.
138. Lessler J, Reich NG, Brookmeyer R, Perl TM, Nelson KE, Cummings DA (2009) Incubation periods of acute respiratory viral infections: a systematic review. Lancet Infect Dis 9: 291-300.
139. Hall WC, Kovatch RM, Herman PH, Fox JG (1971) Pathology of measles in rhesus monkeys. Vet Pathol 8: 307-319.
140. Sakaguchi M, Yoshikawa Y, Yamanouchi K, Sata T, Nagashima K, Takeda K (1986) Growth of measles virus in epithelial and lymphoid tissues of cynomolgus monkeys. Microbiol Immunol 30: 1067-1073.
141. Finkeldey W (1931) Über Riesenzellbefunde in den Gaumenmandeln, zugleich ein Beitrag zur Histopathologie der Mandelveränderungen im Maserninkubationsstadium. Virchows Arch 281: 323-329.
142. Warthin AS (1931) Occurrence of numerous large giant cells in the tonsils and pharyngeal mucosa in the prodromal stage of measles. Arch Pathol 11: 864-874.
143. Sattentau Q (2008) Avoiding the void: cell-to-cell spread of human viruses. Nat Rev Microbiol 6: 815-826.
144. Good RA, Zak SJ (1956) Disturbances in gamma globulin synthesis as “experiments of nature”. Pediatrics 18: 109-149.
145. Nahmias A, Griffith D, Salsbury C, Yoshida K (1967) Thymic aplasia with lymphopenia, plasma cells, and normal immunoglobulins. JAMA 201: 103-108.
146. Burnet FM (1968) Measles as an index of immunological function. Lancet 292: 610-613.
147. Permar SR, Rao SS, Sun Y, Bao S, Buzby AP, Kang HH, Letvin NL (2007) Clinical measles after measles virus challenge in simian

immunodeficiency virus-infected measles virus-vaccinated rhesus monkeys. J Infect Dis 196: 1784-1793.
148. Van Binnendijk RS, Poelen MCM, Kuijpers KC, Osterhaus ADME, UytdeHaag FGCM (1990) The predominance of CD8+ T cells after infection with measles virus suggests a role for CD8+ class I MHC-restricted cytotoxic T lymphocytes (CTL) in recovery from measles. J Immunol 144: 2394-2399.
149. Jaye A, Magnusen AF, Sadiq AD, Corrah T, Whittle HC (1998) Ex vivo analysis of cytotoxic T lymphocytes to measles antigens during infection and after vaccination in Gambian children. J Clin Invest 102: 1969-1977.
150. Van Binnendijk RS, Poelen MCM, De Vries P, Voorma HO, Osterhaus ADME, UytdeHaag FGCM (1989) Measles virus-specific human T cell clones. Characterization of specificity and function of CD4+ helper/cytotoxic and CD8+ cytotoxic T cell clones. J Immunol 142: 2847-2854.
151. Frey S, Krempl CD, Schmitt-Graff A, Ehl S (2008) Role of T cells in virus control and disease after infection with pneumonia virus of mice. J Virol 82: 11619-11627.
152. Permar SR, Moss WJ, Ryon JJ, Douek DC, Monze M, Griffin DE (2003) Increased thymic output during acute measles virus infection. J Virol 77: 7872-7879.
153. Permar SR, Klumpp SA, Mansfield KG, Carville AA, Gorgone DA, Lifton MA, Schmitz JE, Reimann KA, Polack FP, Griffin DE, Letvin NL (2004) Limited contribution of humoral immunity to the clearance of measles viremia in rhesus monkeys. J Infect Dis 190: 998-1005.
154. Pueschel K, Tietz A, Carsillo M, Steward M, Niewiesk S (2007) Measles virus specific CD4 T cell activity does not correlate with protection against lung infection or viral clearance. J Virol 81: 8571-8578.
155. Chen RT, Markowitz LE, Albrecht P, Stewart JA, Mofenson LM, Preblud SR, Orenstein WA (1990) Measles antibody: reevaluation of protective titers. J Infect Dis 162: 1036-1042.
156. Frank SA, Bush RM (2009) Barriers to antigenic escape by pathogens: trade-off between reproductive rate and antigenic mutability. BMC Evol Biol 7: 229.
157. Black FL, YANNET H (1960) Inapparent measles after gamma globulin administration. JAMA 173: 1183-1188.
158. Racaniello V (2011) An exit strategy for measles virus. Science 334: 1650-1651.
159. Tamashiro VG, Perez HH, Griffin DE (1987) Prospective study of the magnitude and duration of changes in tuberculin reactivity during uncomplicated and complicated measles. Pediatr Infect Dis J 6: 451-454.
160. Von Pirquet CE (1908) Das Verhalten der kutanen Tuberkulin-reaktion während der Masern. Dtsch Med Wochenschr 34: 1297-1300.
161. Ryon JJ, Moss WJ, Monze M, Griffin DE (2002) Functional and phenotypic changes in circulating lymphocytes from hospitalized Zambian children with measles. Clin Diagn Lab Immunol 9: 994-1003.
162. Bankamp B, Hodge G, McChesney MB, Bellini WJ, Rota PA (2008) Genetic changes that affect the virulence of measles virus in a rhesus macaque model. Virology 373: 39-50.
163. Premenko-Lanier M, Rota PA, Rhodes GH, Bellini WJ, McChesney MB (2004) Protection against challenge with measles virus (MV) in infant macaques by an MV DNA vaccine administered in the presence of neutralizing antibody. J Infect Dis 189: 2064-2071.
164. Avota E, Avots A, Niewiesk S, Kane LP, Bommhardt U, Ter Meulen V, Schneider-Schaulies S (2001) Disruption of Akt kinase activation is important for immunosuppression induced by measles virus. Nat Med 7: 725-731.
165. Hirsch RL, Griffin DE, Johnson RT, Cooper SJ, Lindo de Soriano I, Roedenbeck S, Vaisberg A (1984) Cellular immune responses during complicated and uncomplicated measles virus infections of man. Clin Immunol Immunopathol 31: 1-12.
166. Ward BJ, Johnson RT, Vaisberg A, Jauregui E, Griffin DE (1991) Cytokine production in vitro and the lymphoproliferative defect of natural measles virus infection. Clin Immunol Immunopathol 61: 236-248.
167. Griffin DE, Ward BJ (1993) Differential CD4 T cell activation in measles. J Infect Dis 168: 275-281.
168. Fugier-Vivier I, Servet-Delprat C, Rivailler P, Rissoan M-C, Liu Y-J, Rabourdin-Combe C (1997) Measles virus suppresses cell-mediated immunity by interfering with the survival and functions of dendritic and T cells. J Exp Med 186: 813-823.
169. Grosjean I, Caux C, Bella C, Berger I, Wild F, Banchereau J, Kaiserlian D (1997) Measles virus infects human dendritic cells and blocks their allostimulatory properties for CD4+ T cells. J Exp Med 186: 801-812.
170. Griffin DE, Ward BJ, Jauregui E, Johnson RT, Vaisberg A (1989) Immune activation in measles. N Engl J Med 320: 1667-1672.
171. Condack C, Grivel J-C, Devaux P, Margolis L, Cattaneo R (2007) Measles virus vaccine attenuation: suboptimal infection of lymphatic tissue and tropism alteration. J Infect Dis 196: 541-549.
172. Enders JF, Peebles TC (1954) Propagation in tissue cultures of cytophatic agents from patients with measles. Proc Soc Exp Biol Med 86: 277-286.
173. Rauh LW, Schmidt R (1965) Measles immunization with killed virus vaccine. Am J Dis Child 109: 232-237.
174. Polack FP, Auwaerter PG, Lee SH, Nousari HC, Valsamakis A, Leiferman KM, Diwan A, Adams RJ, Griffin DE (1999) Production of atypical measles in rhesus macaques: evidence for disease mediated by immune complex formation and eosinophils in the presence of fusion-inhibiting antibody. Nat Med 5: 629-634.
175. Fulginiti VA, Eller JJ, Downte AW, Kempe CH (1967) Altered reactivity to measles virus. Atypical measles in children previously immunized with inactivated measles virus vaccines. JAMA 202: 1075-1080.
176. Nader PR, Horwitz MS, Rousseau J (1968) Atypical exanthem following exposure to natural measles: eleven cases in children previously inoculated with killed vaccine. J Pediatr 72: 22-28.
177. WHO (2004) Measles vaccines. Wkly Epidemiol Rec 79: 130-142.
178. Katz SL (1965) Immunization with live attenuated measles virus vaccines: five years' experience. Arch Gesamte Virusforsch 16: 222-230.
179. Clements CJ, Cutts FT (1995) The epidemiology of measles: thirty years of vaccination. Curr Top Microbiol Immunol 191: 13-33.
180. Moss WJ, Clements CJ, Halsey NA (2003) Immunization of children at risk of infection with human immunodeficiency virus. Bull World Health Organ 81: 61-70.
181. De Quadros CA, Olive JM, Hersh BS, Strassburg MA, Henderson DA, Brandling-Bennett D, Alleyne GA (1996) Measles elimination in the Americas. Evolving strategies. JAMA 275: 224-229.
182. Henao-Restrepo AM, Strebel P, Hoekstra E.J., Birmingham M, Bilous J (2003) Experience in global measles control, 1990-2001. J Infect Dis 187 Suppl 1: S15-S21.
183. Otten M, Kezaala R, Fall A, Masresha B, Martin R, Cairns L, Eggers R, Biellik R, Grabowsky M, Strebel P, Okwo-Bele JM, Nshimirimana D (2005) Public-health impact of accelerated measles control in the WHO African Region 2000-03. Lancet 366:

832-839.
184. Wolfson LJ, Strebel PM, Gacic-Dobo M, Hoekstra EJ, McFarland JW, Hersh BS (2007) Has the 2005 measles mortality reduction goal been achieved? A natural history modelling study. Lancet 369: 191-200.
185. Angel JB, Walpita P, Lerch RA, Sidhu MS, Masurekar M, DeLellis RA, Noble JT, Snydman DR, Udem SA (1998) Vaccine-associated measles pneumonitis in an adult with AIDS. Ann Intern Med 129: 104-106.
186. Albrecht P, Ennis FA, Saltzman EJ, Krugman S (1977) Persistence of maternal antibody in infants beyond 12 months: mechanism of measles vaccine failure. J Pediatr 91: 715-718.
187. Leuridan E, Van Damme P (2007) Passive transmission and persistence of naturally acquired or vaccine-induced maternal antibodies against measles in newborns. Vaccine 25: 6296-6304.
188. Cutts FT, Grabowsky M, Markowitz LE (1995) The effect of dose and strain of live attenuated measles vaccines on serological responses in young infants. Biologicals 23: 95-106.
189. Diaz-Ortega JL, Forsey T, Clements CJ, Milstien J (1994) The relationship between dose and response of standard measles vaccines. Biologicals 22: 35-44.
190. Gans HA, Arvin AM, Galinus J, Logan L, DeHovitz R, Maldonado Y (1998) Deficiency of the humoral immune response to measles vaccine in infants immunized at age 6 months. JAMA 280: 527-532.
191. De Vries RD, Stittelaar KJ, Osterhaus ADME, De Swart RL (2008) Measles vaccination: new strategies and formulations. Expert Rev Vaccines 7: 1215-1223.
192. Henderson DA (1982) Global measles eradication. Lancet 320: 208.
193. Bellini WJ, Rota PA (2011) Biological feasibility of measles eradication. Virus Res 162: 72-79.
194. Moss WJ, Strebel P (2011) Biological feasibility of measles eradication. J Infect Dis 204 Suppl 1: S47-S53.
195. Cochi SL, Linkins RW (2012) The final phase of polio eradication: new vaccines and complex choices. J Infect Dis 205: 169-171.
196. De Swart RL, Duprex WP, Osterhaus ADME (2012) Rinderpest eradication: lessons for measles eradication? Curr Opin Virol 2: 330-334.
197. Essbauer S, Pfeffer M, Meyer H (2010) Zoonotic poxviruses. Vet Microbiol 140: 229-236.
198. Reynolds MG, Damon IK (2012) Outbreaks of human monkeypox after cessation of smallpox vaccination. Trends Microbiol 20: 80-87.
199. Sanders R, Dabbagh A, Featherstone D (2011) Risk analysis for measles reintroduction after global certification of eradication. J Infect Dis 204 Suppl 1: S71-S77.
200. Qiu W, Zheng Y, Zhang S, Fan Q, Liu H, Zhang F, Wang W, Liao G, Hu R (2011) Canine distemper outbreak in rhesus monkeys, China. Emerg Infect Dis 17: 1541-1543.
201. Liniger M, Zuniga A, Naim HY (2007) Use of viral vectors for the development of vaccines. Expert Rev Vaccines 6: 255-266.
202. Singh M, Cattaneo R, Billeter MA (1999) A recombinant measles virus expressing hepatitis B virus surface antigen induces humoral immune responses in genetically modified mice. J Virol 73: 4823-4828.
203. Zuniga A, Wang Z, Liniger M, Hangartner L, Caballero M, Pavlovic J, Wild P, Viret JF, Glueck R, Billeter MA, Naim HY (2007) Attenuated measles virus as a vaccine vector. Vaccine 25: 2974-2983.
204. Brandler S, Lucas-Hourani M, Moris A, Frenkiel MP, Combredet C, Fevrier M, Bedouelle H, Schwartz O, Despres P, Tangy F (2007) Pediatric Measles Vaccine Expressing a Dengue Antigen Induces Durable Serotype-specific Neutralizing Antibodies to Dengue Virus. PLoS Negl Trop Dis 1: e96.
205. Despres P, Combredet C, Frenkiel MP, Lorin C, Brahic M, Tangy F (2005) Live measles vaccine expressing the secreted form of the West Nile virus envelope glycoprotein protects against West Nile virus encephalitis. J Infect Dis 191: 207-214.
206. Liniger M, Zuniga A, Tamin A, Azzouz-Morin TN, Knuchel M, Marty RR, Wiegand M, Weibel S, Kelvin D, Rota PA, Naim HY (2008) Induction of neutralising antibodies and cellular immune responses against SARS coronavirus by recombinant measles viruses. Vaccine 26: 2164-2174.
207. Lorin C, Delebecque F, Labrousse V, Da SL, Lemonnier F, Brahic M, Tangy F (2005) A recombinant live attenuated measles vaccine vector primes effective HLA-A0201-restricted cytotoxic T lymphocytes and broadly neutralizing antibodies against HIV-1 conserved epitopes. Vaccine 23: 4463-4472.
208. Lorin C, Mollet L, Delebecque F, Combredet C, Hurtrel B, Charneau P, Brahic M, Tangy F (2004) A single injection of recombinant measles virus vaccines expressing human immunodeficiency virus (HIV) type 1 clade B envelope glycoproteins induces neutralizing antibodies and cellular immune responses to HIV. J Virol 78: 146-157.
209. Reyes del Valle J, Devaux P, Hodge G, Wegner NJ, McChesney MB, Cattaneo R (2007) A vectored measles virus induces hepatitis B surface antigen antibodies while protecting macaques against measles challenge. J Virol 81: 10597-10605.
210. Griffin DE, Lin WH, Pan CH (2012) Measles virus, immune control, and persistence. FEMS Microbiol Rev 36: 649-662.
211. Rota J, Lowe L, Rota P, Bellini W, Redd S, Dayan G, Van Binnendijk RS, Hahné S, Tipples G, Macey J, Espinoza R, Posey D, Plummer A, Bateman J, Gudino J, Cruz-Ramirez E, Lopez-Martinez I, naya-Lopez L, Holy AT, Giffin S, Carrion V, de Filippis AM, Vicari A, Tan C, Wolf B, Wytovich K, Borus P, Mbugua F, Chege P, Kombich J, koua-Koffi C, Smit S, Bukenya H, Bwogi J, Baliraine FN, Kremer J, Muller C, Santibanez S (2006) Identical genotype B3 sequences from measles patients in 4 countries, 2005. Emerg Infect Dis 12: 1779-1781.
212. Esolen LM, Ward BJ, Moench TR, Griffin DE (1993) Infection of monocytes during measles. J Infect Dis 168: 47-52.
213. Griffin DE, Ward BJ, Esolen LM (1994) Pathogenesis of measles virus infection: an hypothesis for altered immune responses. J Infect Dis 170 (Suppl. 1): S24-S31.
214. Yanagi Y, Takeda M, Ohno S (2006) Measles virus: cellular receptors, tropism and pathogenesis. J Gen Virol 87: 2767-2779.
215. Janeway CA, Travers P, Walport MJ, and Shlomchik M (2004) Immunobiology. Garland Publishing.
216. Turville SG, Santos JJ, Frank I, Cameron PU, Wilkinson J, Miranda-Saksena M, Dable J, Stossel H, Romani N, Piatak M, Jr., Lifson JD, Pope M, Cunningham AL (2004) Immunodeficiency virus uptake, turnover, and 2-phase transfer in human dendritic cells. Blood 103: 2170-2179.
217. Erlenhoefer C, Wurzer WJ, Loffler S, Schneider-Schaulies S, Ter Meulen V, Schneider-Schaulies J (2001) CD150 (SLAM) is a receptor for measles virus but is not involved in viral contact-mediated proliferation inhibition. J Virol 75: 4499-4505.
218. Ono N, Tatsuo H, Hidaka Y, Aoki T, Minagawa H, Yanagi Y (2001) Measles viruses on throat swabs from measles patients use signaling lymphocytic activation molecule (CDw150) but not CD46 as a cellular receptor. J Virol 75: 4399-4401.

219. Van Binnendijk RS, Versteeg-van Oosten JPM, Poelen MCM, Brugghe HF, Hoogerhout P, Osterhaus ADME, UytdeHaag FGCM (1993) Human HLA class I- and HLA Class II-restricted cloned cytotoxic T lymphocytes identify a cluster of epitopes on the measles virus fusion protein. J Virol 67: 2276-2284.
220. Sallusto F, Lanzavecchia A (1994) Efficient presentation of soluble antigen by cultured human dendritic cells is maintained by granulocyte/macrophage colony-stimulating factor plus interleukin 4 and downregulated by tumor necrosis factor alpha. J Exp Med 179: 1109-1118.
221. de Waal L, Suzer Y, Wyatt LS, Sintnicolaas K, Sutter G, Moss B, Osterhaus ADME, De Swart RL (2006) T cell responses to respiratory syncytial virus fusion and attachment proteins in human peripheral blood mononuclear cells. Viral Immunol 19: 669-678.
222. Ebner S, Ehammer Z, Holzmann S, Schwingshackl P, Forstner M, Stoitzner P, Huemer GM, Fritsch P, Romani N (2004) Expression of C-type lectin receptors by subsets of dendritic cells in human skin. Int Immunol 16: 877-887.
223. Engering A, van Vliet SJ, Hebeda K, Jackson DG, Prevo R, Singh SK, Geijtenbeek TBH, van Krieken H, van Kooyk Y (2004) Dynamic populations of dendritic cell-specific ICAM-3 grabbing nonintegrin-positive immature dendritic cells and liver/lymph node-specific ICAM-3 grabbing nonintegrin-positive endothelial cells in the outer zones of the paracortex of human lymph nodes. Am J Pathol 164: 1587-1595.
224. Granelli-Piperno A, Pritsker A, Pack M, Shimeliovich I, Arrighi JF, Park CG, Trumpfheller C, Piguet V, Moran TM, Steinman RM (2005) Dendritic cell-specific intercellular adhesion molecule 3-grabbing nonintegrin/CD209 is abundant on macrophages in the normal human lymph node and is not required for dendritic cell stimulation of the mixed leukocyte reaction. J Immunol 175: 4265-4273.
225. Soilleux EJ, Morris LS, Leslie G, Chehimi J, Luo Q, Levroney E, Trowsdale J, Montaner LJ, Doms RW, Weissman D, Coleman N, Lee B (2002) Constitutive and induced expression of DC-SIGN on dendritic cell and macrophage subpopulations in situ and in vitro. J Leukoc Biol 71: 445-457.
226. Bleharski JR, Niazi KR, Sieling PA, Cheng G, Modlin RL (2001) Signaling lymphocytic activation molecule is expressed on CD40 ligand-activated dendritic cells and directly augments production of inflammatory cytokines. J Immunol 167: 3174-3181.
227. McDonald D, Wu L, Bohks SM, KewalRamani VN, Unutmaz D, Hope TJ (2003) Recruitment of HIV and its receptors to dendritic cell-T cell junctions. Science 300: 1295-1297.
228. Richardson CD, Scheid A, Choppin PW (1980) Specific inhibition of paramyxovirus and myxovirus replication by oligopeptides with amino acid sequences similar to those at the N-termini of the F1 or HA2 viral polypeptides. Virology 105: 205-222.
229. Richardson CD, Choppin PW (1983) Oligopeptides that specifically inhibit membrane fusion by paramyxoviruses: studies on the site of action. Virology 131: 518-532.
230. Murabayashi N, Kurita-Taniguchi M, Ayata M, Matsumoto M, Ogura H, Seya T (2002) Susceptibility of human dendritic cells (DCs) to measles virus (MV) depends on their activation stages in conjunction with the level of CDw150: role of Toll stimulators in DC maturation and MV amplification. Microbes Infect 4: 785-794.
231. Lee B, Leslie G, Soilleux E, O'Doherty U, Baik S, Levroney E, Flummerfelt K, Swiggard W, Coleman N, Malim M, Doms RW (2001) cis Expression of DC-SIGN allows for more efficient entry of human and simian immunodeficiency viruses via CD4 and a coreceptor. J Virol 75: 12028-12038.
232. Moris A, Nobile C, Buseyne F, Porrot F, Abastado JP, Schwartz O (2004) DC-SIGN promotes exogenous MHC-I-restricted HIV-1 antigen presentation. Blood 103: 2648-2654.
233. Moris A, Pajot A, Blanchet F, Guivel-Benhassine F, Salcedo M, Schwartz O (2006) Dendritic cells and HIV-specific CD4+ T cells: HIV antigen presentation, T-cell activation, and viral transfer. Blood 108: 1643-1651.
234. Van Binnendijk RS, Van Baalen CA, Poelen MCM, De Vries P, Boes J, Cerundolo V, Osterhaus ADME, UytdeHaag FGCM (1992) Measles virus transmembrane fusion protein synthesized de novo or presented in immunostimulating complexes is endogenously processed for HLA class I- and class II-restricted cytotoxic T cell recognition. J Exp Med 176: 119-128.
235. Farina C, Theil D, Semlinger B, Hohlfeld R, Meinl E (2004) Distinct responses of monocytes to Toll-like receptor ligands and inflammatory cytokines. Int Immunol 16: 799-809.
236. De Witte L, Bobardt M, Chatterji U, Degeest G, David G, Geijtenbeek TBH, Gallay P (2007) Syndecan-3 is a dendritic cell-specific attachment receptor for HIV-1. Proc Natl Acad Sci U S A 104: 19464-19469.
237. Jahnsen FL, Strickland DH, Thomas JA, Tobagus IT, Napoli S, Zosky GR, Turner DJ, Sly PD, Stumbles PA, Holt PG (2006) Accelerated antigen sampling and transport by airway mucosal dendritic cells following inhalation of a bacterial stimulus. J Immunol 177: 5861-5867.
238. Bieback K, Lien E, Klagge IM, Avota E, Schneider-Schaulies J, Duprex WP, Wagner H, Kirschning CJ, Ter Meulen V, Schneider-Schaulies S (2002) Hemagglutinin protein of wild-type measles virus activates toll-like receptor 2 signaling. J Virol 76: 8729-8736.
239. Steinman RM, Hemmi H (2006) Dendritic cells: translating innate to adaptive immunity. Curr Top Microbiol Immunol 311: 17-58.
240. Heath WR, Carbone FR (2001) Cross-presentation, dendritic cells, tolerance and immunity. Annu Rev Immunol 19: 47-64.
241. Trombetta ES, Mellman I (2005) Cell biology of antigen processing in vitro and in vivo. Annu Rev Immunol 23: 975-1028.
242. Dudziak D, Kamphorst AO, Heidkamp GF, Buchholz VR, Trumpfheller C, Yamazaki S, Cheong C, Liu K, Lee HW, Park CG, Steinman RM, Nussenzweig MC (2007) Differential antigen processing by dendritic cell subsets in vivo. Science 315: 107-111.
243. Villadangos JA, Schnorrer P (2007) Intrinsic and cooperative antigen-presenting functions of dendritic-cell subsets in vivo. Nat Rev Immunol 7: 543-555.
244. Valladeau J, zutter-Dambuyant C, Saeland S (2003) Langerin/CD207 sheds light on formation of birbeck granules and their possible function in Langerhans cells. Immunol Res 28: 93-107.
245. Hladik F, Sakchalathorn P, Ballweber L, Lentz G, Fialkow M, Eschenbach D, McElrath MJ (2007) Initial events in establishing vaginal entry and infection by human immunodeficiency virus type-1. Immunity 26: 257-270.
246. Patterson BK, Landay A, Siegel JN, Flener Z, Pessis D, Chaviano A, Bailey RC (2002) Susceptibility to human immunodeficiency virus-1 infection of human foreskin and cervical tissue grown in explant culture. Am J Pathol 161: 867-873.
247. Valladeau J, Ravel O, zutter-Dambuyant C, Moore K, Kleijmeer M, Liu Y, Duvert-Frances V, Vincent C, Schmitt D, Davoust J, Caux C, Lebecque S, Saeland S (2000) Langerin, a novel C-type lectin specific to Langerhans cells, is an endocytic receptor that induces the formation of Birbeck granules. Immunity 12: 71-81.
248. Girolomoni G, Valle MT, Zacchi V, Costa MG, Giannetti A, Manca F (1996) Cultured human Langerhans' cells are superior to fresh cells at presenting native HIV-1 protein antigens to specific CD4+ T-cell lines. Immunology 87: 310-316.

249. Klechevsky E, Morita R, Liu M, Cao Y, Coquery S, Thompson-Snipes L, Briere F, Chaussabel D, Zurawski G, Palucka AK, Reiter Y, Banchereau J, Ueno H (2008) Functional specializations of human epidermal Langerhans cells and CD14+ dermal dendritic cells. Immunity 29: 497-510.
250. Romani N, Holzmann S, Tripp CH, Koch F, Stoitzner P (2003) Langerhans cells - dendritic cells of the epidermis. APMIS 111: 725-740.
251. Idoyaga J, Cheong C, Suda K, Suda N, Kim JY, Lee H, Park CG, Steinman RM (2008) Cutting edge: langerin/CD207 receptor on dendritic cells mediates efficient antigen presentation on MHC I and II products in vivo. J Immunol 180: 3647-3650.
252. Matsuo M, Nagata Y, Sato E, Atanackovic D, Valmori D, Chen YT, Ritter G, Mellman I, Old LJ, Gnjatic S (2004) IFN-gamma enables cross-presentation of exogenous protein antigen in human Langerhans cells by potentiating maturation. Proc Natl Acad Sci U S A 101: 14467-14472.
253. Nagata Y, Ono S, Matsuo M, Gnjatic S, Valmori D, Ritter G, Garrett W, Old LJ, Mellman I (2002) Differential presentation of a soluble exogenous tumor antigen, NY-ESO-1, by distinct human dendritic cell populations. Proc Natl Acad Sci U S A 99: 10629-10634.
254. Stoitzner P, Tripp CH, Eberhart A, Price KM, Jung JY, Bursch L, Ronchese F, Romani N (2006) Langerhans cells cross-present antigen derived from skin. Proc Natl Acad Sci U S A 103: 7783-7788.
255. De Witte L, De Vries RD, Van der Vlist M, Yüksel S, Litjens M, De Swart RL, Geijtenbeek TBH (2008) DC-SIGN and CD150 have distinct roles in transmission of measles virus from dendritic cells to T-lymphocytes. PLoS Pathog 4: e1000049.
256. Lemon K, De Vries RD, Mesman AW, McQuaid S, Van Amerongen G, Yüksel S, Ludlow M, Rennick LJ, Kuiken T, Rima BK, Geijtenbeek TBH, Osterhaus ADME, Duprex WP, De Swart RL (2011) Early target cells of measles virus after aerosol infection of non-human primates. PLoS Pathog 7: e1001263.
257. Steineur MP, Grosjean I, Bella C, Kaiserlian D (1998) Langerhans cells are susceptible to measles virus infection and actively suppress T cell proliferation. Eur J Dermatol 8: 413-420.
258. Watari E, Shimizu M, Takahashi H (2005) Langerhans cells stimulated by mechanical stress are susceptible to measles virus infection. Intervirology 48: 145-152.
259. Weidmann A, Fischer C, Ohgimoto S, Ruth C, Ter Meulen V, Schneider-Schaulies S (2000) Measles virus-induced immunosuppression in vitro is independent of complex glycosylation of viral glycoproteins and of hemifusion. J Virol 74: 7548-7553.
260. Quaranta V, Tanigaki N, Ferrone S (1981) Distribution of antigenic determinants recognized by three monoclonal antibodies (Q2/70, Q5/6 and Q5/13) on human Ia-like alloantigens and on their subunits. Immunogenetics 12: 175-182.
261. Minagawa H, Tanaka K, Ono N, Tatsuo H, Yanagi Y (2001) Induction of the measles virus receptor SLAM (CD150) on monocytes. J Gen Virol 82: 2913-2917.
262. Geijtenbeek TBH, Torensma R, van Vliet SJ, van Duijnhoven GC, Adema GJ, van Kooyk Y, Figdor CG (2000) Identification of DC-SIGN, a novel dendritic cell-specific ICAM-3 receptor that supports primary immune responses. Cell 100: 575-585.
263. Lanzavecchia A, Abrignani S, Scheidegger D, Obrist R, Dorken B, Moldenhauer G (1988) Antibodies as antigens. The use of mouse monoclonal antibodies to focus human T cells against selected targets. J Exp Med 167: 345-352.
264. Schnorr JJ, Dunster LM, Nanan R, Schneider-Schaulies J, Schneider-Schaulies S, Ter Meulen V (1995) Measles virus-induced down-regulation of CD46 is associated with enhanced sensitivity to complement-mediated lysis of infected cells. Eur J Immunol 25: 976-984.
265. De Vries RD, Lemon K, Ludlow M, McQuaid S, Yüksel S, Van Amerongen G, Rennick LJ, Rima BK, Osterhaus ADME, De Swart RL, Duprex WP (2010) In vivo tropism of attenuated and pathogenic measles virus expressing green fluorescent protein in macaques. J Virol 84: 4714-4724.
266. McCoombe SG, Short RV (2006) Potential HIV-1 target cells in the human penis. AIDS 20: 1491-1495.
267. De Jong MAWP, De Witte L, Taylor ME, Geijtenbeek TBH (2010) Herpes simplex virus type 2 enhances HIV-1 susceptibility by affecting Langerhans cell function. J Immunol 185: 1633-1641.
268. de Jong MA, Vriend LE, Theelen B, Taylor ME, Fluitsma D, Boekhout T, Geijtenbeek TB (2010) C-type lectin Langerin is a beta-glucan receptor on human Langerhans cells that recognizes opportunistic and pathogenic fungi. Mol Immunol 47: 1216-1225.
269. Bolt G, Pedersen IR, Blixenkrone-Moller M (1999) Processing of N-linked oligosaccharides on the measles virus glycoproteins: importance for antigenicity and for production of infectious virus particles. Virus Res 61: 43-51.
270. Chatwell L, Illarionova V, Illarionov B, Eisenreich W, Huber R, Skerra A, Bacher A, Fischer M (2008) Structure of lumazine protein, an optical transponder of luminescent bacteria. J Mol Biol 382: 44-55.
271. Sigal LJ, Crotty S, Andino R, Rock KL (1999) Cytotoxic T-cell immunity to virus-infected non-haematopoietic cells requires presentation of exogenous antigen. Nature 398: 77-80.
272. Bedoui S, Whitney PG, Waithman J, Eidsmo L, Wakim L, Caminschi I, Allan RS, Wojtasiak M, Shortman K, Carbone FR, Brooks AG, Heath WR (2009) Cross-presentation of viral and self antigens by skin-derived CD103+ dendritic cells. Nat Immunol 10: 488-495.
273. Henri S, Guilliams M, Poulin LF, Tamoutounour S, Ardouin L, Dalod M, Malissen B (2010) Disentangling the complexity of the skin dendritic cell network. Immunol Cell Biol 88: 366-375.
274. Dubois B, Lamy PJ, Chemin K, Lachaux A, Kaiserlian D (2001) Measles virus exploits dendritic cells to suppress CD4+ T-cell proliferation via expression of surface viral glycoproteins independently of T-cell trans-infection. Cell Immunol 214: 173-183.
275. Schlender J, Schnorr J-J, Spielhofer P, Cathomen T, Cattaneo R, Billeter M, Ter Meulen V, Schneider-Schaulies S (1996) Interaction of measles virus glycoproteins with the surface of uninfected peripheral blood lymphocytes induces immunosuppression in vitro. Proc Natl Acad Sci USA 93: 13194-13199.
276. Burgdorf S, Kautz A, Bohnert V, Knolle PA, Kurts C (2007) Distinct pathways of antigen uptake and intracellular routing in CD4 and CD8 T cell activation. Science 316: 612-616.
277. Burgdorf S, Scholz C, Kautz A, Tampe R, Kurts C (2008) Spatial and mechanistic separation of cross-presentation and endogenous antigen presentation. Nat Immunol 9: 558-566.
278. WHO (2009) Global reductions in measles mortality 2000-2008 and the risk of measles resurgence. Wkly Epidemiol Rec 84: 509-516.
279. Smith EC, Popa A, Chang A, Masante C, Dutch RE (2009) Viral entry mechanisms: the increasing diversity of paramyxovirus entry. FEBS J 276: 7217-7227.
280. Shirogane Y, Takeda M, Tahara M, Ikegame S, Nakamura T, Yanagi Y (2010) Epithelial-mesenchymal transition abolishes the susceptibility of polarized epithelial cell lines to measles virus. J Biol Chem 285: 20882-20890.

281. El Mubarak HS, Yüksel S, Van Amerongen G, Mulder PGH, Mukhtar MM, Osterhaus ADME, De Swart RL (2007) Infection of cynomolgus macaques (Macaca fascicularis) and rhesus macaques (Macaca mulatta) with different wild-type measles viruses. J Gen Virol 88: 2028-2034.
282. Lemon K, Rima BK, McQuaid S, Allen IV, Duprex WP (2007) The F gene of rodent brain-adapted mumps virus is a major determinant of neurovirulence. J Virol 81: 8293-8302.
283. Dubus JC, Vecellio L, De Monte M, Fink JB, Grimbert D, Montharu J, Valat C, Behan N, Diot P (2005) Aerosol deposition in neonatal ventilation. Pediatr Res 58: 10-14.
284. Lemon K, Ludlow M, De Vries RD, Nambulli S, Wilson MR, McQuaid S, De Swart RL, Duprex WP (2012) Wild-type measles virus uses cotton rat PVRL4 for cell-to-cell spread in vivo. submitted .
285. El Mubarak HS, De Swart RL, Osterhaus ADME, Schutten M (2005) Development of a semi-quantitative real-time RT-PCR for the detection of measles virus. J Clin Virol 32: 313-317.
286. Ibrahim SA, Mustafa OM, Mukhtar MM, Saleh IA, El Mubarak HS, Abdallah A, El Hassan AM, Osterhaus ADME, Groen J, De Swart RL, Zijlstra EE (2002) Measles in suburban Khartoum: an epidemiological and clinical study. Trop Med Int Health 7: 442-449.
287. Kawamata N, Xu B, Nishijima H, Aoyama K, Kusumoto M, Takeuchi T, Tei C, Michie SA, Matsuyama T (2009) Expression of endothelia and lymphocyte adhesion molecules in bronchus-associated lymphoid tissue (BALT) in adult human lung. Respir Res 10: 97.
288. Ferreira CS, Frenzke M, Leonard VH, Welstead GG, Richardson CD, Cattaneo R (2010) Measles virus infection of alveolar macrophages and dendritic cells precedes spread to lymphatic organs in transgenic mice expressing human signaling lymphocytic activation molecule (SLAM, CD150). J Virol 84: 3033-3042.
289. Sternberg S (1997) Histology for pathologists. Philadelphia: Lippincott & Raven. 1200 p.
290. Pabst R, Tschernig T (2010) Bronchus-associated lymphoid tissue: an entry site for antigens for successful mucosal vaccinations? Am J Respir Cell Mol Biol 43: 137-141.
291. Toyoshima M, Chida K, Sato A (2000) Antigen uptake and subsequent cell kinetics in bronchus-associated lymphoid tissue. Respirology 5: 141-145.
292. Teitelbaum R, Schubert W, Gunther L, Kress Y, Macaluso F, Pollard JW, McMurray DN, Bloom BR (1999) The M cell as a portal of entry to the lung for the bacterial pathogen Mycobacterium tuberculosis. Immunity 10: 641-650.
293. Morin MJ, Warner A, Fields BN (1994) A pathway for entry of reoviruses into the host through M cells of the respiratory tract. J Exp Med 180: 1523-1527.
294. Enders JF, Katz SL, Milovanovic MV, Holloway A (1960) Studies on an attenuated measles-virus vaccine I. Development and preparation of the vaccine: techniques for assay of effects of vaccination. N Engl J Med 263: 153-159.
295. Schwarz AJ (1962) Preliminary tests of a highly attenuated measles vaccine. Am J Dis Child 103: 386-389.
296. De Quadros CA, Izurieta H, Carrasco P, Brana M, Tambini G (2003) Progress toward measles eradication in the region of the Americas. J Infect Dis 187(Suppl.1): S102-S110.
297. Hilleman MR (2001) Current overview of the pathogenesis and prophylaxis of measles with focus on practical implications. Vaccine 20: 651-665.
298. Peebles TC, McCarthy K, Enders JF, Holloway A (1957) Behavior of monkeys after inoculation of virus derived from patients with measles and propagated in tissue culture together with observations on spontaneous infections of these animals by an agent exhibiting similar antigenic properties. J Immunol 78: 63-74.
299. Naniche D, Yeh A, Eto DS, Manchester M, Friedman RM, Oldstone MBA (2000) Evasion of host defenses by measles virus: wild-type measles virus infection interferes with induction of alpha/beta interferon production. J Virol 74: 7478-7484.
300. De Swart RL, Kuiken T, Fernandez de Castro J, Papania MJ, Valdespino JL, Minor P, Witham C, Yüksel S, Vos HW, Van Amerongen G, Osterhaus ADME (2006) Aerosol measles vaccination in macaques: preclinical studies of immune responses and safety. Vaccine 24: 6424-6436.
301. Valdespino-Gomez JL, De Lourdes Garcia-Garcia M, Fernandez de Castro J, Henao-Restrepo AM, Bennett J, Sepulveda-Amor J (2006) Measles aerosol vaccination. Curr Top Microbiol Immunol 304: 165-193.
302. Tober C, Seufert M, Schneider H, Billeter MA, Johnston IC, Niewiesk S, Ter Meulen V, Schneider-Schaulies S (1998) Expression of measles virus V protein is associated with pathogenicity and control of viral RNA synthesis. J Virol 72: 8124-8132.
303. Valsamakis A, Schneider H, Auwaerter PG, Kaneshima H, Billeter MA, Griffin DE (1998) Recombinant measles viruses with mutations in the C, V, or F gene have altered growth phenotypes in vivo. J Virol 72: 7754-7761.
304. Devaux P, von Messling V, Songsungthong W, Springfeld C, Cattaneo R (2007) Tyrosine 110 in the measles virus phosphoprotein is required to block STAT1 phosphorylation. Virology 360: 72-83.
305. Fontana JM, Bankamp B, Bellini WJ, Rota PA (2008) Regulation of interferon signaling by the C and V proteins from attenuated and wild-type strains of measles virus. Virology 374: 71-81.
306. Gould E (1974) Variants of measles virus. Med Microbiol Immunol 160: 211-219.
307. Garonne P, Neidhardt E-M, Garcia E, Galibert L, van Kooten C, Banchereau J (1995) Fas ligation induces apoptosis of CD40-activated human B lymphocytes. J Exp Med 182: 1265-1273.
308. Allard SD, Pletinckx K, Breckpot K, Heirman C, Bonehill A, Michiels A, Van Baalen CA, Gruters RA, Osterhaus ADME, Lacor P, Thielemans K, Aerts JL (2008) Functional T-cell responses generated by dendritic cells expressing the early HIV-1 proteins Tat, Rev and Nef. Vaccine 26: 3735-3741.
309. Stittelaar KJ, Kuiken T, De Swart RL, Van Amerongen G, Vos HW, Niesters HGM, van Schalkwijk P, van der Kwast T, Wyatt LS, Moss B, Osterhaus ADME (2001) Safety of modified vaccinia virus Ankara (MVA) in immune-suppressed macaques. Vaccine 19: 3700-3709.
310. Van Binnendijk RS, Poelen MCM, Van Amerongen G, De Vries P, Osterhaus ADME (1997) Protective immunity in macaques vaccinated with live attenuated, recombinant, and subunit measles vaccines in the presence of passively acquired antibodies. J Infect Dis 175: 524-532.
311. Plemper RK, Compans RW (2003) Mutations in the putative HR-C region of the measles virus F2 glycoprotein modulate syncytium formation. J Virol 77: 4181-4190.
312. Tahara M, Takeda M, Yanagi Y (2005) Contributions of matrix and large protein genes of the measles virus edmonston strain to growth in cultured cells as revealed by recombinant viruses. J Virol 79: 15218-15225.

313. Tahara M, Takeda M, Seki F, Hashiguchi T, Yanagi Y (2007) Multiple amino acid substitutions in hemagglutinin are necessary for wild-type measles virus to acquire the ability to use receptor CD46 efficiently. J Virol 81: 2564-2572.
314. Permar SR, Klumpp SA, Mansfield KG, Kim WK, Gorgone DA, Lifton MA, Williams KC, Schmitz JE, Reimann KA, Axthelm MK, Polack FP, Griffin DE, Letvin NL (2003) Role of CD8+ lymphocytes in control and clearance of measles virus infection of rhesus monkeys. J Virol 77: 4396-4400.
315. Tompkins V, Macaulay JC (1955) A characteristic cell in nasal secretions during prodromal measles. J Am Med Assoc 157: 711.
316. Fulton RE, Middleton PJ (1975) Immunofluorescence in diagnosis of measles infections in children. J Pediatr 86: 17-22.
317. Lloyd-Smith JO, Schreiber SJ, Kopp PE, Getz WM (2005) Superspreading and the effect of individual variation on disease emergence. Nature 438: 355-359.
318. De Vries RD, McQuaid S, Van Amerongen G, Yüksel S, Verburgh RJ, Osterhaus ADME, Duprex WP, De Swart RL (2012) Measles immune suppression: lessons from the macaque model. PLoS Pathog 8: e1002885.
319. Choi YK, Simon MA, Kim DY, Yoon BI, Kwon SW, Lee KW, Seo IB, Kim DY (1999) Fatal measles virus infection in Japanese macaques (Macaca fuscata). Vet Pathol 36: 594-600.
320. MacArthur JA, Mann PG, Oreffo V, Scott GBD (1979) Measles in monkeys: an epidemiological study. J Hyg 83: 207-212.
321. Willy ME, Woodward RA, Thornton VB, Wolff AV, Flynn BM, Heath JL, Villamarzo YS, Smith S, Bellini WJ, Rota PA (1999) Management of a measles outbreak among Old World nonhuman primates. Lab Anim Sci 49: 42-48.
322. Kobune F, Sakata H, Sugiura A (1990) Marmoset lymphoblastoid cells as a sensitive host for isolation of measles virus. J Virol 64: 700-705.
323. Verkaik NJ, Nguyen DT, de Vogel CP, Moll HA, Verbrugh HA, Jaddoe VWV, Hofman A, Van Wamel WJB, van den Hoogen BG, Buijs-Offerman RMGB, Ludlow M, De Witte L, Osterhaus ADME, van Belkum A, De Swart RL (2011) Streptococcus pneumoniae exposure is associated with human metapneumovirus seroconversion and increased susceptibility to in vitro HMPV infection. Clin Microbiol Infect 17: 1840-1844.
324. Duprex WP, McQuaid S, Hangartner L, Billeter MA, Rima BK (1999) Observation of measles virus cell-to-cell spread in astrocytoma cells by using a green fluorescent protein-expressing recombinant virus. J Virol 73: 9568-9575.
325. Eccles R (2005) Understanding the symptoms of the common cold and influenza. Lancet Infect Dis 5: 718-725.
326. Hall CB, Douglas Jr. RG, Schabel KC, Geiman JM (1981) Infectivity of respiratory syncytial virus by various routes of inoculation. Infect Immun 33: 779-783.
327. Lu R, Yu X, Wang W, Duan X, Zhang L, Zhou W, Xu J, Xu L, Hu Q, Lu J, Ruan L, Wang Z, Tan W (2012) Characterization of human coronavirus etiology in Chinese adults with acute upper respiratory tract infection by real-time Rt-PCR assays. PLoS ONE 7: e38638.
328. Burke CW, Mason JN, Surman SL, Jones BG, Dalloneau E, Hurwitz JL, Russell CJ (2011) Illumination of parainfluenza virus infection and transmission in living animals reveals a tissue-specific dichotomy. PLoS Pathog 7: e1002134.
329. van Riel D, Munster VJ, de Wit E, Rimmelzwaan GF, Fouchier RAM, Osterhaus ADME, Kuiken T (2006) H5N1 virus attachment to lower respiratory tract. Science 312: 399.
330. van Riel D, den Bakker MA, Leijten LM, Chutinimitkul S, Munster VJ, de Wit E, Rimmelzwaan GF, Fouchier RAM, Osterhaus ADME, Kuiken T (2010) Seasonal and pandemic human influenza viruses attach better to human upper respiratory tract epithelium than avian influenza viruses. Am J Pathol 176: 1614-1618.
331. Bloch AB, Orenstein WA, Ewing WM, Spain WH, Mallison GF, Herrmann KL, Hinman AR (1985) Measles outbreak in a pediatric practice: airborne transmission in an office setting. Pediatrics 75: 676-683.
332. Coleman KP, Markey PG (2010) Measles transmission in immunized and partially immunized air travellers. Epidemiol Infect 138: 1012-1015.
333. Ehresmann KR, Crouch N, Henry PM, Hunt JM, Habedank TL, Bowman R, Moore KA (2004) An outbreak of measles among unvaccinated young adults and measles seroprevalence study: implications for measles outbreak control in adult populations. J Infect Dis 189 Suppl 1: S104-S107.
334. Paunio M, Peltola H, Valle M, Davidkin I, Virtanen M, Heinonen OP (1998) Explosive school-based measles outbreak: intense exposure may have resulted in high risk, even among revaccinees. Am J Epidemiol 148: 1103-1110.
335. Christensen PE, Schmidt H, Bang HO, Andersen V, Jordal B, Jensen O (1953) An epidemic of measles in southern Greenland, 1951; measles in virgin soil. II. The epidemic proper. Acta Med Scand 144: 430-449.
336. Woolhouse ME, Dye C, Etard JF, Smith T, Charlwood JD, Garnett GP, Hagan P, Hii JL, Ndhlovu PD, Quinnell RJ, Watts CH, Chandiwana SK, Anderson RM (1997) Heterogeneities in the transmission of infectious agents: implications for the design of control programs. Proc Natl Acad Sci U S A 94: 338-342.
337. Sinn PL, Williams G, Vongpunsawad S, Cattaneo R, McCray PB, Jr. (2002) Measles virus preferentially transduces the basolateral surface of well-differentiated human airway epithelia. J Virol 76: 2403-2409.
338. McQuillin J, Bell TM, Gardner PS, Downham PS (1976) Application of immunofluorescence to a study of measles. Arch Dis Child 51: 411-419.
339. Scheifele DW, Forbes CE (1972) Prolonged giant cell excretion in severe African measles. Pediatrics 50: 867-873.
340. Lightwood R, Nolan R (1970) Epithelial giant cells in measles as an acid in diagnosis. J Pediatr 77: 59-64.
341. De Jong JG, Winkler KC (1964) Survival of measles virus in air. Nature 201: 1054-1055.
342. Herfst S, Schrauwen EJ, Linster M, Chutinimitkul S, de WE, Munster VJ, Sorrell EM, Bestebroer TM, Burke DF, Smith DJ, Rimmelzwaan GF, Osterhaus AD, Fouchier RA (2012) Airborne transmission of influenza A/H5N1 virus between ferrets. Science 336: 1534-1541.
343. Imai M, Watanabe T, Hatta M, Das SC, Ozawa M, Shinya K, Zhong G, Hanson A, Katsura H, Watanabe S, Li C, Kawakami E, Yamada S, Kiso M, Suzuki Y, Maher EA, Neumann G, Kawaoka Y (2012) Experimental adaptation of an influenza H5 HA confers respiratory droplet transmission to a reassortant H5 HA/H1N1 virus in ferrets. Nature 486: 420-428.
344. Permar SR, Moss WJ, Ryon JJ, Monze M, Cutts F, Quinn TC, Griffin DE (2001) Prolonged measles virus shedding in human immunodeficiency virus-infected children, detected by reverse transcriptase-polymerase chain reaction. J Infect Dis 183: 532-538.
345. Naniche D, Garenne M, Rae C, Manchester M, Buchta R, Brodine SK, Oldstone MBA (2004) Decrease in measles virus-specific CD4 T cell memory in vaccinated subjects. J Infect Dis 190: 1387-1395.
346. Dhiman N, Ovsyannikova IG, Howe RC, Ryan JE, Jacobson RM, Poland GA (2004) Interleukin-4 induced by measles virus and

measles-derived peptides as measured by IL-4 receptor-blocking ELISA. J Immunol Methods 287: 217-225.
347. Gans HA, Maldonado Y, Yasukawa LL, Beeler J, Audet S, Rinki MM, DeHovitz R, Arvin AM (1999) IL-12, IFN-gamma, and T cell proliferation to measles in immunized infants. J Immunol 162: 5569-5575.
348. Ndhlovu ZM, Angenendt M, Heckel D, Schneck JP, Griffin DE, Oelke M (2009) Development of an artificial-antigen-presenting-cell-based assay for the detection of low-frequency virus-specific CD8(+) T cells in whole blood, with application for measles virus. Clin Vaccine Immunol 16: 1066-1073.
349. Stittelaar KJ, Wyatt LS, De Swart RL, Vos HW, Groen J, Van Amerongen G, Van Binnendijk RS, Rozenblatt S, Moss B, Osterhaus ADME (2000) Protective immunity in macaques vaccinated with a Modified Vaccinia virus Ankara-based measles virus vaccine in the presence of passively acquired antibodies. J Virol 74: 4236-4243.
350. Van Els CACM, Nanan R (2002) T cell responses in acute measles. Viral Immunol 15: 435-450.
351. Van Baalen CA, Kwa D, Verschuren EJ, Reedijk ML, Boon AC, de Mutsert G., Rimmelzwaan GF, Osterhaus ADME, Gruters RA (2005) Fluorescent antigen-transfected target cell cytotoxic T lymphocyte assay for ex vivo detection of antigen-specific cell-mediated cytotoxicity. J Infect Dis 192: 1183-1190.
352. Van Binnendijk RS, Poelen MCM, De Vries P, UytdeHaag FGCM, Osterhaus ADME (1991) A role for CD8+ class I MHC-restricted CTLs in recovery from measles: implications for the development of inactivated measles vaccines. In: Brown F, Chanock RM, Ginsberg HS, Lerner RA, editors. Vaccines 91. Cold Spring Harbor: Cold Spring Harbor Laboratory Press. pp. 299-303.
353. de Waal L, Yüksel S, Brandenburg AH, Langedijk JPM, Sintnicolaas K, Verjans GMGM, Osterhaus ADME, De Swart RL (2004) Identification of a common HLA-DP4-restricted T cell epitope in the conserved region of the respiratory syncytial virus G protein. J Virol 78: 1775-1781.
354. Chávez-Galán L, Arenas-Del Angel MC, Zenteno E, Chávez R, Lascurain R (2009) Cell death mechanisms induced by cytotoxic lymphocytes. Cell Mol Immunol 6: 15-25.
355. Lisse I, Samb B, Whittle H, Jensen H, Soumare M, Simondon F, Aaby P (1998) Acute and long-term changes in T-lymphocyte subsets in response to clinical and subclinical measles. A community study from rural Senegal. Scand J Infect Dis 30: 17-21.
356. Schnorr J-J, Xanthakos S, Keikavoussi P, Kampgen E, Ter Meulen V, Schneider-Schaulies S (1997) Induction of maturation of human blood dendritic cell precursors by measles virus is associated with immmunosuppression. Proc Natl Acad Sci USA 94: 5326-5331.
357. De Vries RD, Mesman AW, Geijtenbeek TBH, Duprex WP, De Swart RL (2012) The pathogenesis of measles. Curr Opin Virol 2: 248-255.
358. Huddlestone JR, Lampert PW, Oldstone MBA (1980) Virus-lymphocyte interactions: infection of Tg and Tm subsets by measles virus. Clin Immunol Immunopathol 15: 502-509.
359. Sullivan JL, Barry DW, Lucas SJ, Albrecht P (1975) Measles infection of human mononuclear cells. I. Acute infection of peripheral blood lymphocytes and monocytes. J Exp Med 142: 773-784.
360. Forthal DN, Aarnaes S, Blanding J, De la Maza L, Tilles JG (1992) Degree and length of viremia in adults with measles. J Infect Dis 166: 421-424.
361. Langermans JA, Andersen P, van Soolingen D, Vervenne RA, Frost PA, van der Laan T, van Pinxteren LA, van den Hombergh J, Kroon S, Peekel I, Florquin S, Thomas AW (2001) Divergent effect of bacillus Calmette-Guerin (BCG) vaccination on Mycobacterium tuberculosis infection in highly related macaque species: implications for primate models in tuberculosis vaccine research. Proc Natl Acad Sci U S A 98: 11497-11502.
362. Nguyen DT, De Witte L, Ludlow M, Yüksel S, Wiesmuller K-H, Geijtenbeek TBH, Osterhaus ADME, De Swart RL (2010) The synthetic bacterial lipopeptide Pam3CSK4 modulates respiratory syncytial virus infection independent of TLR activation. PLoS Pathog 6: e1001049.
363. De Salort J, Sintes J, Llinas L, Matesanz-Isabel J, Engel P (2011) Expression of SLAM (CD150) cell-surface receptors on human B-cell subsets: from pro-B to plasma cells. Immunol Lett 134: 129-136.
364. De Vries RD, Yüksel S, Osterhaus ADME, De Swart RL (2010) Specific CD8+ T-lymphocytes control dissemination of measles virus. Eur J Immunol 40: 388-395.
365. Mongkolsapaya J, Jaye A, Callan MFC, Magnusen AF, McMichael AJ, Whittle HC (1999) Antigen-specific expansion of cytotoxic T lymphocytes in acute measles virus infection. J Virol 73: 67-71.
366. Moussallem TM, Guedes F, Fernandes ER, Pagliari C, Lancellotti CLP, De Andrade Jr. HF, Duarte MIS (2007) Lung involvement in childhood measles: severe immune dysfunction revealed by quantitative immunohistochemistry. Hum Pathol 38: 1239-1247.
367. Sallusto F, Lenig D, Forster R, Lipp M, Lanzavecchia A (1999) Two subsets of memory T lymphocytes with distinct homing potentials and effector functions. Nature 401: 708-712.
368. Griffin DE (2010) Measles virus-induced suppression of immune responses. Immunol Rev 236: 176-189.
369. Hahm B (2009) Hostile communication of measles virus with host innate immunity and dendritic cells. Curr Top Microbiol Immunol 330: 271-287.
370. Schneider-Schaulies S, Niewiesk S, Schneider-Schaulies J, Ter Meulen V (2001) Measles virus induced immunosuppression: targets and effector mechanisms. Curr Mol Med 1: 163-181.
371. Servet-Delprat C, Vidalain P-O, Bausinger H, Manie S, Le Deist F, Azocar O, Hanau D, Fischer A, Rabourdin-Combe C (2000) Measles virus induces abnormal differentiation of CD40 ligand-activated human dendritic cells. J Immunol 164: 1753-1760.
372. Vidalain P-O, Azocar O, Rabourdin-Combe C, Servet-Delprat C (2001) Measles virus-infected dendritic cells develop immunosuppressive and cytotoxic activities. Immunobiol 204: 629-638.
373. Beineke A, Puff C, Seehusen F, Baumgartner W (2009) Pathogenesis and immunopathology of systemic and nervous canine distemper. Vet Immunol Immunopathol 127: 1-18.
374. McCullough B, Krakowka S, Koestner A (1974) Experimental canine distemper virus-induced lymphoid depletion. Am J Pathol 74: 155-170.
375. De Swart RL, Vos HW, UytdeHaag FGCM, Osterhaus ADME, Van Binnendijk RS (1998) Measles virus fusion protein- and hemagglutinin-transfected cell lines are a sensitive tool for the detection of specific antibodies by a FACS-measured immunofluorescence assay. J Virol Methods 71: 35-44.
376. Lin CY, Lin MT, Hsieh YL, Tsao LY (1988) Transient disappearance of immunologic disorders and remission after intercurrent measles infections in children with chronic idiopathic thrombocytopenic purpura. J Clin Immunol 8: 207-213.

377. Simpanen E, van ER, Isomaki H (1977) Remission of juvenile rheumatoid arthritis (Still's disease) after measles. Lancet 2: 987-988.
378. Yoshioka K, Miyata H, Maki S (1981) Transient remission of juvenile rheumatoid arthritis after measles. Acta Paediatr Scand 70: 419-420.
379. Moss WJ, Scott S, Ndhlovu Z, Monze M, Cutts FT, Quinn TC, Griffin DE (2009) Suppression of human immunodeficiency virus type 1 viral load during acute measles. Pediatr Infect Dis J 28: 63-65.
380. Ruel TD, Achan J, Gasasira AF, Charlebois ED, Mehbratu T, Rosenthal PJ, Dorsey G, Kamya MR, Kekitiinwa A, Wong J, Havlir DV (2008) HIV RNA suppression among HIV-infected Ugandan children with measles. J Acquir Immune Defic Syndr 48: 225-227.
381. Kretschmer R, Janeway CA, Rosen FS (1968) Immunologic amnesia. Study of an 11-year-old girl with recurrent severe infections associated with dysgammaglobulinemia, lymphopenia and lymphocytotoxic antibody, resulting in loss of immunologic memory. Pediat Res 2: 7-16.
382. Blancou J (2004) Dog distemper: imported into Europe from South America? Hist Med Vet 29: 35-41.
383. Rockborn G (1958) Canine distemper virus in tissue culture. Arch Gesamte Virusforsch 8: 485-492.
384. Liu C, Coffin DL (1957) Studies of canine distemper infection by means of fluorescein-labeled antibody. I. The pathogenesis, pathology, and diagnosis of the disease in experimentally infected ferrets. Virology 3: 115-131.
385. Friedlander JM, Summers BA, Appel MJG (1985) Persistence of virulent canine distemper virus in lymphoblastoid cell lines. Arch Virol 86: 47-62.
386. Wunschmann A, Kremmer E, Baumgartner W (2000) Phenotypical characterization of T and B cell areas in lymphoid tissues of dogs with spontaneous distemper. Vet Immunol Immunopathol 73: 83-98.
387. Summers BA, Appel MJG (1994) Aspects of canine distemper virus and measles virus encephalomyelitis. Neuropathol Appl Neurobiol 20: 525-534.
388. Baron MD (2005) Wild-type Rinderpest virus uses SLAM (CD150) as its receptor. J Gen Virol 86: 1753-1757.
389. Seki F, Ono N, Yamaguchi R, Yanagi Y (2003) Efficient isolation of wild strains of canine distemper virus in Vero cells expressing canine SLAM (CD150) and their adaptability to marmoset B95a cells. J Virol 77: 9943-9950.
390. Langedijk JPM, Janda J, Origgi FC, Orvell C, Vandevelde M, Zurbriggen A, Plattet P (2011) Canine distemper virus infects canine keratinocytes and immune cells by using overlapping and distinct regions located on one side of the attachment protein. J Virol 85: 11242-11254.
391. Sawatsky B, Wong XX, Hinkelmann S, Cattaneo R, von Messling V (2012) Canine distemper virus epithelial cell infection is required for clinical disease but not for immunosuppression. J Virol 86: 3658-3666.
392. Pratakpiriya W, Seki F, Otsuki N, Sakai K, Fukuhara H, Katamoto H, Hirai T, Maenaka K, Techangamsuwan S, Lan NT, Takeda M, Yamaguchi R (2012) Nectin4 is an epithelial cell receptor for canine distemper virus and involved in the neurovirulence. J Virol 86: 10207-10210.
393. Appel MJG, Yates RA, Foley GL, Bernstein JJ, Santinelli S, Spelman LH, Miller LD, Arp LH, Anderson M, Barr M, Pearce-Kelling S, Summers BA (1994) Canine distemper epizootic in lions, tigers, and leopards in North America. J Vet Diagn Invest 6: 277-288.
394. Mainka SA, Qiu X, He T, Appel MJG (1994) Serologic survey of giant pandas (Ailuropoda melanoleuca), and domestic dogs and cats in the Wolong Reserve, China. J Wildl Dis 30: 86-89.
395. Harder TC, Kenter M, Appel MJG, Roelke-Parker ME, Barrett T, Osterhaus ADME (1995) Phylogenetic evidence of canine distemper virus in Serengeti's lions. Vaccine 13: 521-523.
396. Appel MJG, Summers BA (1995) Pathogenicity of morbilliviruses for terrestrial carnivores. Vet Microbiol 44: 187-191.
397. Anderson EC (1995) Morbillivirus infections in wildlife (in relation to their population biology and disease control in domestic animals). Vet Microbiol 44: 319-332.
398. Roelke-Parker ME, Munson L, Packer C, Kock R, Cleaveland S, Carpenter M, O'Brien SJ, Pospischil A, Hofmann-Lehmann R, Lutz H, Mwamengele GL, Mgasa MN, Machange GA, Summers BA, Appel MJ (1996) A canine distemper virus epidemic in Serengeti lions (Panthera leo). Nature 379: 441-445.
399. Quigley KS, Evermann JF, Leathers CW, Armstrong DL, Goodrich J, Duncan NM, Miquelle DG (2010) Morbillivirus infection in a wild siberian tiger in the Russian Far East. J Wildl Dis 46: 1252-1256.
400. Hur K, Bae JS, Choi JH, Kim JH, Kwon SW, Lee KW, Kim DY (1999) Canine distemper virus infection in binturongs (Arctictis binturong). J Comp Pathol 121: 295-299.
401. Hirama K, Goto Y, Uema M, Endo Y, Miura R, Kai C (2004) Phylogenetic analysis of the hemagglutinin (H) gene of canine distemper viruses isolated from wild masked palm civets (Paguma larvata). J Vet Med Sci 66: 1575-1578.
402. Itakura C, Nakamura K, Nakatsuka J, Goto M (1979) Distemper infection in lesser pandas due to administration of a canine distemper live vaccine. Nihon Juigaku Zasshi 41: 561-566.
403. Cattet MR, Duignan PJ, House CA, Aubin DJ (2004) Antibodies to canine distemper and phocine distemper viruses in polar bears from the Canadian arctic. J Wildl Dis 40: 338-342.
404. Kotani T, Jyo M, Odagiri Y, Sakakibara Y, Horiuchi T (1989) Canine distemper virus infection in lesser pandas (Ailurus fulgens). Nihon Juigaku Zasshi 51: 1263-1266.
405. Roscoe DE (1993) Epizootiology of canine distemper in New Jersey raccoons. J Wildl Dis 29: 390-395.
406. Grachev MA, Kumarev VP, Mamaev LV, Zorin VL, Baranova LV, Denikjna NN, Belikov SI, Petrov EA, Kolesnik VS, Kolesnik RS, Dorofeev VM, Beim AM, Kudelin VN, Nagieva FG, Sidorov VN (1989) Distemper virus in Baikal seals. Nature 338: 209.
407. Kennedy S, Kuiken T, Jepson PD, Deaville R, Forsyth M, Barrett T, Van de Bildt MWG, Osterhaus ADME, Eybatov T, Duck C, Kydyrmanov A, Mitrofanov I, Wilson S (2000) Mass die-Off of Caspian seals caused by canine distemper virus. Emerg Infect Dis 6: 637-639.
408. Svansson V, Blixenkrone-Möller M, Skirnisson K, Have P, Heje NI, Nielsen J, Lund E (1993) Infection studies with canine distemper virus in harbour seals. Arch Virol 131: 349-359.
409. Appel MJG, Reggiardo C, Summers BA, Pearce-Kelling S, Mare CJ, Noon TH, Reed RE, Shively JN, Örvell C (1991) Canine distemper virus infection in javelinas (collared peccaries). Arch Virol 119: 147-152.
410. Yoshikawa Y, Ochikubo F, Matsubara Y, Tsuruoka H, Ishii M, Shirota K, Nomura Y, Sugiyama M, Yamanouchi K (1989) Natural infection with canine distemper virus in a Japanese monkey (Macaca fuscata). Vet Microbiol 20: 193-205.
411. Sun Z, Li A, Ye H, Shi Y, Hu Z, Zeng L (2010) Natural infection with canine distemper virus in hand-feeding Rhesus monkeys in China. Vet Microbiol 141: 374-378.

412. Sakai K, Nagata N, Ami Y, Seki F, Suzaki Y, Iwata-Yoshikawa N, Suzuki T, Fukushi S, Mizutani T, Yoshikawa T, Otsuki N, Kurane I, Komase K, Yamaguchi R, Hasegawa H, Saijo M, Takeda M, Morikawa S (2012) Lethal canine distemper virus outbreak in cynomolgus monkeys in Japan in 2008. J Virol in press.
413. Beauverger P, Buckland R, Wild TF (1993) Measles virus antigens induce both type-specific and canine distemper virus cross-reactive cytotoxic T lymphocytes in mice: localization of a common Ld-restricted nucleoprotein epitope. J Gen Virol 74: 2357-2363.
414. Strating A (1975) Measles vaccine in dogs: efficacy against aerosol challenge with virulent canine distemper virus. J Am Vet Med Assoc 167: 59-62.
415. Nicolle C (1931) La maladie du jeune age des chiens est transmissible experimentalement a l'homme sous forme inapparente. Arch Inst Pasteur Tunis 20: 321-323.
416. Raizantseva NE (1956) Experimental measles in puppies. Zh Mikrobiol Epidemiol Immunobiol 27: 22-29.
417. Moura RA, Warren J (1961) Subclinical infection of dogs by canine-adapted measles virus evidenced by their subsequent immunity to canine distemper virus. J Bacteriol 82: 702-705.
418. Osterhaus ADME (1989) A morbillivirus causing mass mortality in seals. Vaccine 7: 483-484.
419. Kuiken T, Kennedy S, Barrett T, Van de Bildt MWG, Borgsteede FH, Brew SD, Codd GA, Duck C, Deaville R, Eybatov T, Forsyth MA, Foster G, Jepson PD, Kydyrmanov A, Mitrofanov I, Ward CJ, Wilson S, Osterhaus ADME (2006) The 2000 canine distemper epidemic in Caspian seals (Phoca caspica): pathology and analysis of contributory factors. Vet Pathol 43: 321-338.
420. DeLay PD, Stone SS, Karzon DT, Katz S, Enders J (1965) Clinical and immune response of alien hosts to inoculation with measles, rinderpest, and canine distemper viruses. Am J Vet Res 26: 1359-1373.
421. Imagawa DT, Goret P, ADAMS JM (1960) Immunological relationships of measles, distemper, and rinderpest viruses. Proc Natl Acad Sci U S A 46: 1119-1123.
422. Sheshberadaran H, Norrby E, McCullough KC, Carpenter WC, Örvell C (1986) The antigenic relationship between measles, canine distemper and rinderpest viruses studied with monoclonal antibodies. J Gen Virol 67: 1381-1392.
423. Örvell C, Norrby E (1974) Further studies on the immunological relationships among measles, distemper, and rinderpest viruses. J Immunol 113: 1850-1858.
424. Gould EA, Armstrong M, Shirodaria PV, De'Ornellas D (1981) Examination of the immunological relationship between measles virus and canine distemper virus using monospecific measles antisera. J Med Virol 7: 51-60.
425. Taylor J, Pincus S, Tartaglia J, Richardson C, Alkhatib G, Briedis D, Appel MJG, Norton E, Paoletti E (1991) Vaccinia virus recombinants expressing either the measles virus fusion or hemagglutinin glycoprotein protect dogs against canine distemper virus challenge. J Virol 65: 4263-4274.
426. Krakowka S, Wallace AL (1979) Lymphocyte-associated immune responses to canine distemper and measles viruses in distemper-infected gnotobiotic dogs. Am J Vet Res 40: 669-672.
427. Adams JM (1952) Pathological and serological relationships between canine distemper and a respiratory tract infection of human beings. AMA Am J Dis Child 84: 466-468.
428. Reed LJ, Muench H (1938) A simple method of estimating fifty percent endpoints. Am J Hygiene 27: 493-497.
429. Fulcher ML, Gabriel S, Burns KA, Yankaskas JR, Randell SH (2005) Well-differentiated human airway epithelial cell cultures. Methods Mol Med 107: 183-206.
430. Anderson JF, Goldberger J (1911) Experimental measles in the monkey: a supplemental note. Public Health Reports 26: 887-895.
431. Avota E, Gassert E, Schneider-Schaulies S (2010) Measles virus-induced immunosuppression: from effectors to mechanisms. Med Microbiol Immunol 199: 227-237.
432. Samb B, Aaby P, Whittle HC, Seck AMC, Rahman S, Bennett J, Markowitz L, Simondon F (1995) Serologic status and measles attack rates among vaccinated and unvaccinated children in rural Senegal. Pediatr Infect Dis J 14: 203-209.
433. Permar SR, Griffin DE, Letvin NL (2006) Immune containment and consequences of measles virus infection in healthy and immunocompromised individuals. Clin Vaccine Immunol 13: 437-443.
434. Bautista-Lopez N, Ward BJ, Mills E, McCormick D, Martel N, Ratnam S (2000) Development and durability of measles antigen-specific lymphoproliferative response after MMR vaccination. Vaccine 18: 1393-1401.
435. Ward BJ, Boulianne N, Ratnam S, Guiot MC, Couillard M, Deserres G (1995) Cellular immunity in measles vaccine failure: demonstration of measles antigen-specific lymphoproliferative responses despite limited serum antibody production after revaccination. J Infect Dis 172: 1591-1595.
436. Helfand RF, Kim DK, Gary HEJ, Edwards GL, Bisson GP, Papania MJ, Heath JL, Schaff DL, Bellini WJ, Redd SC, Anderson LJ (1998) Nonclassic measles infections in an immune population exposed to measles during a college bus trip. J Med Virol 56: 337-341.
437. Muller CP, Huiss S, Schneider F (1996) Secondary immune responses in parents of children with recent measles. Lancet 348: 1379-1380.
438. Jacobson RM, Ovsyannikova IG, Vierkant RA, Pankratz VS, Poland GA (2012) Independence of measles-specific humoral and cellular immune responses to vaccination. Hum Immunol 73: 474-479.
439. Amanna IJ, Slifka MK (2011) Contributions of humoral and cellular immunity to vaccine-induced protection in humans. Virology 411: 206-215.
440. Sheridan BS, Lefrancois L (2011) Regional and mucosal memory T cells. Nat Immunol 12: 485-491.

About the author

Curriculum vitae

PhD portfolio

List of publications

Curriculum vitae

De auteur van dit proefschrift werd geboren op 4 februari 1982 te Schiedam. In 2000 behaalde hij zijn gymnasiumdiploma aan het Stedelijk Gymnasium te Schiedam en begon zijn studie Biomedische Wetenschappen aan de Universiteit Leiden. Na het afronden van de Bachelor-fase in 2003, heeft hij in de Master-fase twee onderzoeksstages doorlopen op het TNO te Leiden en de afdeling Virologie van het Erasmus MC te Rotterdam. Na het behalen van het Masterdiploma in 2006, werd hij door deze afdeling betrokken bij een onderzoeksproject gericht op antivirale resistentie van het herpesvirus in keratitis patiënten. In 2007 startte hij zijn promotieonderzoek gericht op het ontrafelen van de pathogenese van mazelen. Dit onderzoek werd uitgevoerd onder begeleiding van Dr. Rik de Swart en Prof.dr. Ab Osterhaus, in samenwerking met Prof.dr. Theo Geijtenbeek (AMC te Amsterdam) en Dr. Paul Duprex (Boston University), resulterend in dit proefschrift.

PhD PORTFOLIO

Name: Rory Dylan de Vries
Research group: Erasmus MC department Viroscience
Research school: Post-graduate Molecular Medicine
PhD period: 2007 - 2013
Promotor: Prof.dr. Albert D.M.E. Osterhaus
Co-promotor: Dr. Rik L. de Swart
Dr. W. Paul Duprex

In-depth courses:

☐	Course in confocal microscopy (Erasmus MC)	2007
☐	Course in virology (Molmed)	2008
☐	Course in immunology (LUMC)	2008
☐	Course in phylogeny and genetics (Molmed)	2008
☐	Course in training laboratory primates (BPRC)	2008
☐	Course in adobe photoshop / illustrator (Molmed)	2011
☐	Course in adobe indesign (Molmed)	2012
☐	Research integrity course (Molmed)	2012

Poster presentations:

☐	12th Molecular medicine day (Rotterdam)	2008
☐	13th Molecular medicine day (Rotterdam)	2009
☐	Negative strand meeting (Brugge)	2010
☐	16th Molecular medicine day (Rotterdam)	2012

Oral presentations:

☐	Post-infectious diseases symposium (Rotterdam)	2007
☐	18th Measles Meeting (Wurzburg)	2008
☐	Measles virus workshop (Belfast)	2009
☐	SGM spring meeting (Harrogate)	2009
☐	NVVM scientific spring meeting (Papendal)	2009
☐	19th Measles Meeting (Wurzburg)	2009
☐	Bert Rima measles symposium (Belfast)	2010
☐	20th Measles Meeting (Wurzburg)	2010
☐	15th Molecular medicine day (Rotterdam)	2011
☐	Dutch annual virology symposium (Amsterdam)	2011
☐	FNIH scientific advisory board (Boston)	2011
☐	21th Measles Meeting (Wurzburg)	2011
☐	NVVI (Noordwijkerhout)	2011

PhD PORTFOLIO

Attended meetings:

☐	Virology meeting (Greece)	2007
☐	Joint vaccine meeting (Utrecht)	2007
☐	Dutch annual virology symposium (Amsterdam)	2008
☐	Mucosal immunology sympsoium (Rotterdam)	2008
☐	Virology meeting (Dakar)	2009
☐	FNIH scientific advisory board (Belfast)	2010
☐	PhD day (Rotterdam)	2012

Supervision & teaching activities:

☐	Co-supervision MSc student (MH)	2007 - 2008
☐	Co-supervision BSc student (JvdL)	2008 - 2009
☐	Supervision “maatschappelijk stage” (RdH)	2009 - 2010
☐	Co-supervision BSc student (LS)	2010 - 2011
☐	Coach “viruskenner”	2012
☐	Multiple supervisions geneeskunde rotations	2008 - 2009
☐	Multiple supervisions I & I Master rotations	2011 - 2012
☐	FACS introductory lecture	2012

Miscellaneous

☐	Member of SGM	2009 - 2011
☐	Reviewer for tropical health & international medicine	
☐	Reviewer for advances in virology	
☐	Reviewer for european journal of immunology	
☐	Reviewer for journal of biotechnology	
☐	Reviewer for journal of general virology	
☐	Reviewer for journal of pediatrics	
☐	Visits to Belfast for dual immunofluorescence	

List of publications

Published

- DC-SIGN and CD150 have distinct roles in transmission of measles virus from dendritic cells to T-lymphocytes
  Lot de Witte, **Rory D. de Vries***, Michiel van der Vlist*, Selma Yüksel, Manja Litjens, Rik L. de Swart, Teunis B.H. Geijtenbeek
  PLoS Pathog 2008; 4(4):e1000049
- Acyclovir-resistant corneal HSV-1 isolates from patients with herpetic keratitis
  Rui Duan*, **Rory D. de Vries***, Albert D.M.E. Osterhaus, Lies Remeijer, Georges M.G.M. Verjans
  J Infect Dis 2008; 198(5):659-63
- Measles vaccination: new strategies and formulations
  Rory D. de Vries, Koert J. Stittelaar, Albert D.M.E. Osterhaus, Rik L. de Swart
  Expert Rev Vaccines 2008; 7(8):1215-23. Review
- Acyclovir susceptibility and genetic characteristics of sequential herpes simplex virus type 1 corneal isolates from patients with recurrent herpetic keratitis
  Rui Duan, **Rory D. de Vries**, Jessica M. van Dun, Freek B. van Loenen, Albert D.M.E. Osterhaus, Lies Remeijer, Georges M.G.M. Verjans
  J Infect Dis 2009; 200(9):1402-14
- Specific $CD8^+$ T-lymphocytes control dissemination of measles virus
  Rory D. de Vries, Selma Yüksel, Albert D.M.E. Osterhaus, Rik L. de Swart
  Eur J Immunol 2010; 40(2):388-95
- *In vivo* tropism of attenuated and pathogenic measles virus expressing green fluorescent protein in macaques
  Rory D. de Vries, Ken Lemon, Martin Ludlow, Stephen McQuaid, Selma Yüksel, Geert van Amerongen, Linda J. Rennick, Bert K. Rima, Albert D.M.E. Osterhaus, Rik L. de Swart, W. Paul Duprex
  J Virol 2010; 84(9):4714-24
- Early target cells of measles virus after aerosol infection of non-human primates
  Ken Lemon*, **Rory D. de Vries***, Annelies W. Mesman, Stephen McQuaid, Geert van Amerongen, Selma Yüksel, Martin Ludlow, Linda J. Rennick, Thijs Kuiken, Bertus K. Rima, Teunis B.H. Geijtenbeek, Albert D.M.E. Osterhaus, W. Paul Duprex, Rik L. de Swart
  PLoS Pathog 2011; 7(1):e1001263
- Human Langerhans cells capture measles virus through Langerin and present viral antigens to $CD4^+$ T-cells but are incapable of cross-presentation
  Michiel van der Vlist, Lot de Witte*, **Rory D. de Vries***, Manja Litjens, Marein A.W.P. de Jong, Donna Fluitsma, Rik L. de Swart, Teunis B.H. Geijtenbeek
  Eur J Immunol 2011; 41(9):2619-31
- The pathogenesis of measles
  Rory D. de Vries, Annelies W. Mesman, Teunis B.H. Geijtenbeek, W. Paul Duprex, Rik L. de Swart
  Curr Opin Virol 2012; 2(3):248-55. Review
- Recombinant canine distemper virus strain Snyder Hill expressing green or red fluorescent protein causes meningoencephalitis in the ferret
  Martin Ludlow, D. Tien Nguyen, D. Silin, O. Lyubomska, **Rory D. de Vries**, Veronika von Messling, Stephen McQuaid, Rik L. de Swart, W. Paul Duprex
  J Virol 2012; 86(14):7508-19
- Evaluation of synthetic infection-enhancing lipopeptides as adjuvants for a live-attenuated canine distemper virus vaccines administered intra-nasally to ferrets
  D. Tien Nguyen, Martin Ludlow, Geert van Amerongen, **Rory D. de Vries**, Selma Yüksel, R. Joyce Verburgh, Albert D.M.E. Osterhaus, W. Paul Duprex, Rik L. de Swart
  Vaccine 2012; 30(34):5073-80

List of publications

- Evaluating measles vaccines: can we assess cellular immunity?
  Rory D. de Vries, Rik L. de Swart
  Expert Rev Vaccines 2012; 11(7):779-82. Key paper evaluation
- Measles immune suppression: lessons from the macaque model
  Rory D. de Vries, Stephen McQuaid, Geert van Amerongen, Selma Yüksel, R. Joyce Verburgh, Albert D.M.E. Osterhaus, W. Paul Duprex, Rik L. de Swart
  PLoS Pathog 2012; 8(8):e1002885

Accepted for publication

- A prominent role for DC-SIGN$^+$ dendritic cells in initiation and dissemination of measles virus infection in non-human primates
  Annelies W. Mesman, **Rory D. de Vries**, Stephen McQuaid, W. Paul Duprex, Rik L. de Swart, Teunis B.H. Geijtenbeek
  PLoS One in press

Submitted for publication

- Virulence and tropism of recombinant EGFP-expressing canine distemper virus in naive or measles-vaccinated non-human primates
  Rory D. de Vries, Martin Ludlow, Geert van Amerongen, Selma Yüksel, R. Joyce Verburgh, D. Tien Nguyen, Stephen McQuaid, Albert D.M.E. Osterhaus, Rik L. de Swart, W. Paul Duprex
- Measles virus infection of epithelial cells in the macaque upper respiratory tract is mediated by sub-epithelial immune cells
  Martin Ludlow, Ken Lemon, **Rory D. de Vries**, Stephen McQuaid, Emma Millar, Geert van Amerongen, Selma Yüksel, R. Joyce Verburgh, Albert D. M. E. Osterhaus, Rik L. de Swart, W. Paul Duprex

Manuscript in preparation

- The measles virus epithelial cell receptor Nectin-4 is necessary for efficient cell-to-cell spread in cotton rats
  Ken Lemon, Martin Ludlow, **Rory D. de Vries**, Sham Nambulli, Micheal R. Wilson, Stephen McQuaid, Rik L. de Swart, W. Paul Duprex
- Infection of epithelial cells in the macaque nasopharynx and destruction of tonsillar epithelium is associated with high levels of transmissable measles virus
  Martin Ludlow*, **Rory D. de Vries***, Stephen McQuaid, Ken Lemon, Geert van Amerongen, Selma Yüksel, R. Joyce Verburgh, Emma Millar, Albert D.M.E. Osterhaus, Rik L. de Swart, W. Paul Duprex
- Paramyxovirus infections in *ex vivo* lung slice cultures of different host species
  D. Tien Nguyen, **Rory D. de Vries**, Martin Ludlow, Bernadette van den Hoogen, Ken Lemon, Geert van Amerongen, Albert D.M.E. Osterhaus, Rik L. de Swart,W. Paul Duprex
- Measles virus, a respiratory virus causing systemic disease
  Rory D. de Vries, Rik L. de Swart

** both authors contributed equally*

Dankwoord

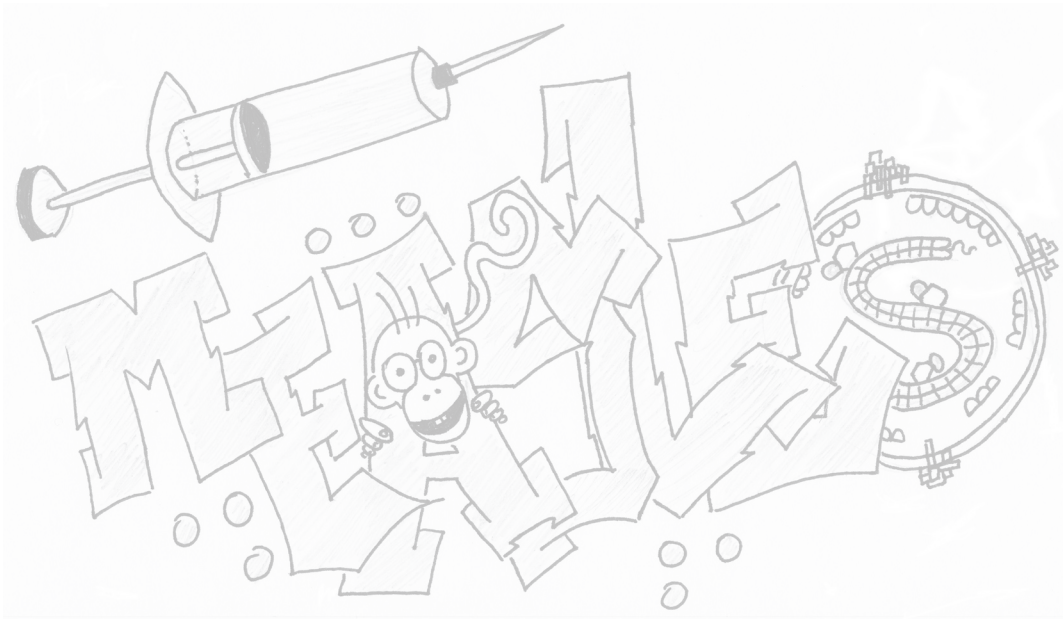

Dankwoord

Zoals gebruikelijk in een proefschrift, wil ik ook graag mijn dank aan een grote groep mensen uiten, die een directe of indirecte bijdrage hebben geleverd aan de totstandkoming van dit proefschrift. Door de vele samenwerkingen is de lijst lang, maar toch hoop ik niemand te vergeten.

Allereerst gaat mijn dank uit naar Ab, mijn promotor. Ik weet dat morbillivirussen één van je passies zijn, dus mijn dank voor de interesse in mijn project. Verder wil ik je bedanken voor de mogelijkheden die ik heb gekregen met het werk op de 17e.

Rik, ik had me geen betere co-promotor dan jij kunnen wensen. Weinig mensen in jouw positie kunnen denk ik zo goed advies geven, zowel op het gebied van schrijven als op het gebied van labwerk! Naast het werk, konden we gelukkig goed met elkaar opschieten, en ondanks dat we als personen erg verschillend zijn konden we ook goed samenwerken en was er veel ruimte voor lol. Mijn dank voor de jaren supervisie, zowel als Master-student, AIO, en hopelijk nog in de toekomst.

Paul, in the beginning of my period working for Rik I only knew you as the little funny guy from Belfast! Who would have thought you would end up to be my second co-promoter. I want to extend my sincere gratitude for the humongous amount of work that you have contributed to this thesis. We always had fun, worked well together and I am very happy that we decided to add you as my co-promotor. I admire your scientific “political” skills and hope that we will still be working together in the future. I will always remember the blood tap that Tien did in our room ☺, and the last night out at the measles meeting in WB, even though you probably don’t remember.

Selma, alles wat ik ongeveer op een lab kan heb ik van jou geleerd. Bedankt voor al je hulp en de fantastische samenwerking, in goede en slechte tijden. Weinig mensen kunnen zo pipetteren als jij, dus ik kan met zekerheid zeggen dat ik het van de beste heb geleerd!

Mijn paranimfen! Joyce, ik ben nog steeds blij dat je onze groep bent komen versterken. In het begin van mijn promotie was je vooral steun en kamergenoot, maar in de laatste periode was je mijn grootste hulp! Bedankt hiervoor, en ook bedankt voor de zelfstandige inzet en prettige samenwerking. Werner, ik ken je alweer sinds je start als student bij Georges en Monique op de 17e. Leuk hoe het uiteindelijk tussen ons gaat en thanks voor je al je praktische adviezen, hulp wanneer nodig en de toch best frequente samenwerking. Verder denk ik dat ik het zonder jouw knuffels niet door mijn laatste apenproef had gered ☺.

“Zeg, duurt het nog lang!!” is de uitspraak van jou die ik me met name zal herinneren. Geert, de samenwerking met jou was fantastisch! Bedankt voor je inzet in mijn project, ik denk dat jij bij alle papers in dit proefschrift betrokken bent geweest. Verder was het altijd leuk om samen weer beneden te zijn, en lekker zinloos te ouwehoeren over van alles en nog wat. Sport, werk, vrouwen, het kon eigenlijk over van alles gaan en overal had je een zeer genuanceerde mening over. En je hebt me toch nog een keer een kooi ingekregen!

Voor steun en toeverlaat ben ik vooral mijn directe mede-AIO's erg dankbaar. Monique, bij jou kan ik altijd met alles terecht, labzaken, promotiezaken en persoonlijke zaken, mijn dank hiervoor. Ook waren we echte FACS-matties ☺, met name de BD lunches waren goed te doen. Tien, als er iemand is met aparte ideeën en eigen manieren ben jij het wel (lees: eigenwijs). Maar het was erg leuk om samen te werken en samen nog een longplakjes paper te doen. Verder heb ik het nog altijd erg naar mijn zijn in kamer Ee1724. Freek, Sara, Gijs en Fatiha bedankt voor de gezelligheid! Natuurlijk gaat mijn dank voor gezelligheid ook uit naar onze buren: Arno (koffie is klaar!), Maarten (helaas is er geen genomics meer van gekomen) en Jan-Henk (de vaste koffiebackup). Speciale dank nog voor naar Stella (K.), zonder jou had ik waarschijnlijk nooit de pedel gebeld! Helaas heeft "so you wanna be a paranimf" het niet gered, en heb je het "koffie is klaar" nooit onder de knie gekregen ☺. Ik blijf het jammer vinden dat je niet meer op onze afdeling bent!

A special word of gratitude for Stephen. Thanks for all your invested effort and time. I don't know how I would obtained my PhD without you as an expert in doing all histology and pathology. I always enjoyed working with you in Belfast and thanks again for having me as a guest in your house. Martin, Linda, Ken and Bert, thanks for all your help, and I hope this Rotterdam/Boston collaboration will be long and fruitful!

Collega's uit Amsterdam: Theo, bedankt voor het plaatsnemen in mijn leescommissie en bedankt voor de wijze lessen! Dankzij jou weet ik exact hoe ik op de juiste plek aan een tafel met een etentje op congres kom te zitten, zodat ik zo min mogelijk met vervelende mensen hoef te socializen. Lot, bedankt voor je wijsheden, ik ken weinig mensen zo intelligent als jij. Michiel bedankt voor je hardnekkigheid. Het LC / mazelen paper was geen succesverhaal, maar toch een mooie publicatie geworden! Annelies bedankt voor de samenwerking en de publicaties samen. Veel succes gewenst in jouw verdere promotie-traject.

Een speciaal bedankje gaat uit naar de dames van het secretariaat. Mijn advies aan alle AIO's zal zijn om Simone, Loubna, Anouk en Maria goed te vriend te houden. Dames, jullie zijn onmisbaar geweest in de laatste fase van mijn promotietraject! Natuurlijk moet ik hierbij ook Robert en Wim bedanken voor alle ondersteuning, op het gebied van proefdierexperimenten en op financieel/contract/personeelszaken gebied.

Collega's die ik graag nog even wil noemen: Petra, soms was het toch alsof mijn moeder op de afdeling rondliep, maar bedankt voor al je praatjes, gezelligheid en adviezen! Miranda, ik hoop dat onze House en pizzadates nog steeds door blijven gaan! Sander H., vooral in het begin van mijn promotie (en eind van jouw promotie) was jij mijn vaste 'partner in crime' in het weekend. Ik weet nog hoe balen het was toen de secretariaat deur niet meer met sleutel 30 geopend kon worden. Eefje, succes met jouw promotie, en ik hoop dat we nog voor gastoptredens als Maria Carey op sintekerst worden gevraagd. Georges, bedankt voor de overbrugging als analist. Verder wil ik graag nog Anna (de G.), Debby, Thijs, Judith, Joost, Rogier, Bernadette, Koert, Leon, Leontine, Leo, Helma en Rui noemen.

Zonder ontspanning geen inspanning, en daarom wil ik ook enkele vrienden in het bijzonder bedanken:

Roy, bedankt dat je er altijd voor me bent en voor de lange en bijzondere vriendschap. Ik hoop dat we nog lang beste vrienden blijven en wil je alle succes wensen in de toekomst.
Tim, bedankt voor alle mogelijkheden die jouw sportschool mij geboden heeft om te groeien als persoon, ik hoop nog lang goede vrienden met je te zijn en samen te kunnen werken.
Corine, als ik bij iemand terecht zou moeten met problemen zou ik bij jou komen. Bedankt dat je er altijd voor me bent wanneer het nodig is.
Lydia, zeker in de beginfase van mijn promotie hadden we een goede band, mijn dank hiervoor.
Ingrid, bedankt voor onze speciale band. Al zou ik jou 3 jaar niet spreken of zien, zouden we nog steeds net zo close zijn als nu denk ik.
Jeffrey M., bedankt voor de klaaguurtjes in de laatste fase van mijn promotie ☺. Ondanks dat ik je bijna alleen zie met sporten, voelt de vriendschap toch hecht en bijzonder!
Jeffrey V., bedankt voor alle gezelligheden en afspraken, en ik ben vereerd dat je me gevraagd hebt als paranimf! Nogmaals mijn dank hiervoor en ik kijk nu al uit naar je promotie.

Tenslotte nog de belangrijkste bedankjes voor mijn familie. Bedankt voor alle gegeven steun. Tante Els, ik wil jou graag noemen in het bijzonder! Bedankt voor alles, voor de alle interesse, betrokkenheid bij alles wat ik doe en de gezelligheid.
Papa en Mama, ik kan mijn dank aan jullie niet op papier uiten. Jullie weten hoe dankbaar ik jullie ben, voor de steun, inspanning en schoppen onder mijn hol zo nu en dan. Zonder jullie zou ik niet zijn wie ik nu ben en zowel op werk als persoonlijk gebied niet bereikt hebben wat ik nu heb. Bedankt voor alles!